Alma Mater Studiorum – Università di Bologna

DOTTORATO DI RICERCA IN
SCIENZE CHIMICHE
Ciclo XXVI
Settore Concorsuale di Afferenza: 03/A1
Settore Scientifico Disciplinare: CHIM/01

DEVELOPMENT AND APPLICATIONS OF HOLLOW FIBER FLOW FIELD-FLOW FRACTIONATION IN THE BIOANALYTICAL FIELD. STUDIES OF AGGREGATION PHENOMENA IN COMPLEX PROTEIN SAMPLES

Presentata da: **Dott.ssa Otilia Maya Tănase**

Coordinatore dottorato:
Chia.mo Prof. Aldo Roda

Relatore:
Chia.mo Prof. Pierluigi Reschiglian

Esame finale anno 2014

Dottoranda: Otilia Maya Tănase

Tutor: prof. Pierluigi Reschiglian

Curriculum, indirizzo: Scienze Chimiche, CHIM/01(03/A1)

Titolo tesi: Development and applications of hollow fiber flow field-flow fractionation in the bioanalytical field. Studies of aggregation phenomena in complex protein samples.

Il lavoro della Dott.ssa Otilia Maya Tănase nel triennio di frequenza del Dottorato in Scienze Chimiche si è rivolto allo sviluppo di metodi di frazionamento in campo-flusso (FFF) in particolare basati sull'impiego e sviluppo della versione miniaturizzata del canale separativo FFF chiamata *hollow fiber FFF* (HF5), in accoppiamento a tecniche di caratterizzazione spettroscopica e ottica, come metodi analitici innovativi per lo studio di campioni proteici complessi e fenomeni di aggregazione. Questo studio trova applicazioni in diversi campi che spaziano dal campo delle proteine terapeutiche, allo studio dei processi di *aging* alla base dello sviluppo di malattie neurodegenative.

Nel corso dei primi due anni di dottorato, il lavoro di ricerca è stato rivolto allo sviluppo di metodi HF5 accoppiati a tecniche di rivelazione molto sensibili (spettroscopia UV/Vis, fluorescenza e multi-angle light scattering – MALS) per la caratterizzazione dimensionale e morfologica di aggregati proteici spesso presenti nei biofarmaci (anticorpi e/o proteine utilizzate come veicolanti per biofarmaci) e formati durante il processo di sviluppo della loro formulazione. Tali metodi sono risultati caratterizzati da elevata sensibilità, selettività e riproducibilità dimostrandosi particolarmente adatti ad un controllo di qualità (QC) di campioni proteici ad elevato perso molecolare. I risultati ottenuti hanno dimostrato anche la superiorità dell'HF5 rispetto alla cromatografia ad esclusione dimensionale (SEC) – il punto di riferimento nelle pratiche di controllo qualità per proteine terapeutiche. La HF5 accoppiata a tecniche di rivelazione sensibili offre una notevole selettività rispetto alla SEC potendo separare analiti in un ampio intervallo di pesi molecolari, pertanto permette un'accurata valutazione della composizione delle formulazioni proteiche; spesso in SEC lo spazio cromatografico disponibile per la separazione di specie ad alto peso molecolare è molto limitato, causando la co-eluizione di specie con pesi molecolari simili.

Nel terzo anno del Dottorato, la Dott.ssa Otilia Maya Tănase ha trascorso un periodio di ricerca all'estero presso il Laboratorio di Patologia, Immunologia e Microbiologia (Albert Einstein College of Medicine, Yeshiva University, NY, Stati Uniti) sotto la supervisione della prof. Laura Santambrogio. Durante tale periodo si è occupata dell'inserimento della tecnologia HF5 nei laboratori e procedure biochimiche utilizzate per lo studio dei fenomeni di aggregazione proteica attinenti al processo di aging (immunosenescenza). Ha quindi sviluppato un metodo Hf5-MALS per la caratterizzazione dimensionale e conformazionale di questi sistemi proteici complessi. L'HF5 accoppiata al MALS è stata applicata come prima dimensione separativa per lisati cellulari interi, di origine diversa e a diversi stadi dell'*aging*, pertanto contenenti diversi livelli e tipologie (covalenti e non-covalenti) di aggregati proteici. Inoltre, ha avuto l'opportunità di apprendere conoscenze su tecniche complementari per la caratterizzazione di tali aggregati (SDS-PAGE, Native PAGE e FPLC). I risultati hanno confermato la capacità dell'HF5 accoppiata al MALS per colmare il "gap" di tecniche adatte per la caratterizzazzione di aggregegati proteici sub micrometrici.

Il lavoro di ricerca all'estero è stato concluso con un manuscritto in fase avanzata di preparazione, che verrà inviato alla rivista Nature Methods.

Il progetto di dottorato ha permesso Dott.ssa Otilia Maya Tănase di approfondire le ricerche nel campo della chimica analitica/tecniche separative, iniziate con il lavoro di tesi e proseguite nel periodo successivo come borsista.. Durante il periodo di tesi la dottoranda ha dimostrato serietà nel lavoro di laboratorio e capacità di lavoro autonomo. La dottoranda ha trascorso un periodo di formazione presso Wyatt Technology Europe (Germania), azienda con la quale il gruppo di ricerca in Chimica Analitica ha una collaborazione stretta. La collaborazione ha avuto come frutto l'implementazione del prototipo miniaturizzato HF5 nel sistema separativo Eclipse® DUALTEC™ prodotto dall'azienda tedesca, il primo sistema FFF commerciale del suo genere – sistema che ha costituito la strumentazione fondamentale nel lavoro di ricerca della dottoranda.

Nell'ambito del suo progetto di ricerca, la Dott.ssa Otilia Maya Tănase ha mostrato un'elevata capacità di adattamento a diversi ambienti culturali e diverse strutture organizzative, ha contribuito a mettere le basi e mantenere collaborazioni internazionali e ha messo alla prova le sue capacità di *problem-solving* mediante la proposta e sviluppo di soluzioni innovative. Le sue doti naturali verso l'apprendimento delle lingue straniere, l'orientamento verso l'organizzazione, l'attenzione ai dettagli, la pazienza e la precisione, le hanno permesso di lavorare con costanza ed in modo efficace sul raggiungimento degli obiettivi a lungo termine, mostrandosi responsabile per il proprio lavoro e per le persone di cui ha coordinato il lavoro in laboratorio.

Ha inoltre svolto attività di tutorato nel laboratorio di Chimica Analitica presso il CdL in Scienze Farmaceutiche Applicate (Imola) dimostrando buone capacità organizzative e didattiche. Inoltre, la Dott. ssa Otilia Maya Tănase si è mostrata disponibile e responsabile ad organizzare, coordinare e seguire il lavoro sperimentale di laureandi nel laboratorio di Chimica Analitica (Scienze della separazione) del Dipartimento "G. Ciamician".

L'attività svolta dalla dottoranda si è finora concretizzata con due articoli pubblicati su riviste internazionali con referee; altri manoscritti sono in fase di avanzata preparazione e saranno presto inviati a riviste internazionali. La dottoranda è stata anche co-autore di sei comunicazioni a congressi nazionali e internazionali, mostrando spiccate capacità di raccolta, elaborazione e preparazione del materiale scientifico da divulgare. Inoltre, la dottoranda ha regolarmente illustrato il suo lavoro mediante relazioni scritte e presentazioni orali in riunioni con gli altri collaboratori del progetto durante tutto il triennio.

Recent advances in the fast growing area of therapeutic/diagnostic proteins and antibodies - novel and highly specific drugs - as well as the progress in the field of functional proteomics regarding the correlation between the aggregation of damaged proteins and (immuno) senescence or aging-related pathologies, underline the need for adequate analytical methods for the detection, separation, characterization and quantification of protein aggregates, regardless of the their origin or formation mechanism.

Hollow fiber flow field-flow fractionation (HF5), the miniaturized version of FlowFFF and integral part of the Eclipse DUALTEC FFF separation system, was the focus of this research; this flow-based separation technique proved to be uniquely suited for the hydrodynamic size-based separation of proteins and protein aggregates in a very broad size and molecular weight (MW) range, often present at trace levels. HF5 has shown to be (a) highly selective in terms of protein diffusion coefficients, (b) versatile in terms of bio-compatible carrier solution choice, (c) able to preserve the biophysical properties/molecular conformation of the proteins/protein aggregates and (d) able to discriminate between different types of protein aggregates. Thanks to the miniaturization advantages and the online coupling with highly sensitive detection techniques (UV/Vis, intrinsic fluorescence and multi-angle light scattering), HF5 had very low detection/quantification limits for protein aggregates. Compared to size-exclusion chromatography (SEC), HF5 demonstrated superior selectivity and potential as orthogonal analytical method in the extended characterization assays, often required by therapeutic protein formulations. In addition, the developed HF5 methods have proven to be rapid, highly selective, sensitive and repeatable. HF5 was ideally suitable as first dimension of separation of aging-related protein aggregates from whole cell lysates (proteome pre-fractionation method) and, by HF5-(UV)-MALS online coupling, important biophysical information on the fractionated proteins and protein aggregates was gathered: size (rms radius and hydrodynamic radius), absolute MW and conformation (shape and mass distribution about the gravity center).

Hollow fiber flow field-flow fractionation, HF5

Multi-angle light scattering, MALS

Intrinsic fluorescence detection, FLD

Analytical techniques hyphenation/coupling

Antibody instability

Therapeutic protein formulation

Protein aggregation, aggregation mechanisms

Antibody self-association

HF5 performance, specificity, repeatability, FFF selectivity, robustness, resolution, efficiency, sample recovery

Limit of Detection, LoD and Limit of Quantification, LoQ

Reactive oxygen species, ROS

Senescence, immunosenescence

Oxidative stress

Protein carbonylation, age-related post-translational modifications

Irreversible protein damage and protein aggregation

Paraquat

TABLE OF CONTENTS

PREAMBLE

This dissertation addresses two major aspects regarding the aggregation phenomena occurring in complex protein samples: the first regards the emerging field of *protein therapeutics* and the current need for adequate *characterization methods for protein formulations*; while the second one regards the study of aggregation phenomena occurring in living organisms as a consequence of the natural process of *aging*, as well as the cause of notorious *neurodegenerative disorders*.

Therapeutic proteins and, in particular, antibodies, are the compounds most used as biopharmaceuticals. However, the biggest problem is their instability which often leads to aggregation. While aggregation is necessary in particular cases for the proteins to perform their biological activity, the presence of aggregated proteins for therapeutic use is undesirable. Even at very low levels, the aggregates of any kind may not preserve or, even worse, it may impede the desired biological functionality and above all, may represent a potential immunogenic risk. Hence the need to carefully evaluate their clinical relevance [Cromwell et al. 2006].

In order to ensure the efficacy and safety of biopharmaceuticals it is essential to employ suitable analytical methods to monitor/evaluate efficiently and accurately the phenomenon of aggregation during development, production and storage of products. Usually, the various aggregation mechanisms are acting simultaneously and have not been fully elucidated [Mahler et al. 2009, Philo and Arakawa 2009,

Engelsman et al. 2011]. Moreover, the formed aggregates have sizes in a very wide dimensional range (few nm-mm). The limitations of currently employed analytical methods in terms of sensitivity, speed of analysis, robustness, range of application (Figure 1) or sample complexity and recovery, together with the fact that the term "aggregate" is constantly redefined as a consequence of continuous new findings in the clinical field, have created a "gap"[Philo 2006].

Biological aging, also known as *senescence*, is a fundamental process which is the main risk factor regarding the development of cancer, cardiovascular and neurodegenerative diseases (Alzheimer, Parkinson and Huntington disease) in vertebrates. In particular, immunosenescence represents the progressive deterioration of the immune system caused by the natural aging process. Inside any living organism, damaged cells are constantly being replaced and proteins are degraded to their constituting amino-acids (proteasome degradation or chaperone-mediated autophagy by lysosome) and re-synthesized. Following senescence, the body gradually loses its ability to repair itself. This is due to loss of equilibrium between the oxidizing species (in particular, the reactive oxygen species) and antioxidants, leading to a pathological condition called *oxidative stress* [Bandyopadhyay et al. 1999, Squier 2001]. Upon oxidation (most frequently resulting in the carbonylation of particular side chains), the proteins lose their native conformation, becoming thermodynamically unstable, and have a high propensity to form larger assemblies. Moreover, since the degradation mechanisms no longer work efficiently, the aggregates accumulate in the endosomal compartments, increasing in size with advancing age [Cannizzo et al. 2011, Cannizzo et al. 2012]. An appropriate proteomics technology platform, based on a separation technique capable of separating protein aggregates based on their biophysical properties, would allow further analysis on how protein sequence/structure determine their tendency to aggregate, how different post-translational modifications affect unfolding and aggregation and the proteomic machinery associated with their degradation.

Moreover, it would open a world of possibilities towards the discovery of novel drug targets and early disease markers [Garbis et al. 2005].

Figure 1 [Zölls et al. 2012] depicts the size range of application of the currently employed analytical methods for the characterization of protein particles. As therapeutic proteins, as well as aging proteins can form different types and sizes of aggregates and particles, a case-by-case selection of the appropriate analytical characterization methods is required, since there is no "*general solution*" to fit all.

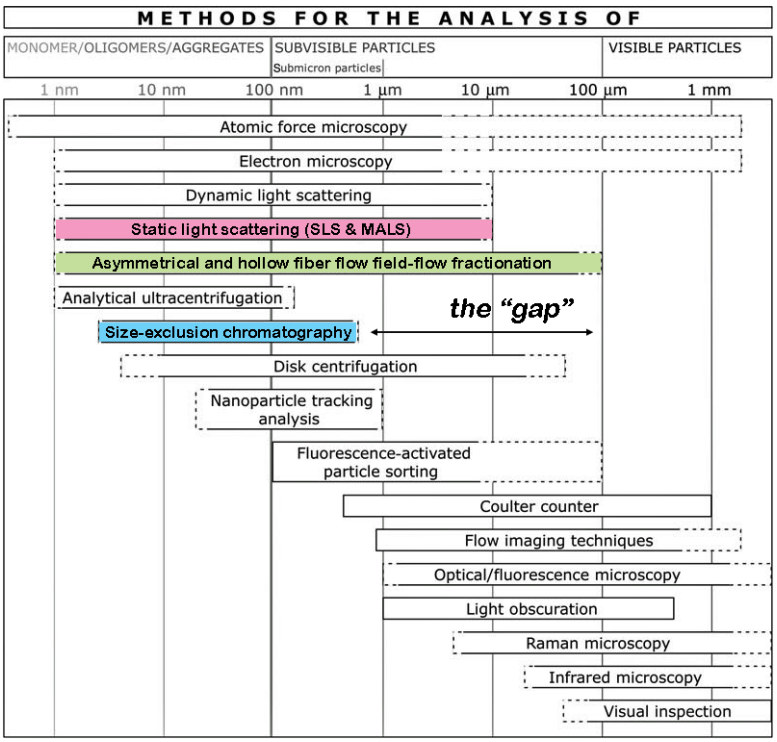

Figure 1 – Approximate size range of current analytical methods for the size characterization of sub-visible and visible (protein) particles [Zölls et al. 2012]

The figure shows that no single method is capable of providing a complete characterization, which would cover the whole nm-mm aggregates size range, therefore making the combination of several methods (usually based on different measurement/separation principles) mandatory for an extensive characterization [Philo 2006, Zölls et al. 2012]. The second challenge lies within the data interpretation; since different measurement/separation principle are applied, results may not always be directly comparable and need to be evaluated case-by-case

considering the underlying theory. The possibility of applying several orthogonal characterization methods has been proposed as means to bridge this "gap", by selecting one or more methods for sample-to-sample comparison and searching for trends rather than concentrate on actual numbers. [Carpenter et al. 2010, Carpenter et al. 2012, Zölls et al. 2012].

Both protein aggregation topics were faced with the help of ***field-flow fractionation*** (FFF), a chromatographic – like flow-based separation technique [Giddings 1966], which is particularly suited for the separation of macromolecules (proteins and protein complexes/aggregates) in a very broad MW range [Zattoni et al. 2007]. FFF and liquid chromatography (LC) employ almost the same instrumental setup, but, since the separation in based on a different principle, the separation device in FFF is an empty *channel* instead of a chromatographic column. In FFF, the retention does not rely on interaction of the analytes with a stationary phase, but with an external *field* that is applied perpendicularly to direction of the mobile phase *flow.* Hence the *field-flow* dualism required for the separation [Giddings 1973, Giddings 2000].
In flow FFF (Fl FFF or F4), the applied field consists in a second stream of mobile phase applied through the channel section, therefore called *cross-flow* [Reschiglian and Moon 2008]. This is the FFF variant of choice for the studies reported in this Thesis because of its ability to separate macromolecules and particles in a very wide size (few nm - μm) and MW range. Moreover, the *flow* field offers intrinsic advantages for the separation of proteins and protein aggregates: (i) the gentle separation mechanism and the lack of a stationary phase; (ii) bio-friendly, and virtually any type of mobile phase can be used; (iii) offers high selectivity in terms of diffusion coefficient differences. Features (i) and (ii) imply that interactions between the proteins and the separation device are negligible. This makes it possible to preserve the native molecular conformation, a fundamental bio-physical property. Feature (iii) is correlated to the separation principle in F4, based on differences in *diffusion coefficients*.

The *diffusion coefficient* (*D*) is a key parameter which relates to the protein size, shape and surface properties. [Reschiglian and Moon 2008].

In particular, this dissertation is centered on the applications in the bioanalytical field of the miniaturized version of F4, called *hollow fiber flow field-flow fractionation* (hollow fiber F4 or HF5), which is characterized by a symmetrical channel geometry represented by a cylindrical channel with porous walls. [Johann et al. 2010].

Many efforts have been employed over the years by the Analytical Chemistry research team of the "G. Ciamician" Chemistry Department into developing the HF5 separation device prototype. Thanks to the successful collaboration between the Analytical Chemistry team and Wyatt Technology Europe (Dernbach, Germany), once the HF5 separation device achieved its ready-to-market phase, it was implemented in the Eclipse® DUALTEC™ FFF separation system. This novel implementation made "the first commercial FFF system using both HF5 and AF4 technique integrated into one instrument", which was launched on the market in 2012. The commercial HF5 channel is equipped with an Enhanced Sealing Technology (EST, patented) facilitating the channel assembly and is also leakage-proof.

In addition to the key advantages offered by F4, HF5 distinguishes itself through unique features, such as: (i) low channel volume, which reduces sample dilution with fractionation, (ii) low flow rates, which makes it possible to be successfully coupled on-line with MS; (iii) disposable usage, which eliminates sample carry-over and possible sample contamination. Features (i) and (ii) also lead to a higher sensitivity by increasing the limit of detection/quantification for protein aggregates. Thanks to all these key advantages, which have led to the promising results described in the literature [Reschiglian et al. 2002, Reschiglian et al. 2004, Reschiglian et al. 2005, Silveira et al. 2005, Roda et al. 2006, Rambaldi et al. 2007, Kang et al. 2008, Kim et al. 2008, Lee et al. 2009, Kang et al. 2010, Lee et al. 2010], HF5 offers unparalleled

performances that are fundamental for the characterization of proteins and protein aggregates.

The analytical information was enhanced by HF5 on-line coupled with highly sensitive *spectroscopic* detection methods, such as **UV absorbance** and **fluorescence emission** detection, or with *optical* detection methods, like **multi-angle light scattering** (**MALS**), which measures the light scattered at multiple angles by the proteins and protein aggregates fractionated through HF5.

Combined with a concentration detector (like a UV detector), MALS is able to provide directly the *size* (root mean square radius or *rms radius,* the mass-average distance between each point in the macromolecule and the center of mass), and the *absolute molar weight* (MW) of the fractionated proteins and protein aggregates as a function of their elution time. Comparing the *rms radius* values obtained from the MALS measurements with the *hydrodynamic radius* (r_H) values, which are readily obtained from the experimental retention time, HF5-MALS allows obtaining information regarding the shape and mass distribution inside the protein aggregates [Reschiglian and Moon 2008].

In Part 1 of this dissertation (*Chapter 4*, *sub-chapter 4.1*), HF5 coupled online with MALS, UV-Vis and/or fluorescence detection was proposed to bridge the "gap" of suitable techniques for the characterization of the sub-μm particles. A fast method is proposed for the characterization of a standard protein mixture, with particular regard to the repeatability, resolution, sensitivity, selectivity and robustness. The superior performance of HF5 is demonstrated, especially from the *selectivity* point of view, when compared to *size-exclusion chromatography* (SEC) – the benchmark in quality control (QC) of therapeutic proteins. Exploratory methods are proposed for the separation and characterization of *self-associated* immunoglobulins (IgGs) under different experimental conditions, showing the versatility and the sensitivity of HF5 when coupled with fluorescence detection (FLD) and MALS. The advantages of miniaturization are explored further, sensitivity is improved even more when

employing a hollow fiber with a smaller inner diameter for the separation of an IgG with low aggregates levels. A fast method is proposed to compare HF5 and SEC performance, employing an IgG1 monoclonal antibody, once again demonstrating the HF5 superiority in terms of *selectivity*. Finally, a highly repeatable and sensitive HF5-MALS method, providing insight on the biophysical nature of aggregates, was developed employing an avidin derivate as sample model (AvidinOX®, provided by Sigma Tau).

The aging-related protein aggregation topic, occurring under the effects of oxidative stress, was addressed in collaboration with the Laboratory of Pathology, Microbiology and Immunology, Albert Einstein College of Medicine of Yeshiva University (New York, USA), and the analytical information was enhanced or corroborated by complementary assays performed by the above-mentioned laboratory. In Part 2 of the dissertation (*Chapter 4, sub-chapter 4.2)*, it is demonstrated that HF5 can be used as a first dimension of separation of aging-related protein aggregates from whole cell lysates and, by coupling HF5 with MALS, important biophysical information on the separated aggregates can be gathered (size, molecular weight and conformation). The effectiveness of the separation method was confirmed by both native-PAGE and proteomic analysis of the high molecular weight aggregates. It is shown how, under the effect of the oxidative stress (either induced or naturally occurring in aging organism), protein aggregates are modified and have a smaller size when compared to native aggregates of same molecular weight. Moreover it is shown that oxidative stress-related proteins aggregate and have a different, more compact, molecular conformation. The ability to separate cell lysates under both physiological and denaturing conditions confirmed what previously reported: most of aging-related aggregates are urea-insoluble. Moreover, offline coupling of HF5 with Mass Spectrometry confirmed the presence of several proteins previously reported to be insoluble or with increased tendency to aggregate during aging.

REFERENCES

[Bandyopadhyay et al. 1999] Bandyopadhyay U.; Das D. and Banerjee R. K. (1999). "*Reactive oxygen species: Oxidative damage and pathogenesis*." CURRENT SCIENCE **77** (5): 658-666.

[Cannizzo et al. 2012] Cannizzo E.; Clement C. C.; Morozova K.; Valdor R.; Kaushik S.; Almeida L. N.; Follo C.; Sahu R.; Cuervo A. M.; Macian F. and Santambrogio L. (2012). "*Age-related oxidative stress compromises endosomal proteostasis*." Cell Press **2** (1): 136-149.

[Cannizzo et al. 2011] Cannizzo E.; Clement C. C.; Sahu R.; Follo C. and Santambrogio L. (2011). "*Oxidative stress, inflamm-aging and immunosenescence*." Journal of Proteomics **74** (11): 2313–2323.

[Carpenter et al. 2012] Carpenter J. F.; Cherney B. and Rosenberg A. S. (2012). *The Critical Need for Robust Assays for Quantitation and Characterization of Aggregates of Therapeutic Proteins*. Analysis of Aggregates and Particles in Protein Pharmaceuticals. Mahler H.-C. and Jiskoot W. Hoboken, NJ, USA, John Wiley & Sons, Inc.

[Carpenter et al. 2010] Carpenter J. F.; Randolph T. W.; Jiskoot W.; Crommelin D. J. A.; Middaugh C. R. and Winter G. (2010). "*Potential Inaccurate Quantitation and Sizing of Protein Aggregates by Size Exclusion Chromatography: Essential Need to Use Orthogonal Methods to Assure the Quality of Therapeutic Protein Products*." Journal of Pharmaceutical Sciences **99** (5): 2200–2208.

[Cromwell et al. 2006] Cromwell M. E. M.; Hilario E. and Jacobson F. (2006). "*Protein aggregation and bioprocessing*." AAPS Journal **8** (3): E572–E579.

[Engelsman et al. 2011] Engelsman J. d.; Garidel P.; Smulders R.; Koll H.; Smith B.; Bassarab S.; Seidl A.; Hainzl O. and Jiskoot W. (2011). "*Strategies for the Assessment of Protein Aggregates in Pharmaceutical Biotech Product Development*." Pharmaceutical Research **28** (4): 920-933.

[Garbis et al. 2005] Garbis S.; Lubec G. and Fountoulakis M. (2005). "*Limitations of current proteomics technologies*." Journal of Chromatography A **1077** (1): 1-18.

[Giddings 1966] Giddings J. C. (1966). "*A New Separation Concept Based on a Coupling of Concentration and Flow Nonuniformities*." Separation Science **1** (1): 123-125.

[Giddings 1973] Giddings J. C. (1973). "*The conceptual basis of field-flow fractionation*." Journal of Chemical Education **50** (10): 667-669.

[Giddings 2000] Giddings J. C. (2000). *Chapter 1: The Field-Flow Fractionation Family: Underlying principles*. Field-Flow Fractionation Handbook. Schimpf M. E.; Caldwell K. and Giddings J. C. New York, Wiley**:** 3-30.

[Johann et al. 2010] Johann C.; Elsenberg S.; Roesch U.; Rambaldi D. C.; Zattoni A. and Reschiglian P. (2010). "*A novel approach to improve operation and performance in flow field-flow fractionation*." Journal of Chromatography A **1218** (27): 4126–4131.

[Kang et al. 2010] Kang D.; Ji E. S.; Moon M. H. and Yoo J. S. (2010). "*Lectin-Based Enrichment Method for Glycoproteomics Using Hollow Fiber Flow Field-Flow Fractionation: Application to Streptococcus pyogenes*." Journal of proteome research **9** (6): 2855–2862.

[Kang et al. 2008] Kang D.; Oh S.; Reschiglian P. and Moon M. H. (2008). "*Separation of mitochondria by flow field-flow fractionation for proteomic analysis*." Analyst (133): 505-515.

[Kim et al. 2008] Kim K. H.; Kang D.; Koo H. M. and Moon M. H. (2008). "*Molecular mass sorting of proteome using hollow fiber flow field-flow fractionation for proteomics*." Journal of Proteomics **71** (1): 123–131.

[Lee et al. 2009] Lee J. Y.; Kim K. H. and Moon M. H. (2009). "*Evaluation of multiplexed hollow fiber flow field-flow fractionation for semi-preparative purposes*." Journal of Chromatography A **1216** (37): 6539–6542.

[Lee et al. 2010] Lee J. Y.; Min H. K.; Choi D. and Moon M. H. (2010). "*Profiling of phospholipids in lipoproteins by multiplexed hollow fiber flow field-flow fractionation and nanoflow liquid chromatography–tandem mass spectrometry*." Journal of Chromatography A **1217** (10): 1660–1666.

[Mahler et al. 2009] Mahler H.-C.; Friess W.; Grauschopf U. and Kiese S. (2009). "*Protein aggregation: Pathways, induction factors and analysis*." Journal of Pharmaceutical Sciences **98** (9): 2909–2934.

[Philo 2006] Philo J. S. (2006). "*Is Any Measurement Method Optimal for All Aggregate Sizes and Types?* ." The AAPS Journal **8** (3).

[Philo and Arakawa 2009] Philo J. S. and Arakawa T. (2009). "*Mechanisms of Protein Aggregation*." Current Pharmaceutical Biotechnology (10): 348-351.

[Rambaldi et al. 2007] Rambaldi D. C.; Zattoni A.; Casolari S.; Reschiglian P.; Roessner D. and Johann C. (2007). "*An Analytical Method for Size and Shape Characterization of Blood Lipoproteins*." Clinical Chemistry **53** (11): 2026-2029.

[Reschiglian and Moon 2008] Reschiglian P. and Moon M. H. (2008). "*Flow field-flow fractionation: A pre-analytical method for proteomics*." Journal of Proteomics **71** (3): 265–276.

[Reschiglian et al. 2002] Reschiglian P.; Roda B.; Zattoni A.; Min B. R. and Moon M. H. (2002). "*High performance, disposable hollow fiber flow field-flow fractionation for bacteria and cells. First application to deactivated Vibrio cholerae**." Journal of Separation Science (25): 490-498.

[Reschiglian et al. 2004] Reschiglian P.; Zattoni A.; Cinque L. and Roda B. (2004). "*Hollow-Fiber Flow Field-Flow Fractionation for Whole Bacteria Analysis by Matrix-Assisted Laser Desorption/Ionization Time-of-Flight Mass Spectrometry*." Analytical Chemistry **76** (7): 2103–2111.

[Reschiglian et al. 2005] Reschiglian P.; Zattoni A.; Roda B. and Cinque L. (2005). "*On-Line Hollow-Fiber Flow Field-Flow Fractionation-Electrospray Ionization/Time-of-Flight Mass Spectrometry of Intact Proteins*." Analytical Chemistry **77** (1): 47-56.

[Roda et al. 2006] Roda A.; Parisi D.; Guardigli M.; Zattoni A. and Reschiglian P. (2006). "*Combined Approach to the Analysis of Recombinant Protein Drugs Using Hollow-Fiber Flow Field-Flow Fractionation, Mass Spectrometry, and Chemiluminescence Detection*." Analytical Chemistry **78** (4): 1085–1092.

[Silveira et al. 2005] Silveira J. R.; Raymond G. J.; Hughson A. G.; Race R. E.; Sim V. L.; Hayes S. F. and Caughey B. (2005). "*The most infectious prion protein particles*." Nature (437): 257-261.

[Squier 2001] Squier T. C. (2001). "*Oxidative stress and protein aggregation during biological aging*." Experimental Gerontology **36** (9): 1539–1550.

[Zattoni et al. 2007] Zattoni A.; Casolari S.; Rambaldi D. C. and Reschiglian P. (2007). "*Hollow-fiber flow field-flow fractionation*." Current Analytical Chemistry **3** (4): 310-323.

[Zölls et al. 2012] Zölls S.; Tantipolphan R.; Wiggenhorn M.; Winter G.; Jiskoot W.; Friess W. and Hawe A. (2012). "*Particles in therapeutic protein formulations, Part 1: Overview of analytical methods*." Journal of Pharmaceutical Sciences **101** (3): 914–935.

CHAPTER 1:
PROTEIN AGGREGATION PHENOMENA

1.1. INTRODUCTION TO THE ANALYTICAL PROBLEM: PROTEIN AGGREGATION

Aggregation is a general term that surrounds several types of protein-protein interactions or characteristics; protein aggregates may emerge from several mechanisms [Philo and Arakawa 2009, Wang et al. 2010] and may be classified in numerous ways, including soluble/insoluble, covalent/non-covalent, reversible/irreversible, and native/denatured. [Cromwell et al. 2006]. In order to address protein aggregation as an issue, an accurate definition of "*protein aggregate*" is required, even though not often available and definitely, not general.

Protein aggregates sizes cover a very wide size spectrum, from small oligomers to visible "*snow*" or "*flakes*" and precipitates, and, as a rule of thumb, only the smaller species have a reversible character. Furthermore, even though less acknowledged, aggregates also display an ample range of life spans, and this aspect impacts greatly on the *choice of appropriate detection methods*. In addition, the measurement itself may destroy or create aggregates, hence impact on aggregates levels; this aspect represents a *major analytical challenge* and is decisive as well for appropriate method selection [Philo 2006].

Consequently, there is no "*general solution to fit all*", since no single analytical method or approach is able to provide a complete answer and, at the same time, able to work in *all* situations and on *all* different samples. Despite all the efforts to define the analytical challenge at stake and all the information currently available on the protein aggregation topic, many pharmaceutical scientists fail to acknowledge protein aggregation as an encompassing phenomenon and its implications on the measurement approach and on the data interpretation. In fact, the case-by-case use of *complementary (orthogonal) characterization methods* is recommended, as well as identifying trends in the obtained results instead on concentrating on raw numbers [Philo 2006, Carpenter et al. 2010, Carpenter et al. 2012, Zölls et al. 2012].

1.1.1. THE PROTEIN AGGREGATES HAVE A WIDE SIZE RANGE

Due to the complexity of the protein aggregation phenomenon, there is no universal terminology to describe the numerous aggregate sizes or types; however, some of the commonly occurring aggregates are classified by [Philo 2006] as follows: (1) rapidly reversible, non-covalent small oligomers (dimer, trimer, tetramer, and so forth); (2) irreversible, non-covalent oligomers; (3) covalent oligomers (for instance, linked through Schiff bases or disulfide bonds); (4) "*large*" aggregates (≥ decamer); (5) "*very large*" aggregates (diameter ~50 nm - 3 μm); and (6) visible particulates ("*snow*", "*flakes*" or "*floaters*"), which are, most likely, irreversible. Except for the visible particulates, there is a chance that the *large* and *very large* protein aggregates have a reversible character, if associated through non-covalent bonds.

In addition, protein aggregates are characterized by the tendency to "*evolve*" over time, typically into larger and less reversible/irreversible species; moreover, it is highly likely for a protein sample to contain more than one of these types or classes [Philo 2006, Philo and Arakawa 2009].

1.1.2. Most Protein Aggregates are reversible

Despite the common tendency to make a *black vs. white* distinction, which usually is interpreted as a permanent and irrevocable classification of aggregates into "*reversible*" and "*irreversible"*, in reality, though, an aggregate that is irreversible in one context can become reversible in another, indicating the existence of a continuum of aggregation states between reversible and irreversible [Philo 2006].

1.1.3. The life span of Protein Aggregates is variable

The ample range of life spans feature of reversible protein aggregates (their permanence in time) is probably their most neglected; the rates of association/dissociation phenomena between oligomers vary greatly, ranging from ms to several days. Many analytical methods, more in particular, separation techniques, allow only the detection the longer life span species; proteins displaying dynamic self-association (rapid and reversible protein self-assembly), under the effects of the separation method, find themselves under a constant struggle between *separation* and *re-equilibration*, because of the law of mass action. Consequently, the separation results often depend on the *rates* of the association/dissociation process, as well as the equilibrium constants [Philo 2006].

Although either SEC and SV-AUC or Flow FFF methods may successfully resolve multiple peaks, in fact, neither of those peaks represents a pure, individual oligomer, but more likely a dynamic mixture of multiple oligomers; however, if the association/dissociation reactions occur very slowly compared to the duration of the separation, the self-associated protein system behaves like a true mixture, therefore individual oligomers can be resolved. Such reversible, but extremely slow association/dissociation reactions, responsible for the existence of so-called "*metastable oligomers*", are rather common [Philo 2006, Philo and Arakawa 2009].

1.1.3. THE SEPARATION IS INTRINSICALLY DISTRESSING FOR PROTEIN AGGREGATES

When analyzing protein aggregates, one of the fundamental problems is represented by the simple fact that most characterization techniques and, in particular, separation techniques, have a chance of perturbing the distribution of protein species in the sample to be analyzed; not only the measurement itself may destroy or cause the loss of some aggregates, but new aggregates can also be created by or during the measurement[Philo 2006, Engelsman et al. 2011].

For instance, both SEC and FFF (AF4 or HF5) produce a high sample dilution of the sample during the separation, which potentially induces the dissociation of the reversible aggregates. Moreover, SEC is also infamous for filtration effects and poor sample recovery, which makes the use of an elution buffer containing high levels of salts and/or organic modifiers mandatory; these carrier solution additives may modify the distribution of non-covalent aggregates. Generally less problematic that SEC, the protein recovery in FFF (AF4 and HF5) may also suffer from non-specific adsorption of proteins to the channel wall, therefore some adjustments of the carrier solution are in order. As for the creation of new aggregates, the major impacting factor is the composition of the carrier solution (and changes thereof); however, in both SEC and FFF, protein aggregates may also arise from pre-dilution of the sample with the separation buffer, whose composition is usually different than the protein formulation buffer [Arakawa et al. 2010, Carpenter et al. 2012, Zölls et al. 2012].

1.1.5. IS IT POSSIBLE TO REPLACE SEC?

Despite its notoriety, it is very likely that SEC (and its macro-column version, fast protein chromatography, FPLC) will continue to be the workhorse tool for protein aggregates characterization in the near future. Alternative analytical platforms, such as SV-AUC and FFF (AF4 and HF5) with or without *multi-angle scattering* (MALS) detection, still have one or more of the following drawbacks: (1) they are not robust

enough (do not provide repeatable results) or/and easy to use as routine QC procedures, therefore difficult to validate for lot release, (2) they have low throughput, (3) they require expensive equipment (SV-AUC) or extensive method development (FFF), therefore highly trained personnel, and (4) the software may be very far from being 21 CFR part 11 compliant [FDA 1997].

Despite these shortcomings, the above mentioned analytical methodologies proved themselves to be invaluable as orthogonal methods for SEC, whose purpose is to help determining the reliability of the results provided by SEC. Such cross-validation practices are usually time and resources-efficient, and they can be implemented fairly easily at all stages of drug development, as well as technological platforms in functional and structural proteomics. In addition, these complementary methods can help guiding the development and the improvement of SEC methods [Philo 2006, Arakawa et al. 2010, Carpenter et al. 2010, Engelsman et al. 2011, Carpenter et al. 2012, Zölls et al. 2012].

For all the reasons described in the previous paragraphs, the protein aggregation phenomenon needs a targeted approach; two main fields of research and their applications are explored in this dissertation, and various aspects are described in order to obtain a wholesome understanding of the protein aggregation issue. Moreover, a critical evaluation of the most frequently employed analytical methodologies, which are currently dedicated to the study of protein aggregation, is due in order to find the best course of action in each described case.

In this dissertation, the miniaturized variant of Flow FFF (hollow fiber FFF or HF5) online coupled with spectroscopic and/or optical detection methods, is employed for the study of protein aggregation phenomena. Various aspects, ranging from instrumental and method robustness (and validation), to detection sensitivity and instrumental/method versatility, in terms of aggregates size-range and MW range, as well as versatility in terms of carrier solution choice (enabling the discrimination of different types of protein aggregates), are explored.

1.2. PROTEIN AGGREGATION PHENOMENA RELATED TO BIOLOGICAL AGING (SENESCENCE)

From the pathological and immunological point of view, *protein aggregation* is a general terminology which describes the association of proteins into larger assembly, following loss of the secondary, tertiary or quaternary protein structure and often leading to loss of biological activity. Protein aggregation is a common biological phenomenon associated to the cellular inability to maintain the homeostasis of their proteome (proteostasis). In physiological conditions, the tendency to aggregate of *de novo* synthesized unfolded proteins is balanced by the several chaperones that aid their folding [Kopito 2000]. Soluble aggregation is also commonly observed in ubiquitinated unfolded proteins before proteasome degradation or in oxidatively damaged proteins before translocation into the lysosomes by chaperone-mediated autophagy [Kiffin et al. 2004]. Additionally, temporal changes to the cellular homeostasis (temperature, pH, water content and salt/ions concentration) can induce transitory protein unfolding and soluble aggregation. Lately, it has been reported that, during physiological aging, proteostasis becomes gradually compromised and several hundred proteins tend to become more insoluble and aggregate. These proteins have been shown to have common biochemical and biological properties, such as a primary structure with amino acids stretches often found in proteins associated with neurodegenerative diseases and secondary structure with increased beta-sheets [David et al. 2010] or present extensive oxidative post-translational modifications [Cannizzo et al. 2012].

During *pathological conditions*, protein aggregation is also a very common occurrence giving rise to the group of diseases collectively known as *protein conformational diseases*. In many degenerative diseases of the CNS, such as Alzheimer's, Parkinson's and Huntington's disease, protein aggregation is a common pathological hallmark [Rubinsztein et al. 2005]. Protein aggregates can be classified according to their biochemical and biophysical characteristics. Biochemically, aggregates can be formed

by covalent bonds, through Schiff-base formation, or non covalent bonds, mainly mediated by hydrogen bonds, hydrophobic and electrostatic interactions. The former are irreversible aggregates whereas the latter can be, at least partially, reversed by cellular molecular chaperones. Size-wise aggregates can range considerably, from protein oligomers up to visible cytosolic inclusions, known as the aggresome [Kopito 2000]. The sub cellular location of these aggregates can also vary, from perinuclear to peri-ER or intra-endosomal.

Recently, there has been a strong interest in analyzing protein aggregates for different reasons: (i) to determine how protein primary and secondary structure influence their tendency to aggregate during physiological or pathological conditions; (ii) to map the post-translational modifications observed in chronic inflammatory, metabolic and degenerative diseases that induce protein aggregation, and (iii) to analyze the machinery recruited to the aggregate to aid its disaggregation or to dispose them through proteasomal or autophagy-mediated endosomal degradation.

Consequently, several methods have been employed to separate protein aggregates, including filter assay, analytical ultracentrifugation (AUC), gel electrophoresis and size exclusion chromatography (SEC) [Stegemann et al. 2005, Ishii et al. 2007, Linetsky et al. 2008, Scharf et al. 2013]. However, the first two methods separate the aggregates as a total, thus, making it impossible to analyze the biochemical composition of the aggregates with different MW, shape and biophysical properties. SEC is limited by the pores size of the column used for fractionation (therefore allow for a specific size range of aggregates to be separated), and by the amount of detergent that can be used during the run (which can, in turn, affect the size and composition of the aggregates). Gel electrophoresis does not allow for an accurate analysis of their MW, nor does provide any additional information on the biophysical properties of the aggregates.

Therefore, an analytical methodology with the ability to separate soluble aggregates from terminal aggregates or aggregates with different biophysical properties would

allow for a more functional analysis. Indeed, in prion disease, a correlation between the size and the infectivity of the protein's aggregate was reported [Silveira et al. 2005].

1.3. PROTEIN AGGREGATION PHENOMENA IN THERAPEUTIC PROTEIN FORMULATIONS

Antibodies, the most developed therapeutic proteins, are large multi-domain proteins. In particular, *human monoclonal antibodies* (mAbs) display poor biophysical properties characterized by low stability and unfavorable tendency towards aggregation. Among the factors that lead to these shortcomings, protein formulation plays an important role, even though the core of problem is the primary sequence of the protein itself; moreover, since mAb therapeutic action is so specific, there are significant differences among them (related to F_{ab} differences and the particular antigen specificity of the monoclonal), which explains the differences in stability and aggregation propensity between antibodies [Lowe et al. 2011].

The final formulation of a therapeutic mAb therefore must be carefully chosen; not only to ensure drug quality (stability and purity), but also to allow drug manufacture at an appropriate scale. Moreover, an effective therapeutic drug requires high-concentration liquid formulations, e.g higher than 100 mg/mL. The mAbs can lose stability and aggregate also, as a result of conformational changes [Schwegman et al. 2009] which can occur upon storage (usually freezing in high-volume vessels [Singh et al. 2009]. Moreover, the constituting amino acids may undergo post-translational modifications during expression, purification, or storage, leading to loss of stability and eventually aggregation [Jenkins et al. 2008].

Known effects of aggregation among therapeutic proteins are: lower in vivo efficacy, increased variability among batches, and perhaps most importantly, immunogenicity in patients [Cordoba-Rodriguez 2008]. Therefore, it is vitally important that for each of the steps of expression, purification, concentration, formulation, storage, and final

filling of the mAb, protein degradation, such s aggregation, must be minimized [Lowe et al. 2011].

In the biopharmaceutical field, the *aggregates* are defined as high molecular weight (MW) protein assemblies; formed either spontaneously, through electrostatic/hydrophobic/hydrogen bonds interactions between native-state monomeric units (also known as protein *self-association*), or by association between denatured (damaged) monomers. Both types represent a concern from the immunological point a view, and their capacity to enhance immune responses to the monomeric form has been known for over a half a century [Rosenberg 2006]. While large aggregates are more easily identified and separated (eliminated through filtration; for example), as their presence is rigorously regulated by FDA [Zölls et al. 2012], little is known about the immunological effects of protein *self-association* phenomenon, which may impede the effectiveness of the therapeutic protein by neutralizing the monomer action.

Although it was initially believed that protein-protein favorable interactions can only occur if hydrophobic surfaces are exposed upon denaturation (intended as irreversible damage), leading to aggregation and often causing severe precipitation, an increasing concern regarding the native protein interactions has recently emerged [Cromwell et al. 2006]. In fact, recent literature indicates that even small perturbations in the protein structure may cause the exposure of hydrophobic surface: it is belied that the formation of self-associated antibody species is mediated by electrostatic interactions [Liu et al. 2005], while dipole-dipole interactions are believed to be the cause of fibrillogenic association of b–sheets [Fernández 2005].

Comprehension on how to control the aggregation phenomenon, through thermodynamic and kinetic studies, helps assessing the danger correlated to the presence of associated species during the formulation development of therapeutic proteins. The main rising concerns of the biopharmaceutical industry, which impacts on the safety and efficacy of therapeutic proteins, is represented by protein aggregation and particulate formation in protein formulations, with their very wide

size range (nm-μm) being the most pressing issue since no single analytical method is able to resolve it. In fact, many efforts have been employed to fill the "gap" of techniques able to identify, separate and characterize the presence of undesired protein aggregates in the sub-μm size range [Cao et al. 2009, Zölls et al. 2012].

Moreover, many efforts have been developing in order to optimize the time and resources required for protein formulations by means of high-throughput techniques for formulation screening [Capelle et al. 2007, Goldberg et al. 2011], as well as of simplification and customization of the protein formulation process through FDA regulations based on Design of Experiments [Hinz 2006, Feng et al. 2012].

1.4. THE NEED FOR APPROPRIATE ANALYTICAL METHODOLOGIES

The need for adequate analytical methods for the detection, separation and characterization of protein aggregates, regardless of their origin or formation mechanism, justifies the sudden growth of new analysis methods. Since therapeutic proteins, as well as aging proteins, can form different types and sizes of aggregates and particles, a case-by-case selection of the appropriate analytical characterization methods is required: there is no "general solution" to fit all.

No single method is indeed capable to cover the nm-mm aggregates size range, therefore making the combination of several methods (usually based on different measurement/separation principles, therefore *orthogonal*) mandatory for an extensive characterization, as means to bridge this "gap"[Philo 2006, Zölls et al. 2012].

1.5. REFERENCES

[Arakawa et al. 2010] Arakawa T.; Ejima D.; Li T. and Philo J. S. (2010). "*The Critical Role of Mobile Phase Composition in Size Exclusion Chromatography of Protein Pharmaceuticals*." Journal of Pharmaceutical Sciences **99** (4): 1674-1692.

[Cannizzo et al. 2012] Cannizzo E.; Clement C. C.; Morozova K.; Valdor R.; Kaushik S.; Almeida L. N.; Follo C.; Sahu R.; Cuervo A. M.; Macian F. and Santambrogio L. (2012). "*Age-related oxidative stress compromises endosomal proteostasis*." Cell **2** (1): 136-149.

[Cao et al. 2009] Cao S.; Pollastrini J. and Jiang Y. (2009). "*Separation and characterization of protein aggregates and particles by field flow fractionation*." Current Pharmaceutical Biotechnology **10** (4): 382-390.

[Capelle et al. 2007] Capelle M. A. H.; Gurny R. and Arvinte T. (2007). "*High throughput screening of protein formulation stability: Practical considerations*." European Journal of Pharmaceutics and Biopharmaceutics **65** (2): 131-148.

[Carpenter et al. 2012] Carpenter J. F.; Cherney B. and Rosenberg A. S. (2012). *The Critical Need for Robust Assays for Quantitation and Characterization of Aggregates of Therapeutic Proteins*. Analysis of Aggregates and Particles in Protein Pharmaceuticals. Mahler H.-C. and Jiskoot W. Hoboken, NJ, USA, John Wiley & Sons, Inc.

[Carpenter et al. 2010] Carpenter J. F.; Randolph T. W.; Jiskoot W.; Crommelin D. J. A.; Middaugh C. R. and Winter G. (2010). "*Potential Inaccurate Quantitation and Sizing of Protein Aggregates by Size Exclusion Chromatography: Essential Need to Use Orthogonal Methods to Assure the Quality of Therapeutic Protein Products*." Journal of Pharmaceutical Sciences **99** (5): 2200–2208.

[Cordoba-Rodriguez 2008] Cordoba-Rodriguez R. V. (2008). "*Aggregates in MAbs and Recombinant Therapeutic Proteins: A Regulatory Perspective*." BioPharm International **21** (11): 44–53.

[Cromwell et al. 2006] Cromwell M. E. M.; Hilario E. and Jacobson F. (2006). "*Protein aggregation and bioprocessing*." AAPS Journal **8** (3): E572–E579.

[David et al. 2010] David D. C.; Ollikainen N.; Trinidad J. C.; Cary M. P.; Burlingame A. L. and Kenyon C. (2010). "*Widespread Protein Aggregation as an Inherent Part of Aging in C. elegans*." PLoS Biology **8** (8): e1000450.

[Engelsman et al. 2011] Engelsman J. d.; Garidel P.; Smulders R.; Koll H.; Smith B.; Bassarab S.; Seidl A.; Hainzl O. and Jiskoot W. (2011). "*Strategies for the Assessment of Protein Aggregates in Pharmaceutical Biotech Product Development*." Pharmaceutical Research **28** (4): 920-933.

[Fda, 06 January 2013]. "*CFR - Code of Federal Regulations Title 21*." Retrieved 22 February, 2014, from http://www.accessdata.fda.gov/scripts/cdrh/cfdocs/cfcfr/cfrsearch.cfm?cfrpart=11.

[Feng et al. 2012] Feng Y. W.; Ooishi A. and Honda S. (2012). "*Aggregation factor analysis for protein formulation by a systematic approach using FTIR, SEC and design of experiments techniques*." Journal of Pharmaceutical and Biomedical Analysis **57**: 143-152.

[Fernández 2005] Fernández A. (2005). "*What factor drives the fibrillogenic association of beta-sheets?*" FEBS Lett.(579): 6635 - 6640.

[Goldberg et al. 2011] Goldberg D. S.; Bishop S. M.; Shah A. U. and Sathish H. A. (2011). "*Formulation development of therapeutic monoclonal antibodies using high-throughput fluorescence and static light scattering techniques: Role of conformational and colloidal stability*." Journal of Pharmaceutical Sciences **100** (4): 1306–1315.

[Hinz 2006] Hinz D. C. (2006). "*Process analytical technologies in the pharmaceutical industry: the FDA's PAT initiative*." Analytical and Bioanalytical Chemistry **384** (5): 1036-1042.

[Ishii et al. 2007] Ishii T.; Yamada T.; Mori T.; Kumazawa S.; Uchida K. and Nakayama T. (2007). "*Characterization of acrolein-induced protein cross-links*." informa healthcare **41** (11): 1253-1260.

[Jenkins et al. 2008] Jenkins N.; Murphy L. and Tyther R. (2008). "*Post-translational Modifications of Recombinant Proteins: Significance for Biopharmaceuticals*." Molecular Biotechnology **39** (2): 113-118.

[Kiffin et al. 2004] Kiffin R.; Christian C.; Knecht E. and Cuervo A. M. (2004). "*Activation of Chaperone-mediated Autophagy during Oxidative Stress*." Molecular Biology of the Cell **15** (11): 4829–4840.

[Kopito 2000] Kopito R. R. (2000). "*Aggresomes, inclusion bodies and protein aggregation*." Trends in Cell Biology **10** (12): 524-530.

[Linetsky et al. 2008] Linetsky M.; Shipova E.; Cheng R. and Ortwerth B. J. (2008). "*Glycation by ascorbic acid oxidation products leads to the aggregation of lens proteins*." Biochimica et Biophysica Acta (BBA) - Molecular Basis of Disease **1782** (1): 22-34.

[Liu et al. 2005] Liu J.; Nguyen M. D. H.; Andya J. D. and Shire S. J. (2005). "*Reversible self-association increases the viscosity of a concentrated monoclonal antibody in aqueous solution*." Journal of Pharmaceutical Sciences **94** (9): 1928–1940.

[Lowe et al. 2011] Lowe D.; Dudgeon K.; Rouet R.; Schofield P.; Jermutus L. and Christ D. (2011). "*Aggregation, stability, and formulation of human antibody therapeutics*." Advances in Protein Chemistry and Structural Biology **84**: 41-61.

[Philo 2006] Philo J. S. (2006). "*Is Any Measurement Method Optimal for All Aggregate Sizes and Types?* ." The AAPS Journal **8** (3).

[Philo and Arakawa 2009] Philo J. S. and Arakawa T. (2009). "*Mechanisms of Protein Aggregation*." Current Pharmaceutical Biotechnology(10): 348-351.

[Rosenberg 2006] Rosenberg A. (2006). "*Effects of protein aggregates: An immunologic perspective*." The AAPS Journal **8** (3): E501-E507.

[Rubinsztein et al. 2005] Rubinsztein D. C.; Difiglia M.; Heintz N.; Nixon R. A.; Qin Z. H.; Ravikumar B.; Stefanis L. and Tolkovsky A. (2005). "*Autophagy and its possible roles in nervous system diseases, damage and repair*." Autophagy **1** (1): 11-22.

[Scharf et al. 2013] Scharf B.; Clement C. C.; Yodmuang S.; Urbanska A. M.; Suadicani S. O.; Aphkhazava D.; Thi M. M.; Perino G.; Hardin J. A.; Cobelli N.; Vunjak-Novakovic G. and Santambrogio L. (2013). "*Age-Related Carbonylation of Fibrocartilage Structural Proteins Drives Tissue Degenerative Modification*." Chemistry & Biology **20** (7): 922-934.

[Schwegman et al. 2009] Schwegman J. J.; Carpenter J. F. and Nail S. L. (2009). "*Evidence of partial unfolding of proteins at the ice/freeze-concentrate interface by infrared microscopy*." Journal of Pharmaceutical Sciences **98** (9): 3239–3246.

[Silveira et al. 2005] Silveira J. R.; Raymond G. J.; Hughson A. G.; Race R. E.; Sim V. L.; Hayes S. F. and Caughey B. (2005). "*The most infectious prion protein particles*." Nature(437): 257-261.

[Singh et al. 2009] Singh S. K.; Rathore N.; Mcauley A. and Rathore A. S. (2009). "*Best Practices for Formulation and Manufacturing of Biotech Drug Products*." BioPharm International **22** (6): 32-48.

[Stegemann et al. 2005] Stegemann J.; Ventzki R.; Schrödel A. and Marco A. d. (2005). "*Comparative analysis of protein aggregates by blue native electrophoresis and subsequent sodium dodecyl sulfate-polyacrylamide gel electrophoresis in a three-dimensional geometry gel*." Proteomics **5** (8): 2002-2009.

[Wang et al. 2010] Wang W.; Nema S. and Teagarden D. (2010). "*Protein aggregation—Pathways and influencing factors*." International Journal of Pharmaceutics **390** (2): 89–99.

[Zölls et al. 2012] Zölls S.; Tantipolphan R.; Wiggenhorn M.; Winter G.; Jiskoot W.; Friess W. and Hawe A. (2012). "*Particles in therapeutic protein formulations, Part 1: Overview of analytical methods*." Journal of Pharmaceutical Sciences **101** (3): 914–935.

CHAPTER 2: FIELD-FLOW FRACTIONATION (FFF)

2.1. THE PROPOSED ANALYTICAL SOLUTION: FIELD-FLOW FRACTIONATION

Albeit a little slower and less visible, but in parallel with traditional techniques such as electrophoresis (gel, GE or capillary, CZE), liquid chromatography (LC) and flow cytometry (FC) [Reschiglian et al. 2005], the development and improvement of ***field-flow fractionation*** (FFF) were motivated by the potential of FFF to fulfill many of the needs described in the previous Chapters. Since early stages of FFF "*the great application range, resolution and versatility for macromolecular and supra-molecular samples, by providing high selectivity and speed, simultaneous measurement, simplified coupling to other measurement devices (…) and applicability to diverse samples over a broad mass-size range, gentleness in separating delicate species, and flexibility in targeting specific problem areas*" make it the ideal candidate for the study of protein aggregation phenomena [Giddings 1993].

Although LC and electrophoresis are still the most employed (traditional) methods for the separation and characterization of biological samples, field-flow fractionation arises as a highly selective, chromatographic-like flow-based separation technique

particularly suited for processing macromolecular and supra-molecular samples that range over 15 orders of magnitude in molecular weight [Giddings 2000] – incidentally, proteins and protein complexes/aggregates – under gentle instrumental conditions [Zattoni et al. 2007, Roda et al. 2009].

The major strength of FFF is its *versatility*, because of the numerous field types which can be applied (Table 1), the instrumental setup, channel design and modes of operation, and not to mention the wide choice of experimental conditions. FFF is therefore suitable for the separation-characterization of a very wide selection of macromolecular and particulate samples [Giddings 2000].

Table 1 – Field types and corresponding FFF techniques

Field	FFF technique
Cross-flow (Fl)	*Flow FFF (FlFFF)*
Sedimentation (Sd)	*Sedimentation FFF (SdFFF)*
Gravitational (Gr)	*Gravitational FFF (GrFFF)*
Thermal (Th)	*Thermal FFF (ThFFF)*
Electrical (El)	*Electrical FFF (ElFFF)*
Magnetic (Mg)	*Magnetic FFF (MgFFF)*
Dielectric (Dl)	*Dielectric FFF (DlFFF)*

Many types of fields have been employed for the FFF separation (displayed in order of their relevance in Table 1) in order to explore its versatility trait and motivated by the fact that they have different size ranges and areas of applicability.

Its greatest strength it is also its major flaw; the wide choice of options (in terms of field, instrumentation or experimental conditions), as well as the broad applications range, have led the way to dispersive efforts being spent exploring the limits of FFF. Exploring the FFF "maze", even though showing the resolution of topical issues and highlighting the particular FFF features [Reschiglian et al. 2005, Roda et al. 2009] , has left a relevant gap between *potential* and *realization*, therefore made this technique generally "*good at everything*" but, unfortunately, "*not specific enough for a particular*

purpose" and, more importantly, not yet able to replace any of the above-mentioned reference techniques [Giddings 2000].

2.1.1. PRINCIPLES OF FFF

The FFF concept and separation principle was described for the first time in 1966 by Calvin Giddings [Giddings 1966]; together with his research team, has contributed significantly during the four stages of FFF development described by [Wahlund and Nilsson 2012]. FFF is a flow-based separation family of techniques which, thanks to the "flow" concept, belongs to the wider chromatographic category; FFF and liquid LC employ almost the same instrumental setup.

The typical FFF operation mode consists in injecting the sample in a narrow band into a stream flowing through a thin/capillary flow chamber, where the sample is separated into components and which are eventually flushed out towards a detection and /or collection system. As the sample components are driven through the length of the flow chamber, they get separated according to their biophysical features, therefore eluted at different times and sequentially detected and/or collected [Giddings 2000].

Similar to the chromatographic *column* concept, in FFF, the flow chamber that makes sample separation possible is called *channel*. Since the FFF separation principle is not based on differential retention of sample components by the stationary phase as occurring in LC, the FFF channel is empty (no stationary phase required) and is usually made of inert and/or biocompatible material. In FFF, the retention relies on the analytes interaction with an external *field*, applied perpendicularly to direction of the mobile phase *flow*. Hence the *field-flow* duality required for the separation [Giddings 2000]. The lack of a stationary phase reduces considerably unwanted interaction between the analytes and the separation device, therefore makes FFF an

intrinsically "soft" separation method, ideally suited to macromolecular and supra-molecular systems, such as protein aggregates.

2.1.3. MECHANISM OF FFF

In order to understand why FFF is valid candidate for the described problematic, the retention mechanism which lies behind the *soft* separation must be examined.
First, the stream flowing through the thin/capillary empty FFF channel is a *laminar flow* (made of very thin streamlines also called *layers* or *laminae*), governed by an ideally *parabolic flow profile* (Figure 1a); the velocity of the parabolic flow is null in proximity of the channel wall and it gradually increases towards the channel center, where it reaches the maximum value, according to the *law of Poiseuille.*

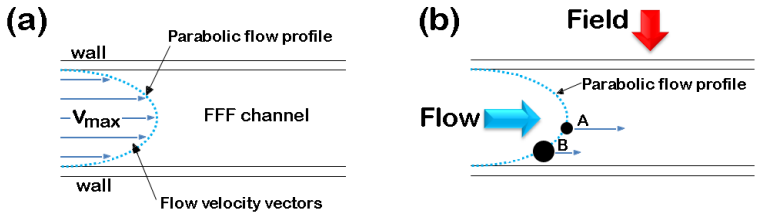

Figure 1 – Separation principle in FFF (a) parabolic flow profile, where v_{max} represents the maximum flow velocity at the center of the parabolic flow profile and (b) differential elution driven by the applied field

In the absence of the applied field, if any particle (macromolecules, supra-molecular species etc.) is set free in the mobile phase flowing through the FFF channel, it will be driven randomly over the short distance between the walls of the channel by the Brownian motion, while being carried downstream by the flow. This random motion of the particle will carry it through stream lines of different velocity (reported in Figure 1a as arrows of different length, proportional to the stream velocity), following a movement called *random walk.* The particle will move downstream very slowly when found near the wall and very fast when near the parabolic flow center;

the average velocity <*v*> will be the same for particles of any size (but small enough to be driven by Brownian motion), therefore will reach the channel exit at the same time [Giddings 2000].

However, when the *field* is applied perpendicularly to the stream of mobile phase, it will drive the different particles in specific zones of the parabolic profile, between the channel walls; under the effect of the field, particles found in a certain region of the parabolic flow profile, will be moved downstream at a velocity equal to the mean flow velocity in that region, therefore carried toward the channel exit at different speeds. An example of differential elution of two analytes (A and B), under the effect of the field, is reported in Figure 1b; A is forced by the field in a stream line characterized by higher flow velocity compared to B, therefore will elute faster.

The field itself must meet three requirements, in order to be effective and actually make the analytes separation possible. Firstly, it needs to be *strong* enough in order to drive forcefully the analytes into specific, highly localized regions of the parabolic flow profile. Secondly, it needs to be *selective* enough, in order to drive the analytes into different streamlines of the parabolic flow profile. Thirdly, it needs to be easily implemented, in order to make instrument development practical and possibly economical and, more importantly, easy to use and reliable [Giddings 2000].

Many field types have been proposed in FFF over its 50 years of existence (Table 1), however their relevance and frequency of usage have changed over time, thanks to the development and improvement of adequate and affordable FFF instrumentation, not to mention their ability to meet the above-described criteria.

2.1.3. FFF MODES OF OPERATION

As the analytes are driven into different localized region within the parabolic flow profile, their relative distribution over the flow streamlines or *laminae* (ideally, only a few μm thick, meaning that the particles would be held essentially at a fixed position

within the parabolic flow profile) dictates their order of elution, selectivity, band broadening or other separation parameters.

There are several types of distributions, also called *operating modes*; their variety adds flexibility to the intrinsically versatile FFF [Giddings 2000]. The most commonly used modes of operation, are: (a) *normal* (Brownian) mode; (b) *steric* mode and (c) *lift-hyperlayer* mode; the *normal mode* will be examined in the following paragraphs. In order to understand how each mode operations, it is fundamental to examine how these distributions are formed.

When a homogeneous population of sample particles enters into an FFF channel, the particles are distributed rather evenly over the channel cross section, at first. When the field begins to act by driving the particles toward the channel wall (or *accumulation wall*), in a process called *sample relaxation*, the particles will respond with forces of transport opposing the external field (whose origin will be discussed further on in this Chapter).

Consequently, even though the field continues to act, the sample relation is completed after a short while because the opposing forces balance themselves and the sample components reach a *steady state*, therefore a corresponding *equilibrium distribution*. The nature of the opposing transport forces exerted by the particles themselves determines the form of the particles distribution, therefore the FFF operating mode and all separation parameters: order of elution, selectivity, resolution etc. [Giddings 2000].

2.1.3.1. NORMAL (BROWNIAN) MODE

The normal (Brownian) mode governs the equilibrium distribution and subsequent elution of most sub-μm particles and virtually all macromolecules (proteins and protein aggregates included); it is the most widely implemented mode, therefore called "*normal*". As the analytes are driven by the field against the accumulation

wall, their concentration builds up, creating a *concentration gradient* and causing the analytes to *diffuse* in the opposite direction (Figure 2a); this transport mechanism holds true until the analytes diffusion force balances the field force [Giddings 2000]. When the Brownian diffusive and the field transport forces reach an equilibrium, the analyte concentration c (relative to the accumulation wall concentration, c_0) approaches an exponential function of elevation x, above the accumulation wall, as reported in *Equation 1* [Giddings 1973, Giddings et al. 1991, Schure et al. 2000] and reported in the enlarged view of Figure 2c, where l is the characteristic elevation of the analyte cloud from the accumulation wall and x is the distance to the channel wall.

$$c = c_0 exp\,(-{}^{x}/_{l})$$

Equation 1

The separation is achieved in *normal mode* because different analytes form exponential distributions / layers of different thickness, as depicted in Figures 2b and 2c; the greater the thickness of the layer, the higher flow velocity streamlines the analyte will reach and, consequently, the faster it will elute.

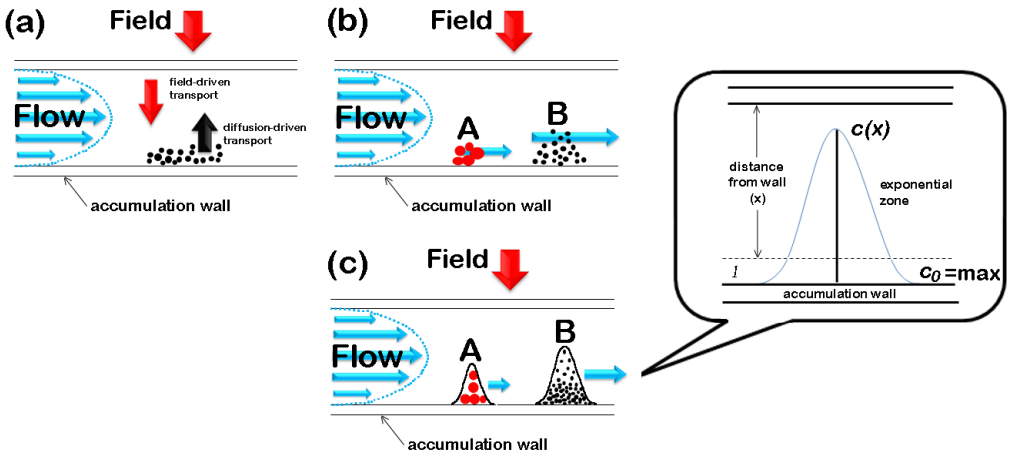

Figure 2 – Normal operative mode: (a) balance between (Brownian) diffusive and field forces; (b) separation of analytes A and B (c) equilibrium distribution analytes A and B in normal mode, enlarged view of the exponential distribution

The thickest layers migrate fastest (analyte A) as opposed to the most compressed distributions (analyte B), which migrate slowest. The sequence of smaller particles eluting faster than larger particles is the characteristic *elution order* in normal mode [Giddings 2000].

The characteristic elevation, l for each analyte represents the ratio between the analyte diffusion coefficient D and the field-induced velocity U (*Equation 2*); the separation is therefore achieved because of differences in diffusion coefficient, since the field force is uniformly exerted.

$$l = {}^{D}/_{|U|}$$

Equation 2

The diffusion coefficient, D is described by Stokes-Einstein equation (*Equation 3*), where k is the Boltzmann constant, T is the absolute temperature, η represents the viscosity of the mobile phase, r_H is the hydrodynamic radius and d_H is the hydrodynamic diameter of the diffusing particle:

$$D = \frac{kT}{6\pi\eta r_H} = \frac{kT}{3\pi\eta d_H}$$

Equation 3

The field-induced velocity, U is described by *Equation 4*, where f represents the friction coefficient:

$$U = {}^{F}/_{f} \quad and \quad f = 3\pi\eta d = 6\pi\eta r$$

Equation 4

At the stationary state, the relationship between l and the force F exerted by the field on a single particle is described by *Equation 5* [Giddings et al. 1991], where k is the Boltzmann constant and T, the absolute temperature:

$$l = {}^{kT}/_{|F|}$$

Equation 5

The distribution thickness (l) is, therefore, inversely related to the primary field force exerted on the particles. In order to achieve optimal levels, the values of l can be controlled by varying the field strength, to which F is directly correlated. Assuming that the sample particles are non-interacting point masses, the velocity V of a cloud of such particles is the average velocity of an exponential distribution within the parabolic flow profile.

The parabolic flow profile is therefore described by *Equation 6* [Schure et al. 2000], where x represents the distance from the wall and x represents the channel thickness (height):

$$V = 6\langle v \rangle \left(\frac{x}{w} - \frac{x^2}{w^2} \right)$$

Equation 6

The retention time of the particles is described by *Equation 7* [Giddings et al. 1991], where L is the channel length.

$$t_R = {}^{L}/_{V}$$

Equation 7

If w is the channel thickness (w>x) and $w >> l$, as it should be for efficient operation, the ratio between a retained and an unretained analyte is given by *Equation 8 [*Schure et al. 2000], where t_0 is the void time (the elution time of an unretained component), R is the retention ratio and represents the delay of a retained analyte caused by its compression by the field. Both t_0 and R have the same meaning as in chromatography.

$$R = \frac{t_0}{t_R} = \frac{w}{6l} = \frac{|F|w}{kT}$$

Equation 8

Equation 8 shows how the retention time of an analyte, t_R is directly proportional to F and represents the fundamental expression that relates retention time to sample

properties in normal FFF; for instance, F (therefore t_R) usually increases with particle size or molecular weight.

2.1.4. FFF TECHNIQUES: FLOW FFF

In Flow FFF (Fl FFF or F4), the applied *field* consists in a second, independent, stream of mobile phase applied across the channel section, therefore called *cross-flow*; the flow field permeates the channel walls and is applied perpendicularly to the to the primary flow stream.

Flow FFF is the most universal of all FFF techniques, the *flow* itself, acting as an universal field (a moving fluid), is able to displace any unattached object [Giddings 2000]; this is the FFF variant of choice in this dissertation, because of its versatility, being able to separate macromolecules and particles in a very wide size (few nm - μm) and MW range. The lower MW/size limit is determined by the MW cut-off of the accumulation wall, which is usually constituted of an ultra filtration membrane able to retain the macromolecular and supra-molecular analytes inside the channel.

Flow FFF became the most frequently employed FFF sub-technique thanks to the rapid growth in the 1990s and 2000s, growth which is motivated by the instrumental and application advancements and its commercialization [Wahlund and Nilsson 2012].

The *flow* field offers intrinsic advantages for the separation of proteins and protein aggregates, which are of interest in this dissertation. Firstly, like all other FFF sub-techniques, Fl FFF has the gentle separation mechanism and does not require a stationary phase for separation. Secondly, its universality implies that virtually any type of mobile phase can be used; in particular, a bio-friendly mobile phase is appropriate for the separation of biological samples. Therefore, due to the lack of stationary phase, the interactions between the proteins and the separation device are negligible and since the separation can be performed in a bio-compatible carrier

solution, make it possible for the proteins and protein aggregates to preserve the *native molecular conformation*, a fundamental bio-physical property.

Thirdly, it offers *high selectivity* in terms of diffusion coefficient differences; this feature is correlated to the separation principle in F4, based on differences in diffusion coefficients, where the *diffusion coefficient* (*D*) is a key parameter which determines the protein size, shape and surface properties, therefore unique [Reschiglian and Moon 2008].

Moreover, Fl FFF is also flexible in channel design, which led to the development and improvement of its sub-techniques: *symmetrical* Fl FFF (F4), *asymmetrical* Fl FFF (AF4), and *hollow-fiber* Fl FFF (HF5). Over the past 20 years, AF4 was of particular interest in the FFF community; however, thanks to its particular features, HF5 gained terrain in the last decade, culminating with its commercialization in 2012.

2.2. FLOW FFF SUB-TECHNIQUES: HOLLOW FIBER FLOW FIELD-FLOW FRACTIONATION (HF5)

HF5 is the miniaturized version of Fl FFF, distinguishing itself through the symmetrical channel geometry and employing a channel with porous walls, represented by a cylindrical ultra-filtration membrane [Johann et al. 2010, Reschiglian et al. 2012]. The idea of *hollow fiber* membranes as tubular, micro-column channels for FFF was proposed initially in the 1970s and complete theories were worked out; however, it never turned into experimentally useful separations (Lee H.L., 1974 and Doshi M.R., 1979). In the late 1980s, HF5 regained interest in the FFF community and a much improved experimental design of the separation device was proposed (Jonsson J.A. and Carlshaf A., 1989-1993); however, technical problems caused by the quality and stability of the hollow fibers impeded further advancements [Wahlund and Nilsson 2012]. HF5 was reborn in the early 2000s [Lee et al. 1999, Kang and Moon 2005, Park et al. 2005, Reschiglian et al. 2005] and, later on, excellent results demonstrated the HF5 potential as *pre-fractionation tool for*

proteomics analysis [Lee et al. 2010]. Moreover, recent advancements suggest that, in the near future, HF5 can potentially replace AF4 as an *extended characterization tool for protein therapeutics* [Reschiglian et al. 2013], therefore complement SEC.

Many efforts have been employed over the years by the Analytical Chemistry research team of the "G. Ciamician" Chemistry Department into developing the HF5 separation device prototype, which was employed during the most experimental work presented in this dissertation. Thanks to the successful collaboration between the Analytical Chemistry team and Wyatt Technology Europe (Dernbach, Germany), once the HF5 separation device achieved its ready-to-market phase, it was implemented in the Eclipse® DUALTEC™ FFF separation system, "the first commercial FFF system using both HF5 and AF4 technique integrated into one instrument" , which was launched on the market in 2011 [Johann et al. 2010]. The commercial HF5 channel is equipped with an Enhanced Sealing Technology (EST, patented) facilitating the channel assembly and is also leakage-proof. The commercial HF5 separation device consists in a 17 cm long PES hollow fiber, with a MWCO of 10 kDa.

In works reported in literature over the past 15 years [Reschiglian et al. 2002, Reschiglian et al. 2003, Roda et al. 2006, Kang et al. 2008, Kim et al. 2008, Lee et al. 2009], the porous membrane was made of a an inert polymeric material, PES (polyethersulfone), CPVC (coated polyvinyl chloride) or PAN (polyacrylonitrile), usually with an internal diameter of 0.8 mm, an optimal length of ~24 cm and a membrane porosity (cut-off) of approximately between 10 and 100 kDa of MW.

In addition to the key advantages offered by F4, the channel miniaturization in HF5 distinguishes itself through unique features. Firstly, the low channel volume (~1/10 of the commercial AF4 channel) reduces considerably the sample dilution. Secondly, due to the reduced size of the separation device, HF5 employs low flow rates, which made it possible to be successfully coupled on-line with Mass Spectrometry [Reschiglian et al. 2005, Lee et al. 2010]. These first two features highlight the

advantages of miniaturization, in particular, the higher sensitivity which is achieved thanks to the increased limit of detection/quantification; this is of particular interest for very low levels of protein aggregates which may be present in therapeutic protein formulations, but also present in the proteome of whole cell lysates. Thirdly, the disposable usage eliminates sample carry-over and possible sample contamination, therefore ideal for biological samples; disposable channels can be particularly appealing for analytical and micro-preparative scale bio-separations, for which either sterility or inter-run reproducibility are critical [Reschiglian and Moon 2008]. HF5 disposable devices have been successfully employed for the fractionation of whole bacteria, yeast and red blood cells [Reschiglian et al. 2002, Reschiglian et al. 2003, Reschiglian et al. 2004]

Because of the promising advancements described in the literature so far [Silveira et al. 2005, Roda et al. 2006, Kang et al. 2008, Kim et al. 2008, Zattoni et al. 2008, Lee et al. 2009, Kang et al. 2010], HF5 had to offer unequalled performances which were fundamental for the purpose of this dissertation.

2.2.1. Separation principles in HF5 applied to proteins and protein aggregates

The principle of HF5 separation relies on differences in diffusion coefficient (D), specific for each protein, correlated to its size (hydrodynamic radius or diameter) through *Equation 3* and molecular weight (MW) [Reschiglian et al. 2013]. Since in HF5 the radial flow, which acts as the separation field, cannot be controlled independently of the longitudinal one, the process of sample relaxation / focus is then performed by simultaneously pumping a stream of mobile phase through the entry and exit of the fiber (Figure 3a); this action results in the focusing of the sample in a narrow band. This aspect is of particular interest in HF5, considering the reduced volume of the fiber compared to that of traditional AF4 channels; if the sample band

is not narrow enough compared to the length of the fiber, it would compromise the separation efficiency.

Therefore, a typical HF5 separation begins by injecting the sample into the hollow fiber, and initially subjecting it to the action of two longitudinal flows entering the channel from opposite sides (Flow in and Flow out), with a typical inlet to outlet flow ratio of 20:80 (Figure 3a). The purpose of this step, called ***sample focus*** step, is the *sample relaxation*, which allows the sample components to reach their equilibrium distributions when the diffusive forces balance the force exerted by the *cross-flow;* a simultaneous result of this action is the *sample concentration* in a narrow band, at the *focus position*, where the resulting longitudinal flow is null.

During the sample focus phase, the flow exiting in a radial direction through the hollow fiber pores, called *focus flow*, represents the sum between Flow in and Flow and has the same meaning as the cross-flow during the sample elution phase; it continues to push the sample components towards the fiber membrane (Figure 3a, black arrows), while being opposed by the proteins diffusive force (Figure 3a, white arrows). Since *D* is specific for each protein, each component will reach a *steady state* at a specific distance from the channel wall, where the diffusive force and the radial field force are in equilibrium.

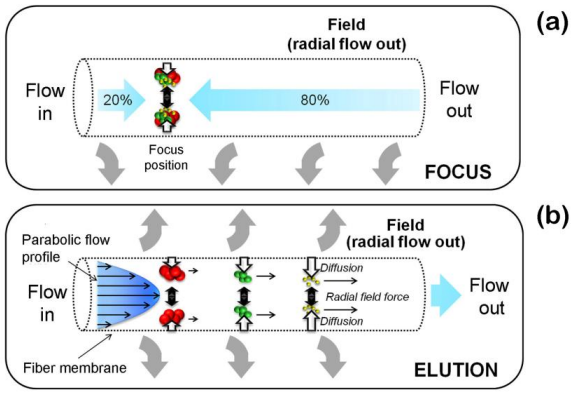

Figure 3 – HF5 separation principles: (a) sample focus/relaxation and (b) sample separation during elution

Once the sample components have reached their steady state and have been distributed in *laminae* embedded in the parabolic flow profile, the ***elution step*** begins: the Flow out is switched off, thus, the Flow in can push the sample components towards the channel exit, while the radial flow continues to push them towards the membrane (Figure 3b), allowing the sample components to maintain their specific distance from the fiber wall.

As described previously in this Chapter, the longitudinal flow has a parabolic profile, characterized by a maximum flow velocity at the center of the hollow fiber and an almost null velocity near the channel wall (Figure 1 and 3b); larger proteins and protein aggregates (with smaller *D*) will find themselves closer to the fiber membrane, into slower velocity stream lines and will be more retained by the radial flow field, while smaller proteins will elute faster (Figure 3b).

This represents the *elution order in normal mode*, as mentioned previously in this Chapter, and applies to proteins and protein aggregates with **5 nm** up to ~ **500 nm** in diameter [Schure et al. 2000]; when the protein aggregate size exceeds this limit, the elution will be switched into the so-called *steric mode*, when the diffusive forces become negligible and characterized by an inverted elution order with respect to the normal one (larger particles, with diameters up to 50 μm, being the first to elute) [Caldwell 2000].

Once the sample run is complete and the components of interest have been separated, the radial flow is switched off (procedure also called "*field release*"), allowing the cleaning of the injection line and flushing away all non-separated sample components, which have been retained for too long in the separation device (if their size exceeds the limits of either normal or steric mode, they have a virtually infinite retention time). The purpose of this phase is to clean the separation device, in order to avoid sample carry-over when the replacement of the hollow fiber is unnecessary.

2.2.2. HF5 RETENTION THEORY IN NORMAL MODE

Assuming a uniform radial flow velocity along the hollow fiber length, through a series of approximations, the retention time of an unretained analyte, t_0 (a.k.a. void time) is expressed by *Equations 9*, where $Flow_{out} = Flow_{in} - Flow_{radial}$ represents the longitudinal flow velocity during elution, V_0 represents the channel void volume, calculated based on R_f, the hollow fiber inner radius and L, the hollow fiber length:

$$t_0 = \frac{V_0}{Flow_{radial}} ln\left(\frac{Flow_{in}}{Flow_{out}}\right) \;\; and \;\; V_0 = \pi L R_f^2$$

Equations 9

Based on a series of approximations [Wijnhoven et al. 1996, Lee et al. 1999], which include an ideal Gaussian concentration profile, the retention time of a separated component, t_R is expressed by *Equation 10*, where D is the diffusion coefficient of the separated component and R_f is the fiber inner radius.

$$t_R = \frac{R_f^2}{8D} ln\left(\frac{Flow_{in}}{Flow_{out}}\right)$$

Equation 10

Taking into consideration the sample focusing/relaxation process [Lee et al. 1999], which occurs at a certain distance from the hollow fiber inlet, called focus position (L_0), the expression of the retention time can be rewritten as Equation 11:

$$t_R = \frac{R_f^2}{8D} ln\left(\frac{Flow_{in} - \left({}^{L_0}/_{L}\right) Flow_{radial}}{Flow_{out}}\right)$$

Equation 11

Correlating Equation 11 with the Stokes-Einstein expression for the diffusion coefficient, D (Equation 3), the relationship between the retention time and the

hydrodynamic diameter, d_H is described by Equation 12, cited in [Zattoni et al. 2007, Reschiglian et al. 2012]:

$$d_H = \frac{8kT}{3\pi\eta R_f^2} ln \left(\frac{Flow_{in} - \left({}^{L_0}/_{L} \right) Flow_{radial}}{Flow_{out}} \right)^{-1} t_R$$

Equation 12

Through *Equation 12* is, then, possible to convert the retention times in the value of the hydrodynamic diameter of the particles and obtain the size distribution of the samples (particle size distribution).

Moreover, the HF5 separation performance can be expressed in terms of number of theoretical plates per unit of time, N directly related to the analyte limit concentration which does not induce overloading, c^* and the analyte limit of detection (minimum detectable concentration), c_{LOD} expressed through Equation 13, cited in [Zattoni et al. 2007, Reschiglian et al. 2012]:

$$\left(\frac{N}{t_R}\right)_{max} = 2\frac{Dc*}{R_f^2 c_{LOD}}$$

Equation 13

Equation 13 shows how the maximum separation efficiency is determined by the analytes biophysical and chemical properties, more specific, by their detectability and tendency towards overloading, a key aspect regarding HF5 applications. A performance decrease is, therefore, expected with increasing MW because of the consequent D decrease (D is inversely proportional to MW), but also because of the consequent c^* decrease with increasing MW (c^* is also inversely proportional to MW) [Moon and Myers 2000].

Equally important, *Equation 13* shows how miniaturization enhances HF5 performance; by further reducing the fiber inner radius the sample dilution is

decreased since the separation would require a lower longitudinal flow rate and by applying higher cross-flow rates, the separation performance improves.

The relationship between D and MW is described by *Equations 14*, where A is a parameter correlated to the nature of the analyte and b is an empirical parameter, whose value can be calculated based on the shape of the particle; for a rigid sphere, the theoretical value of b is 0.33 [Wijnhoven et al. 1996, Valencia and González 2011]:

$$D = A \cdot MW^{-b} \quad and\ D = A \cdot MW^{-1/3}\ \ (rigid\ sphere)$$

Equations 14

2.3. HF5 FOR PARTICLE SIZE-CHARACTERIZATION

Typically, the HF5 separation is monitored by UV/Vis detection and occasionally by fluorescence (FLD) and multi-angle light scattering detection (MALS), which are usually set at a specific wavelength in order to facilitate the detection of the sample components on interest (for proteins, UV detection at 210, 215 and 280 nm is used, while, for florescence detection, an excitation/emission combination of 280 nm/340 nm is usually employed).

The output of such detectors, the sample *elution profile*, representing the sample concentration signal, reported as a function of time and is called *fractogram*, by analogy with the *chromatogram*. A typical HF5 elution profile/fractogram is reported in Figure 4b.

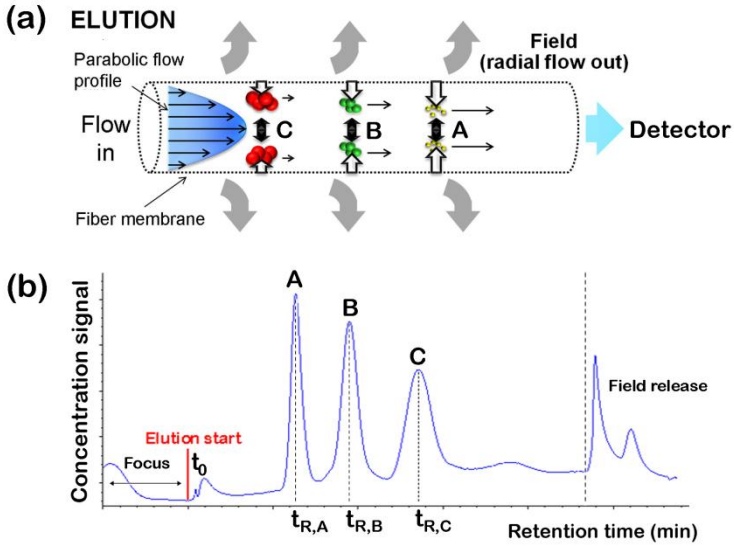

Figure 4 – Retention in HF5: (a) Separation occurring inside the hollow fiber, sample components A, B and C are eluted towards the detector; (b) typical elution profile, depicting the separated components A, B and C as seen by the detector (concentration over time)

As previously stated in this Chapter, the steps of a typical HF5 separation are: (a) sample focus or relaxation, (b) sample separation or elution and (c) field release, all three depicted in figure 4b. Figure 4b also depicts the void time, t_0 which can be determined applying *Equations 9* and the specific retention time for each separated component t_R, from which the size of components A, B and C can be determined though Equation 12. Moreover, the experimental retention time value can be used to determine the diffusion coefficient, *D* through *Equations 3* and *11* and, through a series of approximations and applying *Equation 14*, the MW.

HF5 is, therefore, able not only to separate, but also to characterize the analytes. The particle-size distribution (PSD) can be obtained from the fractogram by means of a numerical conversion of the retention scale. Particle size distribution (PSD) analysis is considered one of the most remarkable trends in analytical science. In fact, many samples of topical analytical interest are found in dispersed form, and information regarding their size distribution is as fundamental as knowledge of their MW.

For instance, in industrial applications, the size characterization of sample particles is routine procedure and is an essential part of the overall quality control (QC)

practices. In the pharmaceutical field, for particles used in drug delivery, the size is a critical factor because it has a strong influence on the particle bio-distribution, hence their performance as carriers, as well as their ability to bind to the active drug. From the hydrodynamic size, the analyte MW can be also derived; however, in this case, assumptions on analyte shape or conformation are required and not always accurate.

2.4. HF5 SEPARATION PERFORMANCE EVALUATION: CRITICAL PARAMETERS

Since FFF (therefore, HF5) is a chromatographic-like technique, many parameters which help evaluate the separation performance can be applied, parameters which will prove useful through this dissertation, especially when HF5 methods are being developed or when the HF5 performance is compared to the one obtained employing other separation techniques.

Figure 5 depicts another typical HF5 elution profile, which will serve as example, used to facilitate the definition of the various separation parameters.

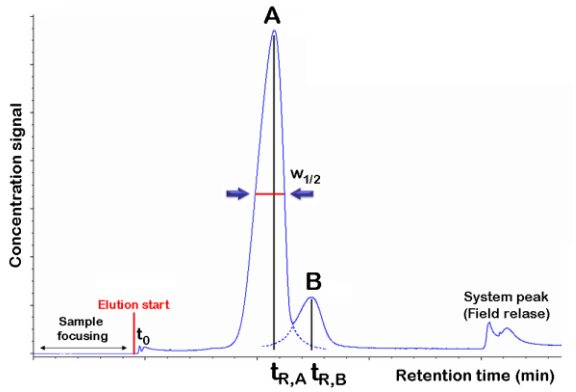

Figure 5 – HF5-UV separation profile depicting the separation of two species and the correlated separation parameters (retention time and peak width at half height)

The extent of *peak broadening* and the *efficiency* of the separation device can be evaluated by means of *number of theoretical plates, N* expressed through *Equation 15*,

and the *height equivalent to a theoretical plate*, *H* (plate height) reported in *Equation 16*, where σ_t^2 represents the variance of the eluted peak and *L* is the length of the separation device [Podzimek 2011]:

$$N = \left(\frac{t_R}{\sigma_t}\right)^2 = 5.54\left(\frac{t_R}{w_{1/2}}\right)^2$$

Equation 15

$$H = \frac{\sigma_t^2}{L} = \frac{Lw_{1/2}^2}{16t_R}$$

Equation 16

Unlike what occurs in chromatography, where the analyte occupies the carrier only for a time equal to t_0, in FFF the analyte occupies the solute at all times, therefore the *axial diffusion* in FFF is inversely proportional to R_s; axial diffusion occurs in FFF as a response to the axial concentration gradients, which cannot be eliminated in FFF. However, this phenomenon is counteracted by the fact that high MW analytes have small *D*, therefore diffuse little. Another source of band broadening in FFF, the main one, is the non-equilibrium, which arises because individual components of the analyte cloud (distribution) are carried downstream at different velocities and resulting in the sample could dispersion along the axial coordinate. Other band broadening effects emerge, for example, from the sample relaxation process or even the sample polydispersity itself [Davis 2000].

Peak symmetry is another parameter which characterizes the quality of a separation device, and is usually software-calculated; peak symmetry is a measure of peak tailing, which usually has a negative impact on resolution; a symmetry > 1.2 indicates the fact that the separation device is compromised and is no longer working properly [Podzimek 2011].

Resolution, R_s is a measure of separation between two bands and, for can be calculated employing Equation 17, where $t_{R,A}$ and $t_{R,B}$ represent the experimental retention time values of species A and B (B eluting after A, Figure 5) and $w_{1/2}$ represents the peak width at half peak height of peak A and B, respectively.

$$R_s = \frac{2.35}{2} \frac{(t_{R,B} - t_{R,A})}{(w_{1/2,A} + w_{1/2,B})}$$

Equation 17

The difference in retention time reflects the *selectivity* of the separation process, whereas w represents the zone spreading that is correlated to the *efficiency* of the process. At a resolution of 1, peaks A and B are not completely separated, but the peak areas overlap is only 2%; complete separation (baseline separation) is achieved at a resolution of 1.25 [Podzimek 2011]. *Equation 17* also shows how resolution is controlled by selectivity and efficiency, meaning that if the separation is not selective enough, a satisfactory resolution cannot be achieved.

In order to achieve a better characterization, the *specific resolution*, R_{sp} can be employed in HF5 similarly to SEC, which takes into account the MW values of the two species, A and B [Podzimek 2011]; the expression for the specific resolution in reported in *Equation 18*:

$$Rsp = \frac{2.35}{2} \frac{(t_{R,B} - t_{R,A})}{\left(w_{1/2,A} + w_{1/2,B}\right)(logMW_B - logMW_A)}$$

Equation 18

Selectivity is the defined as the inherent ability of a technique to separate two components; is FFF can be defined in terms of size, S_d or MW, S_{MW} – *Equations 19* [Schure et al. 2000, Podzimek 2011]:

$$S_d = \left|\frac{d(logt_R)}{d(logd_H)}\right| \quad and\ S_{MW} = \left|\frac{d(logt_R)}{d(logMW)}\right|$$

Equations 19

High selectivity is a fundamental FFF feature, which makes it an appealing separation tool; high selectivity means a significant change in retention time corresponding to a small change in particle size or MW. Selectivity depends on the retention characteristics and is independent from band broadening (efficiency); the limit of maximum selectivity is approached as the retention levels increase. Maximum selectivity in Flow FFF varies between 0.5 – 0.7, comparable to SEC selectivity values of ~ 0.1, even though the SEC efficiency is much higher [Schure et al. 2000].

On the other hand, the SEC *selectivity* is related to the slope of the calibration curve, meaning that SEC columns which are highly efficient do not necessarily provide a good resolution, unless the calibration curve is low enough. The SEC calibration curves, although slightly curved, can be approximated by a linear function in a certain range of t_R, *Equation 20* [Podzimek 2011]:

$$\log MW = a + b \cdot t_R \quad => slope\ b = \frac{log(MW_A) - log(MW_B)}{t_{R,B} - t_{R,A}}$$

Equation 20

The separation (selectivity) in SEC increases inversely to the slope value and depends also on the pore size of the column packing material; however, the calibration curves and, consequently, the slope *b* can be different for different MW regions separated on the same SEC column [Podzimek 2011].

Finally, the *fractionating power* is even more specific for a technique than selectivity, because it defines the relative increment in particle diameter of MW which can be separated with unit resolution (R_s = 1). Similarly to selectivity, it can be defined as

size-based fractionating power, F_d or MW-based fractionating power, F_{MW} – *Equations 21* [Schimpf 2000]:

$$F_d = \frac{R_s}{\delta d/_d} = \frac{t_R}{4\sigma_t} S_d \quad and \quad F_{MW} = \frac{R_s}{\delta MW/_{MW}} = \frac{t_R}{4\sigma_t} S_d$$

Equations 21

Substituting *Equation 13* in either of the *Equations 21*, the fractionating power can be rewritten as a function of efficiency and selectivity – *Equation 22*:

$$F_{d,MW} = \left(1/_4\right) \cdot N^{1/_2} \cdot S_{d,MW}$$

Equation 22

Consequently, the choice of working at high retention levels is motivated by higher selectivity values, as well as increased *N* [Schimpf 2000]. Equation 22 justifies the fact that SEC is given an advantage at lower MWs (< 100 kDa), while FFF quickly overtakes SEC at higher MW values (FFF is superior starting from MWs of few hundreds of kDa). Moreover, a uniform fractionating power can be achieved in FFF (HF5) by gradually decreasing the field strength during the experiments [Schure et al. 2000]

Similar to the SEC capacity factor, *k* (or chromatographic partition coefficient), the *retention level*, R_L in FFF (HF5) is defined through *Equations 23* [Wahlund 2013]:

$$k = \left|\frac{V_R - V_0}{V_0}\right| \qquad and \qquad R_L = \frac{t_R}{t_0}$$

Equations 23

The recommended R_L differs from sample to sample, as observed by [Litzen et al. 1993, Wahlund 2013]; however, they should be kept below a value of 50. Therefore, both selectivity and fractionating power can increase only up to a certain point.

On the other hand, in SEC, contrary to other types of chromatography, resolution can be controlled only through selectivity and column efficiency, since the capacity factor, *k* does not play a role [Podzimek 2011].

Most separation parameters are software-calculated (for example, by ChemStation – the chromatography software for the Agilent Technologies HPLC instrumentation); however, the software does not have the ability to correct the HF5 retention time by subtracting the focus time.

2.5. REFERENCES

[Caldwell 2000] Caldwell K. D. (2000). *Chapter 5: Steric Field-Flow Fractionation and the Steric Transition*. Field-Flow Fractionation Handbook. Schimpf M. E.; Caldwell K. and Giddings J. C. New York, Wiley**:** 79-94.

[Davis 2000] Davis J. M. (2000). *Chapter 3: Band Broadening and Plate Height*. Field-Flow Fractionation Handbook. Schimpf M. E.; Caldwell K. and Giddings J. C. New York, Wiley**:** 49-70.

[Giddings 1966] Giddings J. C. (1966). "*A New Separation Concept Based on a Coupling of Concentration and Flow Nonuniformities*." Separation Science **1** (1): 123-125.

[Giddings 1973] Giddings J. C. (1973). "*The conceptual basis of field-flow fractionation*." Journal of Chemical Education **50** (10): 667-669.

[Giddings 1993] Giddings J. C. (1993). "*Field-flow fractionation: analysis of macromolecular, colloidal, and particulate materials*." Science **260** (5113): 1456-1465

[Giddings 2000] Giddings J. C. (2000). *Chapter 1: The Field-Flow Fractionation Family: Underlying principles*. Field-Flow Fractionation Handbook. Schimpf M. E.; Caldwell K. and Giddings J. C. New York, Wiley**:** 3-30.

[Giddings et al. 1991] Giddings J. C.; Moon M. H.; Williams P. S. and Myers M. N. (1991). "*Particle size distribution by sedimentation/steric field-flow fractionation: development of a calibration procedure based on density compensation*." Analytical Chemistry **63** (14): 1366–1372.

[Johann et al. 2010] Johann C.; Elsenberg S.; Roesch U.; Rambaldi D. C.; Zattoni A. and Reschiglian P. (2010). "*A novel approach to improve operation and performance in flow field-flow fractionation*." Journal of Chromatography A **1218** (27): 4126–4131.

[Kang et al. 2010] Kang D.; Ji E. S.; Moon M. H. and Yoo J. S. (2010). "*Lectin-Based Enrichment Method for Glycoproteomics Using Hollow Fiber Flow Field-Flow Fractionation: Application to Streptococcus pyogenes*." Journal of proteome research **9** (6): 2855–2862.

[Kang and Moon 2005] Kang D. and Moon M. H. (2005). "*Hollow Fiber Flow Field-Flow Fractionation of Proteins Using a Microbore Channel*." Analytical Chemistry **77** (13): 4207–4212.

[Kang et al. 2008] Kang D.; Oh S.; Reschiglian P. and Moon M. H. (2008). "*Separation of mitochondria by flow field-flow fractionation for proteomic analysis*." Analyst (133): 505-515.

[Kim et al. 2008] Kim K. H.; Kang D.; Koo H. M. and Moon M. H. (2008). "*Molecular mass sorting of proteome using hollow fiber flow field-flow fractionation for proteomics*." Journal of Proteomics **71** (1): 123–131.

[Lee et al. 2009] Lee J. Y.; Kim K. H. and Moon M. H. (2009). "*Evaluation of multiplexed hollow fiber flow field-flow fractionation for semi-preparative purposes*." Journal of Chromatography A **1216** (37): 6539–6542.

[Lee et al. 2010] Lee J. Y.; Min H. K.; Choi D. and Moon M. H. (2010). "*Profiling of phospholipids in lipoproteins by multiplexed hollow fiber flow field-flow fractionation and nanoflow liquid chromatography–tandem mass spectrometry*." Journal of Chromatography A **1217** (10): 1660–1666.

[Lee et al. 1999] Lee W. J.; Min B.-R. and Moon M. H. (1999). "*Improvement in Particle Separation by Hollow Fiber Flow Field-Flow Fractionation and the Potential Use in Obtaining Particle Size Distribution*." Analytical Chemistry (71): 3446-3452.

[Litzen et al. 1993] Litzen A.; Walter J. K.; Krischollek H. and Wahlund K. G. (1993). "*Separation and Quantitation of Monoclonal Antibody Aggregates by Asymmetrical Flow Field-Flow Fractionation and Comparison to Gel Permeation Chromatography*." Analytical Biochemistry **212** (2): 469-480.

[Moon and Myers 2000] Moon M. H. and Myers M. N. (2000). *Chapter 13: Experimental Field-Flow Fractionation: Practices and Precautions*. Field-Flow Fractionation Handbook. Schimpf M. E.; Caldwell K. and Giddings J. C. New York, Wiley**:** 119-212.

[Park et al. 2005] Park I.; Paeng K.-J.; Kang D. and Moon M. H. (2005). "*Performance of hollow-fiber flow field-flow fractionation in protein separation*." Journal of Separation Science (16): 2043–2049.

[Podzimek 2011] Podzimek S. (2011). *Chapter 3: Size Exclusion Chromatography*. Light scattering, size exclusion chromatography and asymmetric flow field flow fractionation. Powerful tools for the characterization of polymers, proteins and nanoparticles. Wiley. Hoboken, New Jersey, Wiley**:** 99-206.

[Podzimek 2011] Podzimek S. (2011). *Chapter 5: Asymmetric Flow Field-Flow Fractionation*. Light scattering, size exclusion chromatography and asymmetric flow field flow fractionation. Powerful tools for the characterization of polymers, proteins and nanoparticles. Wiley. Hoboken, New Jersey, Wiley**:** 259-306.

[Reschiglian and Moon 2008] Reschiglian P. and Moon M. H. (2008). "*Flow field-flow fractionation: A pre-analytical method for proteomics*." Journal of Proteomics **71** (3): 265–276.

[Reschiglian et al. 2002] Reschiglian P.; Roda B.; Zattoni A.; Min B. R. and Moon M. H. (2002). "*High performance, disposable hollow fiber flow field-flow fractionation for bacteria and cells. First application to deactivated Vibrio cholerae**." Journal of Separation Science (25): 490-498.

[Reschiglian et al. 2013] Reschiglian P.; Roda B.; Zattoni A.; Tanase M.; Marassi V. and Serani S. (2013). "*Hollow-fiber flow field-flow fractionation with multi-angle laser scattering detection for aggregation studies of therapeutic proteins*." Analytical and Bioanalytical Chemistry (Field-Flow Fractionation).

[Reschiglian et al. 2013] Reschiglian P.; Roda B.; Zattoni A.; Tanase M.; Marassi V. and Serani S. (2013). "*Hollow-fiber flow field-flow fractionation with multi-angle laser scattering detection for aggregation studies of therapeutic proteins*." Anal Bioanal Chem.

[Reschiglian et al. 2004] Reschiglian P.; Zattoni A.; Cinque L. and Roda B. (2004). "*Hollow-Fiber Flow Field-Flow Fractionation for Whole Bacteria Analysis by Matrix-Assisted Laser Desorption/Ionization Time-of-Flight Mass Spectrometry*." Analytical Chemistry **76** (7): 2103–2111.

[Reschiglian et al. 2005] Reschiglian P.; Zattoni A.; Roda B. and Cinque L. (2005). "*On-Line Hollow-Fiber Flow Field-Flow Fractionation-Electrospray Ionization/Time-of-Flight Mass Spectrometry of Intact Proteins*." Analytical Chemistry **77** (1): 47-56.

[Reschiglian et al. 2003] Reschiglian P.; Zattoni A.; Roda B.; Cinque L.; Melucci D.; Min B. R. and Moon M. H. (2003). "*Hyperlayer hollow-fiber flow field-flow fractionation of cells*." Journal of Chromatography A **985** (1-2): 519–529.

Reschiglian P.; Zattoni A.; Roda B.; Michelini E. and Roda A. (2005) Field-flow fractionation and biotechnology. Trends in Biotechnology **23**, 475-483 DOI: 10.1016/j.tibtech.2005.07.008

[Reschiglian et al. 2005] Reschiglian P.; Zattoni A.; Roda B.; Michelini E. and Roda A. (2005). "*Field-flow fractionation and biotechnology*." Trends in Biotechnology **23** (9): 475–483.

[Reschiglian et al. 2012] Reschiglian P.; Zattoni A.; Roda B.; Rambaldi D. C. and Moon M. H. (2012). *Chapter 3: Hollow-Fiber Flow Field-Flow Fractionation: A Pipeline to Scale Down Separation and Enhance Detection of Proteins and Cells*. Field-Flow Fractionation in Biopolymer Analysis. Williams S. K. R. and Caldwell K. D. Vienna, Springer Vienna**:** 37-55.

[Roda et al. 2006] Roda A.; Parisi D.; Guardigli M.; Zattoni A. and Reschiglian P. (2006). "*Combined Approach to the Analysis of Recombinant Protein Drugs Using Hollow-Fiber Flow Field-Flow Fractionation, Mass Spectrometry, and Chemiluminescence Detection*." Analytical Chemistry **78** (4): 1085–1092.

[Roda et al. 2009] Roda B.; Zattoni A.; Reschiglian P.; Moon M. H.; Mirasoli M.; Michelini E. and Roda A. (2009). "*Field-flow fractionation in bioanalysis: A review of recent trends*." Analytica Chimica Acta **Volume 635** (2): 132–143.

[Schimpf 2000] Schimpf M. E. (2000). *Chapter 4: Resolution and Fractionating Power*. Field-Flow Fractionation Handbook. Schimpf M. E.; Caldwell K. and Giddings J. C. New York, Wiley**:** 71-78.

[Schure et al. 2000] Schure M. R.; Schimpf M. E. and Schettler P. D. (2000). *Chapter 2: Retention - normal mode*. Field-Flow Fractionation Handbook. Schimpf M. E.; Caldwell K. and Giddings J. C. New York, Wiley**:** 31-48.

[Silveira et al. 2005] Silveira J. R.; Raymond G. J.; Hughson A. G.; Race R. E.; Sim V. L.; Hayes S. F. and Caughey B. (2005). "*The most infectious prion protein particles*." Nature (437): 257-261.

[Valencia and González 2011] Valencia D. P. and González F. J. (2011). "*Understanding the linear correlation between diffusion coefficient and molecular weight. A model to estimate diffusion coefficients in acetonitrile solutions*." Electrochemistry Communications (13): 129–132.

[Wahlund 2013] Wahlund K.-G. (2013). "*Flow field-flow fractionation: Critical overview*." Journal of Chromatography A **1287** (2013): 97– 112.

[Wahlund and Nilsson 2012] Wahlund K.-G. and Nilsson L. (2012). *Chapter 1: Flow FFF – Basics and Key Applications*. Field-Flow Fractionation in Biopolymer Analysis. Williams S. K. R. and Caldwell K. D. Netherlands, Springer Vienna**:** 1-21.

[Wijnhoven et al. 1996] Wijnhoven J. E. G. J.; Bommel M. R. v.; Poppe H. and Kok W. T. (1996). "*Practical Experience with Organic Solvent Flow Field-Flow Fractionation*." Chromatographia **42** (7/8): 409-415.

[Zattoni et al. 2007] Zattoni A.; Casolari S.; Rambaldi D. C. and Reschiglian P. (2007). "*Hollow-fiber flow field-flow fractionation*." Current Analytical Chemistry **3** (4): 310-323.

[Zattoni et al. 2008] Zattoni A.; Rambaldi D. C.; Roda B.; Parisi D.; Roda A.; Moon M. H. and Reschiglian P. (2008). "*Hollow-fiber flow field-flow fractionation of whole blood serum*." Journal of Chromatography A **1183** (1–2): 135–142.

CHAPTER 3: HF5 INSTRUMENTAL SETUP AND DETECTION SYSTEMS

3.1. HF5 INSTRUMENTAL SETUP

The HF5 instrumentation required for samples separation and characterization adopts the same components of a HPLC system (automated autosampler, pump, degasser and detection systems), but a hollow fiber FFF channel as a separation device instead of the HPLC or SEC column. The HF5 channel (also called cartridge) is implemented in the Eclipse® DUALTEC™ FFF separation system (provided Wyatt Technology Europe, Germany). The FFF module, also automated, is controlled by a specific driver, implemented in the software which controls the HPLC instrumentation; in this dissertation, a 1200 Agilent HPLC system (Agilent Technologies, Santa Clara, USA) was used in all experiments, together with its correlated software, ChemStation®.

The main purpose of the detector in an FFF system is to determine quantitatively the number of particles, and the volume or mass concentrations of the separated fractions through FFF according to size. Consequently, the sample concentration can be derived employing appropriate detection systems, which are able to correlate the signal intensity with the sample concentration through the Lambert-Beer law; for example, UV-Vis and refractive index detectors are also called *concentration detectors*.

Moreover, online detectors such as multi-angle light scattering (MALS) or quasi-elastic light scattering (QELS) detectors, are able to provide further information on the size, as well as on the MW distribution of the sample.

An analytical separation technique requires a detection method which is able to respond to some or all of the components that elute from the separation system. The choice of the detector is, therefore, usually determined by sample requirements. In the FFF family of techniques, many of the detection systems have evolved from those used in LC. The detection can be performed either online, with a detector coupled to the stream of mobile phase, or by collecting sample fractions followed by subsequent analysis. For example, mass spectrometry and gel electrophoresis were used during the experimental work described in this dissertation as offline methods to characterize the HF5 fractions.

When choosing a detector and designing the experimental setup, one needs to consider the concentration of the analyte, the sensitivity of the detector, the level of the background noise, as well as the detection limit. The maximum sample amount that can be injected is usually limited by the sample overloading limit [Moon and Myers 2000], which is a main limitation of FFF, resulting in inter-particle interactions that disturb separation. Therefore, a limit of detection well below the sample overloading concentration is required in order to be able to quantify the analytes without excessive background noise.

3.2. DETECTION SYSTEMS

It is a widely known fact that, since conformation of protein molecules affects their biological activity, their tendency towards aggregation, and consequently the immune responses directed towards such aggregates, are tightly correlated to conformational changes endured by the native form. Conformational studies of the protein molecules in soluble aggregates (native-form aggregates) may be performed

either directly in the protein formulation or after the isolation of the aggregate population of interest. Methods such as: fluorescence spectroscopy (intrinsic, with fluorescence dyes or quenching), UV absorbance and near-UV circular dichroism spectroscopy, binding to conformationally-dependent antibodies for tertiary structure investigations and infrared and far-UV circular dichroism spectroscopy are usually employed for the analysis of the protein structure (tertiary, quaternary). Some native-state aggregated proteins may also lead to the loss of their active property. In some cases, large and insoluble protein aggregates can be separated from their formulation and studied with these same spectroscopic methods [Carpenter et al. 2012] (and references therein).

Just like liquid chromatography (LC, SEC), FFF systems (therefore HF5), may employ standard concentration detectors, such as refractive index (RI), UV absorbance, fluorescence detectors and/or light scattering detectors, in order to monitor the elution process. [Qureshi and Kok 2011] (and references therein)

HF5 separates according to the hydrodynamic size of the sample components. In the previous Chapter was shown how HF5-UV coupling can provide additional sample information, such as PSD. FFF is not only used in combination with UV or fluorescence detectors, but also with light scattering detectors (e.g., multi-angle light scattering, MALS), which enhance the analytical information by accurately determining the MW of the protein aggregates, either soluble or insoluble [Mahler et al. 2009] (and references therein).

Static light scattering detection, usually in the multi-angle light scattering (MALS) version, is often used in a multitude of application fields. MALS detection can provide the absolute MW of proteins and protein aggregates, and the size (*rms radius*) can be obtained without any approximation on particle shape. Another interesting possibility is the recently developed online coupling of HF5 with dynamic light scattering (DLS), which is now commercially available. Online DLS provides immediate information regarding the hydrodynamic size or the diffusion coefficient

of the separated proteins and aggregate populations [Qureshi and Kok 2011] (and reference therein).

FFF coupled with appropriate detection methods can be particularly suitable for the separation and characterization of *soluble aggregates* with sizes above 100 nm, where SEC or SDS-PAGE fail because of their operational range limitation. FFF is therefore able to fill the "*gap*" of suitable separation methods in this range [Mahler et al. 2009, Zölls et al. 2012] (and references therein). In SEC, the upper size limit of detectable protein aggregate is dictated by the column characteristics; larger aggregates can be filtered out by frits in the system or by the column itself, therefore large protein aggregates may be disrupted and be overlooked in the analysis [Engelsman et al. 2011] (and references therein).
In addition, since the FFF operational size range is wide enough, it makes it also suitable for the separation and characterization of *insoluble aggregates*, up to the sub-visible size region (~500 nm – 50μm) [Mahler et al. 2009, Zölls et al. 2012] (and references therein).

In a recent review, [Engelsman et al. 2011] critically analyzed the current analytical methods employed for the study of protein aggregation phenomena. For the purpose of this dissertation, only some of them – reported in Table 1 – will be discussed.

Table 1 - Typical use of analytical techniques in the biopharmaceutical industry with respect to aggregate analysis [Engelsman et al. 2011]

Method	Validation	Quantification	Robustness	Sensitivity	Sample throughput	QC method
AUC	*No*	*Yes*	*Low*	*Medium*	*Low*	*No*
SEC	*Yes*	*Yes*	*High*	*Medium*	*High*	*Yes*
AF4	*Yes*	*Yes*	*Medium*	*Medium*	*High*	*No*
SEC-MALS	*No*	*No (MALS part)*	*Medium*	*High*	*High*	*No*
UV-VIS spectroscopy	*No*	*No*	*Medium*	*Medium*	*High*	*No*
Fluorescence spectroscopy	*No*	*No*	*Medium*	*N/A*	*High*	*No*

Table 1 (full table in [Engelsman et al. 2011]) helps classify and suggest the appropriate use of an analytical technique in the industry as analytical quality control (QC) and extended characterization assays (EC) particularly suited when the routine QC methods provide atypical/inconsistent results.

For example, SEC robustness combined with sample throughput makes it the ideal candidate for QC assays, for which it has been routinely employed in the biopharmaceutical industry, despite its known shortcomings. On the other hand, even though FFF operates in a wider size range and has many advantages over SEC, it is not yet employed during QC of therapeutic proteins because it is less robust than SEC, less mature as a technique, and it often requires time-consuming method development.

Nonetheless, FFF is extremely valuable during the *extended characterization* (EC) assays that are applied during all stages of therapeutic protein formulation development. Implementing the EC assays early in the product development can mitigate the presence of undesired protein aggregates in formulations during production. Since in vitro or in vitro tests for immunogenic reactions are not currently available, some effects of protein aggregation is only observed during the human trials or even only after commercialization [Engelsman et al. 2011] (and references therein).

Implementing the FFF technology in the biopharmaceutical industry as EC assay has been suggested also by [Pollastrini et al. 2012], who highlight the FFF versatility at all stages of drug development, from the identification of the lead product candidate, to process scale-up, formulation development and process control maintenance (strongly recommended by FDA, [Hinz 2006, DiMasi and Grabowski 2007]), pre-clinical and clinical development (drug stability tests) and last, but not least, to commercial product investigations.

3.2.1. SPECTROSCOPIC DETECTION SYSTEMS

3.2.1.1. UV/VIS SPECTROMETRY

UV-Vis spectrophotometers are the most commonly used detectors in FFF applications, mainly due to their availability, simplicity and low cost. Coupled with an FFF system, they have a dual purpose: monitor the separation process and allow the sample quantification (concentration detectors).

For homogeneous samples (i.e. proteins), which absorb specific wavelengths, the relationship between sample absorption and concentration is straightforward, described by the Lambert-Beer law. However, when dealing with particulate samples (very large particles, usually > 1μm), their signal is a combination of light scattering and absorption. Therefore it needs to be corrected for scattering contributions [Sharpe 2012]. Consequently, the quantification of the separated particles is not straightforward, since the UV signal is actually a turbidimetric measure. The UV/Vis detector might be "blinded" by the light scattered in the forward direction. This leads to underestimating the fraction of the largest particles in a sample, especially when the particle size is close to the wavelength of the incident beam [Reschiglian et al. 1997].

However, for chromatographic applications, UV/Vis spectrophotometers have been designed for use as absorption detectors. They have a very low internal volume, which helps minimizing the sample band broadening.

The simplest detectors operate at a single, yet variable, wavelength (variable wavelength detector, VWD), while more complex instruments allow for the simultaneous detection of different wavelengths to match the spectral properties of the analyte (diode array detectors, DAD). Moreover, DAD allows registering the entire UV/Vis spectra of eluting samples. UV/Vis spectra are particularly useful for monitoring (chemical or physical) changes in sample composition during separation.

The detection *wavelength* is generally chosen with the intent to maximize the sensitivity to the analyte while avoiding interferences, such as absorption by the carrier liquid. For instance, high concentration acetate buffer, succinate, citrate buffer, phthalate and barbiturate are known to absorb strongly at 215 nm [Aitken and Learmonth 2002], which is also one of the main protein absorption bands.

In particular, *protein quantification* is usually made possible thanks to the specific protein absorption in the near UV region (280 nm), which depends on the *amino acid (AA) content*; tyrosine (Tyr) and tryptophan (Trp) are the major contributors, although a very small contribution to the UV absorption is also due to phenylalanine (Phe), and to the presence of disulfide bonds [Aitken and Learmonth 2002].

Since the AA sequence and content varies greatly from protein to protein, leading to different absorption intensities among proteins, a specific absorption for each protein must be determined. The *extinction coefficient* ε relates the protein concentration with its absorption intensity. For protein solutions at 1 mg/mL, most $\varepsilon_{0.1\%}^{280nm}$ values are between 0.5 and 1.5 (average 1.0). Moreover, the protein absorption at 280 nm can be employed to determine the protein AA composition, and the Trp, Thy and Phe %. Absorption interferences at 280 nm may exist, due to nucleic acids contamination. However, DNA contamination can be confirmed and quantified by detection at 260 nm [Aitken and Learmonth 2002].

The protein *peptide bond* has a very strong, specific absorbance in the far UV (maximum at 190 nm, but usually detected between 205 and 215 nm), which can be exploited for protein quantification. However, due to oxygen interference at 190 nm, measurements are more convenient at 205 nm, where the absorbance is ~ half than that at 190 nm. As previously mentioned, at these wavelengths (205-215 nm) possible interference from the mobile phase composition (especially highly concentrated salts) may hinder detection, therefore protein quantification. Since protein absorption in the far UV region is not due to AA side chains, it does not distinguish among proteins, and it can be employed as an *absolute method for protein quantification* [Aitken and Learmonth 2002].

Protein quantification by spectrometric methods is based on the *Lambert-Beer law*, which can be expressed as *Equation 1*, where A represents the absorption intensity, ε represents the molar extinction coefficient (a proportionality constant which correlates the absorption intensity and the sample concentration), c represents the sample concentration (molarity, M) and l represents the path length [IUPAC 2014]:

$$A = \varepsilon \cdot c \cdot l$$

Equation 1

A particular version Equation 1 is its adapted version for *flow systems*, expressed by *Equation 2*, where F represents the volumetric flow rate:

$$A \cdot F = \varepsilon \cdot c \cdot l$$

Equation 2

Equation 2 describes the inverse proportionality between sample absorbance and elution flow rate; this relationship can be exploited to increase detection sensitivity in flow systems. According to *Equation 2*, a smaller flow rate implies a larger area under the peak, therefore decreased sample limit of detection (LOD) and quantification (LOQ), leading to higher detection sensitivity. By further reducing the fiber inner radius, both efficiency and sensitivity (c_{LOD}) increase, according to Equation 13 in sub-chapter 2.2.2 (Chapter 2). Thanks to a smaller fiber inner radius, the separation would require a lower longitudinal flow rate, thus decreasing sample dilution and, by applying higher cross-flow rates, the separation performance improves (higher efficiency).

Other methods for protein quantification are represented by offline, specific tests, like the Bradford assay or the BCA assay, which involve protein binding to an absorbing molecule (chromophores).

3.2.1.2. FLUORESCENCE SPECTROSCOPY

Fluorescence spectroscopy is classified by [Engelsman et al. 2011] as an indirect method for assessing protein folding state, by detection of fluorescence emission (intrinsic or extrinsic) which aids observing the protein tertiary/quaternary structure. Its advantages comprise the non-destructive nature, the multiple fluorescence techniques, the possibility of combining fluorescence with microscopic tools, as well as the online detection possibility, which is one of the most appealing features when coupling with a separation technique is considered.

Protein fluorescence is analyzed to monitor changes in the tertiary structure and the environment of the fluorescent amino acids, mainly tryptophan. *Intrinsic protein fluorescence* is attributed to tryptophan (Trp or W), tyrosine (Tyr or Y)), and phenylalanine (Phe or F), with fluorescence intensities decreasing in this order. The absorption/emission maxima in aqueous solution are: 280 nm/350 nm for Trp, 275 nm/304 nm for Tyr and 258 nm/282 nm for Phe. Trp is the mostly monitored fluorophore, since it exhibits the strongest fluorescence and is selectively excitable at wavelengths between 295 and 300 nm. However, Trp is usually very poorly represented in the AA structure of proteins. Moreover, its presence highly varies from protein to protein (i.e., Bovine Serum Albumin contains 2 Trp residues in the AA sequence, while Thyroglobulin contains 40 – [SwissPDB 2014]). Therefore the Trp fluorescence emission cannot be used as a method of identification or quantification [Zölls et al. 2012] (and references therein).

The Trp fluorescence intensity changes dependent on the polarity of the environment. For this reason the Trp property is used to monitor changes in the protein structure and the consequent formation of aggregates. However, fluorescence is only suitable to detect relative structural changes (qualitative information) and not to determine the absolute tertiary structure [Zölls et al. 2012] (and references therein).

Optical detectors are available for online coupling with separation techniques, such as UV/Vis absorbance and fluorescence detectors, that are highly sensitive in detecting chromophores. This allows characterizing proteins with a good S/N ratio for protein concentrations as low as 10 μg/mL [Mahler et al. 2009] (and references therein).

In addition to intrinsic fluorescence, *fluorescent dyes* (*extrinsic fluorescence*) can also be used to examine the conformation and other properties of protein aggregates. Fluorescent dyes can be covalently or non-covalently attached to the protein of interest. Covalently attached fluorescent dyes can be used to analyze protein aggregates and particles in complex buffers or directly in serum. Non-covalent fluorescent dyes, bound by hydrophobic or electrostatic interactions, are usually more interesting for the study of therapeutic protein aggregates and particles because their fluorescence intensity changes with the polarity of the environment (behavior similar to intrinsic Trp). The fluorescence intensity of non-covalent dyes such as ANS (8-anilino-1-naphthalenesulfonate), bis-ANS (4,4-dianilino-1,1-binaphthyl-5,5-disulfonate), SYPRO orange, or Nile Red can be employed to study the exposure of hydrophobic protein regions by unfolding and aggregation. Extrinsic dyes can provide information about structural changes and/or the formation of aggregates, as well as the properties of the formed aggregates, just like intrinsic fluorophores. However, the formation or suppression of protein aggregation should be carefully considered, known to be caused by the organic solvent in which they are prepared or caused by the fluorescent dye itself. [Zölls et al. 2012] (and references therein)
Extrinsic fluorescence detection allows the characterization of very dilute samples employing fluorescent labels. However, careful consideration of protein label (dye) is due, because the extrinsic dye might alter the protein sample (protein-protein interactions), thus creating artifacts (for instance, protein aggregates). The addition of the dye itself may indeed induce artifacts by shifting the equilibrium between different conformational states of the protein [Mahler et al. 2009] (and references

therein). For the study of larger/insoluble aggregates, fluorescent dyes are mostly employed for visualization in fluorescence microscopy or for Fluorescence activated Particle Sorting, FAPS [Zölls et al. 2012] (and references therein).

Intrinsic fluorescence proved to be extremely valuable in evaluating the structural/molecular conformational changes which occur as a consequence of changes in the environmental conditions, responsible for different degrees of protein aggregation [Song et al. 1999] (and references therein).

Intrinsic fluorescence of tryptophan was employed to highlight differences between lyophilized and non lyophilized antibodies and to study the effects of sample lyophilization on antibody stability, leading to aggregation [Wang et al. 2007] (and references therein). IgG aggregation by means of fluorescence emission was also studied by [Demeule et al. 2007].

A recent study, where a fluorescent dye was added to the carrier solution or the sample, showed that SEC performed better for the separation of monomers and dimers, but AF4 was able to provide a higher recovery for larger aggregates. The increased fluorescence intensity observed upon heating an IgG antibody was correlated to IgG aggregates formation, as well as to structural changes in the IgG conformation [Qureshi and Kok 2011].

Intrinsic Trp fluorescence spectroscopy (emission wavelengths of 300-450nm, using an excitation wavelength of 295nm) was employed successfully for the study of antibody conformational changes leading to non-native aggregation, which occurred during the denaturation process; the unfolding/refolding process of the antibody was induced by either treatment with concentrated GuHCl or at elevated temperature [Brummitt et al. 2011] (and references therein).

Finally, intrinsic and extrinsic fluorescence spectroscopy coupled to an AF4 system, together with Differential Scanning Calorimetry (DSC), circular dichroism (CD) and FTIR were employed for the determination of the melting temperature and onset temperature of unfolding of an antibody during its formulation development; a

progressive destabilization of the native protein structure is usually observed as the temperature is increased, often leading to (irreversible) aggregation. This qualitative study of the conformational changes by means of sensitive and fast fluorescence detection, related to the degradation of the tertiary structure during formulation development, demonstrated the role of conformational stability, as well as colloidal stability on the final protein formulations [Hawe et al. 2012] (and references therein).

3.2.2. OPTICAL DETECTION SYSTEMS:

LIGHT SCATTERING

Many analytical methods for the study of colloids are based on the interaction of particles with light; therefore light scattering techniques play a central role in protein particle characterization, as well [Zölls et al. 2012]. Since the intensity of light scattering increases with the sixth power of the aggregate radius, the sensitivity of light scattering detectors for large aggregates is considerably higher than UV, FLD or RI detection. However, when protein aggregates are present at low levels and only the light scattering signal is detected, the determination of MW and the quantification of the aggregates (as mass fraction) cannot be made performed, but light scattering can still provide a qualitative tool for monitoring the presence of aggregates [Carpenter et al. 2010].

Upon sample illumination, the light scattering phenomenon can be observed as a very fast sequence of photon absorption followed by an almost instantaneous emission of another photon. The absorbed energy can be released from the virtual state as photons in two different ways: (1) if the scattered photon has the same energy/frequency as the absorbed photon, the phenomenon is called *elastic light scattering*, characteristic for scatterers smaller than the wavelength of the incident light (or Rayleigh scattering) and for scatterers in the range of the wavelength of the incident light and above (Mie scattering); (2) if the scattered photon has an

energy/frequency different from that of the absorbed photon, the phenomenon is called *inelastic* or *Raman scattering* and occurs only for 10^{-3} of all scattered photons.

Rayleigh/Mie scattering (1) is employed for dynamic light scattering (DLS) or quasi-elastic light scattering (QELS), nanoparticles tracking analysis (NTA), and static light scattering (SLS), while Raman scattering (2) is the basis for Raman spectroscopy [Zölls et al. 2012].

The most used light scattering techniques for the characterization of protein aggregates are dynamic light scattering and static light scattering (multi-angle light scattering); both can be used either as standalone (batch) techniques, or on-line coupled with FFF, although the on-line coupling is more advantageous. A quick review of the two techniques is reported in Table 2, adapted from [Engelsman et al. 2011].

Since DLS was not employed during the experimental part described in this dissertation, the focus will be directed towards MALS.

Table 2 - Light scattering techniques for the analysis of protein aggregates [Engelsman et al. 2011]

Method	**Static light scattering MALS**	**Dynamic light scattering DLS**
Principle	Time-averaged light scattering intensity of particles, detected at multiple angles	Fluctuations in scattered light intensity due to Brownian motion
Observable	Molar mass, size (*rms radius*)	Hydrodynamic size
Size range	10^3Da – 10^9 Da	1 nm – 5 μm
Advantages	High sensitivity; absolute determination of size; commonly used as online detector	Easy to perform (batch mode); non-destructive; high sensitivity; low sample consumption
Disadvantages	Solute concentration must be known; complicated data analysis; not quantitative; limited use in batch mode; very sensitive to sample contamination	Complicated data analysis; not quantitative; low resolution (weak differentiation between particle species); less suitable for polydisperse samples; very sensitive to contamination (e.g. dust)

Although other methods, such as Mass Spectrometry, membrane osmometry or sedimentation equilibrium allow the determination of the absolute MW, MALS is

non-destructive and the determination of the MW and size of the particles is performed without any calibration; therefore can be considered an *absolute technique*. These characteristics, combined with a relatively short analysis times, make MALS a fast and accurate analysis method, optimal for the characterization of macromolecules in solution.

3.2.2.1. MULTI-ANGLE LIGHT SCATTERING (MALS)

The analytical information provided by HF5-UV or HF5-FLD detection can be enhanced even further by online coupling with *optical* detection methods, like *multi-angle light scattering* (MALS), which measures the light scattered at multiple angles by the proteins and protein aggregates, previously fractionated by means of HF5. Combined with a concentration detector (like a UV detector), MALS is able to provide directly the *size* (root mean square radius or *rms radius*, the mass-average distance between each point in the macromolecule and the center of mass) the *absolute molar weight* (MW) of the fractionated proteins and protein aggregates as a function of their elution time. Comparing the *rms radius* values obtained from the MALS measurements with the *hydrodynamic radius* (r_h), which is readily obtained from the experimental retention time, HF5-MALS allows obtaining information regarding the shape (conformation) and mass distribution inside the protein aggregates [Reschiglian and Moon 2008]

The coupling between a miniaturized separation device (HF5) and a highly sensitive detection method such as light scattering has a synergetic effect on decreasing the limit of detection, which proves particularly useful for the characterization of protein samples containing low levels of aggregates. Therefore, the HF5-(UV/FLD)-MALS coupling appears to be the ideal solution for the characterization of the widely-sized protein aggregates present in therapeutic formulations, as well as a possible new technological platform in functional and structural proteomics.

As previously mentioned, *static light scattering* can provide information about the size and MW of the proteins and protein aggregates in the measured solution. In SLS, the *excess Rayleigh's ratio* is measured, this excess ratio represents the time-averaged intensity of scattered light by the particles at a certain angle, compared with the scattering intensity of the solvent. SLS is suitable for molecules which scatter light roughly isotropically, with a radius of gyration smaller than 1/20 of the incident wavelength (up to ~ 30 nm, as laser wavelengths in the range of 600–700 nm are mostly used).

MALS is a particular case of static light scattering, where the scattered light is measured at multiple angles; MALS is necessary to obtain more detailed information about molecules whose scattering type is no longer isotropic (such as high MW protein aggregates) [Zölls et al. 2012]

Parallel to Mass Spectrometry, the development of multi-angle light scattering instruments represented a breakthrough in particle sizing [Wyatt 1968]. In a typical light scattering measurement, the MALS detector and a concentration detector (UV/Vis or a DRI detector) are connected in series after the fractionation device; MALS detection is applicable in a size range from 1 nm to over 1 μm, and its sensitivity increases proportionally to the particle size.

The Zimm equation [Zimm 1948, Wyatt 1993] is used to calculate the size (rms radius, which represents the mass-averaged distance from each scattering point in the particle from its center of gravity) and the MW of the analyzed species from the angle-dependent light scattering intensities, which are also correlated to the sample concentration and the refractive index difference between analyte and solution. The dependence of the radius on MW yields information on the molecular conformation of the species in dispersion.

As previously mentioned, MALS can also be employed as a stand-alone technique, for batch measurements; however when applied to heterogeneous samples, like aggregated protein formulations, only a *Z*-average value for the MW of *all species* present in the solution is provided. Consequently, in protein aggregation analytics,

MALS is mostly used as a detector for SEC or FFF (AF4 or HF5), in combination with UV and/or refractive index detection (to measure the concentration that is needed to calculate the molecular weight). The available MALS software, although powerful in most situations, is limited for the characterization of highly dispersed samples with very broad MW distributions are obtained and especially when the sample components characteristics (e.g. shape/conformation) vary over time [Wahlund 2013].

The major advantage of MALS hyphenation with separation techniques is the possibility to calculate the MW and size of the individually eluting species; this makes the use of MW standards obsolete (i.e. standards for SEC column calibration); therefore, misinterpretation of aggregate sizes based on different elution behavior of standards can be avoided [Zölls et al. 2012].

Consequently, the combination of MALLS with SEC or AF4 is the method of choice for the analysis of protein aggregates and particles as shown by numerous publications; moreover SEC and FFF complement each other, since FFF can pick up aggregates characterization when SEC fails to provide reliable results.

SEC, as standalone technique, has been the workhorse in the biopharmaceutical industry for QC practices and batch release; however, cross-validation of SEC methods for aggregate analysis is nearly always required, by means of orthogonal methods, such as AUC, batch-mode SLS or DLS and FFF [Philo 2006, Arakawa et al. 2010, Carpenter et al. 2010, Carpenter et al. 2012, Liu et al. 2012].

AF4 and SV-AUC were employed as orthogonal methods for the characterization and quantification of soluble aggregates of acid stressed/unstressed recombinant humanized monoclonal antibody, initially measured by SEC and analyzed by SEDFIT/c(s); SV-AUC and AF4 were able to detect markedly higher total aggregate levels than SEC in equivalent antibody samples. Moreover, SEC failed to detect higher MW soluble aggregates due to probable antibody physical adsorption to column matrix, which were apparent in SV-AUC and AF4 analyses, leading to incomplete mass recovery. An aggregation model, based on nearly linear end-to-end

assembly of monomeric subunits, is proposed and corroborated by SV-AUC, SEC, AF4, and DLS measurements [Gabrielson et al. 2007].

SEC-MALS is very useful throughout product development as EC assay; however, due to MALS shortcomings, it is not recommended as a routine QC method. One of the major disadvantages of MALS in general is its sensitivity biased towards large-sized particulate (including non-protein particulates, such as contaminations) and consequent prolonged equilibration times to obtain a stable baseline. Moreover, since data evaluation is so time consuming, its robustness is, therefore, significantly compromised [Engelsman et al. 2011].

This hyphenation between separation and detection techniques, like FFF (HF5)-UV/FLD/RI-MALS, has contributed greatly to the development of Flow FFF as an analytical separation method; this coupling has become a very popular instrumental setup for the determination of absolute MW, MW distribution and size-characterization (z-average *rms radius*) of separated sample populations [Wahlund 2013]. Here below, some of the most recent applications are briefly described.

The aggregation of a monoclonal IgG1 type antibody, induced by freeze–thawing and elevated temperature, and the protein aggregates structural properties were studied by AF4 with UV and MALLS detection, and HP-SEC with UV and online fluorescent dye detection; the study demonstrated that thermal stress led to an increased formation of dimers and soluble oligomers, observed by both HP-SEC and AF4 [Hawe et al. 2008].

A combination of spectroscopic techniques (UV-absorption, CD, ATR-FTIR and fluorescence), light obscuration, dynamic light scattering, SDS-PAGE, AF4 with UV and MALLS detection, and HP-SEC with UV and online fluorescent dye detection was employed in a study aimed to characterize the structural properties of aggregates formed after freeze–thawing and thermal stressing (typical stress factors during development, production and storage) of a humanized monoclonal IgG1

antibody; an increased formation of dimers and soluble oligomers was observed by both HP-SEC and AF4 [Hawe et al. 2009].

Like many other protein misfolding diseases, Prion diseases are notoriously known through the formation of abnormal protein aggregates, whose size ranges from oligomers to large amyloid fibrils and plaques; among the many approaches which were considered for the task of fractionating and characterizing abnormal prion protein particles, only AF4-MALS was effective. AF4-MALS was employed successfully by [Barton et al. 2012] in order to assess the infectivity associated with the widely-sized PrP^{res} in a study which showed that, even though large amyloid fibrils of PrP^{res} are still able to transmit disease, the most infectious J-particles, identified by [Silveira et al. 2005], are smaller oligomeric species.

The time-dependent $A\beta_{1-42}$ aggregation pattern, representing the self-assembly of the 42-amino-acid-long amyloid peptide $A\beta_{1-42}$ into insoluble fibrillar deposits in the brain and a crucial event in the pathogenesis of Alzheimer's disease, was studied by AF4 with on-line multi-angle light scattering detection; the fibril deposition occurs through an aggregation process involving transient and metastable oligomeric intermediates, which are intrinsically difficult to be accurately monitored and characterized by traditional methods. On-line AF4-MALS coupling allowed the separation and the determination of the MW and size distribution of both the early-forming soluble aggregates and the late pre-fibrillar and fibrillar species, demonstrating unique information on the dynamic aggregation kinetics [Rambaldi et al. 2009].

Using different analytical methods, which included visual inspection, turbidity, light obscuration, size exclusion chromatography, and dynamic light scattering, the aggregation behavior of an IgG1 stressed by shaking or heat following static storage was investigated, to determine whether protein aggregates exist in equilibrium; the study demonstrated obvious differences between shaken and heated samples upon storage [Kiese et al. 2010].

A combination of intrinsic/extrinsic fluorescence (FL), circular dichroism, calorimetry, chromatography, capillary electrophoresis, and laser light scattering was used for the study of an IgG1 antibody under acidic conditions, as a function of solution pH; protein unfolding, refolding, native colloidal interactions, aggregate structure and morphology, and aggregate dissociation were observed [Brummitt et al. 2011].

A combination of dynamic light scattering, size exclusion chromatography (SEC) and field flow fractionation (FFF) was employed to study the effect of pH and salt concentration, on the stability and aggregation kinetics of IgG solutions under the conditions typically encountered in downstream processing. The oligomer distributions provided by SEC and FFF are consistent, demonstrating that, for the given antibody, low pH and presence of salt induce conformational changes that are responsible for progressive, but reversible aggregation, proportional to the salt concentration [Arosio et al. 2011].

A recent HF5-MALS-based application, consisting in a customized, fast and accurate method for characterization of therapeutic proteins, using as a model sample an oxidized form of Avidin (AvidinOX®), showed the boost in detection sensitivity obtained by combining a miniaturized separation device (HF5) and a highly sensitive detection method (MALS); the first application developed employing the commercial hollow fiber FFF miniaturized channel [Reschiglian et al. 2013].

A wide range of opportunities for inspiration and exploitation of the distinct characteristics of AF4-MALS throughout the long, winding and multifaceted therapeutic proteins development process are proposed by [Pollastrini et al. 2012]

AF4-MALS was used to study the aggregation properties of antibodies, two different proteins and a protein-polysaccharide conjugate (PPC); the AF4 method was found to be less destructive on the aggregates, but at the expense of separation. Loose protein and antibody aggregates were detected by MALS and their presence was corroborated by complementary spectroscopic and microscopic techniques; the aggregates readily reversed to monomers during AF4 separation. The results

obtained by [Palais et al. 2012] demonstrate the importance of AF4 versatility in terms of experimental conditions (flow combinations), able to characterize the complexity of protein aggregation.

3.3. REFERENCES

[Aitken and Learmonth 2002] Aitken A. and Learmonth M. P. (2002). *Chapter 1: Protein Determination by UV Absorption*. The Protein Protocols Handbook, Second Edition. Walker J. M. Totowa, NJ, Humana Press Ins.

[Arakawa et al. 2010] Arakawa T.; Ejima D.; Li T. and Philo J. S. (2010). "*The Critical Role of Mobile Phase Composition in Size Exclusion Chromatography of Protein Pharmaceuticals*." Journal of Pharmaceutical Sciences **99** (4): 1674-1692.

[Arosio et al. 2011] Arosio P.; Barolo G.; Müller-Späth T.; Wu H. and Morbidelli M. (2011). "*Aggregation Stability of a Monoclonal Antibody During Downstream Processing*." Pharmaceutical Research **28** (8): 1884-1894.

[Barton et al. 2012] Barton K. A.; Sim V. L.; Hughson A. G. and Caughey B. (2012). *Chapter 10: Analysis of Prions by Field-Flow Fractionation*. Field-Flow Fractionation in Biopolymer Analysis. Williams S. K. R. and Caldwell K. D., Springer Vienna**:** 139-149.

[Brummitt et al. 2011] Brummitt R. K.; Nesta D. P.; Chang L.; Chase S. F.; Laue T. M. and Roberts C. J. (2011). "*Nonnative Aggregation of an IgG1 Antibody in Acidic Conditions: Part 1. Unfolding, Colloidal Interactions, and Formation of High-Molecular-Weight Aggregates*." Journal of Pharmaceutical Sciences **100** (6): 2087–2103.

[Carpenter et al. 2012] Carpenter J. F.; Cherney B. and Rosenberg A. S. (2012). *The Critical Need for Robust Assays for Quantitation and Characterization of Aggregates of Therapeutic Proteins*. Analysis of Aggregates and Particles in Protein Pharmaceuticals. Mahler H.-C. and Jiskoot W. Hoboken, NJ, USA, John Wiley & Sons, Inc.

[Carpenter et al. 2010] Carpenter J. F.; Randolph T. W.; Jiskoot W.; Crommelin D. J. A.; Middaugh C. R. and Winter G. (2010). "*Potential Inaccurate Quantitation and Sizing of Protein Aggregates by Size Exclusion Chromatography: Essential Need to Use Orthogonal Methods to Assure the Quality of Therapeutic Protein Products*." Journal of Pharmaceutical Sciences **99** (5): 2200–2208.

[Demeule et al. 2007] Demeule B.; Lawrence M. J.; Drake A. F.; Gurny R. and Arvinte T. (2007). "*Characterization of protein aggregation: The case of a therapeutic immunoglobulin*." Biochimica et Biophysica Acta (BBA) - Molecular Basis of Disease **1774** (1): 146-153.

[DiMasi and Grabowski 2007] Dimasi J. A. and Grabowski H. G. (2007). "*The Cost of Biopharmaceutical R&D: Is Biotech Different?*" MANAGERIAL AND DECISION ECONOMICS (28): 469–479.

[Engelsman et al. 2011] Engelsman J. d.; Garidel P.; Smulders R.; Koll H.; Smith B.; Bassarab S.; Seidl A.; Hainzl O. and Jiskoot W. (2011). "*Strategies for the Assessment of Protein Aggregates in Pharmaceutical Biotech Product Development*." Pharmaceutical Research **28** (4): 920-933.

[Gabrielson et al. 2007] Gabrielson J. P.; Brader M. L.; Pekar A. H.; Mathis K. B.; Winter G.; Carpenter J. F. and Randolph T. W. (2007). "*Quantitation of Aggregate Levels in a Recombinant Humanized Monoclonal Antibody Formulation by Size-Exclusion Chromatography, Asymmetrical Flow Field Flow Fractionation, and Sedimentation Velocity*." Journal of Pharmaceutical Sciences **96**: 268–279.

[Hawe et al. 2008] Hawe A.; Friess W.; Sutter M. and Jiskoot W. (2008). "*Online fluorescent dye detection method for the characterization of immunoglobulin G aggregation by size exclusion chromatography and asymmetrical flow field flow fractionation*." Analytical Biochemistry **378** (2): 115-122.

[Hawe et al. 2009] Hawe A.; Kasper J. C.; Friess W. and Jiskoot W. (2009). "*Structural properties of monoclonal antibody aggregates induced by freeze–thawing and thermal stress*." European Journal of Pharmaceutical Sciences **38** (2): 79-87.

[Hawe et al. 2012] Hawe A.; Wiggenhorn M.; Weert M. v. d.; Garbe J.; Mahler H. and Jiskoot W. (2012). "*Forced Degradation of Therapeutic Proteins*." Journal of Pharmaceutical Sciences **101** (3): 895–913.

[Hinz 2006] Hinz D. C. (2006). "*Process analytical technologies in the pharmaceutical industry: the FDA's PAT initiative*." Analytical and Bioanalytical Chemistry **384** (5): 1036-1042.

[Iupac]. "*Beer–Lambert law (or Beer–Lambert–Bouguer law), IUPAC Goldbook*." Retrieved 24 February, 2014, from http://goldbook.iupac.org/B00626.html.

[Kiese et al. 2010] Kiese S.; Pappenberger A.; Friess W. and Mahler H. C. (2010). "*Equilibrium studies of protein aggregates and homogeneous nucleation in protein formulation*." Journal of Pharmaceutical Sciences **99** (2): 632–644.

[Liu et al. 2012] Liu J.; Zhu Q.; Shire S. J. and Demeule B. (2012). *Chapter 6: Assessing and Improving Asymmetric Flow Field-Flow Fractionation of Therapeutic Proteins*. Field-Flow Fractionation in Biopolymer Analysis. Williams S. K. R. and Caldwell K. D., Springer Vienna**:** 89-101.

[Mahler et al. 2009] Mahler H.-C.; Friess W.; Grauschopf U. and Kiese S. (2009). "*Protein aggregation: Pathways, induction factors and analysis*." Journal of Pharmaceutical Sciences **98** (9): 2909–2934.

[Moon and Myers 2000] Moon M. H. and Myers M. N. (2000). *Chapter 13: Experimental Field-Flow Fractionation: Practices and Precautions*. Field-Flow Fractionation Handbook. Schimpf M. E.; Caldwell K. and Giddings J. C. New York, Wiley**:** 119-212.

[Palais et al. 2012] Palais C.; Capelle M. and Arvinte T. (2012). *Chapter 7: Studies of Loose Protein Aggregates by Flow Field-Flow Fractionation (FFF) Coupled to Multi-Angle Laser Light Scattering (MALLS)*.

Field-Flow Fractionation in Biopolymer Analysis. Williams S. K. R. and Caldwell K. D., Springer Vienna**:** 103-112.

[Philo 2006] Philo J. S. (2006). "*Is Any Measurement Method Optimal for All Aggregate Sizes and Types?* ." The AAPS Journal **8** (3).

[Pollastrini et al. 2012] Pollastrini J.; Narhi L. O.; Jiang Y. and Cao S. (2012). *Chapter 5: Field-Flow Fractionation in Therapeutic Protein Development*. Field-Flow Fractionation in Biopolymer Analysis. Williams S. K. R. and Caldwell K. D., Springer Vienna**:** 73-88.

[Pollastrini et al. 2012] Pollastrini J.; Narhi L. O.; Jiang Y. and Cao S. (2012). *Field-Flow Fractionation in Therapeutic Protein Development*. Field-Flow Fractionation in Biopolymer Analysis. Williams S. K. R. C., Karin D. Vienna, Springer Vienna**:** 73-88.

[Qureshi and Kok 2011] Qureshi R. N. and Kok W. T. (2011). "*Application of flow field-flow fractionation for the characterization of macromolecules of biological interest: a review*." Analytical and Bioanalytical Chemistry **399** (4): 1401-1411.

[Rambaldi et al. 2009] Rambaldi D. C.; Zattoni A.; Reschiglian P.; Colombo R. and Lorenzi E. D. (2009). "*In vitro amyloid Aβ1-42 peptide aggregation monitoring by asymmetrical flow field-flow fractionation with multi-angle light scattering detection*." Analytical and Bioanalytical Chemistry **394** (8): 2145-2149.

[Reschiglian et al. 1997] Reschiglian P.; Melucci D.; Zattoni A. and Torsi G. (1997). "*Quantitative approach to field flow fractionation for the characterization of supermicron particles*." Journal of Microcolumn Separations **9** (7): 545-556.

[Reschiglian and Moon 2008] Reschiglian P. and Moon M. H. (2008). "*Flow field-flow fractionation: A pre-analytical method for proteomics*." Journal of Proteomics **71** (3): 265–276.

[Reschiglian et al. 2013] Reschiglian P.; Roda B.; Zattoni A.; Tanase M.; Marassi V. and Serani S. (2013). "*Hollow-fiber flow field-flow fractionation with multi-angle laser scattering detection for aggregation studies of therapeutic proteins*." Analytical and Bioanalytical Chemistry (Field-Flow Fractionation).

[Sharpe T.]. "*Measuring protein concentration*." Retrieved 20 February, 2014, from http://www.biozentrum.unibas.ch/fileadmin/redaktion/Forschung/Research_Groups/BF/Protocols/Protein_Concentration.pdf.

[Silveira et al. 2005] Silveira J. R.; Raymond G. J.; Hughson A. G.; Race R. E.; Sim V. L.; Hayes S. F. and Caughey B. (2005). "*The most infectious prion protein particles*." Nature (437): 257-261.

[Song et al. 1999] Song J. H.; Kim W.-S.; Park Y. H.; Yu E. K. and Lee D. W. (1999). "*Retention Characteristics of Various Proteins in Flow Field-Flow Fractionation : Effects of pH, Ionic Strength, and Denaturation*." Bulletin of the Korean Chemical Society **20** (10): 1159 - 1164.

[Swisspdb]. "*Swiss PDB*." Swiss Institute of Bioinformatics. Retrieved 20 February, 2014, from http://www.isb-sib.ch/.

[Wahlund 2013] Wahlund K.-G. (2013). "*Flow field-flow fractionation: Critical overview*." Journal of Chromatography A **1287** (2013): 97– 112.

[Wang et al. 2007] Wang W.; Singh S.; Zeng D. L.; King K. and Nema S. (2007). "*Antibody structure, instability, and formulation*." Journal of Pharmaceutical Sciences **96** (1): 1-26.

[Wyatt 1968] Wyatt P. J. (1968). "*Differential Light Scattering: a Physical Method for Identifying Living Bacterial Cells*." Applied Optics **7** (10): 1879-1896

[Wyatt 1993] Wyatt P. J. (1993). "*Light scattering and the absolute characterization of macromolecules*." Analytica Chimica Acta **272** (1): 1–40.

[Zimm 1948] Zimm B. (1948). "*The Scattering of Light and the Radial Distribution Function of High Polymer Solutions*." The Journal of Chemical Physics **16** (1093).

[Zölls et al. 2012] Zölls S.; Tantipolphan R.; Wiggenhorn M.; Winter G.; Jiskoot W.; Friess W. and Hawe A. (2012). "*Particles in therapeutic protein formulations, Part 1: Overview of analytical methods*." Journal of Pharmaceutical Sciences **101** (3): 914–935.

CHAPTER 4:

PART 1: STUDY OF PROTEIN AGGREGATION PHENOMENA IN THERAPEUTIC FORMULATIONS

INTRODUCTION

Therapeutic and diagnostic proteins represent the fastest growing area of biopharmaceutical applications [Daugherty and Mrsny 2006] and, among them, antibodies are the major player, controlling many types of diseases such as cancer, infectious diseases, allergy, autoimmune diseases, and inflammation [Wang et al. 2007]. A fast keyword search on [ClinicalTrials.gov 2013] reports almost 3000 clinical trials involving monoclonal antibodies in 2013, spread globally (Figure 1).

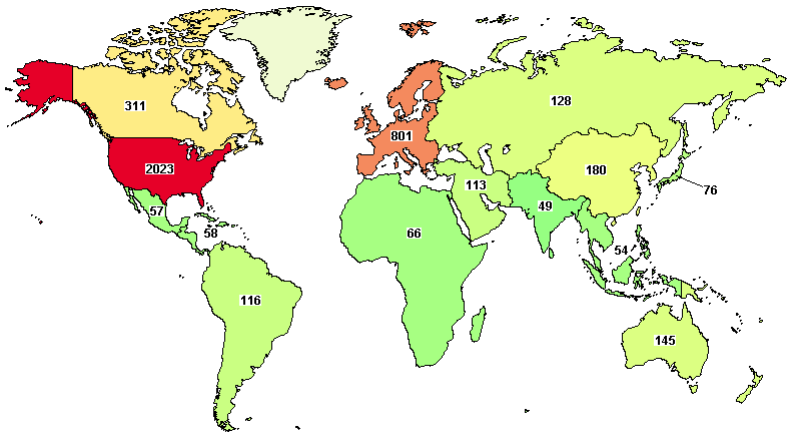

Figure 1 - Clinical studies involving monoclonal antibodies in 2013.
Source: [ClinicalTrials.gov 2013]

Therapeutic protein drugs, antibodies in particular, (a) have a very specific action, therefore lead to less side effects compared to small molecule drugs; (b) may be used for drug delivery, namely conjugated to another therapeutic drug for efficient delivery of this entity to a target site, therefore reducing potential side effects and (c) may be conjugated to radioisotopes for specific diagnostic purposes [Wang et al. 2007]. All these reasons explain why this category of therapeutics is gaining extraordinary drive, as well as widespread recognition. Since the approval of the first monoclonal antibody product in 1986 (-OKT-3) [Wang et al. 2007], the booming increase in protein drugs development (30-fold increase over 7 years, 2006-2013) reflects the relevance of bio-therapeutics and the advances made in antibody

engineering. Most of the FDA-approved drugs target cancer or inflammation, pathologies which have not been previously treated effectively with traditional, small molecule drugs [Daugherty and Mrsny 2006].

Antibody therapeutics are large (MW>150 kDa), complex molecules and must be administered at high levels in order for them to be effective (~1g/dose). Their production and purification scale has reached unpredicted industrial levels, previously assumed impossible. Development of *stable and high concentration formulations*, as well as *effective delivery strategies* of large amounts of complex molecules progressively became pressing issues for the biopharmaceutical industry. *Product stability* soon became a critical aspect, since tightly related to its effectiveness, as well as its potential toxicity [Daugherty and Mrsny 2006].

Consequently, the need for (improved) high throughput methods to optimize the development of protein formulation, the need for sensitive and accurate methods to determine and to monitor over time the composition of the protein formulation, as well as the need for robust QC protocols for batch release have emerged [Capelle et al. 2007, Carpenter et al. 2012].

These needs justify the sudden growth of new analysis methods, aimed at the development of sensitive and selective separation techniques, with a wide range of applications, appropriate resolution and versatility regarding the analysis of complex samples. Among them, albeit a little slower and less visible, the development and improvement of *field-flow fractionation* (FFF) has progressed in parallel to the development of electrophoresis (gel, GE or capillary, CZE), liquid chromatography (LC) and flow cytometry (FC) [Reschiglian et al. 2005].

The development of befitting technologies and scientific understanding of their manufacture and formulation have sustained the consequent booming commercialization of monoclonal antibodies therapeutics (mAbs). [Lowe et al. 2011]

SYNOPSIS: ANTIBODY INSTABILITY

Antibodies are large multi-domain proteins with similar tertiary structures. The multitude of disulfide bonds and tight domain–domain interactions in antibodies make render them relatively stable and more resistant to moderate thermal stress compared to other proteins [Wang et al. 2007]. However, similar to most proteins, many human monoclonal antibodies display poor biophysical properties, such as *low stability* and a *propensity to aggregate*. The factors which contribute to instability and tendency towards aggregation are complex, act simultaneously and are not fully understood [Lowe et al. 2011].

Examples of physical and chemical instabilities regard phenomena such as: denaturation, aggregation, surface adsorption, deamidation, oxidation, isomerization or fragmentation. Due to their highly specific action, there is a significant difference in the primary sequence among different antibodies; therefore, the relative severity of these degradation pathways needs to be studied case-by-case. The most frequent manifestations of antibody instability include: aggregation, deamidation, and isomerization [Wang et al. 2007, Singh et al. 2009].

Due to differences in their stability, some antibody products are formulated in a liquid form, while others are lyophilized. Commercial antibody formulations are either neutral or weakly acidic, indicating the optimal pH range for most antibodies. Among the additives employed to suppress antibody aggregation, surfactants have been used in most of these antibody products. As for the excipients, aimed to assure the product stability over time, the two most commonly used are sucrose and NaCl; they have been equally successful in liquid formulations, while sucrose is preferable to NaCl for lyophilized formulations [Ohtake et al. 2011]. Nonetheless, a case-by-case study of appropriate formulation excipients and buffering agents is due, since antibodies differ at structural level.

Major issues, regarding the antibody formulation challenging task, have emerged: (1)

the development of stable high-concentration formulations and (2) the management of the high-concentration associated viscosity of these formulations. However, the available stability data found in the literature and the information on the commercial antibody products suggest that antibody formulation, compared to other protein drugs, although challenging, is relatively manageable [Wang et al. 2007, Lowe et al. 2011, Zölls et al. 2012].

Although more stable than other proteins, antibodies are subjected to a variety of physical and chemical degradation pathways, which can be observed in liquid, frozen, and lyophilized states. For instance, the glycosylation state of an antibody can significantly affect its degradation; however, in many cases, multiple degradation pathways can occur simultaneously and the degradation mechanism may change depending on the stress conditions. These degradation pathways are divided into two major categories: (A) physical and (B) chemical instabilities [Wang 2005, Wang et al. 2007, Wang et al. 2010] (and references therein).

Understanding how these mechanisms act (and probably interact) is fundamental knowledge because it aids data interpretation, from protein formulation development, industrial process scale-up and manufacturing, choosing the most appropriate analytical tools for stability testing, to ensuring the adequacy of the procedures for stability tests or batch release tests and, ultimately, to ensuring the ***quality*** *(purity and stability) of the finished drug product. Moreover, the development and the implementation of a Process Analytical Technology (PAT) [Hinz 2006] working side-by-side with Design of Experiments (DOE), is strongly suggested by the FDA, aimed to make the therapeutic drugs development more manageable, more time – efficient and more cost-effective [DiMasi and Grabowski 2007].*

A. PHYSICAL INSTABILITY OF ANTIBODIES

There are two major, correlated, pathways through which antibodies display physical instability: *denaturation* and *aggregation*. Protein denaturation leads to aggregation, but aggregation is not necessarily dependent upon antibody denaturation, since it can occur even among native antibody molecules [Cromwell et al. 2006]

DENATURATION

Antibodies can denature under a variety of conditions, including temperature change, shear, and various processing steps; however, antibodies appear to be more resistant to thermal stress compared to other proteins. Shear stress, as well as the lyophilization process, may cause antibody denaturation [Wang et al. 2007]. An example of forced antibody degradation which occurs during lyophilization was illustrated by [Hawe et al. 2008], employing AF4 and SEC coupled with tryptophan intrinsic fluorescence to demonstrate the various extents of protein denaturation.

AGGREGATION

Antibody aggregation is the most common manifestation of physical instability and was extensively discussed in the dedicated Chapter 1 of this dissertation. One of the greatest challenges in therapeutic protein formulation development is the *concentration dependent antibody aggregation* because, in order to be effective, the antibody formulations require high concentrations (>100 mg/mL in liquid formulations) [Lowe et al. 2011].

Increasing the antibody concentration increases the aggregation propensity. Protein aggregates generally have reduced activity and, more worrisome, greater immunogenicity potential because of the multiplicity of epitopes and/or conformational changes [Wang et al. 2007] compared to the native monomeric form.

Antibody aggregates can easily form both in liquid and solid states, under a variety

of conditions. The protein–protein interactions, which ultimately lead to protein aggregation, are influenced by both *diffusion rate* and *geometric constraints* of the interaction sites, therefore are tightly correlated to protein concentration changes, viscosity, ionic strength, pH, and temperature [Saluja and Kalonia 2008, Mahler et al. 2009]. These factors impact greatly on the aggregation extent. Other conditions known to induce protein aggregation include: shaking (can accelerate antibody precipitation), long-term storage, freeze-thaw process [Hawe et al. 2009] and lyophilization process [Hawe et al. 2008].

Lyophilization may induce different *extents* of antibody aggregation, as well as different aggregate *types* (from non covalent- linked monomers and/or even disulfide linked aggregates). Furthermore, antibody aggregation is a common phenomenon during storage in a lyophilized state [Wang 2005].

Thermal treatment (high temperature) is known to accelerate the aggregation process in antibodies, nevertheless, low temperature storage is believed by [Wang et al. 2007] to reduce the hydrophobic interaction (the major force in protein folding) therefore leads to the formation of high molecular weight species. For instance, a well known example is the case of reversible aggregation in serum Cryoglobulins, which precipitate at temperatures below normal body temperature (37°C) and dissolve again if the blood is heated.

Closely related to the low-temperature effect, the *freeze-thaw* process often induces protein aggregation; nonetheless, it does not pose a threat, partly due to the reversibility of antibody aggregates [Wang et al. 2007].

In this dissertation, the reversible freeze/thaw-induced aggregation phenomenon of an IgG_1 type antibody was monitored by HF5-UV in sub-chapter 4.1.3 and, employing the same self-associated antibody, the performance of HF5-UV-MALS was compared to SEC, the benchmark in QC of antibodies, in sub-chapter 4.1.6. In the latter sub-chapter, a wide MW and size range of antibody aggregates was monitored over time and MW-characterized by online MALS detection.

Several protein aggregation mechanisms have been proposed by [Philo and Arakawa 2009] and will be discussed in a separated sub-section, further on in this chapter.

B. CHEMICAL INSTABILITY OF ANTIBODIES

There are several types of chemical degradation pathways which cause antibody instability, which – based on the site of changes – may or may not lead to the loss of antibody activity [Wang et al. 2007].

DISULFIDE FORMATION/EXCHANGE

Disulfide bond formation/exchange is likely the most frequent cross-linking pathway causing chemical aggregation during the various processing steps of antibody formulation development. Furthermore, storage often leads to disulfide-based aggregation [Wang et al. 2007].

DEAMIDATION

This chemical degradation pathway has been widely reported in literature and is so frequent that purified antibody formulations may contain many deamidated forms [Wang 2005].

ISOMERIZATION

Similar to deamidation, the relative rate of isomerization can be influenced strongly by steric effect; the most common isomerization pathway in antibodies is the formation of iso-aspartic acid, from direct isomerization of aspartic acid (Asp), as well as from hydrolysis of the pH-dependent succinimide intermediate [Wang et al. 2007].

OXIDATION

Although not as prevalent as deamidation and isomerization in antibodies, oxidation of amino acid (AA) residues (such as: Met, Tyr, Trp, His, and Cys) can easily occur during storage.

FRAGMENTATION

Fragmentation is a chemical degradation pathway that can easily occur in antibodies even during production processes. A variety of process conditions may accelerate it, for instance: acidic or basic treatment, thermal treatment, freeze/thaw, and storage. The most probable sequences leading to fragmentation in proteins are Asp-Gly and Asp-Pro; however, there are other sequences which can also experience cleavages, like Asn-Ser. Fragments types include monomer species that have lost a light chain (M-LC), a F_{ab} arm (M-F_{ab}), a heavy chain (HC) and the light-chain (LC). Though less commonly, fragments can also be represented by antibody subunits resulting from both peptide and/or disulfide bond cleavage. Furthermore, antibodies are also prone to (UV) radiation-induced cleavages [Wang et al. 2007] (and references therein).

In this dissertation, the presence of fragments of IgG_1 type of antibodies was observed during the exploratory study described in sub-chapter 4.1.4, probably caused by either processing or storage conditions (freeze/thaw). Furthermore, in the same study, it was shown how the specific but undesired UV absorption of the mobile phase (phosphate buffer) can hinder the detection of antibody fragments.

SYNOPSIS: THERAPEUTIC DRUGS FORMULATION

The most obvious and common solution to the antibody instability (ultimately leading to antibody aggregation) is to increase conformational and colloidal stability by changing the drug product *formulation*. The antibody formulation development involves simultaneous variation of multiple parameters (like ionic strength and pH) and the addition of excipients (such as amino acids, sugars, and detergents) [Lowe et al. 2011] (and references therein). Since antibodies are typically prepared in a wide range of formulations, high-throughput methods for structural and colloidal stability analyses, as well as accelerated stability studies are currently required during

therapeutic drug formulation, aimed to explore the optimal combination of parameters. The formulation development can take a significant toll on time, product and expenses. Nonetheless, these current needs led to the development of higher-throughput methods for analysis [Lowe et al. 2011] (and references therein) and more efficient approaches, like the Design of Experiments implementation in the formulation development.

A. LIQUID ANTIBODY FORMULATIONS

Given that the antibody structure itself allows it, liquid dosage form is generally preferable to lyophilized products because it is easier to administer and less expensive to manufacture. Half of the commercial antibodies are stable enough to be formulated in a liquid form [Wang et al. 2007].

EFFECT OF PROTEIN CONCENTRATION

A previously mentioned, the concentration-dependent protein aggregation is the greatest challenge to developing high-concentration protein formulations, since a relatively large amount of antibodies needs to be dosed to achieve any therapeutic effect (otherwise, a large volume of antibody preparation has to be infused). The solubility of antibodies does not pose issues, since it seems to be relatively high and excipients such as surfactants have been effective in increasing it even further. The decrease in antibody solution viscosity is achieved by adding sufficient amounts of NaCl, though even adjusting the formulation pH could produce a similar effect [Wang et al. 2007] (and references therein).

From the analytical point of view, high protein concentration is a problem, as well. In SEC and FFF, both chromatographic flow-based separation systems, the quantification of aggregates levels usually involves not only sample dilution prior to analysis (because high volumes are required in order to provide robust results), but

also a high dilution during the separation itself. Since the sample dilution may induce the disruption of high MW species, it also leads to potential inaccurate aggregates quantification, as reported by [Gabrielson et al. 2007, Arakawa et al. 2010, Carpenter et al. 2010], therefore requiring orthogonal methods for results validation.

In this dissertation, a phenomenon similar to the concentration effect was observed (though in a concentration range much lower than typical antibody formulation) during the study discussed in sub-chapter 4.1.5, where an IgG1 type antibody displayed decreasing aggregates levels, proportional to the injected amount. Other sample loading tests have been performed in order to establish the HF5 overloading limit, a critical parameter given the fact that HF5 is a miniaturized separation device, discussed in sub-chapters 4.1.3 and 4.1.4.

Effect of Formulation pH

The determination of a stable formulation pH is often the starting point of formulation development. The pH has a known effect on the antibody stability, depending on the formulation composition, stress conditions and even antibody concentration, just like for other proteins. Formulation pH may have an effect of the (a) physical stability of antibodies, because it alters the number and distribution of charges on the protein surface, as well as on (b) chemical stability, playing a critical role in controlling many degradation pathways (such as disulfide bond formation/exchange, deamidation, fragmentation and isomerization). Oxidation may even be inhibited by adjusting the pH [Wang et al. 2007] (and references therein).

The formulation pH has to be adjusted in order to balance all the potential antibody pathways leading to degradation/aggregation. The optimum pH value depends on the AA sequence of the antibody; nonetheless, an acidic pH appears to be optimum for the antibody majority. The pH value appears to be an issue even when performing antibody stability tests, therefore depends on the analytical method chosen for these tests [Wang 2005, Wang et al. 2007], which will be discussed further on.

Effect of Buffering Agents

Both the type and concentration of a buffering agent may affect the stability of proteins; therefore, their combination needs to be carefully considered. Choosing the optimal buffering agent can potentially achieve both pH control and stabilization of antibodies [Arakawa et al. 2010]. Seldom, a buffering agent optimal for one antibody may be harmful to another [Wang et al. 2007]. The role of the buffering agent, aside from maintaining the pH stable, is to shield proteins by charge, therefore suppress aggregation. Moreover, as states before, the addition of salts (the most common, NaCl) with the purpose of decreasing the formulation viscosity, also has a shielding effect. The effects of the buffering agents and salts and their concentration on the separation process and antibody aggregates quantification will be discussed further on.

Effect of Formulation Excipients

One of the most convenient and effective methods employed to achieve antibody stability (and suppress/reduce aggregation) in solution is the use of formulation excipients. A plethora of formulation excipients have proven to be effective in protecting the physical and chemical stability of antibodies under different processing conditions and storage, including sugars, polyols, amino acids (arginine), surfactants and polymers [Wang et al. 2007] (and references therein).

Among them, sugars and surfactants are the most commonly used. While they have proven to be useful in reducing shaking/stirring-induced aggregation, surfactants may have negative effects during long-term storage due to the presence of residual level of peroxides (which have been shown to cause protein oxidation), therefore should be carefully considered [Wang et al. 2007]. The addition of common antibody formulation excipients in the carrier solutions employed during the characterization of antibody formulations will be discussed further on.

B. LYOPHILIZED ANTIBODY FORMULATIONS

Lyophilized formulations share common traits with the liquid formulations (previously described). However, they pose some particular issues, as well, since the lyophilization process itself can promote degradation pathways and lead to protein aggregation.

EFFECT OF FORMULATION pH

Although a pH of the solid state could not be defined for lyophilized formulations, the pH of the liquid formulation which is freeze-dried can have a potential effect on the stability of the lyophilized formulation. Therefore, the same precautions need to be taken (in fact, even more) in adjusting the formulation pH by employing various buffering agents, which, consequently, may have an effect on the antibody stability both during lyophilization and storage of the lyophilized products [Wang et al. 2007].

EFFECT OF PROTEIN CONCENTRATION

Often, increasing the protein concentration tends to increase the stability of the protein during lyophilization. However, antibodies do not seem to follow this trend and many of them have shown decreased stability both during lyophilization and storage at high concentrations [Wang et al. 2007] (and references therein).

PRODUCT QUALITY ASSURANCE: PURITY

ANALYTICAL METHODS EMPLOYED FOR ANTIBODY FORMULATION CHARACTERIZATION: SEPARATION AND PROTEIN AGGREGATES LEVELS QUANTIFICATION

SEC has been the benchmark analytical system for determining the composition of protein samples, thanks to the robustness of the data, the wide range of both HPLC systems and commercially available SEC columns and the time-efficient data generation [Arakawa et al. 2010]. Many published examples over the past 20 years, showing the use of SEC for the characterization of mAb formulations and detection of mAb aggregates, as well as the effects of changing buffer composition, pH, use of excipients, and mutations to the antibody sequence, have led to SEC implementation in the QC protocols for antibody formulations batch release [Lowe et al. 2011] (and references therein).

Although a very robust system, which is the main reason for SEC implementation in QC assays, some of the drawbacks of SEC include: compromising between the dynamic range of analysis and the resolution, the possible loss of large aggregates (physically filtered out of the sample, either via the column frits or interaction with the column matrix) and possible sample interactions with the column matrix [Arakawa et al. 2010, Engelsman et al. 2011]. Moreover, when analyzing by SEC, protein samples are often *diluted* in a buffer which usually is quite different from the final formulation that has been chosen for antibody production and storage [Zölls et al. 2012].

Data interpretation, choosing the most appropriate column matrix and the adequate mobile phase, together with employing appropriate known standard samples require a careful consideration [Carpenter et al. 2010, Lowe et al. 2011, Carpenter et al. 2012]. Incomplete sample recovery, compromised selectivity and resolution and inaccurate estimation of aggregates levels are the main reasons why complementary analyses are required when SEC fails.

It is a generally acknowledged fact that, in order to accurately characterize a protein formulation (identification, quantitation, as well as size- and MW-characterization of all present species), it is absolutely vital to employ analytical methods which allow such analyses in an environment as close as possible to the antibody formulation buffer.

First of all, the dynamic ranges in HF5 in virtually unlimited, thanks to the opposite elution order with respect to SEC. This feature is very appealing for the separation of antibody aggregates in a very wide size and MW range (see Chapter 1).

In this dissertation, the possibility to validate an HF5-UV method for the separation of protein mixtures was discussed in sub-chapter 4.1.1. Parameters like: results repeatability (first level of precision), resolution, efficiency, selectivity and robustness show the advancements achieved with a commercial instrumentation when compared to data found in literature on hollow fiber prototypes.
SEC and HF5 performance was compared in the studies described in sub-chapters 4.1.2 (standard protein mixture) and 4.1.6 (IgG1 type antibody). In both sub-chapters, HF5 superiority in terms of selectivity is another appealing feature worth considering for this type of application. Moreover, it was shown how online coupling with MALS can enhance the analytical information.

It is a known fact that the SEC columns offer a limited operational range in terms of pH, as well as aggregates sizes and MW (depending on the material and the size of the pores of the column packing). Even though the choice of commercial hollow fibers is more limited (as material type and MWCO), the same HF5 membrane type (for instance, PES material) can be employed for a wide spectrum of applications (protein aggregates separation included) because they operate in the whole pH range and are highly resistant. Furthermore, since the stationary phase is eliminated in HF5, one does not have to consider possible column packing-mobile phase interactions, which are another SEC limiting factor. In addition, hollow fibers are not

only less expensive than SEC columns, but can also be employed as disposable devices, thus avoiding sample carry-over or contamination.

In order to maintain the sample integrity, thus the aggregates levels, it is highly important to separate in a mobile phase whose composition is as close as possible to the formulation of a given antibody and the FFF (HF5) versatility in terms of carrier solution composition allows doing so.

In this dissertation, the effect of the pH of the carrier solution on the antibody stability and on the separation HF5 performance was discussed in sub-chapter 4.1.4, which describes an exploratory study performed on an IgG_1 type antibody.

Next, since the buffering agent and the (salts) concentrations have shown a great influence on antibody stability during formulation, it is expected for them to influence the antibody behavior during their characterization (and separation), as well.

In this dissertation, an exploratory study employing HF5 coupled with UV detection for the separation of different IgG_1 type antibodies is described in sub-chapter 4.1.4, showing the influence of the buffering agent and its concentration on the separation process, as well as on the sample stability.

The carrier solution ionic strength is another important separation feature in HF5 because it controls (by charge shielding) the protein interactions during separation, therefore influences protein stability and consequently the sample recovery (proteins interacting with the separation device) and the aggregates levels (protein-protein interactions).

In this dissertation, different buffering agents and concentrations thereof, therefore having different ionic strengths, were explored in sub-chapter 4.1.4 with the purpose of observing their influence on antibody stability during HF5 separation and identifying the optimal combination for the aggregates levels quantification of an IgG_1 type antibody.

SEC and HF5 performance is compared for the separation of an IgG1 type antibody in sub-chapter 4.1.6, including aspects like sample recovery, identification of different types of high MW antibody aggregates and the reversibility of the aggregation process (which was monitored by UV-MALS detection).

Seldom, the optimal a buffering agent for one antibody, may be harmful to another.

In this dissertation, an exploratory study involving different buffering agents (phosphate buffer, citrate buffer and a combination of the two), different concentrations and different IgG1 type antibodies was described in sub-chapter 4.1.4; the study shows differences among antibodies behavior during their separation.

While the addition of salts (NaCl is the most common) is required for a complete sample recovery, it is not a guarantee. In fact, SEC requires very high NaCl concentrations (300-500 mM) [Arakawa et al. 2010] (and references therein), with the risk of disturbing the aggregates levels and achieving the opposite effect: incomplete sample recovery. On the other hand, HF5 can achieve complete sample recovery even at lower salt concentrations, added to carrier solutions whose composition is much closer to the antibody formulation (with a better chance of reflecting the true sample composition).

In this dissertation, the HF5 performance for the separation of an IgG1 type antibody was compared to SEC when employing carrier solutions containing different amounts of NaCl and discussed in sub-chapter 4.1.6. In the same sub-chapter, two carrier solutions with a composition similar to the antibody formulation buffer were employed for the HF5 separation and characterization of IgG1 type antibodies.

Moreover, the influence of different types of salt (NaCl and $MgCl_2$, both known chaotropic agents) was observed during the HF5 separation of different IgG1 type antibodies and discussed in sub-chapter 4.1.4.

The addition of excipients (such as sugars or surfactants) to the carrier solution in HF5, in

order to render it more sample-compatible (similar to the formulation buffer), was explored, although results are not shown in the experimental section of this dissertation. Sugars tend to modify the rheological properties of the carrier solution, causing instrumental setbacks and clogs in the HPLC capillaries, while surfactants, as they pass through the FFF system components, have a tendency to foam, therefore can only be employed at very low concentrations (with the risk of not being effective enough to suppress antibody aggregation). The use of low foaming surfactants may be a temporary solution, however, it may have unexpected effects on the antibody stability if they are different from the one used in the original formulation. High concentrations of surfactants (if provided in the original antibody formulation) may lead to the formation on micelles, which impede the aggregates detection and quantification by MALS, since MALS detection does not discriminate them from protein aggregates.

PRODUCT QUALITY ASSURANCE: STABILITY

ANALYTICAL METHODS EMPLOYED FOR THERAPEUTIC PROTEIN STABILITY TESTS

Typically, therapeutic proteins (mAbs as well) are stored over several months between manufacture, filling, and clinical administration. As detailed previously, they are typically formulated at high concentrations (mAb formulations exceed 100 mg/mL, for subcutaneous administration). In order to understand the stability and aggregation tendency of particular mAb in a given formulation, accelerated stability studies are conducted during development, although stability tests are conducted on the finished products, before and even after commercialization [Lowe et al. 2011] (and reference therein). In fact, the FDA regulates the quality of biopharmaceutical drugs (in terms of product purity *and* stability), from development to commercialization.

The stability tests, although rigorously regulated by the FDA, are developed according to the ICH guidelines [ICH 2014] that are somewhat flexible (hence

guidelines, not *rules*), considering the particularities of antibodies, meaning that each test is antibody-customized. The short-term, as well as long-term stability of therapeutic proteins being at stake, suitable analytical tests are required on both liquid and lyophilized protein formulations, in order to monitor the behavior, identify and quantify (possibly discern between various types of) protein aggregates.

The *accelerated stability tests*, also called *stress tests*, whose purpose is to simulate harsh and inappropriate storage conditions, as well as deliberately induce the accelerated formation of aggregates (in order to understand the underlying causes, as well as simulate long-term storage), typically involve the incubation of the antibody formulation at defined temperatures, usually 4 and 40°C over several months. At defined time intervals, samples are removed and subjected to stability analyses. The presence of low MW fragments (degradation products) and high MW aggregates levels, as well as aggregation/degradation rates are measured against previously defined values and used to determine whether the antibody is appropriately stable over long periods of time [Lowe et al. 2011] (and references therein).

Nevertheless, the accelerated stability tests performed on therapeutic proteins (at room temperature or 5-8°C), may or may not be possible or accurate because the presence of complex and multiple degradation pathways – which may have different degree of temperature dependencies – are unpredictable, therefore may not be able to simulate the long-term behavior [Wang et al. 2010] (and reference therein).

In this dissertation, a short-term accelerated stability study conducted by HF5 coupled with UV and MALS detection on a modified protein, stored in lyophilized form (AvidinOX®), was discussed in sub-chapter 4.1.7. The protein aggregates, present at trace levels, were successfully quantified and their MW values were calculated by MALS. The same study also highlighted the miniaturization advantages regarding the decreased limit of detection of protein aggregates and the HF5 versatility regarding the carrier solution composition (the possibility of working in denaturing vs. native mobile phase), which made possible the

distinction and quantification of different types of protein aggregates (covalent vs. non-covalent).

The advantages of miniaturization of the HF5 separation device (employing a hollow fiber with a smaller inner diameter), coupled online with highly sensitive detection methods (intrinsic fluorescence detection and peptide bond absorption) were explored and discussed in sub-chapter 4.1.5. The study showed how the detection limit of antibody aggregates can be decreased to ng of injected sample, even in antibody formulations where the aggregates levels represented only a 2% (mass fraction) of the injected sample.

PROTEIN AGGREGATION MECHANISMS

As thoroughly discussed in Chapter 1, therapeutic proteins (mAbs included) exhibit a wide spectrum of aggregation phenomena, making it virtually impossible to find a single analytical method able to work well in all cases. Moreover, though less recognized, aggregates also exhibit highly different life spans, and their lifetime has important consequences for detection methods. Another major analytical challenge resides in the fact that the measurement itself may destroy or create aggregates and is a key determinant for appropriate method selection [Philo 2006]. Lastly, SEC capabilities are limited, though routinely employed as benchmark analytical method in QC practices, therefore the use of orthogonal techniques is vital for an accurate estimation of the aggregation extent. For this purpose, MALS and (intrinsic) fluorescence are often employed as detection methods during the extended characterization assays, although their implementation as QC methods is currently not possible [Gabrielson et al. 2007, Engelsman et al. 2011, Zölls et al. 2012].

A general understanding of the underlying aggregation mechanisms which occur during formulation development may actually help finding solutions for the aggregation issue, but is just as important in choosing the appropriate characterization methods and data

interpretation. An accurate determination of the extent and type of aggregates contributes ultimately to assuring the quality of the therapeutic drug.

Protein aggregation can occur through a number of distinct mechanisms or pathways, which are not mutually exclusive, therefore can act simultaneously on the same product, although usually one is dominant. A general understanding of the most frequent aggregation mechanisms may point development into the right direction (finding a good formulation, or a method to suppress and remove aggregates) or at least avoiding excipients and processes that are likely to make things worse. The following aggregation mechanisms were proposed by [Philo and Arakawa 2009, Wang et al. 2010] and reviewed by [Amani and Naeem 2013].

MECHANISM 1: REVERSIBLE ASSOCIATION OF THE NATIVE MONOMER

Mechanism 1 describes the intrinsic tendency of the native form of the protein to reversibly associate (aggregate). As the surface of the native protein monomer is self-complementary, it will readily *self-associate* to form reversible small oligomers.

There may be multiple "*sticky*" or complementary zones on the monomer surface and, when the protein concentration rises (or, generally, when the monomers find themselves closer to each other), progressively larger oligomers form, driven by the law of mass action. Over time and as their size increases, these larger aggregates often become irreversible. Due to multiple mechanisms acting at the same time, these irreversible aggregates may be formed through covalent bonds, like disulfide linkages. *Every known protein has an intrinsic tendency to self-associate; however, the aggregation propensity differs from one protein to another*.

For instance, insulin is the most commonly known example of a therapeutic protein which readily (and normally) associates to form reversible oligomers. Although the reversible insulin aggregates do not pose a threat due to their reversible nature, such association can have important consequences for bioactivity, information which led

to the development of important new therapeutic products [Philo and Arakawa 2009] (and references therein).

MECHANISM 2: AGGREGATION OF CONFORMATIONALLY-ALTERED MONOMER

Mechanism 2 is similar to Mechanism 1, but applies to native monomers with a very low propensity to reversibly associate. The first step of Mechanism 2 is a transient conformational change/partial unfolding of the monomer to a non-native state, characterized by a strong tendency to associate. At any given time, the non-native (aggregation-prone) fraction of protein will usually be quite small. Conformational changes and aggregation through Mechanism 2 will be promoted by *stress* (such as thermal, heat or freeze/thaw or shear stress), which may trigger the initial conformational change. Consequently, the aggregates formation will be suppressed by conditions that stabilize the native conformation. This aggregation mechanism does appear to be the dominant one for many proteins [Philo and Arakawa 2009] (and references therein).

In this dissertation, the reversibility of the self-association process between IgG_1 type antibody monomers, which have (most likely) suffered a conformational change due to freeze/thaw process and/or due to the fact that the sample was diluted in a buffer with a composition different from the formulation buffer, was monitored by HF5-UV-MALS (and SEC-UV-MALS) and discussed in sub-chapters 4.1.3 and 4.1.6.

MECHANISM 3: AGGREGATION OF CHEMICALLY- MODIFIED PRODUCT

As discussed previously in this Chapter, the chemical instability of proteins leads to a series of degradation pathways. Mechanism 3 is, in fact, a version of Mechanism 2, where the change in protein conformation is caused by modifications in the covalent structure, which lead to aggregation. Chemical changes may include degradation

pathways like oxidation, deamidation, or proteolysis and may induce the formation of new "*sticky*" patches on the surface, or even change the electric charge leading to reduced electrostatic repulsion between monomers.

A particular feature of this type of aggregation is that the aggregates will be enriched in the modified form. Nonetheless, improving the chemical stability of the monomer will reduce the aggregation extent. Importantly (and intuitively), chemically-altered aggregates can be particularly immunogenic [Philo and Arakawa 2009] (and references therein).

In this dissertation, the self-association process between monomeric units of an oxidized protein (AvidinOX®), which have (most likely) suffered a conformational change due to chemical instability, and/or promoted by the presence of degradation products, was monitored by HF5-UV-MALS and discussed in sub-chapter 4.1.7. The study showed that the AvidinOX® oligomeric species are stable over time and, thanks to the HF5 versatility, non-covalent, as well as covalent aggregates were discriminated, quantified and monitored over time.

MECHANISM 4: NUCLEATION-CONTROLLED AGGREGATION

Mechanism 4 is common mechanism for the formation of visible particulates or precipitates, a process which is similar to growing large crystals by adding micro-crystal "*seeds*" to a saturated solution. The critical nuclei are also sometimes called the "*seeds*" or "*templates*" for aggregate growth. When the native monomer has a low tendency to form small and moderately-sized oligomers (because is not thermodynamically favored), but an aggregate of sufficient size still manages to form, afterwards the growth of this "*seed*"/critical nucleus through addition of monomers is highly favored and the formation of much larger species is very fast. A special feature of Mechanism 4 is that the rate of formation of the large particles or precipitates usually exhibits a *lag phase* (whose length can vary from vial to vial within the same lot), that is, no particles or precipitates can be observed for a long

period of time, but then, all of a sudden, the large species appear and accumulate [Philo and Arakawa 2009] (and references therein).

The main advantage in understanding of the mechanism of aggregation is that it can help guide either upstream or downstream process development. For instance, when proteins are prone to conformational changes (partial or complete unfolding), mechanical stress and exposure to air or solid surfaces, which may lead to adsorption-induced unfolding, must be avoided at all costs. While the addition of "*generic protein stabilizers*"(sucrose, polyols and certain amino acids and salts), may aid against various environmental stresses that cause unfolding by suppressing aggregation via Mechanism 2, in fact will usually significantly increase aggregation via Mechanisms 1 and 4 [Philo and Arakawa 2009] (and references therein).

Some forms of aggregates may be worse than others. High order (high MW) native-like oligomers formed via Mechanism 1are more likely to cross-react with the native monomer, potentially neutralizing it, rather than induce an immune response. On the other hand, non-native aggregated monomers formed via Mechanisms 2-4 are more likely to have altered potency, as well as altered immunogenicity.

Understanding aggregation mechanisms is also important from the analytical point of view, because it may aid in choosing an optimal chromatographic *purification step* in order to remove aggregates during production or by applying pressure-induced aggregates disruption, provided that the chosen purification method does not generate new aggregates. Furthermore, knowing the type of aggregates may even help design a better chromatography method for aggregate removal [Philo and Arakawa 2009] (and references therein).

REFERENCES

[Amani and Naeem 2013] Amani S. and Naeem A. (2013). "*Understanding protein folding from globular to amyloid state. Aggregation: Darker side of protein*." Process Biochemistry **48** (11): 1651–1664.

[Arakawa et al. 2010] Arakawa T.; Ejima D.; Li T. and Philo J. S. (2010). "*The Critical Role of Mobile Phase Composition in Size Exclusion Chromatography of Protein Pharmaceuticals*." Journal of Pharmaceutical Sciences **99** (4): 1674-1692.

[Capelle et al. 2007] Capelle M. A. H.; Gurny R. and Arvinte T. (2007). "*High throughput screening of protein formulation stability: Practical considerations*." European Journal of Pharmaceutics and Biopharmaceutics **65** (2): 131-148.

[Carpenter et al. 2012] Carpenter J. F.; Cherney B. and Rosenberg A. S. (2012). *The Critical Need for Robust Assays for Quantitation and Characterization of Aggregates of Therapeutic Proteins*. Analysis of Aggregates and Particles in Protein Pharmaceuticals. Mahler H.-C. and Jiskoot W. Hoboken, NJ, USA, John Wiley & Sons, Inc.

[Carpenter et al. 2010] Carpenter J. F.; Randolph T. W.; Jiskoot W.; Crommelin D. J. A.; Middaugh C. R. and Winter G. (2010). "*Potential Inaccurate Quantitation and Sizing of Protein Aggregates by Size Exclusion Chromatography: Essential Need to Use Orthogonal Methods to Assure the Quality of Therapeutic Protein Products*." Journal of Pharmaceutical Sciences **99** (5): 2200–2208.

[Clinicaltrials.Gov]. Retrieved 17 February, 2014, from http://clinicaltrials.gov/ct2/results/map?term=monoclonal+antibodies.

[Cromwell et al. 2006] Cromwell M. E. M.; Hilario E. and Jacobson F. (2006). "*Protein aggregation and bioprocessing*." AAPS Journal **8** (3): E572–E579.

[Daugherty and Mrsny 2006] Daugherty A. L. and Mrsny R. J. (2006). "*Formulation and delivery issues for monoclonal antibody therapeutics*." Advanced Drug Delivery Reviews **58** (5-6): 686-706.

[DiMasi and Grabowski 2007] Dimasi J. A. and Grabowski H. G. (2007). "*The Cost of Biopharmaceutical R&D: Is Biotech Different?*" MANAGERIAL AND DECISION ECONOMICS (28): 469–479.

[Engelsman et al. 2011] Engelsman J. d.; Garidel P.; Smulders R.; Koll H.; Smith B.; Bassarab S.; Seidl A.; Hainzl O. and Jiskoot W. (2011). "*Strategies for the Assessment of Protein Aggregates in Pharmaceutical Biotech Product Development*." Pharmaceutical Research **28** (4): 920-933.

[Gabrielson et al. 2007] Gabrielson J. P.; Brader M. L.; Pekar A. H.; Mathis K. B.; Winter G.; Carpenter J. F. and Randolph T. W. (2007). "*Quantitation of Aggregate Levels in a Recombinant Humanized Monoclonal Antibody Formulation by Size-Exclusion Chromatography, Asymmetrical Flow Field Flow Fractionation, and Sedimentation Velocity*." Journal of Pharmaceutical Sciences **96**: 268–279.

[Hawe et al. 2008] Hawe A.; Friess W.; Sutter M. and Jiskoot W. (2008). "*Online fluorescent dye detection*

method for the characterization of immunoglobulin G aggregation by size exclusion chromatography and asymmetrical flow field flow fractionation." Analytical Biochemistry **378** (2): 115-122.

[Hawe et al. 2009] Hawe A.; Kasper J. C.; Friess W. and Jiskoot W. (2009). "*Structural properties of monoclonal antibody aggregates induced by freeze–thawing and thermal stress*." European Journal of Pharmaceutical Sciences **38** (2): 79-87.

[Hinz 2006] Hinz D. C. (2006). "*Process analytical technologies in the pharmaceutical industry: the FDA's PAT initiative*." Analytical and Bioanalytical Chemistry **384** (5): 1036-1042.

[Ich, 2014]. "*ICH Quality Guidelines: Impurities (Q3A-Q3B); Quality of technological Products (Q5A-Q5E) - stability (Q5C); Specifications (Q6A-Q6B)* ". Retrieved 25 February, 2014, from http://www.ich.org/products/guidelines/quality/article/quality-guidelines.html.

[Lowe et al. 2011] Lowe D.; Dudgeon K.; Rouet R.; Schofield P.; Jermutus L. and Christ D. (2011). "*Aggregation, stability, and formulation of human antibody therapeutics*." Advances in Protein Chemistry and Structural Biology **84**: 41-61.

[Mahler et al. 2009] Mahler H.-C.; Friess W.; Grauschopf U. and Kiese S. (2009). "*Protein aggregation: Pathways, induction factors and analysis*." Journal of Pharmaceutical Sciences **98** (9): 2909–2934.

[Ohtake et al. 2011] Ohtake S.; Kitab Y. and Arakawa T. (2011). "*Interactions of formulation excipients with proteins in solution and in the dried state*." Advanced Drug Delivery Reviews **63** (13): 1053-1073.

[Philo 2006] Philo J. S. (2006). "*Is Any Measurement Method Optimal for All Aggregate Sizes and Types?* ." The AAPS Journal **8** (3).

[Philo and Arakawa 2009] Philo J. S. and Arakawa T. (2009). "*Mechanisms of Protein Aggregation*." Current Pharmaceutical Biotechnology (10): 348-351.

[Reschiglian et al. 2005] Reschiglian P.; Zattoni A.; Roda B.; Michelini E. and Roda A. (2005). "*Field-flow fractionation and biotechnology*." Trends in Biotechnology **23** (9): 475–483.

[Saluja and Kalonia 2008] Saluja A. and Kalonia D. S. (2008). "*Nature and consequences of protein–protein interactions in high protein concentration solutions*." International Journal of Pharmaceutics **358** (1-2): 1-15.

[Singh et al. 2009] Singh S. K.; Rathore N.; Mcauley A. and Rathore A. S. (2009). "*Best Practices for Formulation and Manufacturing of Biotech Drug Products*." BioPharm International **22** (6): 32-48.

[Wang 2005] Wang W. (2005). "*Protein aggregation and its inhibition in biopharmaceutics*." International Journal of Pharmaceutics **289** (1-2): 1-30.

[Wang et al. 2010] Wang W.; Nema S. and Teagarden D. (2010). "*Protein aggregation—Pathways and influencing factors*." International Journal of Pharmaceutics **390** (2): 89–99.

[Wang et al. 2007] Wang W.; Singh S.; Zeng D. L.; King K. and Nema S. (2007). "*Antibody structure, instability, and formulation*." Journal of Pharmaceutical Sciences **96** (1): 1-26.

[Zölls et al. 2012] Zölls S.; Tantipolphan R.; Wiggenhorn M.; Winter G.; Jiskoot W.; Friess W. and Hawe A. (2012). "*Particles in therapeutic protein formulations, Part 1: Overview of analytical methods*." Journal of Pharmaceutical Sciences **101** (3): 914–935.

4.1.1. HF5 – UV PERFORMANCE EVALUATION FOR THE SEPARATION OF A STANDARD PROTEIN MIXTURE. HF5-UV METHOD VALIDATION TENTATIVE: SPECIFICITY, REPEATABILITY / FIRST LEVEL OF PRECISION, SELECTIVITY AND ROBUSTNESS.

This chapter is aimed towards deepening the understanding of the critical parameters which affect HF5 performance during the separation of protein formulations and to establish whether HF5 is a valid candidate for the QA (quality assurance) and QC (quality control) of biopharmaceutical products.

In particular, the following characteristics of the proposed HF5 method were investigated: method *specificity*, method *repeatability / first level of precision*, method *selectivity* and method *robustness*. All the experimental work described in this chapter is aimed on evaluating the HF5 separation performance of a mixture consisting in four standard proteins, with molecular weights (MW) ranging from 29 kDa to 670 kDa.

The method *specificity* was tested by comparing the separation profiles obtained during single proteins injections with the separation profile of the protein mixture containing the same proteins. The retention time value was the comparison/matching criteria.

Following the ICH guidelines [ICH 2014] regarding the validation of analytical procedures (Q2 (R1)), aimed to evaluate the quality of biopharmaceutical products, the method *repeatability* was studied employing a sequence of injections of the same sample (in terms of composition, amount and volume), performed under identical experimental conditions. The variability and the trends of the well known separation parameters (retention time, peak width at half height, peak symmetry and sample recovery) were monitored during subsequent analyses, as well as separation resolution and efficiency. The definitions and formulas of all analytical parameters employed for the method validation tentative in this sub-chapter were previously discussed in sub-chapter 2.4 (Chapter2).

The method *molecular weight-based selectivity* (S_{MW}) was calculated using the average values of the retention times, determined during the repeatability study, and the declared MW values.

Finally, the method *robustness* was evaluated by varying simultaneously two critical parameters: channel flow rate and cross-flow rate, therefore by varying of the ratio between them, v_c/v_x.

4.1.1.1. EXPERIMENTAL SETUP

HF5 was performed using an Agilent 1200 system (Agilent Technologies, Santa Clara, CA, USA) consisting in a 1200 Agilent degasser, a 1200 Agilent isocratic pump, a 1200 Agilent auto sampler, and a 1200 Agilent variable wavelength detector combined with an Eclipse® DUALTEC™ prototype FFF separation system (Wyatt Technology Europe, Dernbach, Germany). The software package Wyatt Eclipse @ ChemStation Version B.04.02 [98] (Wyatt Technology Europe) was used to control the FFF separation system.

The hollow-fiber was a 17 cm long polyether-sulfone (PES) fiber, type FUS 0181 available from Microdyn-Nadir (Wiesbaden, Germany) with the following characteristics according to the manufacturer: 0.8mm ID, 1.3mm OD and a molecular weight cut-off (MWCO) of 10 kDa, corresponding to an average pore size of 5 nm. The UV detector response at 215 nm was used to monitor the separation process.

4.1.1.2. SAMPLES AND REAGENTS

The carrier solution (mobile phase) was 50mM NH_4HCO_3 (Fluka) with a pH ~ 8.0. The carrier solution was prepared using water purified by an Elix 3 UV Water Purification System (Millipore, Billerica, USA) and filtered through a 0.1 μm-pore membrane.

The protein mixture stock solution contained 1 mg/mL of each of the following proteins: carbonic anhydrase (CAH), bovine serum albumin (BSA), apoferritin (Ferr) and thyroglobulin (Thy), all obtained from Sigma Aldrich (St. Louis, MO, USA) dissolved in the carrier solution, resulting in a total protein concentration of 4 mg/mL. The standard protein characteristics are summarized in Table 1. The same mixture has been used as a benchmark in various publications [Kang and Moon 2005,

Lee et al. 2009]. The stock solution was diluted 1:10 in carrier solution before injection in HF5.

Table 1 – Standard protein characteristics

Proteins	Abbreviation	Product code (Sigma Aldrich)	MW (kDa)	pI
Carbonic anhydrase (bovine erythrocytes)	CAH	C3934	29.0	5.9
Bovine serum albumin (bovine; fatty acid free, and essentially globulin free)	BSA	A3782	66.7	4.7
Apoferritin (equine spleen)	Ferr	A3641	481.2	4.4
Thyroglobulin (bovine thyroid)	Thy	T1001	660.0 – 690.0	4.5

Single protein samples were solutions of CAH, BSA, Ferr and Thy prepared at a concentration of 1 mg/mL (0.1%) in the carrier solution.

4.1.1.3. METHODS

The "*step gradient*" HF5 method evaluated in this chapter was developed as an improvement of a similar fractionation method proposed in a recent study [Johann et al. 2010] on the same standard protein mixture and using the same separation system. The radial field was reduced as the MW of the proteins increased by placing two steep flow field gradients to reduce as much as possible the time required for the fractionation, while considering the optimal retention factor for each protein. The radial field/cross flow rate (v_x) was maintained constant at 0.85 mL/min for 13.5 min, linearly decreased to 0.5 mL/min in 0.5 min and maintained constant at this value for 7 min. After the 7 min, the flow was linearly reduced to 0.4 mL/min in 0.2 min and maintained constant until the end of the run. The focus-inject step was performed for 4 min at a focus flow rate of 0.85 mL/min. The sample was focused at a distance of approximately 15% fiber length from the channel inlet.

4.1.1.4. RESULTS AND DISCUSSION

A. METHOD SPECIFICITY: PEAK IDENTIFICATION

The specificity of an analytical method is defined in the ICH guidelines as *"the ability to assess unequivocally the analyte in the presence of components which may be expected to be present. Typically these might include impurities, degradants, matrix, etc"*. This definition implies that the proposed method, in order to be specific, it should be able to ensure the identity of an analyte, its purity (regarding the presence of possible contaminants such as related substance test) and the accurate composition of the sample (quantitation of active substance and known impurities) [ICH 2014].

An amount of 2 µg of standard protein mixture (0.5 µg of each protein) was injected and the separation was monitored by a UV detector set at 215 nm for more sensitivity. The choice of two steep field gradients in the method (depicted in Figure 1, black trace) was made not only to speed up the fractionation process, but also in regard to the optimal retention factor for each protein. A field that is too strong not only has a negative effect on the performance of the separation itself, but also on the peak characteristics (shape and width) and on sample recovery. The radial flow was reduced as the MW of the proteins increased.

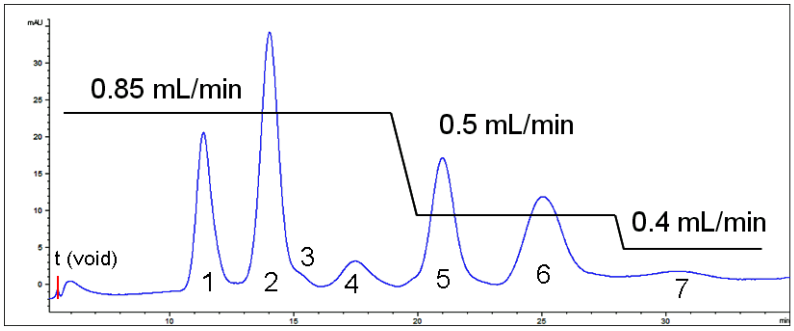

Figure 1 – Separation profile of the standard protein mixture (blue) at 215 nm. The black trace above the fractogram represents the cross-flow rate during the separation.

The fractionations performed on the single proteins (0.5 µg each) simplified the peak identification for the protein mixture and also ensured that there are no interactions between the proteins in the mix. The fractograms reported in Figure 2 show that the retentions times of the proteins in the mixture and the corresponding peaks in the single protein are almost a perfect match.

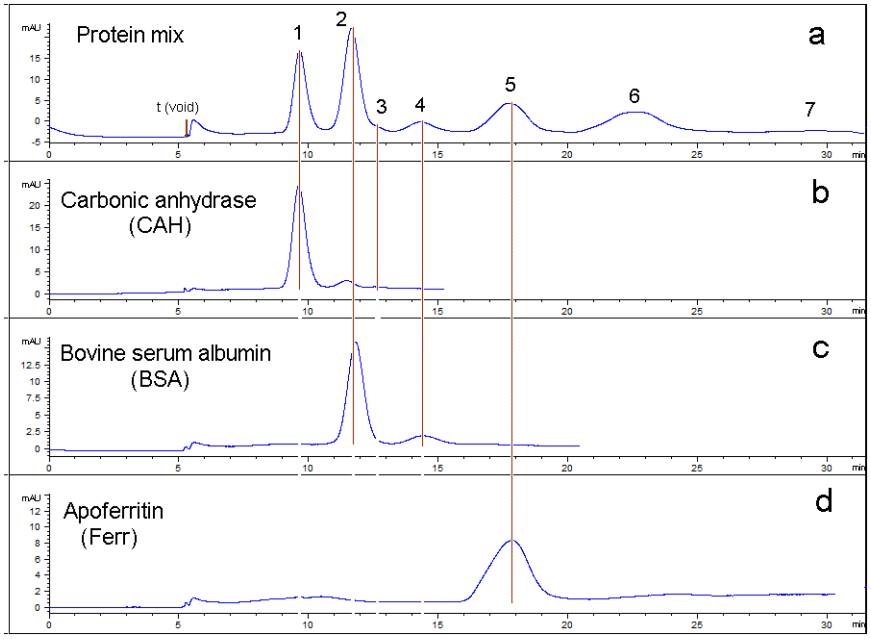

Figure 2 – Separation profiles at 215 nm corresponding to the standard protein mixture (a) and single standard proteins: carbonic anhydrase (b), bovine serum albumin (c) and apoferritin (d). The correspondence between the retention time values for specific proteins and their oligomers is traced in red

Comparing the separation profiles (retention time values) of the single proteins with the profile of the protein mixture, (0.5 µg each), the BSA monomer shoulder was identified as the CAH trimer (peak 3). Moreover, the CAH dimer is completely covered by the BSA monomer (peak 2) and, similarly, the Ferr dimer is covered by the Thy monomer (peak 6). There is little separation between the Thy dimer and the Ferr trimer (peak 7) because of the small difference in MW (about 100 kDa) and because the width of the peaks tends to increase with the MW.

B. METHOD REPEATABILITY (A.K.A. INTRA-ASSAY PRECISION OR THE FIRST LEVEL OF PRECISION)

The **precision** of an analytical method is defined in the ICH guideline as "*the closeness of agreement (degree of scatter) between a series of measurements obtained from multiple sampling of the same homogeneous sample under the prescribed conditions. Precision may be considered at three levels: repeatability, intermediate precision and reproducibility*".

The precision of an analytical procedure is usually expressed as the variance, standard deviation or coefficient of variation of a series of measurements. *Repeatability*, also called *intra-assay precision*, expresses the precision under the same operating conditions over a short interval of time [ICH 2014].

A total amount of 2 µg of protein (0.5 µg each protein) was injected repeatedly (in a series of 13 subsequent injections) in order to assess the *first level of precision* of the method and the results are reported in Figure 3. As it is evident from Figure 3, baseline separation for all proteins in the mixture was obtained in less than 30 min with a good peak shape. A high repeatability is also evident for the overlay of repeated runs, as further analyzed in the next paragraphs.

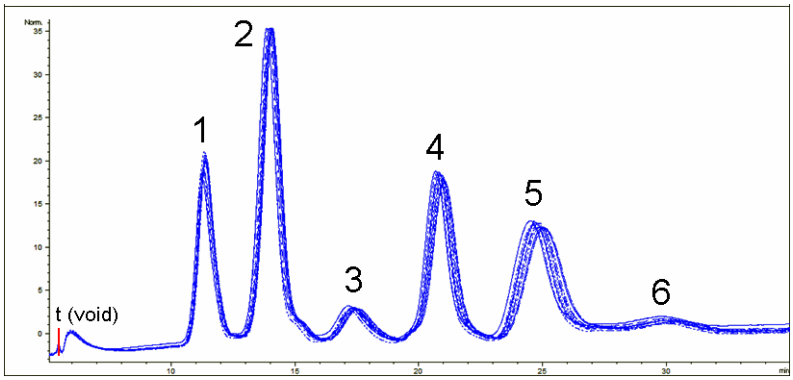

Figure 3 – Separation profiles of the standard protein mixture recorded at 215 nm, representing 13 subsequent injections. Separated species in eluting order: (1) CAH monomer; (2) BSA monomer; (3) BSA dimer, (4) Ferr monomer; (5) Thy monomer and (6) Ferr trimer

Only the completely separated species were considered, therefore the CAH trimer – which eluted as a shoulder of the BSA monomer – was not included in the repeatability study.

The repeatability of the method was evaluated by calculating the *average values* (mean values) of the following parameters: **retention time, peak width, peak shape, resolution between eluting species, efficiency** (in terms of plate height and number of plates per minute) and assessing the *standard deviation* (STDEV) and the *relative standard deviation* (RSD%) values.

C. RETENTION TIME AND PEAK WIDTH

Table 2 and 3 summarize the *average values*, the *standard deviation* and the *relative standard deviation (RSD %)* of the **retention time** and **peak width** over 13 subsequent runs. Peak widths at half height values were considered for the statistical analysis.

Table 2 – Retention time: average values, standard deviation and relative standard deviation over 13 subsequent sample runs

Retention time, tR (min)	Average	STDEV	RSD (%)
CAH monomer	6.34	0.053	0.843
BSA monomer	8.99	0.082	0.912
BSA dimer	12.40	0.134	1.084
Ferr monomer	15.87	0.112	0.707
Thy monomer	19.78	0.171	0.867
Ferr trimer	25.17	0.287	1.141

Table 3 – Peak width at half height: average values, standard deviation and relative standard deviation over 13 subsequent sample runs

Peak width (min)	Average	STDEV	RSD (%)
CAH monomer	0.667	0.007	1.032
BSA monomer	0.773	0.013	1.747
BSA dimer	1.189	0.034	2.878
Ferr monomer	0.966	0.036	3.694
Thy monomer	1.549	0.066	4.254
Ferr trimer	3.029	0.316	10.444

As the MW of the eluted proteins increases, there is a slight but distinct increase in peak width with increasing number of injections. Since there is no significant shift in the retention time (retention time RSD <2% for all the proteins), it suggests that this variation is more likely due to the protein stability over time and consequently to different carry-over effect related to non-specific interaction with channel walls, rather than loss of performance due to the device itself. In fact, the peak width RSD exceeds 4% only above the MW of Thy (the largest and less stable protein in the mixture).

D. SAMPLE RECOVERY

The sample relative recovery was calculated considering the largest peak area as having a 100% sample recovery (for each protein). Table 4 summarizes the *average values*, the *standard deviation* and the *relative standard deviation (RSD %)* of the sample recovery over 13 subsequent runs.

The sample relative recovery has a low variability for three of the eluted species (monomers of BSA, Ferr and Thy) with an RSD < 2%. From the fractograms reported in Figure 3 we can notice that the peaks become wider over time and their height decreases, even though the lowest recovery over 13 runs is about 89%, which is still relatively high for a biological sample. The recovery loss is most probably related to the protein stability over time.

Table 4 – Sample relative recovery: average values, standard deviation and relative standard deviation over 13 subsequent sample runs

Relative recovery* (%)	Average	STDEV	RSD (%)
CAH monomer	93.327	3.853	4.129
BSA monomer	98.518	0.670	0.680
BSA dimer	93.558	3.568	3.814
Ferr monomer	98.587	0.999	1.013
Thy monomer	97.047	1.538	1.585
Ferr trimer	88.963	7.402	8.320
* The largest area corresponds to 100% sample recovery			

E. PEAK SYMMETRY (SHAPE)

Even under optimal experimental conditions, the peak shape in FFF can appear skewed. The peak shape can be easily altered as a consequence of an overloading effect. This effect is present if: (a) a high amount of sample is loaded in the channel and the sample does not have enough physical space for the relaxation step; (b) the radial field is too strong and the sample is pushed too forcefully towards the channel wall causing peak tailing or (c) the channel flow rate is too slow and the sample band is left for too long inside the channel causing peak tailing. Even the MW of the protein appears to have an overloading effect, therefore a smaller amount of sample is required for proteins with high MW values [Moon and Myers 2000, Podzimek 2011].

The peak symmetry measures the peak tailing, which has a negative effect on the resolution. Some peak tailing is normal (symmetry <1.2), but a larger value is an indication of a damaged separation device or the presence of interactions between the analytes and the separation device [Podzimek 2011].

Table 5 summarizes the *average values*, the *standard deviation* and the *relative standard deviation (RSD %)* of the peak symmetry over 13 subsequent runs.

Table 5 – Peak symmetry: average values, standard deviation and relative standard deviation over 13 subsequent sample runs

Peak symmetry	Average	STDEV	RSD (%)
CAH monomer	0.773	0.014	1.858
BSA monomer	0.925	0.005	0.561
BSA dimer	0.804	0.059	7.387
Ferr monomer	0.917	0.018	2.010
Thy monomer	0.794	0.045	5.870
Ferr trimer	1.437	0.145	10.111

BSA and Ferr monomers show an almost Gaussian peak, with symmetry close to 1. CAH monomer, BSA dimer and Thy monomer peaks are slightly fronted (symmetry < 1) and the Ferr trimer peak is tailed (symmetry > 1). The peaks corresponding to

CAH, BSA and Ferr monomers have low peak shape variability (RSD% < 2), but the variability tends to increase for the higher MW species. This effect can be attributed to the instability of Thy, the standard protein with the highest MW, instability which can ultimately lead to non-specific interactions inside the separation device.

F. RESOLUTION

Resolution is a measure of the separation between two zones. The difference in the retention times of two components reflects the *selectivity* of the separation, while *peak width* (*w*) represents the zone spreading that is related to the *efficiency* of the process. Therefore, resolution is controlled by both selectivity and efficiency. A resolution value of 1 indicates that a 2% of the peak areas overlap; therefore the peaks are not completely separated. The complete separation is achieved at a resolution of 1.25. A better evaluation of the separation process can be achieved by calculating the specific resolution (R_{sp}), which takes into account the MW values of the separated species, as well as retention time and peak width [Podzimek 2011].

Table 6 summarizes the *average values*, the *standard deviation* and the *relative standard deviation (RSD %)* of **resolution** between eluting species over 13 subsequent runs.

Table 6 - Resolution: average values, standard deviation and relative standard deviation over 13 subsequent sample runs

Resolution	Average	STDEV	RSD (%)
CAH – BSA monomers	2.163	0.015	0.716
BSA monomer– BSA dimer	1.757	0.030	1.698
BSA dimer – Ferr monomer	1.899	0.066	3.489
Ferr – Thy monomers	1.829	0.049	2.673
Thy monomer – Ferr trimer	1.379	0.085	6.184

All calculated resolution values exceed the 1.25 value, meaning that all considered peaks are completely separated. Figure 4 reports the resolution average values between eluting species.

Resolution is influenced by both retention time and peak width but, since the retention time variability is not significant (RSD% < 2% for all proteins), we can only assume a great influence from the peak width on the corresponding resolution RSD% values.

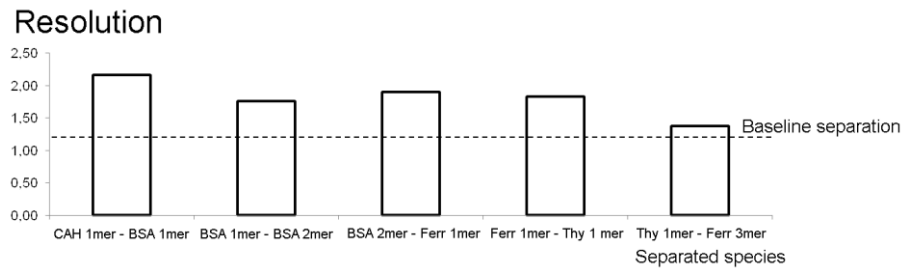

Figure 4 – Average resolution values between eluting species in the standard protein mixure

The resolution average values are always higher than 1.25, with peak symmetry very close to unity, which implies a baseline separation between the eluted species.

G. EFFICIENCY

The efficiency of a separation device is affected by the amount of sample band broadening during the separation process. It is known that, the longer the time an analyte spends inside the separation device, the greater its band broadening will be. Band broadening (also called zone broadening, zone spreading, zone dispersion or axial dispersion) is expressed in terms of *plate height* (*H*) or *number of theoretical plates* (*N*) [Schimpf 2000]. High efficiency is characterized by a large plate count, *N* and a small plate height, *H*. High selectivity means high resolution only if band broadening is minimal, since high selectivity can be ruined by excessive band broadening [Podzimek 2011].

Table 7 summarizes the *average values*, the *standard deviation* and the *relative standard deviation (RSD %)* of **efficiency** over 13 subsequent runs, expressed as plate height.

Table 7 – Separation efficiency (plate height, cm): average values, standard deviation and relative standard deviation over 13 subsequent sample runs

Plate height, H (cm)	Average	STDEV	RSD (%)
CAH	0.034	0.001	1.839
BSA	0.023	0.001	2.577
BSA dimer	0.028	0.001	4.536
Ferr	0.011	0.001	6.131
Thy	0.019	0.001	6.945
Ferr trimer	0.045	0.010	22.014

The separation efficiency for the standard protein mixture is also reported in Figure 5, expressed as number of plates/minute. These values were obtained by dividing the number of plates calculated for each peak by the corresponding retention time.

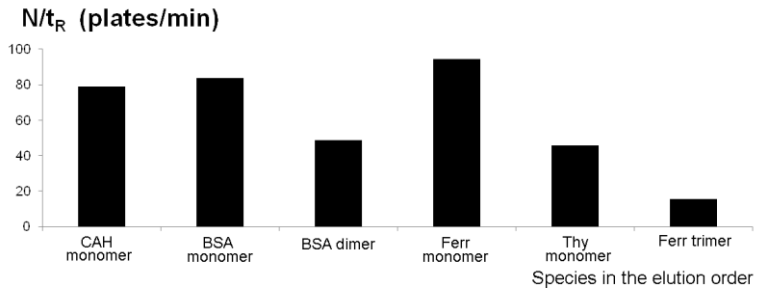

Figure 5 – Average efficiency values expressed as number of plates/minute

A significant increase in efficiency is observed with respect to previous HF5 methods reported in the literature [Park et al. 2005], the plate height values obtained in this study are about 10 times lower than the values reported for the same protein mixture.

H. METHOD SELECTIVITY

Selectivity is a parameter that quantifies the selective dispersion of the sample and represents the difference in retention time with MW of size. High selectivity means that there is a significant change in retention time with a small change in MW or size; therefore, selectivity can be expressed in terms of size (particle diameter, S_d) or MW (S_{MW}). Resolution is the decisive parameter when it comes to evaluate the separation performance, because it takes into account both selectivity and efficiency [Davis 2000, Podzimek 2011].

The FFF selectivity calculated for this study was the *MW-based selectivity* (S_{MW}), defined as the slope of the log (t_R) against the log (MW) plot, derived from the experimental retention time values for the eluted species and standard MW values for proteins reported in Table 1.

If a radial field gradient is to be used in the method, the relationship between the two logarithms is no longer linear. Therefore, when the "*step gradient*" method is employed (Figure 1 and Figure 6a), we can only calculate the selectivity for the first three eluting species, when a constant cross flow rate of 0.85 mL/min was applied.

In Figure 6b, a method, which uses a constant cross-flow rate, was employed to separate the same standard protein mixture, in order to calculate the selectivity for more than 3 separated species.

At a first glance, it can be noted that the peaks corresponding to proteins with higher MW (Ferr and Thy) are much wider, as a consequence of the stronger field (0.85 mL/min). Moreover, if the method in Figure 6b is to be applied, the elution time should be increased in order for the Ferr and Thy oligomers to be eluted.

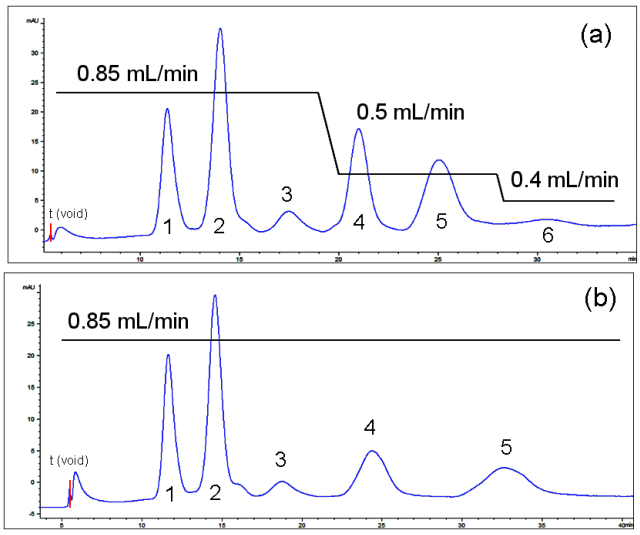

Figure 6 – Separation profiles of the standard protein mixture obtained employing the "*step gradient*" method (a) and the constant field method (b). The cross-flow rate is represented as a black line.

The separation performances of the HF5 methods illustrated in Figure 6 were compared and the results are summarized in Tables 8 ("*step gradient*" method) and 9 (constant field method).

The retention level, R_L (or level of retention) of each analyte was calculated, as proposed by [Wahlund 2013], a parameter similar to the capacity factor, k in column liquid chromatography, as well as the specific resolution, R_{sp} – a parameter which takes in consideration the MW of each species [Podzimek 2011] – previously discussed in sub-chapter 2.4 (Chapter 2) and in the Resolution section of this study, which can easily be applied to FFF separation methods.

As expected, employing a stronger (and constant) field for the whole duration of the separation, the method depicted in Figure 6b offers a higher R_L for all analytes, even though the maximum retention level should be kept, in general, in the range 5 – 50 to avoid band broadening and peak tailing [Litzen et al. 1993, Wahlund and Nilsson 2012]. In fact, at constant strong field, the peaks are broader (Figure 6b), but the specific resolution is very similar to the one offered by "step gradient" method (Figure 6a) because of the analytes eluting at retention times further apart from each other.

Table 8 – Separation performance of the "*step gradient*" HF5 method (Figure 6a), evaluated through the following parameters: analytes retention level, resolution and specific resolution

Peak	Species	MW (g/mol)	t_R (min)	Retention level (R_L)	Resolution (R_s)	Specific resolution (R_{sp})
1	CAH monomer	29000	6.34	14.1		
2	BSA monomer	66700	8.99	20.0	2.163	6.0
3	BSA dimer	133400	12.40	27.6	1.757	5.8
4	Ferr monomer	481200	15.87	35.3	1.899	3.4
5	Thy monomer	670000	19.78	44.0	1.829	12.7
6	Ferr trimer	1443600	25.17	55.9	1.379	4.1

Table 9 – Separation performance of the constant field HF5 method (Figure 6b), evaluated through the following parameters: analytes retention level, resolution and specific resolution

Peak	Species	MW (g/mol)	t_R	Retention level (R_L)	Resolution (R_s)	Specific resolution (R_{sp})
1	CAH monomer	29000	6.6	14.7		
2	BSA monomer	66700	9.5	21.2	2.16	6.0
3	BSA dimer	133400	13.8	30.6	1.93	6.4
4	Ferr monomer	481200	19.3	43.0	1.78	3.2
5	Thy monomer	670000	27.5	61.2	1.89	13.1

This comparison proves that an excessive retention level leads to compromising the separation performance, while the "*step gradient*" method is optimal for the separation of proteins in a wide MW range because it takes into consideration the optimal retention level for each protein in the standard mixture.

The selectivity plots corresponding to both methods are reported in Figure 7.

The equation for the log (t_R) vs log (MW) plot was: y=0.42x-1.05, where the slope (0.42) represents the selectivity of the "*step gradient*" method for the first 3 eluted species. From the calculated MW-based selectivity value and considering a globular shaped protein (d_H proportional to $MW^{1/3}$), the diameter-based selectivity was estimated. A high value of 1.23 was obtained.

The constant field method still provides a good selectivity (slope: 0.34) for the separation of 5 species, although band broadening is much more evident, compromising the separation performance.

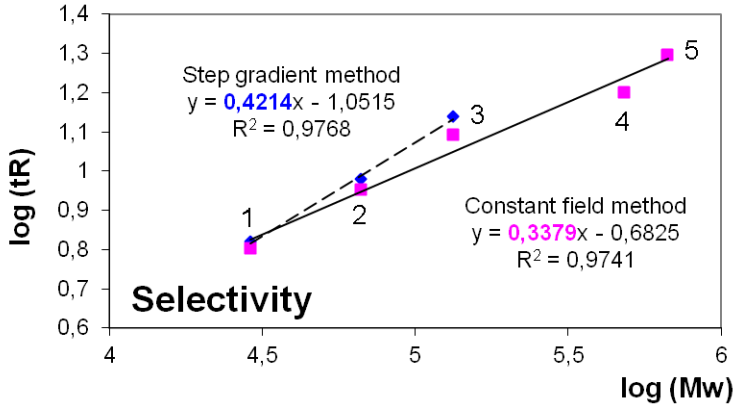

Figure 7 - Selectivity plots: log (tR) plotted against the corresponding log (MW). The slope represents the selectivity value

I. METHOD ROBUSTNESS

As defined in the ICH guidelines, the method robustness is "*a measure of the analytical method to remain unaffected by small but deliberate variations in method parameters and provides an indication of its reliability during normal usage*". Experiment design (fractional factorial design or Plackett-Burmann design) is common and useful to investigate multiple parameters simultaneously [Feng et al. 2012]. This result will help identify critical parameters that will affect the performance of the method [ICH 2014].

As an example, in this study we chose to vary the ratio between the channel flow rate (v_c) and the cross-flow rate (v_x), therefore changing two parameters simultaneously. Moreover, different operators were assigned to perform the required sample injections. Since the obtained results (fractograms) were not significantly different between the two operators, only one set of results is depicted in Figure 8.

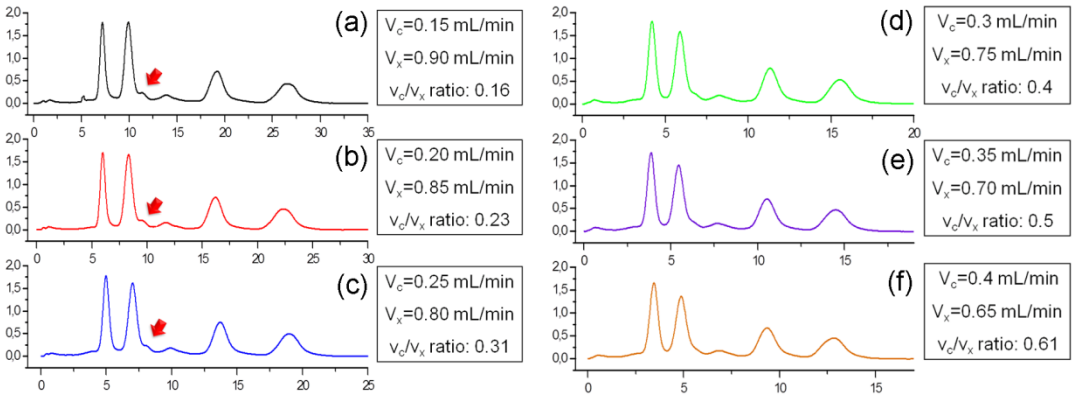

Figure 8 - Robustness of the method, evaluated by varying the ratio between the channel flow rate and the cross-flow rate

It can be noted that, as the ratio between the channel flow rate and the cross-flow increases, the peaks shape and width remain almost constant, for all species. The only differences between the graphs consist, as expected, in the retention time values because as the v_c/v_x ratio increases, the proteins elute faster. Moreover, the CAH trimer can be observed up to a ratio of 0.31 as a shoulder to the BSA monomer, after which it disappears into the peak tail.

4.1.1.4. CONCLUSIONS

The work presented in this chapter shows an improvement of the fractionation performance for protein analysis of an HF5 method, accomplished employing the Eclipse® DUALTEC™ FFF separation system prototype. The "*step gradient*" HF5 method proposed for the fractionation of the standard protein mixture has proved to be effective, reproducible, efficient and highly selective, showing promise as a candidate for the separation of complex protein mixtures.

The use of steep field gradients during sample elution served not only to reduce as much as possible the analysis time, but also considered the optimal retention factor for each protein in the mixture. By comparing the performance of the "*step gradient*"

HF5 method proposed for validation in this sub-chapter with an HF5 method which consists in applying a constant strong field thought the whole elution process of proteins in a wide MW range, it is proved that the first is superior to the latter. The "*step gradient*" method is faster and provides an optimal separation of even more protein species than the constant field method.

The method also proved to be robust, when the flow rates affecting the separation performance were simultaneously varied.

The work presented in this chapter represents a promising step towards the validation of an FFF method for the implementation as QA and/or QC method of biopharmaceutical products, even though many efforts have been and are currently employed towards this topic.

4.1.1.6. REFERENCES

[Davis 2000] Davis J. M. (2000). *Chapter 3: Band Broadening and Plate Height*. Field-Flow Fractionation Handbook. Schimpf M. E.; Caldwell K. and Giddings J. C. New York, Wiley**:** 49-70.

[Feng et al. 2012] Feng Y. W.; Ooishi A. and Honda S. (2012). "*Aggregation factor analysis for protein formulation by a systematic approach using FTIR, SEC and design of experiments techniques*." Journal of Pharmaceutical and Biomedical Analysis **57**: 143-152.

[Ich, 1997]. "*ICH Quality Guidelines, Validation of Analytical Procedures: Methodology (Q2(R1))*." Retrieved 23 February, 2014, from http://www.ich.org/products/guidelines/quality/article/quality-guidelines.html.

[Johann et al. 2010] Johann C.; Elsenberg S.; Roesch U.; Rambaldi D. C.; Zattoni A. and Reschiglian P. (2010). "*A novel approach to improve operation and performance in flow field-flow fractionation*." Journal of Chromatography A **1218** (27): 4126–4131.

[Kang and Moon 2005] Kang D. and Moon M. H. (2005). "*Hollow Fiber Flow Field-Flow Fractionation of Proteins Using a Microbore Channel*." Analytical Chemistry **77** (13): 4207–4212.

[Lee et al. 2009] Lee J. Y.; Kim K. H. and Moon M. H. (2009). "*Evaluation of multiplexed hollow fiber flow field-flow fractionation for semi-preparative purposes*." Journal of Chromatography A **1216** (37): 6539–6542.

[Litzen et al. 1993] Litzen A.; Walter J. K.; Krischollek H. and Wahlund K. G. (1993). "*Separation and Quantitation of Monoclonal Antibody Aggregates by Asymmetrical Flow Field-Flow Fractionation and Comparison to Gel Permeation Chromatography*." Analytical Biochemistry **212** (2): 469-480.

[Moon and Myers 2000] Moon M. H. and Myers M. N. (2000). *Chapter 13: Experimental Field-Flow Fractionation: Practices and Precautions*. Field-Flow Fractionation Handbook. Schimpf M. E.; Caldwell K. and Giddings J. C. New York, Wiley**:** 119-212.

[Park et al. 2005] Park I.; Paeng K.-J.; Kang D. and Moon M. H. (2005). "*Performance of hollow-fiber flow field-flow fractionation in protein separation*." Journal of Separation Science (16): 2043–2049.

[Podzimek 2011] Podzimek S. (2011). *Chapter 3: Size Exclusion Chromatography*. Light scattering, size exclusion chromatography and asymmetric flow field flow fractionation. Powerful tools for the characterization of polymers, proteins and nanoparticles. Wiley. Hoboken, New Jersey, Wiley**:** 99-206.

[Podzimek 2011] Podzimek S. (2011). *Chapter 5: Asymmetric Flow Field-Flow Fractionation*. Light scattering, size exclusion chromatography and asymmetric flow field flow fractionation. Powerful tools for the characterization of polymers, proteins and nanoparticles. Wiley. Hoboken, New Jersey, Wiley**:** 259-306.

[Schimpf 2000] Schimpf M. E. (2000). *Chapter 4: Resolution and Fractionating Power*. Field-Flow Fractionation Handbook. Schimpf M. E.; Caldwell K. and Giddings J. C. New York, Wiley**:** 71-78.

[Wahlund 2013] Wahlund K.-G. (2013). "*Flow field-flow fractionation: Critical overview*." Journal of Chromatography A **1287** (2013): 97– 112.

[Wahlund and Nilsson 2012] Wahlund K.-G. and Nilsson L. (2012). *Chapter 1: Flow FFF – Basics and Key Applications*. Field-Flow Fractionation in Biopolymer Analysis. Williams S. K. R. and Caldwell K. D. Netherlands, Springer Vienna**:** 1-21.

4.1.2. HF5 – MALS AND SEC – MALS PERFORMANCE COMPARISON FOR THE SEPARATION OF A STANDARD PROTEIN MIXTURE.

FFF SELECTIVITY FEATURE

In this chapter, the performance of an HF5 developed for the separation of the standard protein mixture is compared to size exclusion chromatography (SEC), the benchmark for the QA and QC of therapeutic proteins. The performance comparison was made under two different experimental conditions: (a) employing a high ionic strength (optimal/recommended for SEC) mobile phase and (b) employing a low ionic strength mobile phase.

The identification of the separated species was possible due to HF5 and SEC online coupling with UV and MALS detection. This coupling allowed the determination of the absolute MW of the separated species, as well as the calculation of the sample recovery at all times. The separation performance was evaluated in terms of efficiency (N), resolution (R_s) and MW-based selectivity (S_{MW}), as well as sample recovery. In particular, specific separation parameters like retention level (R_L) for HF5 and capacity factor (k) for SEC and specific resolution (R_{sp}) values were compared under each experimental condition. The definitions and formulas of all analytical parameters employed for the comparison in this sub-chapter were previously discussed in sub-chapter 2.4 (Chapter 2).

This study shows the potential of HF5-UV-MALS as orthogonal method for the validation of SEC results during the characterization of protein formulations. Furthermore, the HF5 device employed in this study (having double the length of a commercial, standard device) allowed the scale-up of the injection amount to levels comparable to the SEC requirements, in order to provide reliable and robust results (absolute MW).

4.1.2.1. EXPERIMENTAL SETUP

SEC and HF5 analyses were performed using an Agilent 1200 HPLC system (Agilent Technologies, Santa Clara, CA, USA) consisting in a degasser, an isocratic pump, an auto sampler and a variable wavelength UV detector, combined with an Eclipse® DUALTEC prototype separation system (Wyatt Technology Europe, Dernbach, Germany). The ChemStation version B.04.02 (Agilent Technologies) data system for Agilent instrumentation was used to set and control the instrumentation and for the computation of various separation parameters. The software package Wyatt Eclipse @ ChemStation version 3.5.02 (Wyatt Technology Europe) was used to set and control the FFF separation system. An Agilent 1100 UV-Vis variable wavelength detector operating at a wavelength of 280 nm was used as a concentration detector at all times.

An 18-angle MALS detector model DAWN® HELEOS™ light scattering detector (Wyatt Technology Corporation, Santa Barbara, CA, USA), employing a laser operating at a wavelength of 658 nm, was used in all experiments.

ASTRA® software version 5.3.2.14 (Wyatt Technology Corporation) was used to handle signals from the detectors (MALS and UV) and to compute the proteins MW and concentration values.

The SEC column was a WTC-0305S (Wyatt SEC protein column for MALS, 5µm coated silica beads 300Å, size 7.8x300mm), operating in the MW range from 5.000 to 1.250.000 g/mol.

The HF5 separation device was a 34 cm long cartridge assembled from two commercial (17 cm long) cartridges connected with a union piece, thus called "*double length*" HF5 cartridge. A separation device this size should allow the scale-up of the injection amount to levels comparable to the SEC requirements and provide reliable and robust results (absolute MW).

The hollow-fiber was a 34 cm long polyether-sulfone (PES) fiber, type FUS 0181

available from Microdyn-Nadir (Wiesbaden, Germany) with the following characteristics according to the manufacturer: 0.8mm ID, 1.3mm OD and a molecular weight cut-off of 10 kDa corresponding to an average pore size of 5 nm.

4.1.2.2. SAMPLES AND REAGENTS

The carrier solution/mobile phase was phosphate buffered saline (PBS) prepared at two concentrations, with different ionic strength values:

(A) High/optimal ionic strength PBS, recommended for SEC column by the manufacturer: 50 mM phosphate buffer supplemented with 50 mM NaCl at pH 6.8 (IS = 200 mM).

(B) Low ionic strength PBS: 10 mM PB supplemented with 25 mM NaCl at pH 7.0 (IS = 55 mM).

Both carrier solutions employed during this study were prepared using MilliQ water purified by an Elix 3 UV Water Purification System (Millipore, Billerica, USA) and filtered through 0.2 μm pore membrane sterile filter units (Millipore), at all times.
The protein mixture and the BSA solution at 1.0 mg/mL (0.1%) used for this study were prepared as described in the Samples and Reagents section of sub-chapter 4.1.1.2 (Chapter 4), but the dilutions were prepared in the PBS mobile phase.

4.1.2.3. METHODS

An amount of 40 μg of total protein (10μg of each of the following proteins: CAH, BSA, Ferr and Thy) was injected in the SEC column and the separations were performed at 0.5 mL/min flow rate at all times.

The HF5 methods evaluated in this chapter are similar to the "*step gradient*" HF5 method described in sub-chapter 4.1.1 (Chapter 4), but modified according to the mobile phase ionic strength, which is a known critical parameter in FFF.

The same protein amount (40 μg) was injected in the HF5 separation device during the focus-inject step, which was performed for 4 min at a focus flow rate of 0.85 mL/min. The sample was focused at a distance of approximately 15% fiber length from the channel inlet an eluted afterwards at a channel flow rate of 0.2 mL/min. The cross-flow rate was reduced as the MW of the proteins increased, by placing a steep field gradient to reduce as much as possible the time required for the fractionation, while considering the optimal retention factor for each protein. The HF5 methods for (A) and (B) mobile phases are summarized in Table 1.

Table 1 – HF5 flow rates timetable for the protein mix separations in high IS mobile phase (Method A) and low IS mobile phase (Method B)

Channel flow rate (v_c): 0.2 mL/min			
Focus flow rate (v_{foc}): 0.85 mL/min			
Focus – Inject duration: 3.5 min (0.5 min focus time before focus-inject step)			
Method	v_x start (mL/min)	v_x end (mL/min)	Duration (min)
A (high IS)	0.85	0.85	17.5
	0.85	**0.40**	**0.5**
	0.40	0.40	20.5
	0.00	0.00	2.0
Total analysis time: 42.5 min			
B (low IS)	0.85	0.85	15.5
	0.85	**0.40**	**0.5**
	0.40	0.40	20.5
	0.00	0.00	2.0
Total analysis time: 40.5 min			

4.1.2.4. RESULTS AND DISCUSSION

A. SEC AND HF5-UV-MALS IN HIGH IONIC STRENGTH MOBILE PHASE (200 mM)

The standard proteins mixture was first injected in SEC and HF5 and separated employing the mobile phase recommended for SEC column (IS = 200 mM). The BSA sample was separated by both SEC and HF5 under the same conditions as the protein mixture in order to check the correspondence between the retention times and to confirm that there are not interactions between the proteins in the mixture which might lead to difficulties in the peaks assignment.

The SEC separation profiles at 280 nm of the protein mixture and the BSA sample, confirming the identity of the BSA peak are reported in Figure 1 (a) standard protein mixture and (b) BSA sample and, respectively in Figure 2 for the HF5 separations.

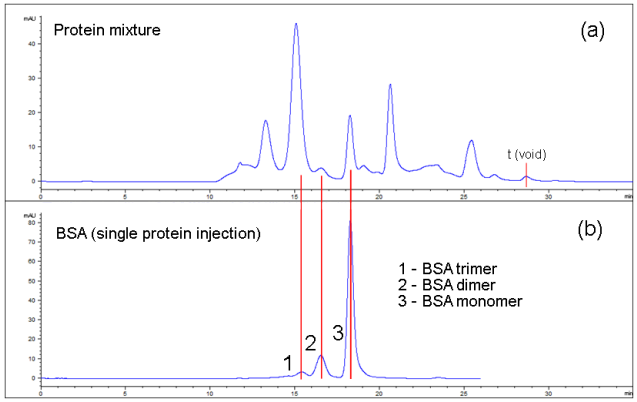

Figure 1 – SEC separation profiles at 280 nm for (a) standard protein mixture and (b) BSA sample. BSA oligomers identification based on the retention times and order of elution

Figure 1b shows that the SEC separation under optimal conditions allows the identification of 3 BSA oligomers. In Figure 1a, when the BSA is mixed with other standard proteins, only the BSA monomer and dimer are visible, while the BSA trimer elutes under the peak of a different species in the mixture (most probably the

Ferr monomer), even though the MW difference is considerable (MW 200 kDa for the BSA trimer vs. MW 481 kDa for the Ferr monomer). This indicates low separation selectivity, topic which would be discussed in the following paragraphs.

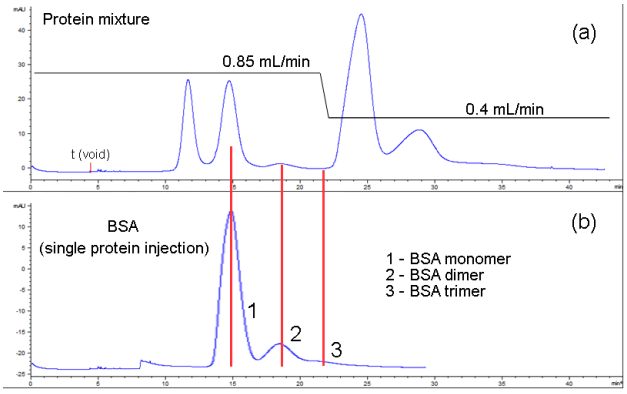

Figure 2 – HF5 separation profiles at 280 nm for (a) standard protein mixture and (b) BSA sample. BSA oligomers identification based on the retention times and order of elution. The black trace represents the cross-flow rates variation during the separation.

Figure 2b allowed the identification of 3 BSA oligomers, just as in SEC, only in reversed elution order. Figure 2a shows that in HF5, when the BSA is mixed with other proteins, the BSA trimer elutes right before the Ferr monomer. This indicates that the HF5 method is more selective compared to the SEC method.

Next, SEC and HF5 were coupled online with a MALS detector for the determination of the absolute MW. The separation profiles, as well as the calculated MW for each separated peak are reported in Figure 3 (SEC) and Figure 4 (HF5).

In both cases the peak assignment was based on the elution order and confirmed afterwards by the absolute MW values derived from MALS data. Both SEC and HF5 separation profiles show the presence of 7 separated species.

The peak identification, as well as other fundamental separation parameters computed by Astra® and ChemStation – with the purpose of comparing the SEC and HF5 performance – is reported in Table 2 for the SEC separation and Table 3 for the HF5 separation.

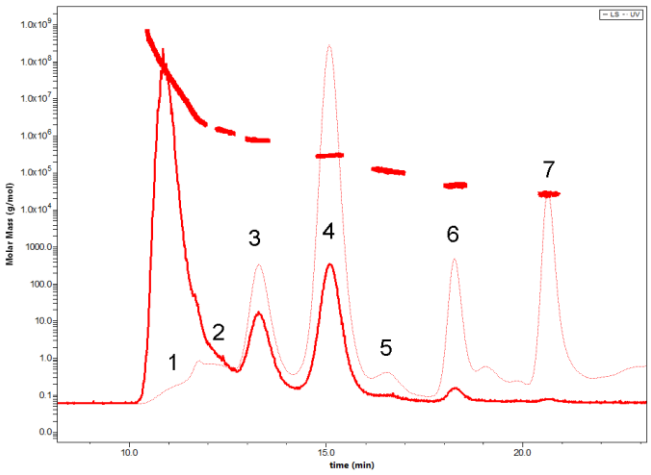

Figure 3 – SEC-UV-MALS elution profile of the standard protein mixture at 200 mM ionic strength. Rayleigh ratio at 90° represented as a thick line and UV signal at 280 nm represented as a dotted thin line.

All SEC peaks are slightly fronted, except for the first one, which represents a polydisperse population of Ferr and Thy oligomers. The complete separation is achieved in less than 30 minutes and the efficiency, expressed as number of plates, is very high. The SEC separation profile shows the presence of unidentified species eluting between the CAH and BSA monomers, which could be attributed to fragments of larger proteins broken or carrier over during the separation. These unidentified peaks may also indicate the malfunction of the SEC column.

Table 2 – SEC separation performance evaluation: separation parameters derived from data at optimal ionic strength (200 mM). Peak assignment in agreement with the calculated MW

Peak #	t_R (min)	Calculated MW (kDa)	Peak assignment	$w_{1/2}$ (min)	Peak symmetry	Plates number	Resolution (R_s)
1	11.75	>3000.0	Thy and Ferr oligomers	0.4311	5.81	4115	
2	12.06	1358.2	Thy 2mer	0.7001	0.21	1644	0.32
3	13.27	679.4	Thy 1mer	0.6673	0.78	2189	1.04
4	15.06	485.1	Ferr 1mer	0.6455	0.93	3016	1.61
5	16.52	137.0	BSA 2mer	0.8954	0.73	1886	1.11
6	18.25	68.2	BSA 1mer	0.415	0.9	10714	1.55
7	20.62	30.1	CAH 1mer	0.4174	0.62	13523	1.0

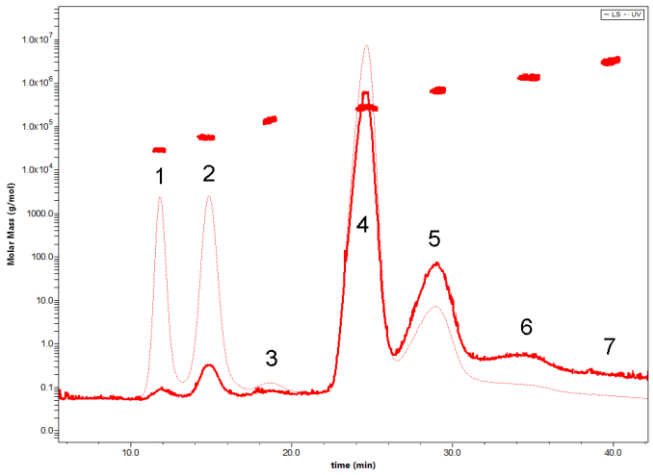

Figure 4 – HF5-UV-MALS elution profile of the standard protein mixture at 200 mM ionic strength. Rayleigh ratio at 90° represented as a thick red line and UV signal at 280 nm represented as a dotted thin red line.

Most HF5 peaks are symmetrical, while the others are slightly tailed. The complete separation is achieved in approximately 40 minutes. The HF5 efficiency, expressed as number of plates, is very low compared to SEC because the HF5 peaks are very broad (it is a known fact that the peaks in FFF are much broader compared to chromatographic peaks). The resolution between species is comparable to SEC. The HF5 separation profile does not contain unidentified species, which confirms that the separation is very gentle and may confirm undesired sample-column matrix interactions observed previously in the SEC elution profile.

Table 3 – HF5 separation performance evaluation: separation parameters derived from data at SEC optimal ionic strength (200 mM). Peak assignment in agreement with the calculated MW

Peak #	t_R (min)	Calculated MW (kDa)	Peak assignment	$w_{1/2}$ (min)	Peak symmetry	Plates number	Resolution (R_s)
1	7.66	29.9	CAH 1mer	0.8736	0.85	426	
2	10.71	68.8	BSA 1mer	1.2765	0.9	390	1.66
3	14.54	135.6	BSA 2mer	2.8455	0.72	144	1.09
4	20.52	483.5	Ferr 1mer	1.9365	1.35	622	1.47
5	24.8	677.2	Thy 2mer	3.2275	1.15	327	0.97
6	27.65	1356.3	Thy 2mer	4.8566	0	179	0.41
7	34.64	> 2000.0	Thy and Ferr oligomers	2.8656	0.96	809	1.06

SPECIFIC SEPARATION PARAMETERS FOR PERFORMANCE EVALUATION

Selectivity is a fundamental parameter in analyses of mixtures, because it is important to avoid co-elution of species. The selectivity was calculated as the MW-based selectivity (S_{MW}), defined as the slope of the log (t_R) against the corresponding log (MW) plot, where the retention times, as well as MW values, were derived from the experimental data. The selectivity plots obtained at high/optimal ionic strength are displayed in Figure 5a for the SEC separation and 5b for the HF5 separation.

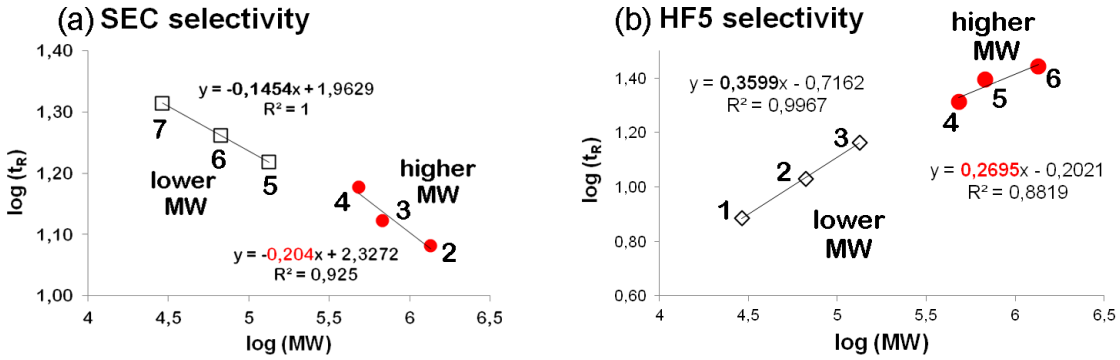

Figure 5 – Selectivity plots obtained at 200 mM ionic strength for (a) SEC and (b) HF5. The numbers near the data points represent the peak numbers in their elution order.

Since the HF5 separation was performed employing two different cross-flow rates (see Figure 2), the selectivity was calculated by dividing the separated species into 2 groups: the ones separated at a constant cross-flow rate of 0.85 mL/min and the ones separated at 0.4 mL/min.

The SEC *selectivity* is related to the slope of the calibration curve, meaning that SEC columns that are highly efficient do not necessarily provide a good resolution, unless the calibration curve is low enough (optimal *b* value: 0.1). Since the separation, therefore the selectivity in SEC, increases inversely to the slope value and depends also on the pore size of the column packing material, a slope value of $b = 0.15$ for the

SEC WTC column indicates a lower selectivity when compared to the separation of polystyrene standards in the same MW range, reported by [Podzimek 2011]. Furthermore, the SEC selectivity decreases with the MW range of the proteins separated on the same column (*b* = 0.2 for peaks 2-4).

On the other hand, maximum selectivity achievable in Flow FFF (therefore HF5) varies between 0.5 – 0.7, comparable to SEC selectivity values of ~ 0.1, even though the SEC efficiency is much higher [Schure et al. 2000]. Flow FFF selectivity also depends on the sample conformation and the carrier solution employed for the separation and varies in the range 0.3-0.7. Generally, the FFF selectivity is higher than SEC selectivity [Podzimek 2011].

As expected, the HF5 selectivity for both small and large proteins is higher compared to SEC, meaning that HF5 is potentially able to detect more species. These species may be overlooked by SEC analysis because they co-elute with proteins with similar MW value. The HF5 selectivity should increase with the MW of the separated species, but this applies to methods which use a constant cross-flow rate during elution (not the case described in this study).

The specific resolution (R_{sp}) is another fundamental separation parameter and was calculated for both SEC and HF5 separations, as well as the retention levels (R_L) and the corresponding retention factor (k) for the SEC separations. The obtained values are reported in Table 4. Peak 1 (SEC) and peak 7 (HF5) were excluded from the calculations because they represent polydisperse populations.

The dead volume of the SEC column was calculated as the volume of the cylinder with the same size characteristics and was found to be 14.33 mL. Therefore, the dead time (t_0) at 0.5 mL/min flow rate was 28.67 min (shown in Figure 1). The t_0 was related to the retention time through *capacity factor* (*k*) for the analytes separated by SEC, instead of the retention level calculated for the analytes separated by HF5.

In HF5, the R_L for the protein with the highest MW is, as expected, the highest of all and above the recommended value (>50) [Litzen et al. 1993, Wahlund 2013]. SEC and HF5 present similar specific resolution values and, except for the high MW proteins

and oligomers, a baseline resolution is achieved with both techniques.

Table 4 – Capacity factor (SEC), retention level (HF5), specific resolution and selectivity for SEC and HF5 at high ionic strength, 200 mM

Peak	Species	Calculated MW (kDa)	t_R (min)	Retention	Specific resolution (R_{sp})	Selectivity
SEC				**Capacity factor (k)**		
2	Thy dimer	1358.2	12.06	0.58		0.2
3	Thy monomer	679.4	13.27	0.54	3.5	
4	Ferr monomer	485.1	15.06	0.47	11.0	
5	BSA dimer	137.0	16.52	0.42	2.0	0.15
6	BSA monomer	68.2	18.25	0.36	5.1	
7	CAH monomer	30.1	20.62	0.28	2.8	
HF5				**Retention level (R_L)**		
1	CAH monomer	29.9	7.66	20.2		0.36
2	BSA monomer	68.8	10.71	28.2	4.6	
3	BSA dimer	135.6	14.54	38.3	3.7	
4	Ferr monomer	483.5	20.52	54.0	2.7	0.27
5	Thy monomer	677.2	24.8	65.3	6.6	
6	Thy dimer	1356.3	27.65	72.8	1.4	

A net distinction in the favor of HF5 is made by *selectivity*; the selectivity of both small and large proteins (and their oligomers) is always higher for HF5. The values reported in Table 4 will also be discussed by comparison with the ones obtained at low ionic strength.

B. SEC AND HF5-UV-MALS IN LOW IONIC STRENGTH MOBILE PHASE (55 mM)

Next, the standard proteins mixture was injected in SEC and HF5 and separated employing the low ionic strength mobile phase (IS = 55 mM). The purpose of employing this mobile phase during the separations was to demonstrate the versatility of HF5 in regard to the wide choice of carrier solutions. SEC and HF5 were coupled online with a MALS detector for the determination of the absolute MW. The separation profiles, as well as the calculated MW for each separated peak are reported in Figure 6 (SEC) and Figure 7 (HF5).

In both cases the peak assignment was based on the elution order and confirmed afterwards by the absolute MW values derived from MALS data. At low ionic strength, both SEC and HF5 separation profiles show the presence of 7 separated species. The peak identification, as well as other fundamental separation parameters computed by Astra® and ChemStation – with the purpose of comparing the SEC and HF5 performance – is reported in Table 5 for the SEC separation and Table 6 for the HF5 separation.

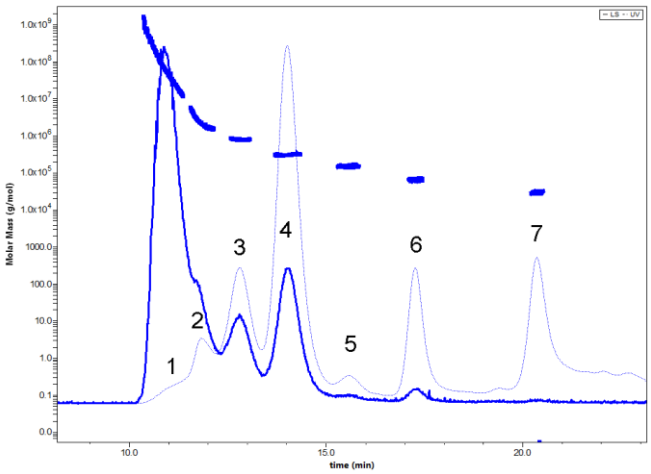

Figure 6 - SEC-UV-MALS elution profile of the standard protein mixture at 55 mM ionic strength. Rayleigh ratio at 90° represented as a thick blue line and UV signal at 280 nm represented as a dotted thin blue line.

Table 5 – SEC separation performance evaluation: separation parameters derived from data at low ionic strength (55 mM). Peak assignment in agreement with the calculated MW

Peak #	t_R (min)	Calculated MW (kDa)	Peak assignment	$w_{1/2}$ (min)	Peak symmetry	Plates number	Resolution (R_s)
1	11.44	>2000.0	Thy and Ferr oligomers	0.5854	0	2123	
2	11.80	1358.2	Thy 2mer	0.6928	0.60	1608	0.33
3	12.78	679.4	Thy 1mer	0.7183	0.91	1755	0.82
4	13.98	485.1	Ferr 1mer	0.6115	0.83	2898	1.06
5	15.56	137.0	BSA 2mer	0.8243	0.67	1976	1.29
6	17.25	68.2	BSA 1mer	0.4125	0.65	9685	1.60
7	20.34	30.1	CAH 1mer	0.5048	0.63	9001	0.99

The peaks are broader compared to the separation at optimal IS, and the consequent decrease in efficiency is significant for the separation of CAH, BSA and Thy monomers. The resolution is not compromised as much as the efficiency when the analysis is performed in a carrier solution with lower salt content. The presence of unidentified species eluting between the CAH and BSA monomers persists, as expected, since the purpose of a high salt content in the carrier solution is to prevent/minimize analyte – matrix interactions. The specific resolution of the species separated by SEC, as well as the capacity factor and the selectivity will be discussed further on.

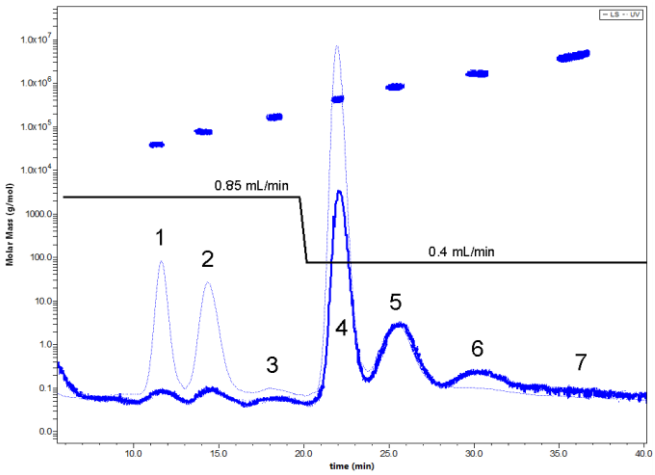

Figure 7 – HF5-UV-MALS elution profile of the standard protein mixture at 55 mM ionic strength. Rayleigh ratio at 90° represented as a thick blue line and UV signal at 280 nm represented as a dotted thin blue line. The black line represents the cross-flow rate trend during the separation

Table 6 – HF5 separation performance evaluation: separation parameters derived from data at low ionic strength (55 mM). Peak assignment in agreement with the calculated MW

Peak #	t_R (min)	Calculated MW (kDa)	Peak assignment	$w_{1/2}$ (min)	Peak symmetry	Plates number	Resolution (R_s)
1	7.48	29.9	CAH 1mer	0.9658	0.86	332	
2	10.22	68.8	BSA 1mer	1.3881	0.73	300	1.37
3	14.13	135.6	BSA 2mer	2.9284	0.84	129	1.06
4	17.82	483.5	Ferr 1mer	1.1939	0.73	1234	1.05
5	21.32	677.2	Thy 2mer	2.3879	0.82	442	1.15
6	24.27	1356.3	Thy 2mer	4.5949	0	155	0.50
7	29.57	> 2000.0	Thy and Ferr oligomers	3.7661	0	342	0.75

In HF5, the separation of 7 species at low ionic strength is achieved in less than 40 min. The peaks become broader compared to the separation at high ionic strength and the separation efficiency consequently decreases. A slight decrease in resolution is also observed. Compared to the SEC separation at low ionic strength, the HF5 separation profile does not show any unidentified peaks. The specific resolution of the species separated by HF5, as well as the retention level and the method selectivity will be discussed separately.

SPECIFIC SEPARATION PARAMETERS FOR PERFORMANCE EVALUATION

The *MW-based selectivity* (S_{MW}) plots obtained at low ionic strength are displayed in Figure 8 (a) for the SEC separation and (b) for the HF5 separation. Peak 1 (SEC) and peak 7 (HF5) were excluded from the calculations because they represent polydisperse populations (not resolved).

The HF5 selectivity was calculated by dividing the separated species into 2 groups: the ones separated at a constant cross-flow rate of 0.85 mL/min and the ones separated at 0.4 mL/min.

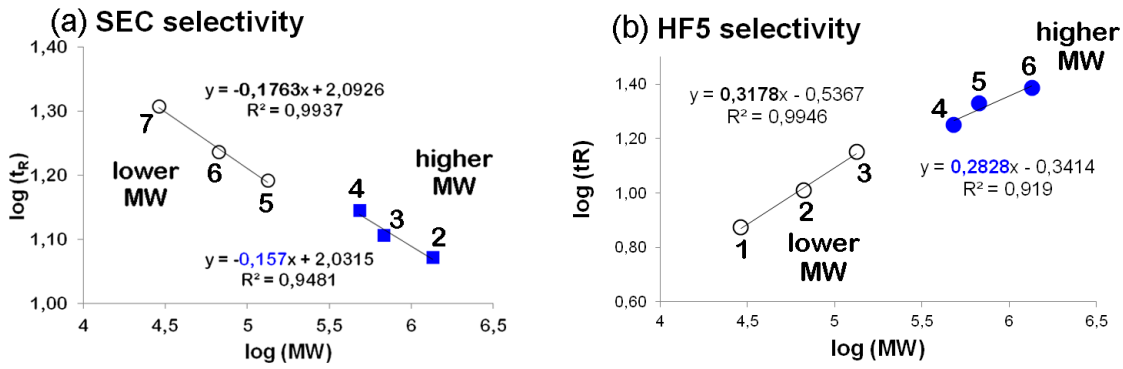

Figure 8 – Selectivity plots obtained at 55 mM ionic strength for (a) SEC and (b) HF5. The numbers near the data points represent the peak numbers in their elution order.

The HF5 selectivity is always higher than SEC selectivity, shown by the corresponding selectivity slope trends for small MW proteins (b = 0.32 in HF5, vs. b = 0.17 in SEC), as well as for high MW proteins (b = 0.28 in HF5, vs. b = 0.16 in SEC). Furthermore, at low IS, the SEC selectivity slope trend does not change significantly between lower and higher MW proteins (b = 0.16-0.17, Table 7), as previously observed at high IS (b = 0.15-0.2, Table 4).

The superior HF5 selectivity indicates that the HF5 method is potentially able to separate more species. These species may be overlooked by SEC analysis because they co-elute with proteins with similar MW value. Employing this "*step gradient*" method, the HF5 selectivity does not increase with the MW, as it would normally do at constant cross-flow rate. The HF5 selectivity for high MW proteins at low ionic strength is slightly higher compared to the value obtained at high ionic strength (Figure 8b and Figure 5b).

The specific resolution (R_{sp}) was calculated for both SEC and HF5 separations, as well as the retention levels (R_L) and the corresponding capacity factor (k) for the SEC separations and the results are reported in Table 7.

Table 7 – Capacity factor (SEC), retention level (HF5), specific resolution and selectivity for SEC and HF5 at low ionic strength, 55 mM

Peak	Species	Calculated MW (kDa)	t_R (min)	Retention	Specific resolution (R_{sp})	Selectivity
SEC				**Capacity factor (k)**		
2	Thy dimer	1358.2	11.8	0.59		0.16
3	Thy monomer	679.4	12.78	0.55	2.7	
4	Ferr monomer	485.1	13.98	0.51	7.2	
5	BSA dimer	137.0	15.56	0.46	2.3	0.17
6	BSA monomer	68.2	17.25	0.40	5.3	
7	CAH monomer	30.1	20.34	0.29	2.8	
HF5				**Retention level (R_L)**		
1	CAH monomer	29.9	7.48	18.7		0.32
2	BSA monomer	68.8	10.22	25.6	3.8	
3	BSA dimer	135.6	14.13	35.3	3.6	
4	Ferr monomer	483.5	17.82	44.6	1.9	0.28
5	Thy monomer	677.2	21.32	53.3	7.9	
6	Thy dimer	1356.3	24.27	60.7	1.7	

At low ionic strength, the SEC capacity factor, *k* shows only a slight increase for all species (2-9% increase), while the retention level, R_L for all species separated by HF5 decreases (7 – 18% decrease), especially for the high MW proteins. The specific resolution R_{sp} obtained in SEC and HF5 is comparable. Even at low ionic strength, HF5 presents a higher selectivity when compared to SEC, for all MW in the protein mixture.

C. SAMPLE RECOVERY AT HIGH AND LOW IONIC STRENGTH

While an accurate MW characterization, as well as effective separation of all existing species in a protein formulation is important, the sample recovery is another fundamental parameter worthwhile taking into consideration. If the sample recovery, usually determined by MALS measurements or estimating the area under the peak at 280 nm (or any other protein specific wavelength), is not complete (100%) during QA or QC protocols based on SEC, a secondary separation/characterization technique is required to understand the reason.

In this study, the sample recovery was calculated by Astra® for both SEC and HF5 separations, and investigated when employing both low and high ionic strength mobile phases. The results are reported in Table 8.

Table 8 – Sample relative recovery in SEC and HF5 in high (200 mM) and low (55 mM) ionic strength mobile phase

Species	SEC 200 mM (μg)	SEC 55 mM (μg)	HF5 200 mM (μg)	HF5 55 mM (μg)
CAH monomer	4,59	3,98	2,99	3,04
BSA monomer	6,59	7,06	11,09	9,47
BSA dimer	2,84	2,27	1,78	1,32
Ferr monomer	13,39	14,78	15,28	12,34
Thy monomer	6,39	6,62	6,58	6,09
Thy dimer	3,34	2,35	1,94	1,52
Total sample recovery (μg)	37,14	37,06	39,66	33,78
Total sample recovery (%)	94.3	94.1	99.3	87.6

First of all, it can be noted that the proteins proportion is no longer in balance (1:1:1:1), shown by both SEC and HF5 results. However, since the total recovered protein is close to the injected amount (40 μg), it may indicate the lack of sample homogeneity during injection.

The SEC results indicate that, in this study, the recovered protein amount was not affected by the change in the salt composition of the mobile phase, as it would be

expected. It is a known fact that SEC requires a high salt content to supress sample-matrix interactions which lead to loss of sample during the separation. However, even under high/optimal ionic strength conditions, SEC does not offer a complete recovery for all proteins.

The highest recovery is observed when HF5 is performed in high ionic strength mobile phase. When the ionic strength is decreased in HF5, it is followed by a decrease in sample recovery, suggesting the presence of non-specific interactions between the proteins and the separation device. The ionic strength in HF5 is as important as it is in SEC when the sample recovery is at stake.

4.1.2.5. CONCLUSIONS

The scale-up of the HF5 separation device allowed a rather high sample amount (40µg) to be separated, detected reliably and, most importantly, recovered.

While the separation efficiency is always higher for SEC thanks to the reduced band broadening, the resolution (R_s and R_{sp}) of SEC and HF5 is comparable and selectivity is always higher in HF5.

However, as suggested by [Zölls et al. 2012], the comparison between results obtained employing techniques which are based on different principles should be done looking for data trends instead on focusing on numbers.

In fact, this study shows that the SEC selectivity trend, even under optimal conditions (recommended by the column manufacturer), is lower than previously reported by [Podzimek 2011] on polystyrene standards with MWs in the same range (b = 0.13 – 0.14 for the protein mix in this study vs. b = 0.09 for the polystyrene standards, much closer to the optimal value of 0.1).

The selectivity in HF5, on the other hand, displays an opposite trend, meaning that the slope values are higher than reported by [Podzimek 2011], on the polystyrene standards mentioned before (b = 0.27 – 0.28 for the protein mixture in this study vs. b

= 0.2 for the polystyrene standards).

This is an appealing (HF5) feature for the separation of complex protein samples, because it allows the detection and quantification of species that otherwise would be overlooked. It was shown that, in SEC, the co-elution of species is very common, even if the MW difference between the separated species is considerable. The possibility to use mobile phases at low ionic strength is another appealing possibility, even though reducing the salt concentration should be considered carefully due to its correlation with sample recovery.

Even if SEC compensates with higher efficiency, it does not earn any extra points if the species are co-eluting. A second SEC column with a different porosity may be coupled online with the first one, in order to ensure the required selectivity. However, placing a second SEC column, in series with the first one, could compromise further the sample recovery.

The SEC sample recovery is incomplete, but still high and it does not change significantly upon ionic strength variation, indicating the robustness of the separation device.

The highest sample recovery is obtained when the separation is performed in HF5 in high ionic strength carrier solution, and a direct correlation between the recovered sample amount and the ionic strength is shown.

4.1.2.6. REFERENCES

[Litzen et al. 1993] Litzen A.; Walter J. K.; Krischollek H. and Wahlund K. G. (1993). "*Separation and Quantitation of Monoclonal Antibody Aggregates by Asymmetrical Flow Field-Flow Fractionation and Comparison to Gel Permeation Chromatography*." Analytical Biochemistry **212** (2): 469-480.

[Podzimek 2011] Podzimek S. (2011). *Chapter 5: Asymmetric Flow Field-Flow Fractionation*. Light scattering, size exclusion chromatography and asymmetric flow field flow fractionation. Powerful tools for the characterization of polymers, proteins and nanoparticles. Wiley. Hoboken, New Jersey, Wiley**:** 259-306.

[Schure et al. 2000] Schure M. R.; Schimpf M. E. and Schettler P. D. (2000). *Chapter 2: Retention - normal mode*. Field-Flow Fractionation Handbook. Schimpf M. E.; Caldwell K. and Giddings J. C. New York, Wiley**:** 31-48.

[Wahlund 2013] Wahlund K.-G. (2013). "*Flow field-flow fractionation: Critical overview*." Journal of Chromatography A **1287** (2013): 97– 112.

[Zölls et al. 2012] Zölls S.; Tantipolphan R.; Wiggenhorn M.; Winter G.; Jiskoot W.; Friess W. and Hawe A. (2012). "*Particles in therapeutic protein formulations, Part 1: Overview of analytical methods*." Journal of Pharmaceutical Sciences **101** (3): 914–935.

4.1.3. FREEZE-THAW INDUCED ANTIBODY SELF-ASSOCIATION MONITORING BY HF5 – UV AND MALS CHARACTERIZATION

In this sub-chapter, the reversible self-association between antibody monomers was observed and monitored over time by HF5 and UV detection. The possible causes for this aggregation phenomenon were identified as freeze/thaw stress on the antibody, as well as sample dilution (previous to separation by HF5) in a buffer with a different composition than the formulation buffer.

One of the main concerns in therapeutic proteins quality control (QC) and quality assurance (QA) is represented by the possible changes that the protein composition may undergo upon sample dilution, especially if the dilution is not performed in the formulation buffer. If the QC tests employ flow-based methods (either SEC or FFF), sample dilution is inevitable during the separation and is often required even before the separation [Arakawa et al. 2010].

In FFF, the sample concentration changes drastically during a normal separation because first, the sample needs to be focused (concentrated in a narrow band) and afterwards, the sample is inevitably diluted during elution. Upon dilution, and especially when the dilution is performed in a buffer different from the formulation buffer (which is usually the case), weakly-bound and/or associated protein species with rapid association/dissociation conversion rates, are likely to be disrupted [Philo 2006, Arakawa et al. 2010, Engelsman et al. 2011].

In this study, the sample dilution was controlled to some extent during elution by adjusting the flow rates and employing a miniaturized separation device (HF5). Since the dissociation occurred very slowly compared to the duration of the separation, the self-associated protein system behaved like a true mixture, therefore individual oligomers could be resolved. Such reversible, but extremely slow association/dissociation reactions, responsible for the existence of so-called "*metastable oligomers*", are rather common [Philo 2006, Philo and Arakawa 2009] and, due to their reversible nature, pose less threat from the immunogenic point of view.

HF5 coupled with UV detection (absorption wavelength of the peptide bond, 215 nm) proved to be rather sensitive in detecting changes in the sample composition, which occurred faster at first and experienced a deceleration over time.

4.1.3.1. INSTRUMENTAL SETUP

HF5 analyses were performed using an Agilent 1200 HPLC system (Agilent Technologies, Santa Clara, CA, USA) consisting in a degasser, an isocratic pump, an auto sampler and a variable wavelength UV detector, combined with an Eclipse® DUALTEC prototype separation system (Wyatt Technology Europe, Dernbach, Germany). The ChemStation version B.04.02 (Agilent Technologies) data system for Agilent instrumentation was used to set and control the instrumentation and for the computation of various separation parameters. The software package Wyatt Eclipse @ ChemStation version 3.5.02 (Wyatt Technology Europe) was used to set and control the FFF separation system. An Agilent 1100 UV-Vis variable wavelength detector operating at a wavelength of 215 nm was used as a concentration detector at all times.

An 18-angle MALS detector model DAWN® HELEOS™ light scattering detector (Wyatt Technology Corporation, Santa Barbara, CA, USA), employing a laser operating at a wavelength of 658 nm, was used in all experiments.

ASTRA® software version 5.3.2.14 (Wyatt Technology Corporation) was used to handle signals from the detectors (MALS and UV) and to compute the proteins MW and concentration values. The hollow fiber was 17 cm long a polyether-sulfone (PES) fiber, type FUS 0181 available from Microdyn-Nadir (Wiesbaden, Germany) with the following characteristics according to the manufacturer: 0.8mm ID, 1.3mm OD and a molecular weight cut-off of 10 kDa corresponding to an average pore size of 5 nm.

4.1.3.2. SAMPLES AND REAGENTS

The mobile phase was 10 mM phosphate buffer supplemented with 25 mM NaCl, at a final pH of 7.2 (total ionic strength: 55 mM), prepared using MilliQ water purified by an Elix 3 UV Water Purification System (Millipore, Billerica, USA) and filtered

through 0.2 μm pore membrane sterile filter units (Millipore).

The sample used in the study was an IgG_1 type antibody, for simplicity named mAb1. The sample was diluted 1:100 in the mobile phase, at a final concentration of 0.385 mg/mL and divided in two aliquots: Vial §1 and Vial §2. Vial §1 was used for analyses immediately after the sample dilution, while Vial §2 was stored at -20°C and thawed before the analyses. Both vials were stored at room temperature during the working days and at 4°C during the night and/or over the week-end.

4.1.3.3. METHODS

An amount of 2 μg of mAb1 (5.2 μL) was injected at all times, unless otherwise specified. The mAb1 sample was injected in the HF5 separation device during the focus-inject step, which was performed at a focus flow rate of 0.85 mL/min for 4 min. The sample was focused at a distance of approximately 15% fiber length from the channel inlet an eluted afterwards at a channel flow rate of 0.35 mL/min under the effect of a constant cross-flow rate of 0.35 mL/min.

The separation was monitored by UV detection at 215 nm and, when specified, by a multi-angle scattering detector. The sample was injected at different time intervals and the oligomers distribution was observed.

4.1.3.4. RESULTS AND DISCUSSION

The purpose of the study presented in this sub-chapter was to observe by HF5-UV the changes that occur in therapeutic protein samples due to dilution, handling and different storage conditions.

First, 2 μg of mAb1, taken from Vial §1, were injected and separated by HF5. The separation was repeated after 6 hours and after 3 days since the first injection. The separation profiles are reported in Figure 1.

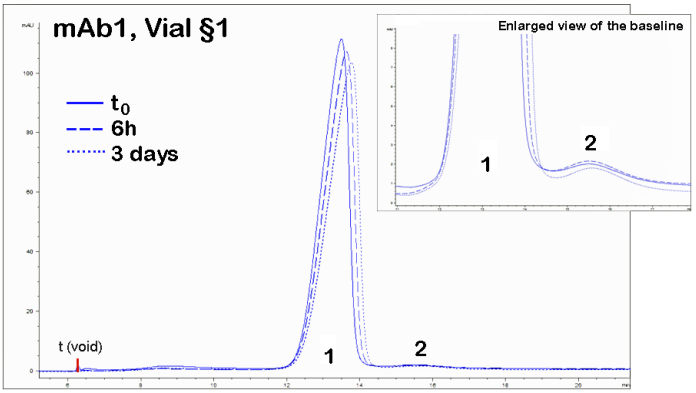

Figure 1 – HF5-UV separation profiles at 215 nm of mAb1 in Vial §1

Figure 1 shows the elution of two species, most likely mAb1 monomer and dimer. Even though the sample was diluted 1:100 in a buffer different than the formulation buffer, the composition of mAb1 in Vial §1 is stable over time. It is very likely that the phosphate buffer employed as carrier solution, as well as dispersion media, stabilizes mAb1. The retention times shift slightly, but this change is very likely due to the hollow fiber usage.

Table 1 reports the exact composition of the sample immediately after dilution, after 6h and 3 days after dilution and overnight storage at 4°C.

Table 1 – mAb1 composition in Vial §1 at different time intervals

Time point	Peak 1 (%)	Peak 2 (%)
t_0	97.95	2.05
6h	97.76	2.24
3 days	97.48	2.52

Based on the retention time value, it was assumed that the first peak corresponded to the mAb1 monomer and the second to the dimer. Their amounts, which are reported in Table 1, confirm the fact that the sample composition did not change significantly over time. The monomer amount decreases slightly over time, suggesting the presence of mAb1 species which self-associate very slowly into dimer.

Next, the stability of mAb1 in Vial §2 was monitored. After dilution, Vial §2 was stored at -20°C to avoid mAb1 composition changes, while the study on Vial §1 was conducted immediately after the sample dilution. The same amount of mAb1 (2 µg), taken from Vial §2, was injected and separated by HF5 at all times. The separation was repeated after 6 hours and after 3 days since the first injection. The separation profiles are reported in Figure 2.

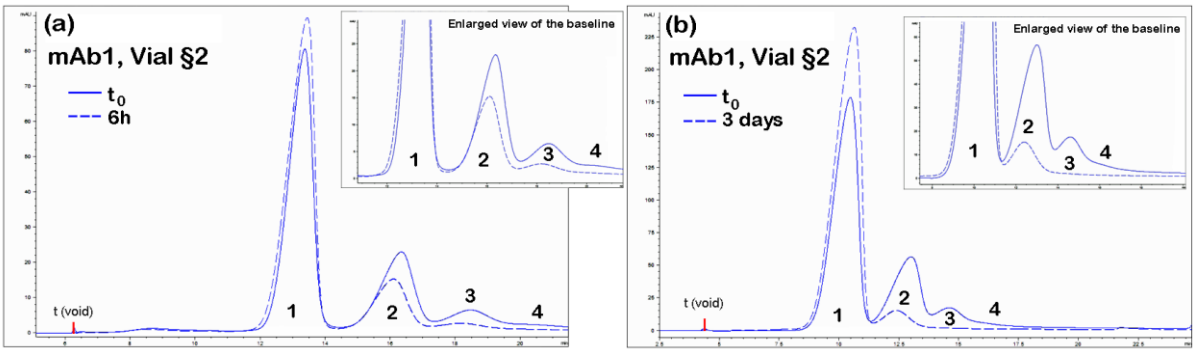

Figure 2 – HF5 separation profiles at 215 nm of mAb1 in Vial §2

Figure 2 shows the elution of two additional mAb1 species (four species in total), whose amounts vary greatly over time. It is very likely that peak 1 corresponds to the monomer and the following peaks (2 – 4) correspond to mAb1 oligomers. The exact sample composition is reported in Table 2.

Table 2 – mAb1 composition in Vial §2 at different time intervals

Time point	Peak 1 (%)	Peak 2 (%)	Peak 3 (%)	Peak 4 (%)
t_0	63.20	25.32	8.80	2.58
6h	77.89	17.22	3.66	1.21
3 days	93.98	5.75	0.25	-
7 days	97.93	2.07	-	-

The mAb1 oligomers amounts reported in Table 2 show the increase of monomer amount over time at the expense of larger oligomers. This situation is opposite to the one observed for mAb1 in Vial §1. After only 6h, approximately 50% of all larger

oligomers have spontaneously dissociated into monomeric units.

The mAb1 oligomers distribution in Vial §2 was assessed after one week (7 days) and the elution profiles are reported in Figure 3. The distribution of mAb1 species in Vial §2 after 7 days is very similar to the one reported for Vial §1 at t0 (Table 2).

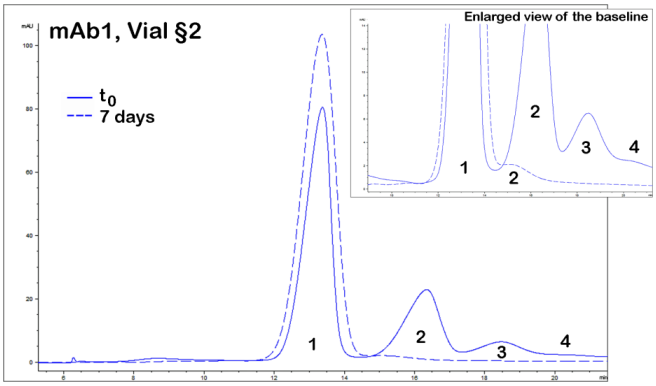

Figure 3 – HF5 separation profiles at 215 nm of mAb1 in Vial §2 immediately after dilution and after 7 days

Figure 3 and the values reported in Table 2 suggest that mAb1 in Vial §2 reaches the species distribution of mAb1 in Vial §1 at t_0 after a week. It is expected that, from this point forward, the oligomers distribution of mAb1 in Vial §2 will follow the trend which was observed for Vial §1.

These findings suggest that mAb1 in Vial §2 experiences two aggregation phenomena. The first is depicted in Figure 2, showing the monomer in dynamic equilibrium with its larger oligomers. The mAb1 oligomers, which are self-assemblies of the monomer, slowly dissociate into monomer over approximately 3 days. The second aggregation phenomenon is the exact opposite, seen for mAb1 in Vial §1 in Figure 1, which is the slow self-association of monomeric units into larger assemblies.

The self-association phenomenon was investigated by coupling the FFF separation system with a DAWN HELEOS multi-angle light scattering detector. The absolute MW values of mAb1 oligomeric species in both Vial §1 and Vial §2 are reported in Figure 4.

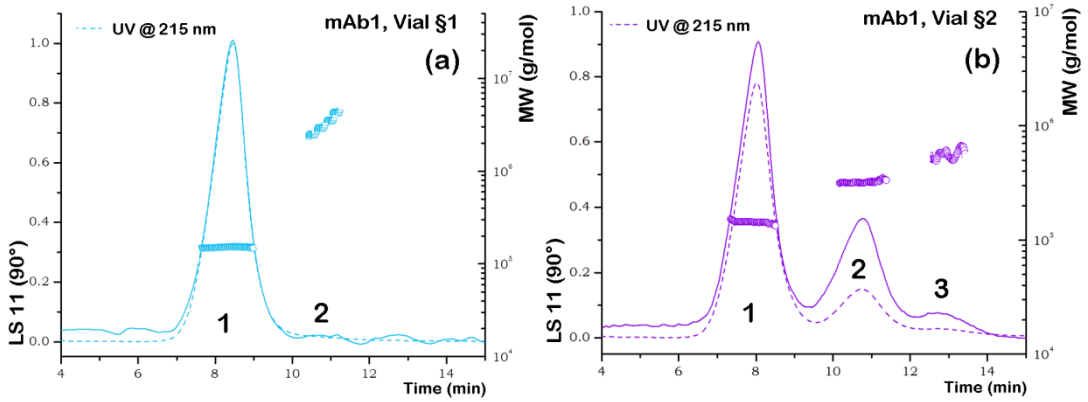

Figure 4 – HF5-MALS elution profiles of mAb1 in Vial §1 and Vial §2 at t0

Figures 4a confirms the monomer assignment to the first peak, but the MW of the second peak does not correspond to the dimer. In fact, peak 2 appears to correspond to very high MW species (2×10^6 – 5×10^6 g/mol) that are present at trace levels and are very compact as size, since they elute very close to the monomer. Figure 4b, on the other hand, shows that mAb1 contains different levels of monomer (peak 1), dimer (peak 2), trimer and tetramer (peak 3). Therefore, it is very likely that peak 4 (which is shown in Figures 2 and 3) corresponds to high MW aggregates, whose MW could not be determined during the separations reported in Figure 4a. These HMW aggregates found in Vial §2 are larger in size than the ones found to co-exist with the monomer in Vial §1, since they elute later than the trimer or tetramer of mAb1.

Finally, increasing amounts of mAb1 from Vial §2 were separated by HF5-UV in order to determine the *sample overloading limit*, which is topic closely related to the sample dilution requirement. Since the HF5 cartridge is a miniaturized device, the protein amount which can be injected into the channel and separated under optimal conditions without the risk of overcrowding is limited by the hollow fiber's internal area (4.27 cm^2) and/or the internal volume (85 μL).

Figure 5 reports the separation profiles of increasing amounts of mAb1 from Vial §2, which were separated subsequently and under identical experimental conditions.

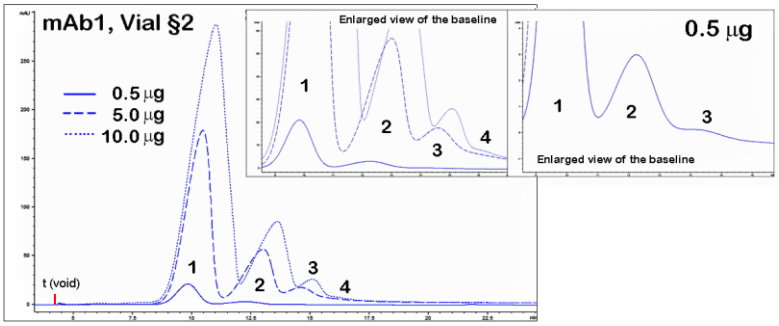

Figure 5 – HF5 separation profiles at 215 nm of different amounts (0.5 – 10.0) of mAb1 from Vial §2

The enlarged view of the baseline for 0.5 µg of mAb1 (Figure 5, far right graph) shows that, when coupled with UV detection at 215 nm, HF5 is very sensitive in detecting and quantifying very low amounts of mAb1 aggregates. The trimer and tetramer amount below *peak 3* represent roughly *44 ng* of mAb1 (8.8% of the sample at t_0). Since its detection and quantitation limit appear to be very low, there is no need for large amounts of sample, which are usually required for data reproducibility for batch release or sample complete workup.

Figure 6 reports the separation profiles of even higher amounts of mAb1 from Vial §2, separated subsequently and under identical experimental conditions.

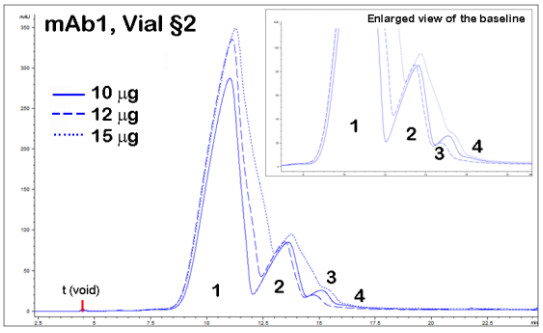

Figure 6 - Separation profiles at 215 nm of different amounts (10.0 – 15.0) of mAb1 from Vial §2

As expected, when the injected amount exceeds the overloading limit, not only the separation is no longer achieved properly because there is not enough physical space for the sample to relax properly during the focus step (at 15 µg, the peaks appear as

if they were "*split*"), but also the larger peaks actually cover below their tail smaller peaks, corresponding to species which are less abundant. For mAb1, the overloading limit appears to be around 10 μg. This amount should be sufficient for the MALS detector to provide reliable MW values for the species separated by HF5.

4.1.3.5. CONCLUSIONS

The HF5 true potential resides in the detection sensibility, especially when coupled with detection techniques which are intrinsically sensitive (such as UV absorption of the protein peptide bond at 215 nm or multi-angle light scattering), therefore it does not require large sample amounts to provide reliable results.

However, a detection method which is too sensitive (like MALS) has its downsides, such as being also very sensitive to large-sized particles, without having the ability to discriminate between protein particles and impurities like dust particles [Zölls et al. 2012].

This is where hyphenated techniques come to the rescue. By online coupling a separation technique such as HF5, which brings its own miniaturization advantages, with a specific sample property (such as protein specific UV absorption and/or fluorescence emission), the analytical information provided by the MALS detector is enhanced. In the absence of specific UV signal, MALS cannot provide information regarding the nature of the sample or its absolute MW, even though it can provide accurate information about the size regardless of the nature of the sample.

In this study was shown how HF5-UV can be employed to monitor antibody composition following dilution, how the freeze/thaw process – following sample dilution – induced dynamic aggregation (probably facilitated by the reduced volume of the sample when in frozen state) and how, once the sample was thawed, HF5-UV was able to monitor the slow dissociation into antibody monomeric units.

"LESS IS MORE"

It is also shown that, when coupled with intrinsically sensitive detection methods (UV at 215 nm and MALS), HF5 reduces considerably the need for large sample amounts in order to detect the presence and quantify trace amounts of antibody aggregates. Moreover, if the sample amount exceeds certain limits (overloading limit), not only has a negative impact on the separation process, but even impedes the detection of low abundant species.

4.1.3.6. REFERENCES

[Arakawa et al. 2010] Arakawa T.; Ejima D.; Li T. and Philo J. S. (2010). "*The Critical Role of Mobile Phase Composition in Size Exclusion Chromatography of Protein Pharmaceuticals*." Journal of Pharmaceutical Sciences **99** (4): 1674-1692.

[Engelsman et al. 2011] Engelsman J. d.; Garidel P.; Smulders R.; Koll H.; Smith B.; Bassarab S.; Seidl A.; Hainzl O. and Jiskoot W. (2011). "*Strategies for the Assessment of Protein Aggregates in Pharmaceutical Biotech Product Development*." Pharmaceutical Research **28** (4): 920-933.

[Philo 2006] Philo J. S. (2006). "*Is Any Measurement Method Optimal for All Aggregate Sizes and Types?* ." The AAPS Journal **8** (3).

[Philo and Arakawa 2009] Philo J. S. and Arakawa T. (2009). "*Mechanisms of Protein Aggregation*." Current Pharmaceutical Biotechnology (10): 348-351.

[Zölls et al. 2012] Zölls S.; Tantipolphan R.; Wiggenhorn M.; Winter G.; Jiskoot W.; Friess W. and Hawe A. (2012). "*Particles in therapeutic protein formulations, Part 1: Overview of analytical methods*." Journal of Pharmaceutical Sciences **101** (3): 914–935.

4.1.4. CARRIER SOLUTION SCREENING EXPLORATORY STUDY BY HF5-UV: INFLUENCE OF PH, SALT TYPE AND CONCENTRATION, IONIC STRENGTH AND BUFFERING AGENT ON THE IMMUNOGLOBULINS (IGGS) STABILITY DURING SEPARATION

In this sub-chapter, the influence of parameters like pH, buffering agent and concentration, salt type and concentration, as well as carrier solution ionic strength (IS) on the stability of antibodies (immunoglobulins, IgGs) during their separation by HF5 was monitored by UV detection.

The same parameters which impact greatly on the antibody stability also play a major role during the HF5 separation. For instance, the ionic strength value of the carrier solution influences the protein interactions during separation, shielding the proteins by charge and the same role (shield by charge) is played by the solution pH and the salt concentration.

A universal buffer cannot be employed for all antibodies, since their structure varies substantially (hence their specific biological function), an optimal buffer for one antibody may be harmful to another. The same effect was observed when the salt type is changed (from NaCl to $MgCl_2$).

Furthermore, the HF5 versatility in terms of carrier solution composition is shown, as well as the wide pH range (allowed by the PES hollow fibers) of carrier solutions that can be employed for the separation. The study also shows how the carrier solution components specific absorption can interfere with detection (in this study, the phosphate buffer absorption interfered with the detection of antibody degradation products/fragments, buy may also interfere with the detection of antibody aggregates), therefore need to be considered carefully.

The phenomenon of *nonspecific protein adsobtion* to the hollow fiber inner wall leading to incomplete recovery, abnormal elution position, loss of peak symmetry and poor resolution is an issue which HF5 (FFF) and SEC have in common. The sample interaction with the column matrix is a known SEC limitation. In this study, this issue was addressed by performing a series of injections of the same sample (*make-up runs)* in order to improve sample recovery. This is a common practice in SEC and recommended by SEC columns manufacturers, therefore was adopted in HF5 as well.

Finally, two mobile phases, with a composition similar to the antibody formulation buffer were employed during the HF5 separation. Nonetheless, even though the sample stability may be maintained, it appears that the low ionic strength leads to poor separation performance, as well as compromised sample recovery (even after make-up runs), therefore not optimal for sample characterization.

4.1.4.1. INSTRUMENTAL SETUP

HF5 analyses were performed using an Agilent 1200 HPLC system (Agilent Technologies, Santa Clara, CA, USA) consisting in a degasser, an isocratic pump, an auto sampler and a variable wavelength UV detector, combined with an Eclipse® DUALTEC prototype separation system (Wyatt Technology Europe, Dernbach, Germany). The ChemStation version B.04.02 (Agilent Technologies) data system for Agilent instrumentation was used to set and control the instrumentation and for the computation of various separation parameters. The software package Wyatt Eclipse @ ChemStation version 3.5.02 (Wyatt Technology Europe) was used to set and control the FFF separation system. An Agilent 1100 UV/Vis variable wavelength detector operating at a wavelength of 280 nm was used as a concentration detector at all times.

The hollow-fiber was a 17 cm long polyether-sulfone (PES) fiber, type FUS 0181 available from Microdyn-Nadir (Wiesbaden, Germany) with the following characteristics according to the manufacturer: 0.8 mm ID, 1.3 mm OD and a molecular weight cut-off of 10 kDa corresponding to an average pore size of 5 nm.

4.1.4.2. SAMPLES AND REAGENTS

The reagents required to prepare the carrier solutions/mobile phases were supplied by Sigma and are reported in Table 1. All carrier solutions were prepared according to the schematic reported in Figure 1, using MilliQ water purified by an Elix 3 UV Water Purification System (Millipore, Billerica, USA) and filtered through 0.2 μm pore membrane sterile filter units (Millipore), at all times.

The samples used in the study were three IgG_1 type monoclonal antibodies, for simplicity named **mAb1**, **mAb2** and **mAb3**. All the available information regarding

the antibodies is reported in Table 2. The sample aliquots were stored at room temperature during the working days and at 4°C during the night and/or over the week-end.

Table 1 – Reagents used for the preparation of the mobile phases

Reagent	Buffer type	Product code from Sigma
$Na_2HPO_4 \cdot 2\ H2O$	Phosphate buffer	342483
$NaH_2PO_4 \cdot 2\ H2O$		S5136
Na citrate	Citrate buffer	W302600
Citric acid		C0759
NaCl	-	S5886
MgCl2	-	M2393

Table 2 – Available information regarding the monoclonal antibodies (mAbs) used in this study

Antibody short name	IgG isotype	pI	MW (kDa)	Initial concentration (mg/mL)
mAb1	IgG_1	8.73	142.2	38.5, in ammonium acetate, pH 5.0
mAb2	IgG_1	N/A	150.0	2.0, formulation N/A
mAb3	IgG_1	8.25	144.2	40.0, in phosphate/citrate buffer, pH 5.0

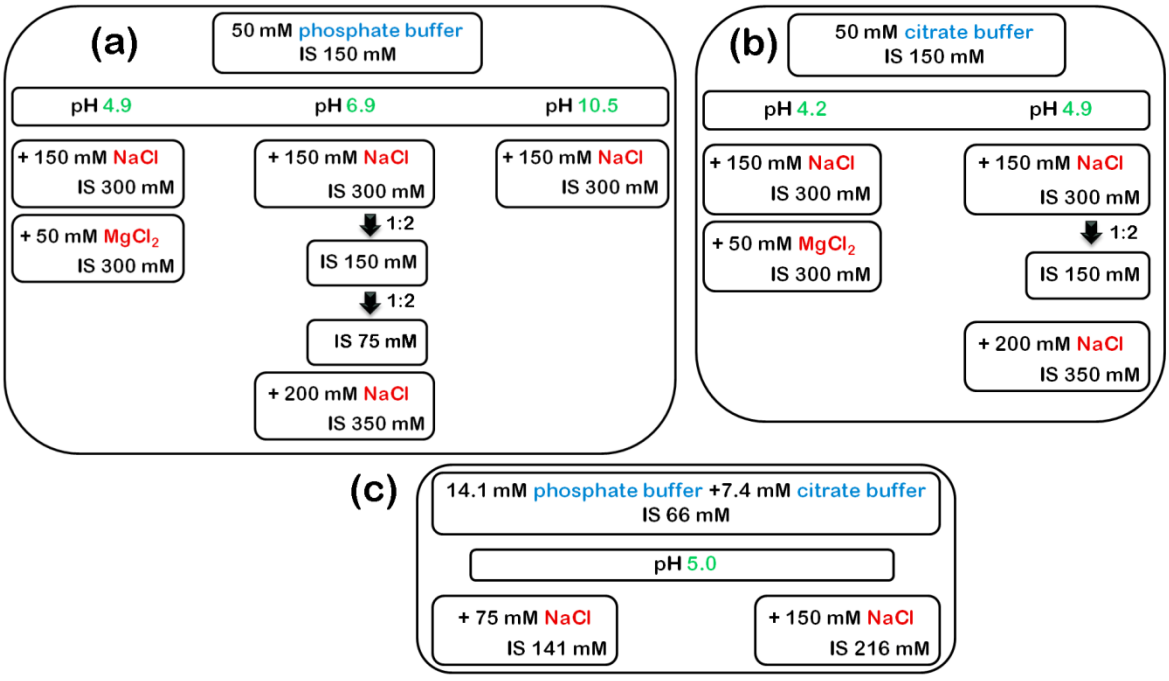

Figure 1 – Carrier solutions preparation (a) phosphate buffer; (b) citrate buffer and (c) phosphate/citrate buffer similar to the formulation buffer for mAb3

4.1.4.3. METHODS

The same amount of each mAb was injected at all times (2 μg of mAb1 and mAb2 and 0.6 μg of mAb3), unless otherwise specified. The samples were injected in the HF5 separation device during the focus-inject step, which was performed at a focus flow rate of 0.85 mL/min for 4 min. The sample was focused at a distance of approximately 15% fiber length from the channel inlet an eluted afterwards at a channel flow rate of 0.35 mL/min under the effect of a constant cross-flow rate of 0.35 mL/min. The separation process was monitored by UV detection at 280 nm

4.1.4.4. RESULTS AND DISCUSSION

The factors which induce aggregation in therapeutic protein formulations were divided in: (a) sample variables (sample concentration) and (b) carrier solution/buffer variables. In the latter category we included: solution pH, buffer composition, solution ionic strength, salt type and salt concentration.

Once the carrier solution variables were identified, their influence on the antibody stability and/or HF5 separation performance was observed under different experimental conditions, reported in Figure 1. The carrier solution variables that were taken into consideration are summarized in Table 3. One parameter was changed at a time, while all the others remained constant.

Two buffer types were used in this study: **phosphate buffer**, which operates between a pH value of 5.7 and 8.0 and **citrate buffer,** which operates in the pH range between 3.0 and 6.2 [Dawson et al. 1986, www.sigmaaldrich.com 2014]. A third buffer, which consisted in a mixture containing both phosphate and citrate buffers (whose composition was very similar to the mAb3 formulation buffer), was employed as carrier solution as well.

Two salts were employed in the study: NaCl and $MgCl_2$, both chaotropic agents

(protein stabilizers) according to the *Hofmeister series*, which divides tested reagents/substances into protein denaturants and protein stabilizers, according to the same principle on which protein salting in/salting out is based. NaCl was also used to adjust the mobile phase ionic strength, which has a known impact on the FFF separation performance, as well as on protein stability.

The solution pH is another parameter that has a great impact on protein stability and therefore on FFF performance of protein samples. The pH extreme values (4.9 and 10.5) were chosen below and above the reliable pH buffering range of the phosphate buffer, avoiding the proximity to the pI of IgGs, which is approximately 7.3 ± 1.2. Considering that no acids/bases were added to the mobile phase during the separations, the buffers maintained their set pH, although sometimes outside their operating range.

Table 3 – Carrier solution variables and values employed in this study

#	Variable	Values	Buffer type	Constant parameters
1	pH	4.9 6.9 10.5	Phosphate	Buffer composition (50 mM) Buffer salt: NaCl (150 mM) Solution ionic strength (300 mM)
2	Salt I	NaCl $MgCl_2$	Phosphate	Buffer composition (50 mM) Solution ionic strength (300 mM) pH: 4.9
3	Ionic strength I	150 mM (A) 75 mM (B) 150 mM (C) 300 mM (D) 350 mM (E)	Phosphate	Buffer type Buffer salt: NaCl pH: 6.9
4	Ionic strength II	150 mM (F) 150 mM (G) 300 mM (H) 350 mM (I)	Citrate	Buffer type Buffer salt: NaCl pH: 4.9
5	Salt II	NaCl $MgCl_2$	Citrate	Buffer composition, 50 mM Solution ionic strength, 300 mM pH: 4.2
6	Ionic strength III	141 mM (J) 216 mM (K)	Phosphate / citrate	Formulation Buffer salt: NaCl pH: 4.9

A. CARRIER SOLUTION pH VALUE – PHOSPHATE BUFFER

The first carrier solution variable observed during this study was the **pH value**. To this purpose, three phosphate buffer solutions were prepared (Figure 1a), each one at a different pH, by adjusting the salts concentration (the ratio between the amounts of $Na_2HPO_4 \cdot 2\ H2O$ and $NaH_2PO_4 \cdot 2\ H2O$) in order to meet as much as possible the desired final pH value. The final pH adjustment (to 4.9, 6.9 and 10.5) was performed by adding concentrated HCl or NaOH.

Once the carrier solutions were prepared and the HF5-HPLC system was "*conditioned*" by fluxing the chosen carrier solution through the separation-detection system until the UV baseline was stable, a series of blank injections were performed. Their purpose was to establish the UV baseline variations during a normal HF5 run.

It is a known fact that the phosphate buffer has a specific absorption in the UV range if its concentration exceeds a certain value [Aitken and Learmonth 2002] (sub-chapter 3.2.1.1). Furthermore, the UV signal responds to pressure changes in the system that usually occur during a normal FFF run. The blank injections performed in phosphate buffer carrier solutions are reported in Figure 2.

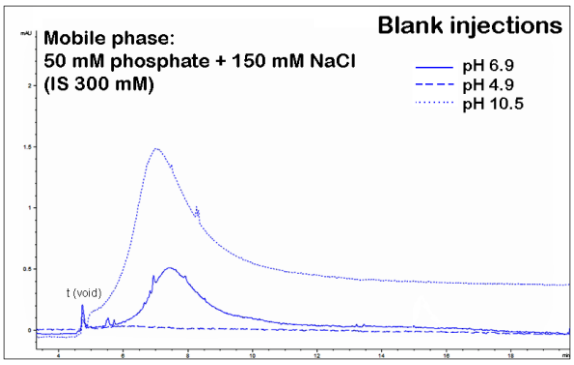

Figure 2 – Blank injections performed in phosphate buffer carrier solutions at different pH

The blank runs reported in Figure 2 show that higher pH values (6.9 and 10.5) of the phosphate buffer have a significant impact on the UV baseline, especially immediately after the elution step begins, which represents the chromatographic

space for the elution of small proteins and/or protein fragments. A UV signal variation in this region could impede the detection of mAb fragments or degradation products.

In order to verify if the above statement applies to mAb1, mAb2 and mAb3, each of them (2 µg of mAb1 and mAb2 and 0.6 µg of mAb3) was separated by HF5-UV and the elution profiles are reported in Figure 3, 4 and 5.

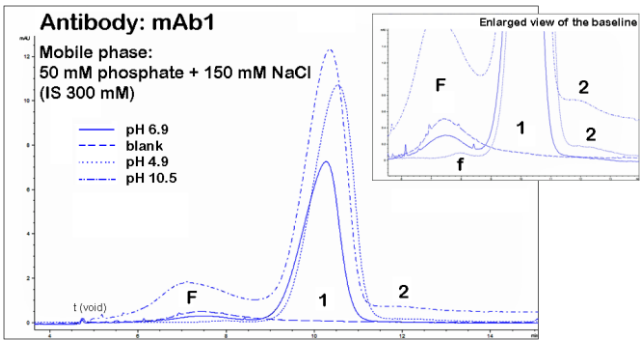

Figure 3 – HF5 separation profiles of mAb1 at 280 nm in phosphate buffer solutions at different pH values. The false baseline signal marked with "F", possible mAb1 fragments marked as "f"

Figure 3 shows the presence of three species corresponding to mAb1, detected by UV at 280 nm. The mAb1 monomer is the predominant species and its peak partly covers the aggregates peak (peak 2). At pH 4.9, peak 2 is not even visible, but it is the only experimental condition which allows the detection of species eluting before the monomer ("f", very likely mAb1 fragments/degradation products). At pH 6.9 and 10.5, the UV baseline false peak "F" impedes the detection of mAb1 fragments.

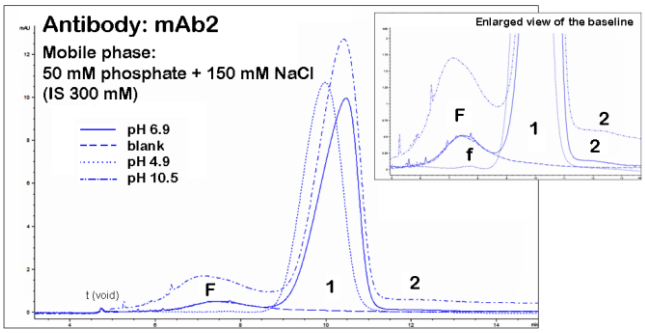

Figure 4 – HF5 separation profiles of mAb2 at 280 nm in phosphate buffer solutions at different pH values. The false baseline signal marked with "F", possible mAb1 fragments marked as "f"

Figure 4 shows the elution profiles of mAb2, which are similar to the ones observed for mAb1. Just as for mAb1, at pH 4.9, peak 2 is not even visible, but it is the only experimental condition which allows the detection of species eluting before the monomer because, at higher pH values, the UV baseline false peak "F" impedes the detection of mAb1 fragments "f".

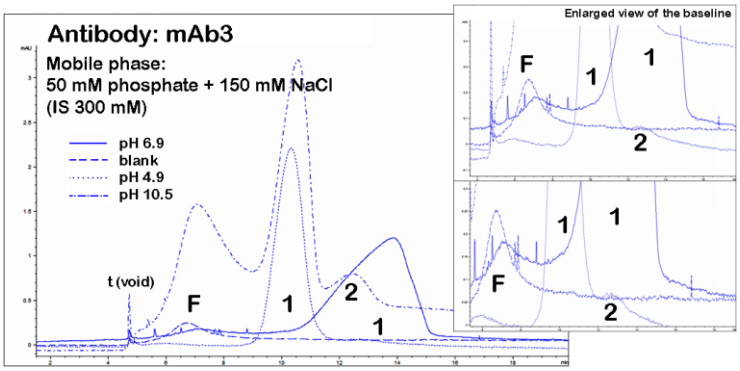

Figure 5 – HF5 separation profiles of mAb3 at 280 nm in phosphate buffer solutions at different pH values. The false baseline signal is marked with "F"

Finally, Figure 5 shows the elution profiles corresponding to mAb3 under different experimental conditions. The UV signal at 280 nm does not detect the presence of fragments eluting before the monomer in any of them. Even though the mAb3 sample amount was the same in every experimental condition, the elution profile at pH 6.9 shows a sample overloading effect consisting in a broad and tailed monomer peak, with delayed retention time. This result indicates that the separation in phosphate buffer at this pH value is not suitable. It is very likely that mAb3 is *unstable* and interacts (non-specifically) with the hollow fiber.

Peak 2, corresponding to mAb3 aggregates, is detected only at low and high pH. Under these experimental conditions the peaks are symmetrical and the highest sample recovery is obtained at high pH.

These experiments have shown how the pH of the carrier solution influences the antibody stability in a very short time (equal to the duration of the HF5 run) and how the instability of an antibody leads to poor/lack of separation and/or interactions with the separation device.

Moreover, the results indicate a correlation between the phosphate buffer pH and the phosphate UV absorption. This specific absorption impedes the detection of antibody fragments/degradation products.

B. CARRIER SOLUTION SALT (I) – PHOSPHATE BUFFER

Next, the **salt type** was considered as variable and the two salts chosen for this study were NaCl and $MgCl_2$. To this purpose, a phosphate buffer solution was prepared at pH 4.9 (Figure 1a) and divided in two containers which were supplemented with the necessary amount of each salt in order to reach a final solution ionic strength of 300 mM. A concentration of 150 mM of NaCl added the same ionic strength to the final mobile phase as 50 mM $MgCl_2$. The final pH adjustment to the desired values (4.9, 6.9 and 10.5) was performed by adding concentrated HCl or NaOH.

As soon as the system was "*conditioned*", a series of blank injections were performed in order to check the UV baseline for variations caused by pressure changes. Since, in this case, there were no UV false peaks; each mAb (2 µg of mAb1 and mAb2 and 0.6 µg of mAb3) was separated under both experimental conditions. The elution profiles are reported in Figures 6, 7 and 8.

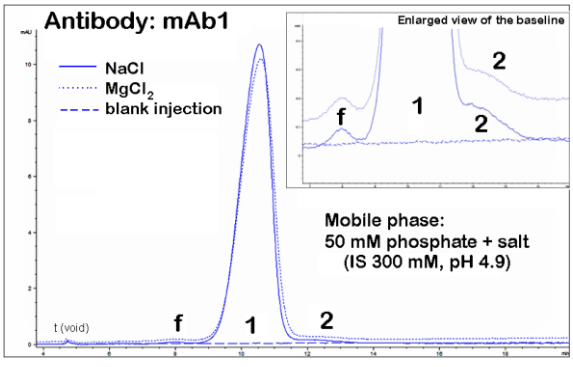

Figure 6 – HF5 separation profile of mAb1 and blank injection at 280 nm in phosphate buffer solutions supplemented with different salts. The mAb1 fragments are marked as "f"

The separation profiles of mAb1 at 280 nm reported in Figure 6 show the elution of 3

peaks, corresponding to mAb1 fragments, monomer and aggregates. Since the monomer is the dominant species, its peak partly covers the aggregates peak. The sample recovery is slightly higher when NaCl is added to the phosphate buffer and the separation performance improves, the band broadening is reduced and the monomer symmetry is closer to a Gaussian peak.

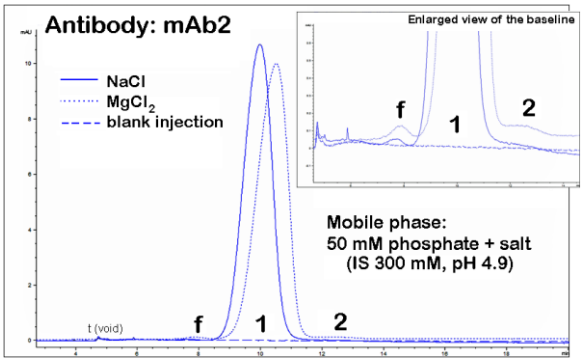

Figure 7 – HF5 separation profiles of mAb2 and blank injection at 280 nm in phosphate buffer solutions supplemented with different salts. The mAb2 fragments are marked as "f"

The separation profiles of mAb2 reported in Figure 7 are very similar to the ones of mAb1 in Figure 6: the aggregates peak (peak 2) is separated better when $MgCl_2$ is added to the carrier solution, but at the expense of sample recovery, peak symmetry and band broadening (separation efficiency).

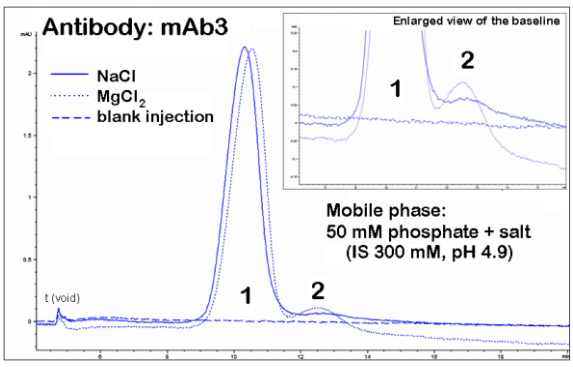

Figure 8 – HF5 separation of mAb3 and blank injection at 280 nm in phosphate buffer solutions supplemented with different salts.

The separation profiles of mAb3 reported in Figure 8 show the presence of two eluting species: mAb3 monomer and aggregates. The resolution between species is

improved visibly when $MgCl_2$ is added to the mobile phase and the sample recovery remains constant. There are no significant differences in terms of peak symmetry or band broadening.

These experiments have shown the importance of choosing the appropriate salt to be added to the carrier solution. The purpose of supplementing the buffer/mobile phase with salt is to improve sample recovery. The ions in solution (in this study, $[Na^+] + [Cl^-]$ and $[Mg^{2+}] + 2[Cl^-]$) surround the protein surface and create an electrostatic shield which suppresses protein interactions (protein-protein or protein-separation device interactions). While the separation of mAb1 and mAb2 is improved in carrier solution containing NaCl, the same effect is observed for mAb3 when adding $MgCl_2$.

C. CARRIER SOLUTION IONIC STRENGTH (I) – PHOSPHATE BUFFER

The third variable considered for this study was the **ionic strength of the carrier solution**. To this purpose, different **phosphate buffer** solutions at pH 6.9 were prepared from a stock solution of 50 mM phosphate buffer supplemented with 150 mM NaCl (IS 300 mM) that was subsequently diluted 1:2 (IS 150 mM) and 1:4 (IS 75 mM). Part of the phosphate buffer solution was left as such (without NaCl supplement, IS 150 mM). The exact composition of the carrier solutions is reported in Table 4.

Table 4 – Composition of phosphate buffer carrier solutions of different ionic strength (pH 6.9)

Carrier	Composition	Ionic strength (mM)
A	50 mM phosphate buffer	150
B	50 mM phosphate buffer + 150 mM NaCl	300
C	25 mM phosphate buffer + 75 mM NaCl	150
D	12.5 mM phosphate buffer + 37.5 mM NaCl	75
E	50 mM phosphate buffer + 200 mM NaCl	350

A series of blank injections was performed under each experimental condition to monitor the behavior of the UV baseline in response to the increasing ionic strength (NaCl amount) and the results are reported in Figure 9.

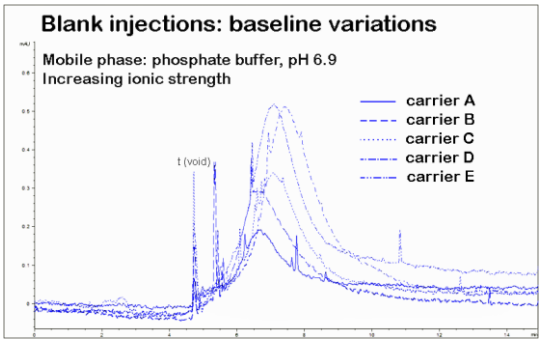

Figure 9 – Blank injections at 280 nm in phosphate buffer solutions with increasing ionic strength.

Figure 9 shows how the UV baseline suffers variations as the ionic strength of the mobile phase in increased, a situation which is similar to the one observed when the pH was varied (Figure 2).

Next, an amount of 2 µg of mAb2 was separated by HF5-UV employing phosphate buffer carrier solutions B, C and D (Table 4) and the elution profiles are reported in Figure 10.

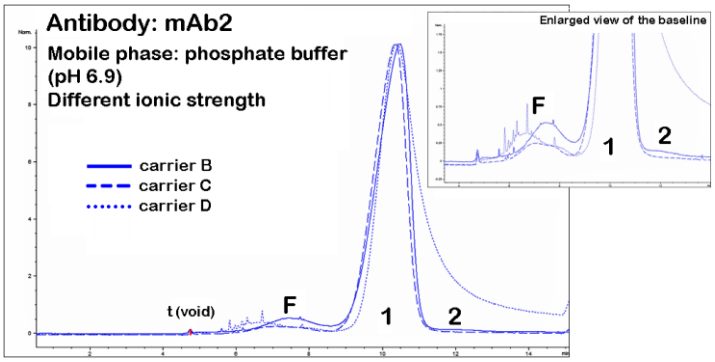

Figure 10 – HF5 separation profiles of mAb2 and blank injection at 280 nm in phosphate buffer solutions of different ionic strength (pH 6.9). The false UV baseline signal is marked with "F"

Figure 10 shows how the separation worsens as the ionic strength is decreased (B > C > D), not only the mAb2 fragments are completely covered by the false peak "F", but

mAb2 starts interacting with the separation device when carrier D is employed (the monomer peak is a broad and highly tailed).

D. CARRIER SOLUTION IONIC STRENGTH (II) – CITRATE BUFFER

In order to determine whether the UV signal variations (that impede the detection of mAb2 fragments) could be avoided, a different type of buffer (**citrate buffer**) was employed as carrier solution for the separation of the antibodies. Four citrate buffer solutions were prepared at different ionic strength values according to the scheme in Figure 1b, at pH 4.9 and their exact composition is reported in Table 5.

Table 5 – Composition of citrate buffer carrier solutions of different ionic strength (pH 4.9)

Carrier	Composition	Ionic strength (mM)
F	50 mM citrate buffer	150
G	25 mM citrate buffer + 75 mM NaCl	150
H	50 mM citrate buffer + 150 mM NaCl	300
I	50 mM citrate buffer + 200 mM NaCl	350

An amount of 2 μg of mAb2 and 0.6 μg of mAb 3 were separated by HF5-UV employing citrate buffer carrier solutions G, H and I (Table 5) and the corresponding elution profiles are reported in Figure 11.

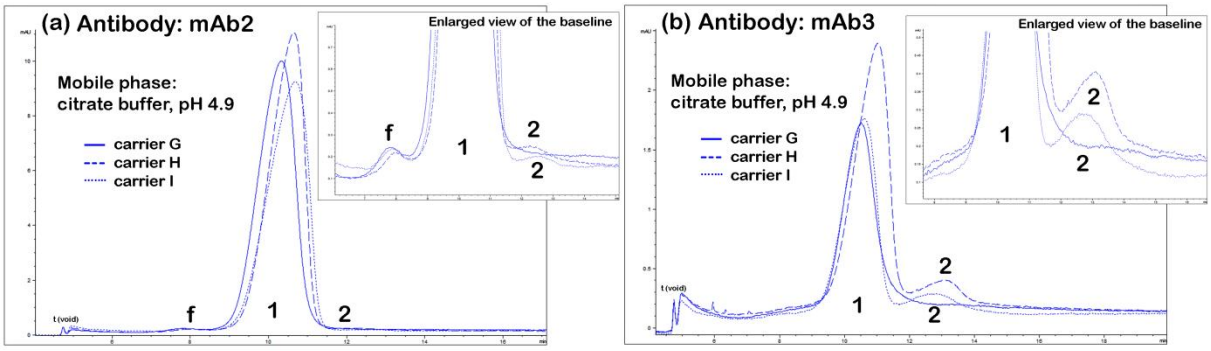

Figure 11 – HF5 separation profiles at 280 nm of (a) mAb2 and (b) mAb3 in citrate buffer solutions of different ionic strength (pH 4.9). Fragments/degradation products of mAb2 are marked as "f".

Figure 11a shows that when citrate buffer is used as carrier solution, instead of phosphate buffer, it allows the detection of mAb2 fragments. Both Figures 11 show that, as the ionic strength is increased (G < H < I), the resolution between peaks 1 and 2 improves. The highest sample recovery for both antibodies is achieved when carrier H is employed. Carrier solution G (IS 75 mM) does not allow the separation of the tested mAbs.

Next, mAb2 and mAb3 separations were performed in buffers (phosphate and citrate) either containing a high NaCl content (200 mM) or not at all. The elution profiles corresponding to mAb2 and mAb3 are reported in Figure 12 and Figure 13, respectively.

Figure 12a reports the separation of mAb2 in carrier solutions which do not contain NaCl. The presence of mAb2 fragments is detected (peak "f"), but the aggregates peak is absent. On the other hand, Figure 12b shows that the presence of high amounts of NaCl in the phosphate buffer leads to the UV false peak "F", which covers the mAb2 fragments. However, the addition on NaCl allowed the separation of the aggregates peak (peak 2) in both phosphate and citrate buffers.

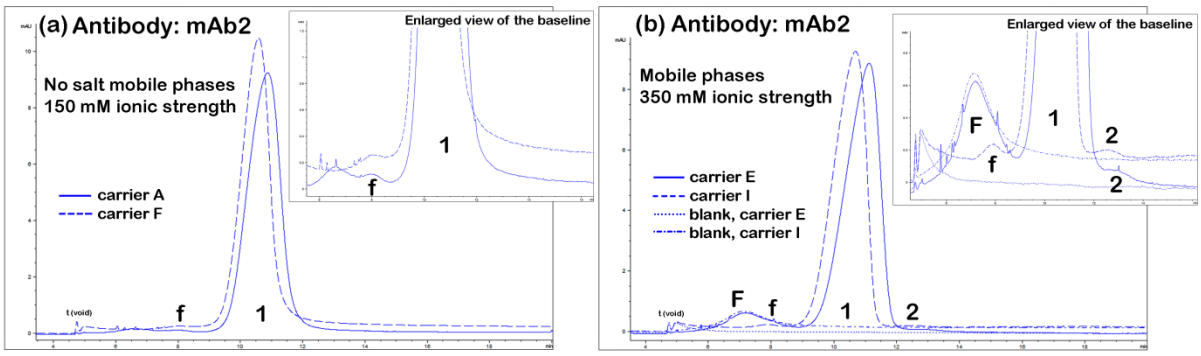

Figure 12 – HF5 separation profiles at 280 nm of mAb2 in (a) carrier solutions without NaCl, A – phosphate and F – citrate and (b) carrier solutions containing a high amount of NaCl, E – phosphate and I – citrate.

The best separation performance and the highest sample recovery were obtained (at both low and high IS) in citrate buffer. It is also very likely that the carrier solution pH had a contribution to improving the separation performance, since the citrate and

the phosphate were employed at different pH values.

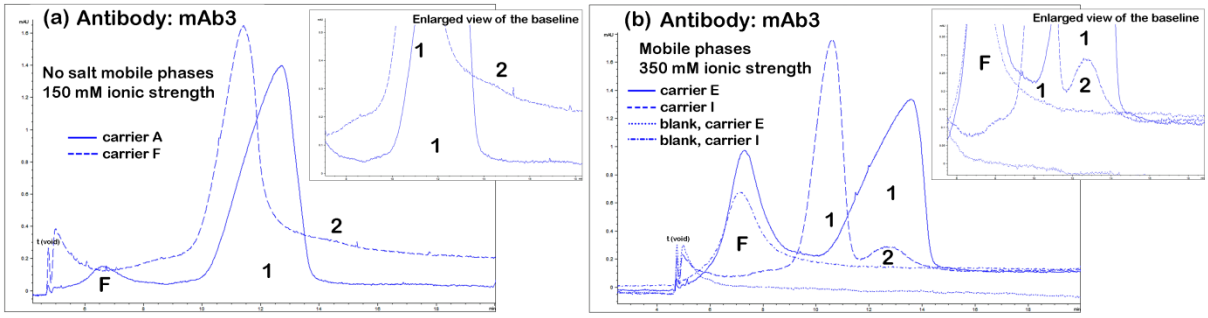

Figure 13 – HF5 separation profiles of mAb2 at 280 nm in (a) carrier solutions without NaCl, A – phosphate and F – citrate and (b) carrier solutions containing a high amount of NaCl, E – phosphate and I – citrate.

Figure 13a reports the separation of mAb2 in carrier solutions which do not contain NaCl. The false UV peak "F" is visible in phosphate buffer, but neither buffer allows detecting the presence of mAb3 aggregates. Figure 13b shows that the presence of NaCl in the phosphate buffer leads to an increased UV false peak "F" that covers the mAb2 fragments, therefore, both phosphate salts and NaCl amounts contribute to its appearance. Furthermore, the separation performance worsens visibly in carrier E. Antibody mAb3 appears to interact with the separation device resulting in a broad, tailed peak. The best separation performance and the highest sample recovery were obtained in citrate carrier I.

These experiments demonstrated how the carrier solution ionic strength affects both mAbs stability and HF5 separation performance. If the ionic strength is too low, the separation does not take place, whereas employing a higher ionic strength can consequently improve sample recovery, as well as aggregates peak separation from the monomer. However, employing phosphate buffer resulted to be problematic, especially at higher salts concentration, leading to system false peak "F" that covered mAb2 fragments. Replacing the buffer type, the UV system peak was eliminated and the separation performance was improved. It is very likely that a lower pH value played a role into improving the mAbs separation.

E. CARRIER SOLUTION SALT (II) – CITRATE BUFFER

Similar to the experiments performed employing phosphate buffer described in subchapter 4.2, the s**alt type** was considered as a variable in the *citrate buffer* composition. To this purpose, the same salts (NaCl and $MgCl_2$) were added separately to a 50 mM citrate buffer solution at pH 4.2, as described in Figure 1b.
Blank injections were performed in order to establish the UV baseline level, followed by sample injections. An amount of 2 µg of mAb2 and 0.6 µg of mAb3 were separated by HF5-UV in citrate buffers and the elution profiles are reported in Figures 14.

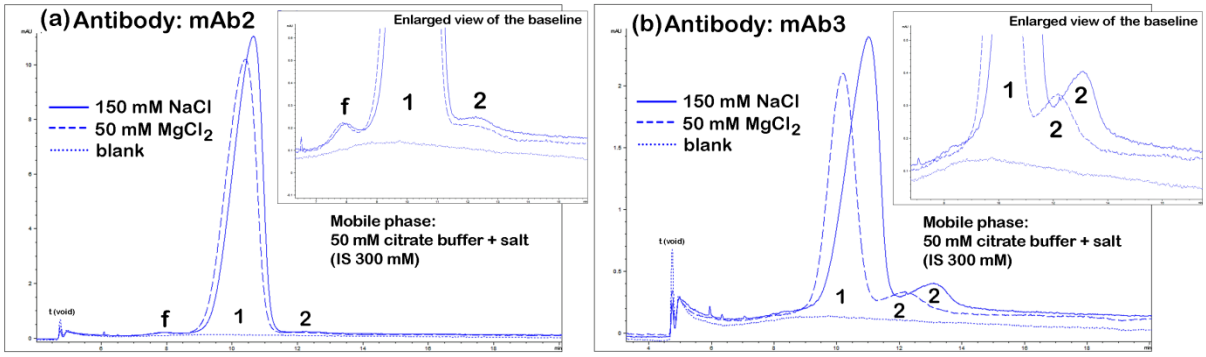

Figure 14 – HF5 separation profiles at 280 nm of (a) mAb2 and (b) mAb3 in phosphate buffer solutions supplemented with different salts. The mAb2 fragments are marked as "f"

Figures 14 show how the presence of $MgCl_2$ in the citrate buffer improves the monomer peak symmetry, unfortunately at the expense of sample recovery, while other separation parameters like the resolution between species and band broadening (separation efficiency) remain unaltered.

These experiments show once again the importance of choosing the appropriate salt to add to the buffer/carrier solution. Both NaCl and MgCl2 provide a good separation performance, while the presence of NaCl is better at assuring a high sample recovery of both mAb2 and mAb3.

Increasing amounts of mAb3 were separated by HF5-UV employing a carrier solution which consisted in 50 mM citrate buffer supplemented with 50 mM $MgCl_2$ in order to establish whether the sample incomplete recovery was caused by the experimental conditions or by an autosampler error. The separation profiles are reported in Figure 15.

The mAb3 total recovery increased when progressively higher sample amounts were injected, established by calculating the area under the peak in each case. The results are reported in Table 6. Since the sample recovery was actually improved when injecting higher amounts, these results exclude a systematic incomplete sample recovery.

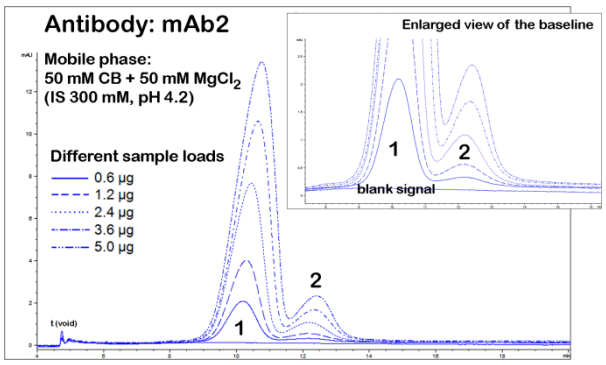

Figure 15 – HF5 separation profiles of mAb3at 280 nm. Increasing amounts of mAb3, separated in 50 mM citrate buffer supplemented with 50 mM $MgCl_2$, pH 4.2

Table 6 – m Ab2 sample recovery calculations based on area under the peak at 280 nm values

Sample amount (µg)	Area under the peak (mAU*s)	Sample relative recovery (%)	Sample recovery increase (%)
0.6	160	100	
1.2	330	103.1	3.1
2.4	706	110.3	10.3
3.6	1110	115.7	15.7
5.0	1597	119.8	19.8

The phenomenon of *nonspecific protein adsobtion* to the hollow fiber inner wall, leading incomplete sample recovery, abnormal elution position, loss of peak symmetry and poor resolution is an issue which HF5 (FFF) and SEC have in

common. The sample interaction with the column matrix is a known SEC limitation. However, this issue can be addressed by performing a series of injections of the same sample known as *make-up runs*, which is a common practice in SEC and recommended by SEC columns manufacturers. The purpose of these make-up runs, which are usually not described in journal articles, is to let the sample adhere to the column matrix until the sample recovery gradually starts to improve, indicating that the non-specific interactions have been diminished because the active "*sticky*" sites have been saturated.

Since it is a proven method to overcome sample loss, this practice was adopted in FFF (HF5). Usually 10-20 μg of sample (or a standard protein, such as BSA) are injected repeatedly and separated by HF5, letting the protein adhere until it saturates the hollow fiber inner wall (HF5).

The downside of this procedure is that, if it is performed with an unstable protein (which might be the case of a protein during formulation development), it might lead to progressive sample accumulation on the hollow fiber wall causing the depletion of the fiber.

These experiments served to demonstrate how sample recovery can be improved by performing a hollow fiber ***make-up*** *procedure, which is a practice adopted from SEC. Therefore, mAb3 separation could be performed in the carrier solution which proved to be optimal from all points of view (separation performance and sample recovery) and the sample recovery was improved by approximately 20%.*

F. CARRIER SOLUTION IONIC STRENGTH (II) – PHOSPHATE / CITRATE BUFFER

Finally, the last set of experiments was performed employing a mixture of phosphate and citrate buffer as carrier solution, at pH 5.0 and supplemented with different amounts of NaCl. This phosphate/citrate combination is very similar to the mAb3 formulation buffer and its preparation is depicted in Figure 1c. The exact carrier solutions composition is reported in Table 7.

Table 7 – Composition of phosphate/citrate buffer carrier solutions, different ionic strength (pH 5.0)

Carrier	Composition	Ionic strength (mM)
J	14.1 mM phosphate buffer + 7.8 citrate buffer + 75 mM NaCl	141
K	14.1 mM phosphate buffer + 7.8 citrate buffer + 150 mM NaCl	216

Blank injections were performed to establish the UV baseline level, followed by sample injections. An amount of 2 µg of mAb2 and 0.6 µg of mAb3 were separated by HF5-UV employing the formulation buffer-like carrier solutions and the elution profiles are displayed in Figure 15.

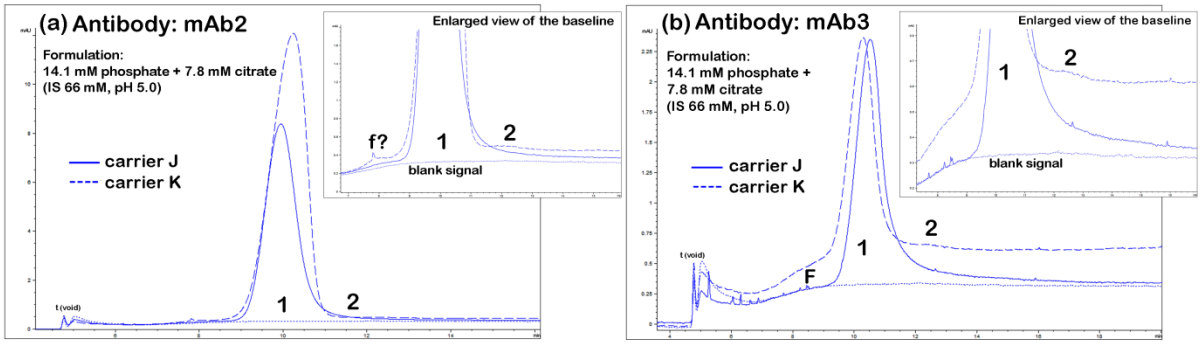

Figure 16 - Separation profiles at 280 nm of (a) mAb2 and (b) mAb3 in phosphate/citrate buffer solutions supplemented with different amounts of NaCl.

Figure 15a, corresponding to the separation profiles of mAb2, shows the presence of fragments and aggregates peaks only in carrier K, with the highest ionic strength

value. On the other hand, the separation profiles of mAb3 depicted in Figure 15b show a poor separation in both cases, as well as false UV peaks probably caused by the phosphate/NaCl salts combination. This carrier solution, even though very similar to the mAb3 formulation buffer, is not suitable for the separation of mAb3.

These experiments demonstrated the possibility to perform separations in carrier solutions whose composition is similar to the formulation buffer of therapeutic proteins. However, separating in such buffers, although guaranteeing less stress on the sample stability, did not lead to good separation results. Sample recovery as well as low abundant mAb species detection and separation may be compromised due to insufficient ionic strength.

4.1.4.5. REFERENCES

[Aitken and Learmonth 2002] Aitken A. and Learmonth M. P. (2002). *Chapter 1: Protein Determination by UV Absorption*. The Protein Protocols Handbook, Second Edition. Walker J. M. Totowa, NJ, Humana Press Ins.

[Dawson et al. 1986] Dawson R. M.; Elliot D. C.; Elliot W. H. and Jones K. M. (1986). *Data for Biochemical Research, 3rd edition*, Oxford Science Publishing.

[Www.Sigmaaldrich.Com]. "*www.sigmaaldrich.com*." Retrieved 23 February, 2014, from http://www.sigmaaldrich.com/life-science/core-bioreagents/biological-buffers/learning-center/buffer-reference-center.html#citric2.

4.1.5. HF5 – FLD METHOD OPTIMIZATION FOR THE QUANTIFICATION OF AGGREGATE LEVELS IN PROTEIN FORMULATIONS.

INTRINSIC FLUORESCENCE-BASED DETECTION OF ANTIBODY AGGREGATES: LOD AND LOQ ESTIMATION.

ADVANTAGES OF MINIATURIZATION: UV DETECTION SENSITIVITY BOOST EMPLOYING A SMALLER INNER DIAMETER HOLLOW FIBER.

This sub-chapter summarizes the exploratory study aimed to demonstrate the advantages of miniaturization of the separation device, online coupled with high sensitivity detection systems, for the detection and quantification of protein aggregates that may be present in antibody formulations. The advantages of using a miniaturized separation device consist not only in a reduced sample dilution during the separation, but also in employing lower flow rates, which – according to Lambert Beer law applied to flow systems (Equation 2, discussed in sub-chapter 3.2.1.1, Chapter 3) – lead to increased detection sensitivity.

Furthermore, the maximum separation efficiency is determined by the analytes biophysical and chemical properties, in particular, by their *detectability* and *tendency*

towards overloading, a key aspect regarding HF5 applications (Equation 13, discussed in sub-chapter 2.2.2, Chapter 2).

The first part of this study describes the method development process of an HF5 method that employs the intrinsic fluorescence of antibodies (in this case, an IgG_1 type antibody) as detection method. Once the HF5 method was optimized, the detection sensitivity was evaluated by means of Limit of Detection (LoD) and Limit of Quantification (LoQ) estimation.

The second part of this study explores other methods of increasing HF5 detection sensibility, which consisted in employing a hollow fiber with a smaller internal diameter and the peptide bond absorption of antibodies as detection method. This study showed that a 4-fold increase in sensitivity as well as a 2-fold increase in efficiency was achieved, even when the antibody aggregates were present at trace levels, when compared to the separation performance obtained with the standard (commercial) hollow fiber membrane.

The definitions and formulas of all analytical parameters employed in this study were previously discussed in sub-chapter 2.4 (Chapter 2).

4.1.5.1. EXPERIMENTAL SETUP

HF5 analyses were performed using an Agilent 1200 HPLC system (Agilent Technologies, Santa Clara, CA, USA) consisting in a degasser, an isocratic pump, an auto sampler, a variable wavelength UV detector and a fluorescence detector, combined with an Eclipse® DUALTEC prototype separation system (Wyatt Technology Europe, Dernbach, Germany). The ChemStation version B.04.02 (Agilent Technologies) data system for Agilent instrumentation was used to set and control the instrumentation and for the computation of various separation parameters. The software package Wyatt Eclipse @ ChemStation version 3.5.02 (Wyatt Technology Europe) was used to set and control the FFF separation system. The fluorescence detector (FLD) was set at an excitation wavelength of 280 nm (specific for proteins) and an emission wavelength of 340 nm, which was the specific fluorescence emission maximum of tryptophan, Trp (therefore for proteins containing this amino acid, such as antibodies).

The hollow-fiber was a 17 cm long polyether-sulfone (PES) fiber, type FUS 0181 available from Microdyn-Nadir (Wiesbaden, Germany) with the following characteristics: 0.8 mm ID, 1.3 mm OD and a molecular weight cut-off of 10 kDa, corresponding to an average pore size of 5 nm. The HF5 separation device was already described in the previous chapters. A hollow fiber membrane with a smaller inner diameter, type FUS 0353 in PES material with 0.5 mm ID and a MWCO of 30 kDa was employed in the last part of this study.

4.1.5.2. SAMPLES AND REAGENTS

The first sample was an IgG_1 antibody, for simplicity named mAb3, at a concentration of 40 mg/mL (stock solution). The sample was initially diluted 1:80 in the mobile phase and a sample volume of 10 µL containing 5 µg of mAb3 was injected at all times during the HF5 method development phase of this study. During the second part of this study – the estimation of LoD and LoQ of the mAb3 aggregate levels – the sample was diluted subsequently until the desired final concentration was achieved. Previous studies on mAb3, discussed in sub-chapter 4.1.4, showed that approximately 10% of the sample was represented by the dimer form of the antibody.

In the third part of this study, where a hollow fiber with a smaller ID was employed to increase detection sensitivity, a different IgG_1 type antibody was used, for simplicity named mAb2, at a concentration of 2 mg/mL. Antibody mAb2 was diluted at a final concentration of 0.5 mg/mL to suit the requirements for this study. During previous studies, reported in Chapter 4.1.4, mAb2 showed very low aggregates levels (1-2%).

The carrier solution/mobile phase employed for the separation of mAb3 was 50 mM citrate buffer supplemented with 50 mM $MgCl_2$, pH 4.2. A different carrier solution, consisting in 50 mM phosphate buffer supplemented with 150 mM NaCl (pH 7.2) was employed for the separation of mAb2. These carrier solutions were found optimal the separation of mAb2 and mAb3, respectively, according to the study conducted in sub-chapter 4.1.4. The carrier solutions were prepared using MilliQ water purified by an Elix 3 UV Water Purification System (Millipore, Billerica, USA) and filtered through 0.2 µm pore membrane sterile filter units (Millipore), at all times.

4.1.5.3. HF5 – (UV) – FLD METHOD DEVELOPMENT FOR mAb3

A. ESTABLISHING THE SIGNAL/NOISE RATIO FOR FLUORESCENCE EMISSION AT 340 nm

First, a previously tested HF5 method was employed for the separation of mAb3, which represented the starting point for the method development. An amount of 5 µg of mAb3 was injected during the focus-inject step, performed at 0.85 ml/mL focus flow rate for 4 min. When the focus step was completed, the sample was eluted at a channel flow rate of 0.35 mL/min, under the effect of a constant cross-flow rate of 0.35 mL/min for 15 min. The fluorescence emission at 340 nm and the absorbance at 280 nm were recorded simultaneously and the separation profiles are reported in Figure 1.

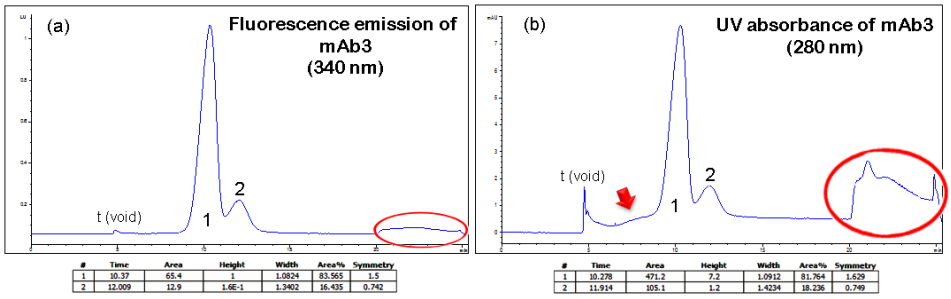

Figure 1 – HD5 separation profiles of mAb3: (a) fluorescence emission at 340 nm and (b) UV absorbance at 280 nm (b) recorded during the same sample run

Previous studies (sub-chapters 4.1.3 and 4.1.4) have confirmed that the UV signal is not only affected by pressure variations during a normal FFF run, in particular when switching between operational modes (such as the signal variations shown in the red circles in Figure 1), but also requires a long period of time to stabilize before a sample run can be performed (usually 45-60 min, called "*system conditioning*"). This is because many salts in the mobile phase composition (such as phosphates, but also

acetate and citrate) have an UV absorbance of their own [Aitken and Learmonth 2002]. It is a known fact that, even though protein absorbance at 210 or 215 nm of the peptide bonds is very intense, it is rarely used because of possible impurities interference (such as the previously mentioned mobile phase salts).

Figure 1b shows how the UV baseline is affected by the pressure changes during mAb3 separation performed in citrate buffer. The red arrow indicates a signal variation which could be easily mistaken for the presence of mAb3 fragments. Fortunately, Figure 1a confirms that mAb3 does not contain any fragments; therefore, the UV signal variation should be attributed to other factors. The lack of specific sample signal represents an important issue, especially when the sample composition is unknown or during the quantification of low protein aggregates levels. This is where the fluorescence detection comes into play. Figure 1a shows that not only the system conditioning is not required (since the mobile phase salts do not fluoresce at 340 nm), but also the baseline remains stable during the entire HF5 sample run.

Once the sample run is completed, the next one can be performed right away, without the need to wait for the baseline to stabilize again. The areas highlighted by the red circles in Figure 1a and 1b show the signal variation when the cross-flow is annulled (also called "*field release*"), allowing the sample components which were not separated to exit the system before the next injection. This "*M*" shaped signal variation is very common and is known as "*system peak*". If the separation system and the online coupled detectors are clean, the height of this peak is constant and is identical even during blank runs (Figure 2a and 2b), therefore, serves as indicator.

Next, the fluorescence emission and the UV absorbance were registered during a blank run in order to establish the signal/noise ratios (S/N) and the profiles are reported in Figure 2.

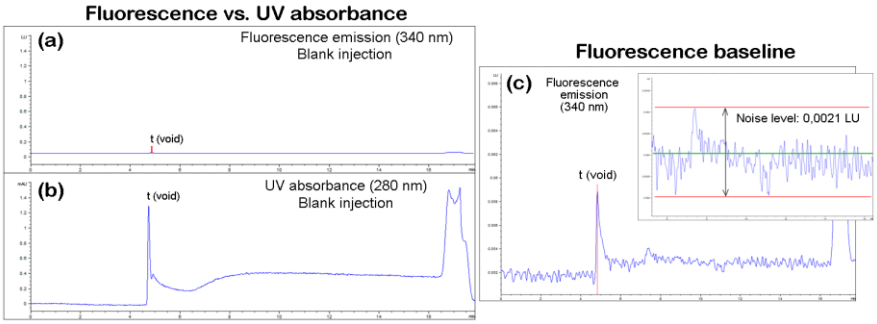

Figure 2 – (a) Fluorescence emission at 340 nm and (b) UV absorption at 280 nm during the same blank run; (c) estimation of the noise level of the fluorescence baseline

The blank run in Figure 2b reflects, once more, the UV signal baseline variations caused by the pressure changes which occur during the normal operation of an FFF system. And, once again, Figure 2a shows that the fluorescence signal is not affected by the pressure changes. The fluorescence signal baseline was examined more closely in Figure 2c and the noise level was established at 0.0021 LU, as the signal random variations above and below the "*zero line*" in green.

B. HF5 – FLD METHOD OPTIMIZATION FOR mAb3

The first HF5 parameter that was optimized was the *focus time*. The same mAb3 amount (5 µg) was injected during the focus-inject step at 0.85 mL/min of focus flow rate, while the focus-inject duration was increased over subsequent runs. The sample was eluted at a channel flow rate of 0.35 mL/min, under the effect of a constant cross-flow rate of 0.35 mL/min. The separation profiles are reported in Figure 3.

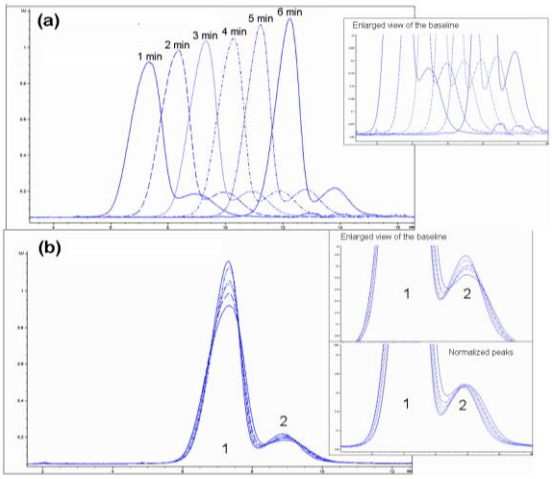

Figure 3 – HF5 separations of mAb3 with different focus-inject durations (a) real scale and (b) peaks overlaid on the monomer retention time at 6 min focus-inject

The mAb3 monomer peak height increases proportionally to the focus – inject duration. Figure 4a shows the importance of the sample relaxation process (sample focus step), which may lead to incomplete separation or even incomplete sample recovery. Figure 4b shows that, as the focus-inject time duration increases, the band broadening is reduced and the peaks become narrower. Moreover, the separation between the two peaks improves, shown by the progressive decrease of the valley height between the peaks.

Table 1 reports the effects of the sample focus time on the separation through parameters like area under the peak, peak height and peak width at half height ($w_{1/2}$), retention times, and peak symmetry.

Table 1 – Sample focus-inject time variation effects on the separation performance

	#	Time	Area	Height	Width	Area%	Symmetry
1 min	1	7.323	66.7	8.6E-1	1.2866	86.431	1.338
	2	8.951	10.5	1.3E-1	1.3536	13.569	0.684
2 min	1	8.354	67	9.3E-1	1.1951	85.613	1.522
	2	9.913	11.3	1.4E-1	1.3426	14.387	0.641
3 min	1	9.299	67	9.8E-1	1.1378	85.760	1.407
	2	10.981	11.1	1.4E-1	1.3003	14.240	0.933
4 min	1	10.283	65.3	1E0	1.0909	85.621	1.555
	2	11.925	11	1.5E-1	1.2606	14.379	0.94
5 min	1	11.214	64.9	1.1	1.0109	85.426	1.469
	2	12.814	11.1	1.5E-1	1.2186	14.574	0.891
6 min	1	12.238	65.9	1.1	0.9924	85.016	1.517
	2	13.783	11.6	1.6E-1	1.2037	14.984	0.841

Increasing the focus time up to 4 min, an improvement in both sample recovery (estimated as total area under the peak) and monomer-dimer resolution is observed. Between 4 min and 6 min, the resolution is constant and only the sample recovery improved slightly. A **4 min focus time** was considered optimal and used in the following experiments.

Next, the *cross—flow rate* was chosen as a variable and all other separation parameters were kept constant. The same mAb3 amount (5 µg) was injected during the focus-inject step at 0.85 mL/min of focus flow rate for 4 min. The sample was eluted at a channel flow rate of 0.35 mL/min, under the effect of different, but constant cross-flow rates. The elution profiles are reported in Figure 4.

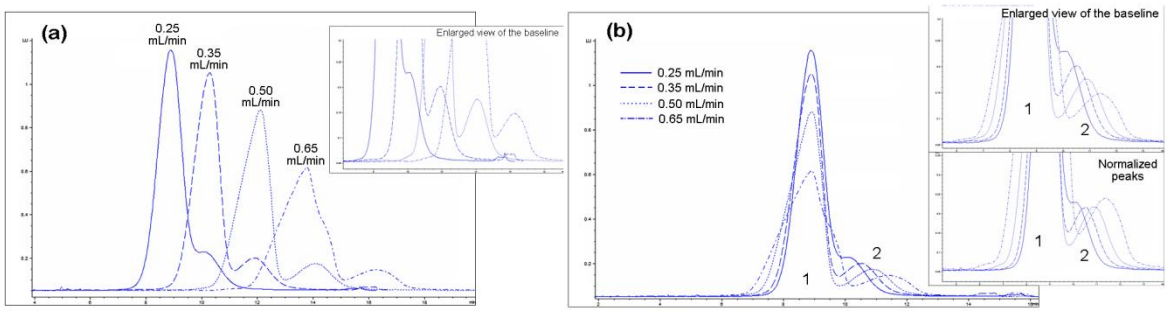

(c)

#	Time	Area	Height	Width	Area%	Symmetry	
1	8.869	71.2	1.1	1.0752	88.123	1.055	0.25 mL/min
2	10.135	9.6	1.7E-1	0.9192	11.877	0.402	
#	Time	Area	Height	Width	Area%	Symmetry	
1	10.283	65.3	1E0	1.0909	85.621	1.555	0.35 mL/min
2	11.925	11	1.5E-1	1.2606	14.379	0.94	
#	Time	Area	Height	Width	Area%	Symmetry	
1	12.093	61.7	8.3E-1	1.2431	85.339	1.979	0.50 mL/min
2	14.027	10.6	1.2E-1	1.466	14.661	0.92	
#	Time	Area	Height	Width	Area%	Symmetry	
1	13.762	59.6	5.7E-1	1.7523	85.866	1.588	0.65 mL/min
2	16.254	9.8	9.5E-2	1.7243	14.134	1.016	

Figure 4 – HF5 separation profiles of mAb3 under the effect of different cross-flow rates (a) real scale and (b) peaks overlaid on the monomer retention time at 0.65 mL/min cross-flow rate and (c) table reporting the separation performance parameters

As the cross-flow rates increases, the resolution between the peaks improves noticeably up to a certain point (0.5 mL/min of cross-flow rate value). The sample recovery decreases slightly as the cross-flow value is increased. Since the sample spends more time inside the hollow fiber, while being retained by progressively

stronger fields, it was expected that the peaks became progressively broader because of the longitudinal diffusion effect (a.k.a. band broadening). The strength of the field (the flow rate) causes the peaks to become increasingly more asymmetrical (tailed). Finally, the effect of a field that is too strong for the separation of mAb3 (0.65 mL/min) causes an effect which resembles very much to the sample overloading effect. This is the reason why the monomer peak looks "*split*" and the separation actually worsens. A **cross-flow rate of 0.5 mL/min** was considered optimal and used in the following experiments.

Next, the *channel (detector) flow rate* was chosen as a variable and all other separation parameters were kept constant. The same mAb3 amount (5 μg) was injected during the focus-inject step at 0.85 mL/min of focus flow rate for 4 min. The sample was eluted at different channel flow rates, under the effect of a constant cross-flow rate of 0.5 mL/min. The elution profiles are reported in Figure 5.

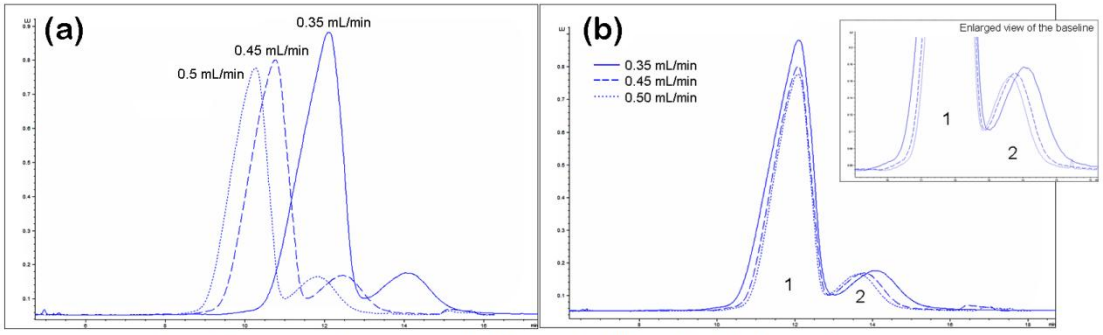

(c)

#	Time	Area	Height	Width	Area%	Symmetry	
1	12.093	61.7	8.3E-1	1.2431	85.339	1.979	0.35 mL/min
2	14.027	10.6	1.2E-1	1.466	14.661	0.92	

#	Time	Area	Height	Width	Area%	Symmetry	
1	10.759	50.3	7.5E-1	1.1213	85.364	1.938	0.45 mL/min
2	12.455	8.6	1.1E-1	1.2557	14.636	1.058	

#	Time	Area	Height	Width	Area%	Symmetry	
1	10.267	45.6	7.2E-1	1.0539	85.567	1.969	0.50 mL/min
2	11.837	7.7	1.1E-1	1.1717	14.433	1.101	

Figure 5 – HF5 separation profiles of mAb3 under the effect of different channel flow rates (a) real scale and (b) peaks overlaid on the monomer retention time at 0.35 mL/min channel flow rate and (c) table reporting the separation performance parameters

As the channel flow rate is increased, the band broadening diminishes (the faster channel flow counteracts the sample longitudinal dispersion). The peaks resolution

remains constant, as well as the valley height between the monomer and dimer. Since the signal intensity increases inversely to the flow rate, a slower channel rate can be used to enhance detection. However, in this study a **channel flow rate of 0.5 mL/min** was considered optimal and used in the following experiments.

Summarizing, the **optimal** HF5-FLD method consisted in injecting the mAb sample during focus, performed at 0.85 mL/min for 4 min. Once the focus step was complete, the sample was eluted at 0.5 mL/min (initially 0.35 mL/min), under the effect of a constant cross-flow rate of 0.5 mL/min (initially 0.35 mL/min).

The comparison between the elution profiles of mAb3, obtained applying the initial HF5 method and the optimized method is reported in Figure 6.

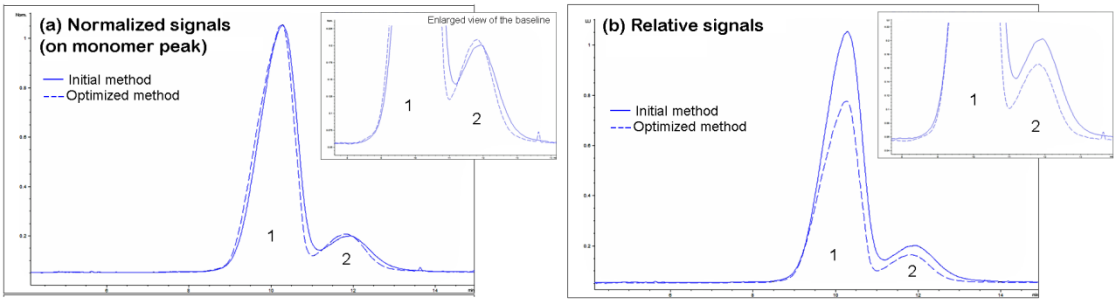

(c)

#	Time	Area	Height	Width	Area%	Symmetry	
1	10.283	65.3	1E0	1.0909	85.621	1.555	Initial method
2	11.925	11	1.5E-1	1.2606	14.379	0.94	

#	Time	Area	Height	Width	Area%	Symmetry	
1	10.267	45.6	7.2E-1	1.0539	85.567	1.969	Optimized method
2	11.837	7.7	1.1E-1	1.1717	14.433	1.101	

Figure 6 – HF5 separation profiles of mAb3: (a) initial HF5 method; (b) optimized HF5 method, (c) table reporting the separation performance parameters

Since the ratio between the channel flow rate and the cross-flow rate did not change (=1), the optimized method allows the separation of mAb3 monomer and dimer in approximately 14 min of analysis time, while the separation performance is improved. This optimized method was employed at all times from this point forward.

4.1.5.4. STUDY FOR THE DETERMINATION OF THE LIMIT OF DETECTION (LOD) AND THE LIMIT OF QUANTIFICATION (LOQ) OF AGGREGATE LEVELS PRESENT IN mAb3 FORMULATION.

A. ASCERTAINING THE LINEARITY INTERVAL FOR THE mAb3 FLUORESCENCE EMISSION AT 340 nm

Signal to Noise Ratio (S/N) is a dimensionless measure of the relative strength of an analytical signal (S) to the average strength of the background instrumental noise (N) for a particular sample and is closely related to the detection level. The ratio is useful for determining the effect of the noise on the relative error of a measurement [Skoog and Leary 1992].

Limit of Blank (LoB), Limit of Detection (LoD), and Limit of Quantification (LoQ) are terms used to describe the smallest concentration of an analyte that can be reliably measured by an analytical procedure.

LoD is a feature of limit assays, usually expressed as %, ppm or ppb and defined by the ICH guidelines as "*the lowest amount of analyte in a sample that can be detected, but not necessarily quantitated under the stated experimental conditions*". There are two approaches for the determination of LoD. The first consists in comparing signals from samples with known levels of impurities with blank signals (the LoD is then established at a ratio of 2:1 or 3:1),while the second approach consists in estimating the LoD from the standard deviation of the signal and the slope of the calibration curve (LoD=3σ/s) [Guidelines 2014].

On the other hand, LoQ is a feature of quantitative assays for low levels of analytes in sample matrices and is defined by the ICH guidelines as "*the concentration of the related substance in the sample that will give a S/N ratio of 10:1*". Impurities in bulk drug substance, as well as degradation products in final therapeutic protein formulations are characterized by means of LoQ. LoQ of an analytical method is influenced by

detector sensitivity, as well as sample preparation procedure at low levels of impurities [Guidelines 2014].

The Limit of Blank can be calculated from: $LoB = mean_{blank} + 1.645 (STDEV_{blank})$.
In this study, five blank injections were performed for the determination of **LoB** and a value of **0.00229** was found ($mean_{blank} = 0.00202$ L.U. and $STDEV_{blank} = 0.000164$ L.U.).

In general, the fluorescence detection cannot be used to quantify (there are a few exceptions, and even so the method for quantifying cannot be validated) because, although directly correlated to the protein amount, an increase in the fluorescence signal can also indicate changes in the protein conformation, therefore not able to distinguish between the two. However, the intrinsic fluorescence signal is highly valuable in determining whether certain experimental conditions change the protein molecular conformation or whether the changes occur in the proximity of a fluorophore (observed as a shift in the emission wavelength or change in fluorescence intensity). Therefore, in general, fluorescence detection only provides qualitative information [Zölls et al. 2012].
Despite all these reasons, since this study did not involve drastic changes in the experimental conditions which would result in conformational modifications, the intrinsic Trp fluorescence is proposed as sensitive method of detection for the quantification of mAb3 aggregates levels.

In order to ascertain of the *linear relationship* between the fluorescence signal intensity and the sample amount, in the concentration range of interest (which was as low as possible, since LoD and LoQ were to be determined), a series of six different sample amounts was injected and each of them was replicated 3 times, each time injecting the same sample volume. The mAb3 dilutions are reported in Table 2.

Table 2 – Sample dilutions of mAb3 in mobile phase

Initial concentration of the stock solution	Dilution	Final concentration (mg/mL)	Injected amount (constant V_{inj}=10 µL)
40 mg/mL	1:80 from 40 mg/mL	0.5	5.000
	1:1.25 from 0.5 mg/mL	0.4	4.000
	1: 2 from 0.5 mg/mL	0.25	2.500
	1:2 from 0.25 mg/mL	0.125	1.250
	1:5 from 0.5 mg/mL	0.1	1.000
	1:3 from 0.1 mg/mL	0.0334	0.334

The elution profiles of the different mAb3 sample amounts are reported in Figure 6. As the sample amount is diminished, the peaks become more symmetric (below 2.5 µg) and the ratio between the monomer and the dimer peak height increases (from 7 to 12.5).

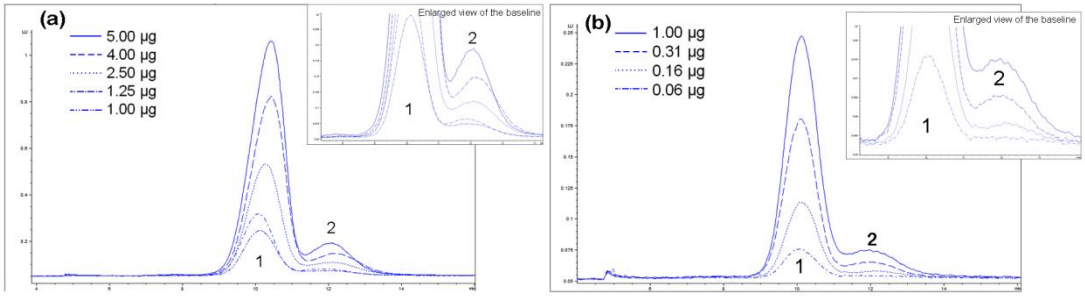

Figure 7 – HF5-FLD separation profiles of different amounts of mAb3, (a) above 1µg and (b) below 1µg

Figure 6b reports the separation profiles of sample amounts below 1 µg of mAb3 sample. The dimer peak cannot be discriminated from the baseline if the injected mAb3 amount is too low (below 0.16 µg).

The *calibration curve*, which correlates the intensity of the fluorescence signal and the sample concentration, was traced by plotting the mAb3 dimer peak height against the corresponding injected (total) sample amount and is reported in Figure 7, along with the separation performance parameters.

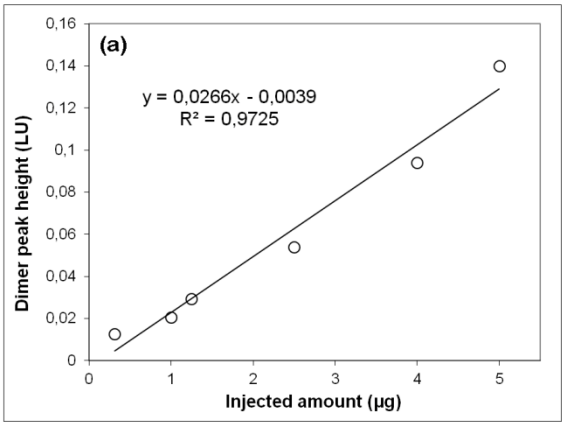

(b)

#	Time	Area	Height	Width	Area%	Symmetry	
1	10.095	8.1	1.3E-1	1.0616	88.177	1.017	0.31 µg
2	12.022	1.1	1.2E-2	1.4757	11.823	0.814	
#	Time	Area	Height	Width	Area%	Symmetry	
1	10.11	12.5	1.9E-1	1.0794	86.842	0.941	1.00 µg
2	11.957	1.9	2.1E-2	1.4871	13.158	0.611	
#	Time	Area	Height	Width	Area%	Symmetry	
1	10.059	16.6	2.6E-1	1.0459	87.138	0.991	1.25 µg
2	11.805	2.4	2.9E-2	1.4315	12.862	0.606	
#	Time	Area	Height	Width	Area%	Symmetry	
1	10.263	31.6	4.8E-1	1.0984	86.597	1.108	2.50 µg
2	12.1	4.9	5.5E-2	1.4695	13.403	0.768	
#	Time	Area	Height	Width	Area%	Symmetry	
1	10.428	51.7	7.7E-1	1.1185	86.249	1.41	4.00 µg
2	12.141	8.2	9.4E-2	1.4615	13.751	0.664	
#	Time	Area	Height	Width	Area%	Symmetry	
1	10.413	66.7	1	1.1052	86.142	1.422	5.00 µg
2	12.084	10.7	1.4E-1	1.2954	13.858	0.907	

Figure 8 – (a) Calibration curve for the mAb3 dimer peak and (b) separation performance parameters, including the dimer peak height values used for the calibration curve

Once the linear relationship was established, the LoD and LoQ for the mAb3 dimer were calculated and the results are reported in Table 3.

Table 3 - LoD and LoQ determination of mAb3 aggregates

Equation	x1 (µg)	x2 (µg)
LoD = y1 = 0.0266 x1 – 0.0039	0.404	
LoQ = y2 = 0.0266 x2 – 0.0039		1.007
Where: LoD = 3 × LoB = 0.006871 L.U. (y1) LoQ = 10 × LoB = 0.022903 L.U. (y2)		

The LoQ and LoD values reported in Table 3 refer to the mAb3 injected amount required for the dimer to the distinguished from the instrumental noise (0.404 µg) and the mAb3 amount required for the dimer to be quantified (1.007µg). When 1 µg of mAb3 was injected, the dimer represented 13.16% of the total amount (Table in Figure 7b), therefore, the smallest quantifiable dimer amount was **132 ng**.

Following the same procedure, the smallest dimer amount that can be detected by the FLD detector was found to be **47.86 ng**, representing 11.82% of the mAb3 injected amount.

4.1.5.5. ADVANTAGES OF MINIATURIZATION: UV SIGNAL SENSIBILITY BOOST WHEN EMPLOYING A HOLLOW FIBER WITH A SMALLER INNER DIAMETER HF5 – UV METHOD FOR THE SEPARATION OF mAb2

STUDY PERFORMED IN COLLABORATION WITH WYATT TECHNOLOGY EUROPE (DERNBACH, GERMANY)

As discussed in sub-chapter 3.2.1.1, the Lambert-Beer law applied to flow systems (*Equation 2*) shows how the sample absorbance (A) is inversely related to the volumetric flow rate value (F). This linear relationship can be affected by sample recovery. The area under the peak for each analyte at a specific wavelength is correlated to the sample recovery through the extinction coefficient (at the same wavelength) and, therefore, inversely proportional to the flow rate at which the analyte is eluted through the UV detection system. Especially when dealing with trace levels of protein aggregates, we can make the most of this relationship by decreasing as much as possible the channel (detector) flow rate. However, we need take into consideration the implications of a slower channel flow rate on band broadening, as reported in the mAb3 method development part of this study.

A relatively simple solution which could resolve the band broadening issue, even at very low channel flow rates, is further miniaturization of the separation device. In theory, this solution can be implemented by simply replacing the standard hollow fiber membrane (PES, ID 800 μm) with a hollow fiber of the same material having a smaller inner diameter.

A variety of hollow fiber materials, pore sizes corresponding to different MWCOs are available from Microdyn Nadir (the supplier for the hollow fibers which are compatible with the HF5 cartridge commercialized by Wyatt Technology Europe), suitable for different fields of application (environment, metal, textile, paper, food, pharmaceutical/biotechnology and chemical). However, the choice in terms of hollow fiber inner diameter (ID) is restricted to a narrow range, from 0.5 to 1.0 mm.

Therefore, the hollow fiber of choice for this sensibility study was the one with the smallest ID, with the following characteristics: type FUS 0353, PES material, ID 0.5 mm, pore size corresponding to a MWCO of 30 kDa and 17 cm of length. One of the main concerns in replacing the standard hollow fiber membrane (with a larger ID, 0.8 mm) was the efficacy of the sealing system. Fortunately, there were no visible leaks when the smaller ID hollow fiber replaced the standard one, therefore we proceeded with the study.

The protein chosen for this study was a different IgG_1 type antibody, mAb2. During previous studies on this particular antibody (described in Chapter 4.1.4), the monomeric form was very stable and only a very small percentage of this mAb2 was found as dimer (roughly 1.5%), also very stable under various environmental changes. Therefore, mAb2 was considered the optimal sample type for this study because it contained only trace amounts of aggregates and they were stable.

A very low amount of mAb2 (0.15 μg, 0.3 μL of a 0.5 mg/mL mAb2 solution) was injected at all times and the separations were performed employing 50 mM phosphate buffer supplemented with 150 mM NaCl (ionic strength: 300 m) at a final pH of 7.2 as mobile phase. A UV/Vis variable wavelength detector set at 205 nm was coupled online with the HF5 module on the Eclipse® DUALTEC™ FFF separation system as a concentration detector and to monitor the separation process.

While the UV signal at 280 nm is specific for the proteins amino acidic side chains (in particular, only three of them are chromophores: tyrosine, phenylalanine and especially tryptophan) and can be employed to identify a particular protein and discriminate between proteins, in the far UV region (between 190 and 230 nm) the protein chains have a very low absorbance compared to the peptide bond. Therefore, the peptide bond absorbance at 205 nm can be considered an absolute means to determine the protein presence in a sample and, even though the protein absorbance maximum intensity is at 190 nm (at 205 nm is only half the value obtained at 190 nm), the 205 nm is the wavelength of choice because there is no oxygen absorbance interference [Aitken and Learmonth 2002].

The HF5 method was adjusted accordingly to suit the new hollow fiber membrane characteristics: the sample runs were performed by injecting the same amount of sample (0.15 µg of mAb2) during focus, performed at 0.22 mL/min for 6 min (to compensate for the very low flow rate). After the completion of the focus step, the sample was eluted at a channel flow rate of 0.22 mL/min under the effect of different cross-flow rates (different filed strengths). The elution profiles obtained under different cross-flow rates are reported in Figure 8.

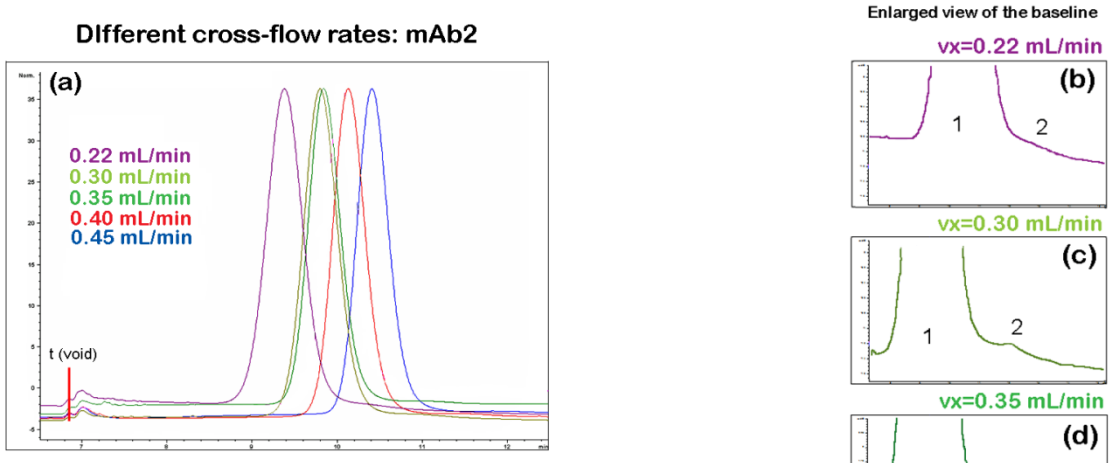

(g)

Vx (mL/min)	Species	t_R (min)	Area (%)	Peak height (mAU)	Peak width (min)	Peak symmetry	Resolution (R_s)	Efficiency (# plates)	Retention level (R_L)
0.22	1mer	2.8780	98.4	34.2	0.5189	0.94		170	1.4
	2mer	3.6330	1.5	0.7	0.4106	-	1.2	434	1.6
0.30	1mer	3.2960	98.7	35.0	0.4903	0.89		250	1.5
	2mer	4.2000	1.4	0.4	0.5368	-	1.2	339	1.6
0.35	1mer	3.3370	98.6	34.8	0.4167	0.87		355	1.5
	2mer	4.4800	1.4	0.4	0.5784	0.35	1.4	332	1.7
0.40	1mer	3.6270	98.2	35.2	0.4167	0.87		420	1.6
	2mer	4.8670	1.8	0.4	0.7350	0.44	1.3	243	1.7
0.45	1mer	3.9060	98.9	33.9	0.4069	0.86		511	1.6
	2mer	5.3210	1.1	0.2	0.8564	0.92	1.3	214	1.8

Figure 9 – HF5 separation profiles of mAb2 at 205 nm, employing a hollow fiber with an ID of 0.5 mm (a – f) and the separation performance parameters table (g)

All separation profiles show that the dimer is not completely separated from the monomer. However, this is not a reflection on the performance, but rather a consequence of the proportion between the two mAb2 species. Since the monomer is present in a very large amount (98.5% of the sample), its peak is very broad

compared to the dimer peak. Consequently, the tail of the monomer peak partly covers the dimer peak.

Applying an increasingly stronger field, the dimer peak is better resolved, shown by Figures 8b through 8f. The separation efficiency for the monomer increases proportionally with the cross-flow rate, while the efficiency for the dimer has an opposite trend. This can be explained by the fact that the dimer peak width increases proportionally with the field strength, but so does the retention level (evaluated through the retention time value, t_R). An opposite trend was observed for the monomer peak width (Table g in Figure 8).

As the cross-flow rate increases, the monomer peak remains symmetric, while the dimer peak becomes tailed under the effect of stronger fields. The peak symmetry was calculated only when the flow conditions allowed the separation of the dimer peak (Figures 8d – 8f).

There were no noticeable trends of the resolution as the cross-flow rate was increased. The monomer-dimer resolution had an acceptable value at all times (1.25 = baseline separation > R_S > 1 = acceptable).

4.1.5.6. CONCLUSIONS

This study provided proof that, when a miniaturized separation device like a very small ID hollow fiber (membrane) is coupled online with a very sensitive detection method, such as UV detection at 205 nm, trace amounts of aggregate levels can be successfully detected and quantified. When injecting only 150 ng of mAb2, an amount as low as 2.25 ng of dimer can be quantified, corresponding to 1.5% of the total protein amount.

The proposed HF5-UV method is not only time-efficient, allowing the mAb2 separation under 13 min, but the use of a smaller ID hollow fiber as separation device also enhances considerably the detection sensitivity.

In Figure 9, a comparison between the separation performance of the commercial hollow fiber membrane and the smaller ID hollow fiber is reported. The fluorescence detection at 340 nm was used as detection method, based on the optimistic results described previously in this sub-chapter, when the sample of choice was mAb3 (which contained a larger amount of dimer).

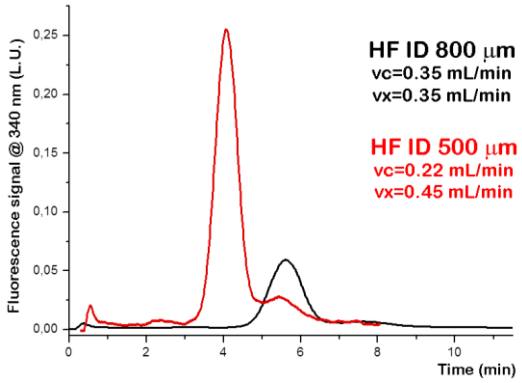

Figure 10 – HF5 separation profiles of mAb2. Comparison between hollow fiber separation devices: standard membrane (ID 0.8 mm, black) and smaller ID membrane (ID 0.5 mm, red). Advantages of miniaturization: sensitivity and separation efficiency

From the dimer peak height ratio obtained under the flow conditions (corresponding to the two hollow fiber devices), we obtain a 4-fold sensitivity increase when the hollow fiber ID is smaller. Similarly, for the same hollow fiber smaller ID, we observe a 2-fold efficiency increase, thanks to the more advantageous retention time/peak width ratio. These results are in agreement with the conclusions drawn from *Equation 13* in sub-chapter 2.2.2 (Chapter 2).

4.1.5.7. REFERENCES

[Aitken and Learmonth 2002] Aitken A. and Learmonth M. P. (2002). *Chapter 1: Protein Determination by UV Absorption*. The Protein Protocols Handbook, Second Edition. Walker J. M. Totowa, NJ, Humana Press Ins.

[Guidelines I. Q., 1997]. "*ICH Quality Guidelines, Validation of Analytical Procedures: Methodology*." Retrieved 23 February, 2014, from http://www.ich.org/products/guidelines/quality/article/quality-guidelines.html.

Skoog D. A. and Leary J. J. (1992). *Principles of Instrumental Analysis/Solution Manual, 4th edition*.

[Zölls et al. 2012] Zölls S.; Tantipolphan R.; Wiggenhorn M.; Winter G.; Jiskoot W.; Friess W. and Hawe A. (2012). "*Particles in therapeutic protein formulations, Part 1: Overview of analytical methods*." Journal of Pharmaceutical Sciences **101** (3): 914–935.

4.1.6. HF5 – MALS AND SEC – MALS PERFORMANCE COMPARISON FOR THE SEPARATION OF IMMUNOGLOBULINS (IgGs).

FFF SELECTIVITY FEATURE

In this sub-chapter, the advantages of HF5 in terms of versatility (carrier solution composition, even similar to the antibody formulation buffer), lower sample dilution and FFF selectivity are the features which make it an ideal candidate as SEC orthogonal method for therapeutic proteins formulation characterization.

The miniaturization of the separation device – thus requiring lower volumetric flow rates – allows less sample dilution during the separation, as well as enhanced detection, according to Lambert-Beer law applied to flow systems (Equation 2, sub-chapter 3.2.1.1, Chapter 3). In addition, the gentle HF5 separation mechanism should be less disruptive of large protein aggregates held together by weak, non-covalent forces.

Thanks to the virtually unlimited chromatographic space for the separation of protein aggregates, when coupled with an appropriate detection system, HF5 should be able to allow the separation of a wide range (sizes and MW) of antibody aggregates, therefore able to quantify them reliably. As shown in the previous sub-chapter 4.1.5, LoD and LoQ for antibody high MW species are in the nanograms range when the peptide bond absorption in the far UV is employed as detection

method.

Although from many points of view a very robust system, SEC presents some drawbacks, including (a) the trade-off between the dynamic range of analysis (size and MW) and the species resolution, (b) the potential loss of large aggregates (physically filtered out, or by adsorption/interaction to the column matrix), (c) the potential disruption of large or "*sticky*" aggregates and even (d) the formation of new aggregates during the separation [Arakawa et al. 2010]. Moreover, protein samples are often diluted into a buffer which is usually different from the final formulation buffer, therefore may experience instability issues during separation [Lowe et al. 2011].

The performance of HF5 online coupled with UV and MALS detection is discussed in comparison with SEC for the separation of the same antibody formulation. The definitions and formulas of all analytical parameters employed for the method validation tentative in this sub-chapter were previously discussed in sub-chapter 2.4 (Chapter 2). Furthermore, the sample recovery and the reversibility of the self-association process were monitored over time by UV detection, like discussed in sub-chapter 4.1.3, showing the sample evolution and the metastable equilibrium between antibody species.

HF5 high selectivity allowed the separation and identification of more antibody species than SEC, which is a fundamental feature for the characterization of complex protein mixtures.

Last, but not least, HF5 versatility is highlighted when employing a carrier solution with very low ionic strength and a carrier solution whose composition is similar to the antibody formulation.

4.1.6.1. EXPERIMENTAL SETUP

SEC and HF5 analyses were performed using an Agilent 1200 HPLC system (Agilent Technologies, Santa Clara, CA, USA) consisting in a degasser, an isocratic pump, an auto sampler and a variable wavelength UV detector, combined with an Eclipse® DUALTEC prototype separation system (Wyatt Technology Europe, Dernbach, Germany). The ChemStation version B.04.02 (Agilent Technologies) data system for Agilent instrumentation was used to set and control the instrumentation and for the computation of various separation parameters. The software package Wyatt Eclipse @ ChemStation version 3.5.02 (Wyatt Technology Europe) was used to set and control the FFF separation system. An Agilent 1100 UV-Vis variable wavelength detector operating at a wavelength of 280 nm was used as a concentration detector at all times.

An 18-angle MALS detector model DAWN® HELEOS™ light scattering detector (Wyatt Technology Corporation, Santa Barbara, CA, USA), employing a laser operating at a wavelength of 658 nm, was used in all experiments.

ASTRA® software version 5.3.2.14 (Wyatt Technology Corporation) was used to handle signals from the detectors (MALS and UV) and to compute the proteins absolute MW and concentration values.

The SEC columns were a WTC-0305S (Wyatt SEC protein column for MALS, 5µm coated silica beads 300Å, size 7.8x300mm), operating in the MW range from 5.000 to 1.250.000 Da (g/mol), and a Mab PAC SEC-1 (Thermo Scientific Dionex, 5µm coated silica beads 300Å, size 4.0x300 mm), operating in a MW range from 10.000 to 1.000.000 Da.

The hollow-fiber was a 17 cm long polyether-sulfone (PES) fiber, type FUS 0181 available from Microdyn-Nadir (Wiesbaden, Germany) with the following characteristics: 0.8 mm ID, 1.3 mm OD and a molecular weight cut-off of 10 kDa, corresponding to an average pore size of 5 nm.

4.1.6.2. MATERIALS AND METHODS

The carrier solution/mobile phase was phosphate buffered saline (PBS) prepared at three concentrations, with different ionic strength values. Their exact compositions are reported in Table 1.

Table 1 – The carrier solutions compositions employed in this study

Carrier	Composition	Comment
A	50 mM phosphate buffer + 300 mM NaCl, pH 6.8 (IS 450 mM)	Typical high IS buffer for the separation of proteins, recommended for Dionex SEC column by the manufacturer
B	50 mM phosphate buffer + 50 mM NaCl, pH 6.8 (IS 200 mM)	Typical buffer recommended for Wyatt SEC column by the manufacturer
C	10 mM phosphate buffer + 150 mM NaCl, pH 7.0 (IS 180 mM)	low IS eluent for mAbs recommended or Dionex SEC column by the manufacturer
C	10 mM phosphate buffer + 25 mM NaCl, pH 7.0 (IS 55 mM)	Employed only in HF5
D	42 mM phosphate buffer + 24 mM citrate buffer + 105.5 mM NaCl, pH 5.0 (IS 171.5 mM)	Employed only in HF5

The carrier solutions were prepared using MilliQ water purified by an Elix 3 UV Water Purification System (Millipore, Billerica, USA) and filtered through 0.2 μm pore membrane sterile filter units (Millipore), at all times.

The sample employed in this study was an IgG_2 type antibody, for simplicity called **mAb4**, prepared at a concentration of 0.329 mg/mL. An amount of 2 μg of mAb4 was injected at all times.

When the Dionex SEC column was employed, the separations were performed at 0.2 mL/min flow rate and when the WTC SEC column was used, mAb4 was eluted at 0.5 mL/min flow rate.

When the separations took place in HF5, mAb4 was injected during focus, performed at 0.85 mL/min focus flow rate for 4.5 min. The sample was focused at a distance of approximately 15% fiber length from the channel inlet and eluted afterwards at a

channel flow rate of 0.35 mL/min under the effect of a constant cross-flow rate of 0.35 mL/min for 20 min.

4.1.6.3. RESULTS

Sample mAb4 was separated by SEC employing two different columns (Dionex SEC and WTC SEC) and the recommended carrier solutions for each SEC column. HF5 separations were performed afterwards under identical separation conditions (employing the same buffers) and the separation performance of the two techniques was compared. The separation was monitored by UV detection at 280 nm (concentration detector) at all times and, by coupling online the Eclipse® DUALTEC™ separation system with a DAWN® HELEOS™ (MALS) detector, the absolute molecular weight (MW) of all eluting species was calculated. A mAbs specific value of $\varepsilon_{0.1\%}^{280\,\mathrm{nm}} = 1.4\,\mathrm{mL/mg \cdot cm}$ was used in all MW calculations.

A. SEC AND HF5-UV-MALS IN VERY HIGH IONIC STRENGTH MOBILE PHASE (450 mM)

First, mAb4 was injected in HF5 and the Dionex SEC column and separated employing the carrier A reported in Table 1 (IS =450 mM), which was also the recommended elution buffer for the SEC column. The separation profiles at 280 nm of mAb4, as well as the MW value corresponding to each eluting peak, are reported in Figure 1, (a) the SEC separation and (b) the HF5 separation. Figure 1a depicts the SEC-UV-MALS elution profile of mAb4 in carrier A. The UV absorption at 280 nm allows the detection of four peaks and their assignment is reported in Table 2, while an additional peak is observed only by light scattering. Since the protein concentration signal is lacking in correspondence of the peak marked as “HMWS” (high MW species), it is not possible to confirm that this peak actually corresponds to protein aggregates.

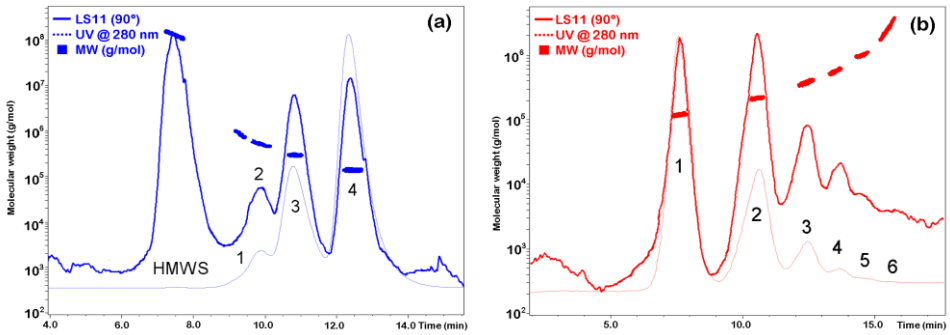

Figure 1 – UV-MALS separation profiles of mAb4 in carrier A employing (a) Dionex SEC column and (b) HF5 channel.

Table 2 – Peak assignment for the SEC separation profile reported in Figure 1a. Absolute MW values derived from MALS measurements.

Peak #	MW (g/mol)	MW_{HMWS}/MW_{1mer}	Peak assignment
HMWS	> 10^8		Polydisperse population
1	850.000	5.8	Hexamer
2	599.200	4.1	Tetramer
3	304.500	2.1	Dimer
4	146.400	1.0	Monomer

Figure 1b shows the HF5-UV-MALS elution profile of mAb4. In this case, the UV signal at 280 detects six eluting species, whose assignment is reported in Table 3.

Table 3 - Peak assignment for the HF5 separation profile reported in Figure 1b. Absolute MW values derived from MALS measurements

Peak #	MW (g/mol)	MW_{HMWS}/MW_{1mer}	Peak assignment
1	143.500	1.0	Monomer
2	244.500	1.7	Dimer
3	397.800	2.8	Trimer
4	587.300	4.1	Tetramer
5	1.188.000	8.3	Octamer
6	2.561.000		Polydisperse population

Aside from the opposite elution order, several observations can be drawn from the comparison between SEC and HF5 results. The most obvious one is that HF5 allows

the separation of two additional mAb4 species (oligomers) that were not separated by SEC: the trimer and the octamer, while the mAb4 hexamer is only present in the SEC elution profile. Since mAb4 is a highly self-associated antibody, most likely induced by the storage conditions, it is possible that the dynamic dissociation of the HMWS into smaller MW species is so fast that its composition changed between the SEC and HF5 analysis. In addition, as demonstrated in sub-chapter 4.1.2 (Chapter 4), it is also very likely that *SEC is not selective enough* and the trimer as well as the octamer co-elute with other species.

Selectivity is a fundamental parameter in the analyses of mixtures, because it is important for the separation technique to allow the separation and detection of *all* species present in the protein formulation. If selectivity is not high enough, the presence of several species can be overlooked, in which case the separation profile would not reflect the true sample composition.

Just like for the protein mixture in sub-chapter 4.1.2, the SEC and HF5 selectivity the separation of mAb4 in carrier A was calculated as the *MW-based selectivity* (S_{MW}), defined as the slope of the log (t_R) against the corresponding log (MW) plot, where the retention times, as well as MW values, were derived from the experimental data. The slopes were calculated on the first four eluting species, where the relationship between the two logarithms is linear, and the selectivity plots are reported in Figure 2, (a) for the SEC separation and (b) for the HF5 separation.

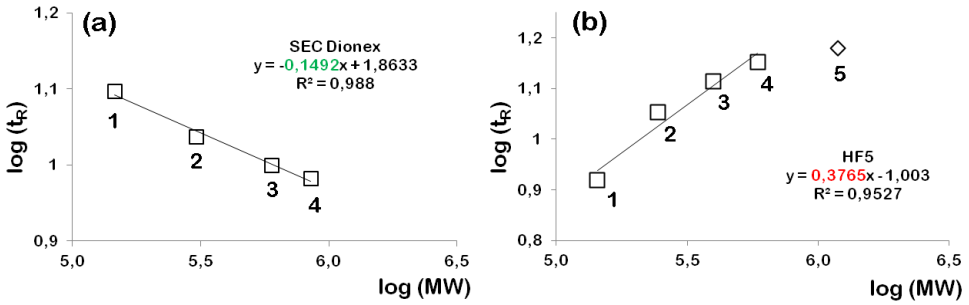

Figure 2 – Selectivity plots obtained in carrier A for (a) SEC and (b) HF5. The numbers near the data points represent the peak numbers in their elution order.

As expected, the HF5 selectivity for the separation of mAb4 is higher compared to

SEC, meaning that, at equal MW values, the difference in retention time is higher in HF5 when compared to SEC. This finding confirms the fact that SEC does not allow the separation / detection of mAb4 trimer and octamer resulting in them co-eluting with other species with similar MW value.

For a more in-depth comparison between SEC and HF5, several specific separation parameters were calculated, like separation efficiency (*N*, number of plates) specific resolution (R_{sp}), HF5 retention level (R_L) and its equivalent in SEC, the capacity factor (*k*), as well as selectivity (S_{MW}) and their values are reported in Table 4. HMWS peak (SEC) was excluded from the calculations because it corresponds to a polydisperse population (non resolved species, whose protein nature was not confirmed).

Table 4 - Separation performance parameters for SEC Dionex and HF5 separations in carrier A

Device	Peak #	t_R (min)	Retention	MW (g/mol)	Efficiency (N)	Resolution R_S	Specific resolution (R_{sp})	Selectivity S_{MW}
			k					
SEC	1	9.6	0.49	850.000	3542			0.15
	2	10.0	0.47	599.200	1964	0.48	3.2	
	3	10.9	0.42	304.500	2975	1.08	3.7	
	4	12.5	0.34	146.400	4649	2.05	6.4	
			R_L					
HF5	1	8.3	21.8	143.500	556			0.38
	2	11.3	29.7	244.500	695	1.89	8.2	
	3	13.0	34.2	397.800	1184	1.09	5.2	
	4	14.2	37.4	587.300	1785	0.82	4.8	
	5	15.1	39.7	1.188.000	1878	0.67	2.2	
	6	16.0	42.1	2.561.000	2108	0.65	1.9	

The dead volume of the SEC column was calculated as the volume of the equivalent cylinder (4.0x300 mm) and was found to be 3.77 mL. The dead time (t_0) at 0.2 mL/min flow rate was 18.85 min. The t_0 was related to the retention time through the capacity factor, *k* (also called chromatographic partition coefficient) for the analytes separated by SEC, instead of the retention level, R_L calculated for the analytes separated by HF5. The SEC capacity factors are in the expected range ($0 < k < 1$) and the HF5 retention levels are in the range recommended by [Wahlund 2013] and [Litzen et al.

1993] (R_L<50).

As expected, efficiency is always higher for SEC because the band broadening in HF5 (FFF in general) is higher. The specific resolution values (R_{sp}), which take into consideration the MW of the resolved species, are similar. Baseline resolution (Rs > 1.25) is achieved only for the first two peaks in HF5 and the last two peaks in SEC, while acceptable resolution is obtained between peaks 2 and 3 (Rs > 1), in both SEC and HF5.

A net distinction in the favor of HF5 is made by selectivity: the selectivity of both small and large mAb4 oligomers is always higher for HF5. The SEC analysis is more time-efficient, but the downside is the reduced chromatographic space available for the separation of all mAb4 oligomers. Altogether, these observations illustrate the net advantages of employing the HF5 separation device for an accurate characterization of mAb4 instead of the SEC Dionex column.

B. SEC AND HF5-UV-MALS IN MODERATE IONIC STRENGTH MOBILE PHASE (200 mM)

Next, mAb4 was injected in HF5 and the WTC SEC column and separated employing the carrier B reported in Table 1 (IS =200 mM), which was also the recommended elution buffer for the SEC column. The separation profiles at 280 nm of mAb4, as well as the MW value corresponding to each eluting peak, are reported in Figure 3, (a) the SEC separation and (b) the HF5 separation.

Figure 3a depicts the SEC-UV-MALS elution profile of mAb4 in carrier B: the UV absorption at 280 nm allows the detection of four peaks and their identification is reported in Table 5, while an additional peak is observed only by light scattering, similar to the one reported in Figure 1a. Not even in this case is possible to confirm that this peak actually corresponds to protein aggregates due to the lack of UV signal in this chromatographic region.

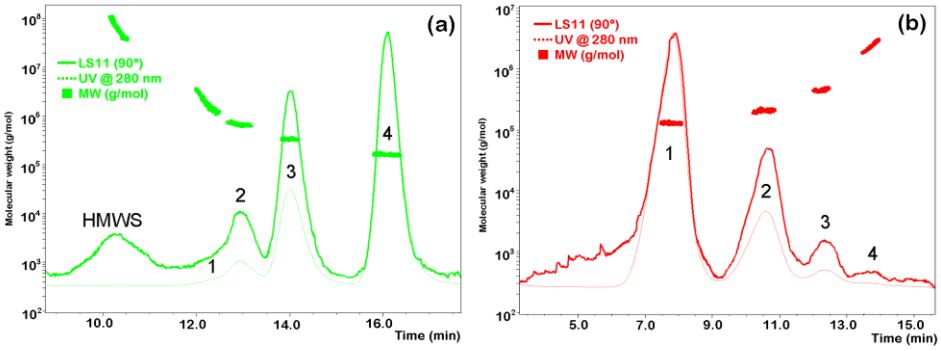

Figure 3 – UV-MALS separation profiles of mAb4 in carrier B employing (a) Dionex SEC column and (b) HF5 channel.

Table 5 – Peak assignment for the SEC separation profile reported in Figure 3a. Absolute MW values derived from MALS measurements.

Peak #	MW (g/mol)	MW_{HMWS}/MW_{1mer}	Peak assignment
HMWS	$> 10^7$		Polydisperse population
1	2.100.589	13.9	Polydisperse population
2	856.500	5.7	Hexamer
3	352.700	2.3	Dimer
4	151.500	1.0	Monomer

Figure 3b shows the HF5-UV-MALS elution profile of mAb4: in this case, the UV signal at 280 detects four eluting species, just like in SEC, whose assignment is reported in Table 6.

Table 6 - Peak assignment for the HF5 separation profile reported in Figure 3b. Absolute MW values derived from MALS measurements

Peak #	MW (g/mol)	MW_{HMWS}/MW_{1mer}	Peak assignment
1	138.500	1.0	Monomer
2	282.300	2.0	Dimer
3	492.600	3.6	Tetramer
4	2.500.000	18.1	Polydisperse population

Both SEC and HF5 allow the separation and detection of four eluting peaks, but the MW values derived from experimental data show that, based on the MW_{HMWS}/MW_{1mer} ratios, SEC and HF5 do not separate exactly the same species. This

is a known issue when comparing results obtained with techniques which employ different principles (in this case the separation mechanism) or when complementary tests are preformed on the same sample: there is no way of knowing which one provides the true sample composition. Nonetheless, due to the reversibility of the antibody self-association, it is conceivable that the sample composition may have changed between the SEC and HF5 analyses or that the SEC and HF5 profiles simply show different stages of the mAb4 oligomers dissociation process.

Moreover, when the sample recovery is incomplete, due to preferential adsorbtion of aggregates, it leads to questionable accuracy on aggregate levels [Carpenter et al. 2010]. For instance, in a recent publication [Gabrielson et al. 2007], where FFF and SV-AUC were proposed as orthogonal techniques when SEC failed to detect the HMWS of mAbs present at trace levels, all three techniques provided different results. SEC not only underestimated the aggregates levels, but modified the aggregates distribution. Moreover, certain oligomers have shown preferential adsorbtion to the SEC column matrix.

Since it was not possible to determine which technique led to erroneous results, the separation performance of SEC and HF5 was compared using the values derived from experimental data. First, the MW-based selectivity of SEC and HF5 for the separation of mAb4 in carrier B was calculated from the experimental retention time and MW values. The slopes were calculated on the first three eluting species, where the relationship between the two logarithms is linear, and the selectivity plots are reported in Figure 4, (a) for the SEC separation and (b) for the HF5 separation.

As expected, even in this case, the HF5 selectivity for the separation of mAb4 is higher compared to SEC, meaning that, at equal MW values, the difference in retention time is higher in HF5 when compared to SEC. In order to compare the SEC and HF5 performance, the same specific separation parameters were calculated as for mAb4 separation by SEC and HF5 in carrier A and their values are reported in Table 7. HMWS peak (SEC) was excluded from the calculations because of the polydisperse nature of the population (non resolved species).

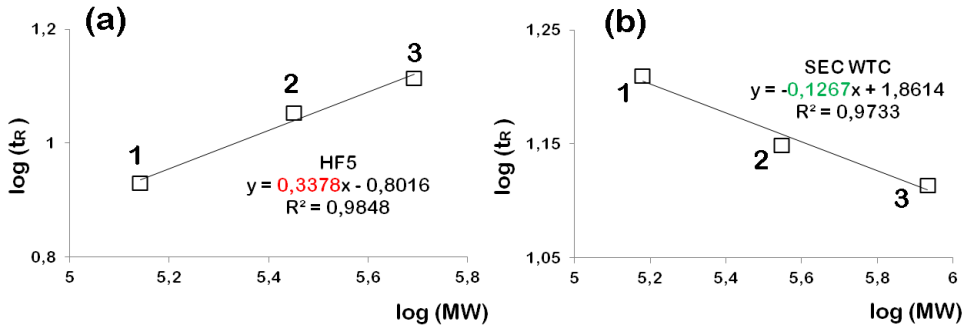

Figure 4 – Selectivity plots obtained in carrier B for (a) SEC and (b) HF5. The numbers near the data points represent the peak numbers in their elution order.

Table 7 – Separation performance parameters for SEC WTC and HF5 separations in carrier B

Device	Peak #	t_R (min)	Retention	MW (g/mol)	Efficiency (N)	Resolution R_S	Specific resolution (R_{sp})	Selectivity S_{MW}
			k					
SEC	1	12.6	0.56	2.100.589	5474			0.13
	2	13.0	0.55	856.500	3084	0.53	1.4	
	3	14.1	0.51	352.700	4661	1.23	3.2	
	4	16.2	0.43	151.500	7293	2.67	7.3	
			R_L					
HF5	1	8.5	22.4	138.500	401			0.34
	2	11.3	29.7	282.300	615	1.60	5.2	
	3	13.0	34.2	492.600	1025	1.03	4.3	
	4	14.2	37.4	2.500.000	1302	0.74	1.0	

The dead volume of the SEC column was calculated as the volume of the equivalent cylinder (7.8x300 mm) and was found to be 14.33 mL. The calculated dead time (t_0) at 0.5 mL/min flow rate was 28.67 min. The t_0 was related to the retention time through the capacity factor, k for the analytes separated by SEC, instead of the retention level, R_L calculated for the analytes separated by HF5.

The SEC WTC column offers higher analytes retention compared to the Dionex column (k factor in Tables 4 and 7). The retention levels obtained in HF5 in carrier B are similar to the values obtained in carrier A (Table 4) and are always in the recommended range (< 50).

As expected, the efficiency in SEC is higher than in HF5 and the SEC WTC column offers an even higher efficiency compared to the Dionex column (Table 4) for the

separation on mAb4. The SEC WTC column is a little more selective than the Dionex column, as well (b closer to 0.1, b = 0.13 for WTC vs. b = 0.15 for Dionex).

As in the previous case (carrier A), reported in section A of this sub-chapter, the specific resolution in SEC and HF5 is similar and the resolution is obtained at baseline (R_s > 1.25) for the first two peaks in HF5 and the last two peaks in SEC, while an acceptable resolution is obtained for peaks 2 and 3 in both SEC and HF5.

Even in this case, selectivity is higher in HF5, which means that HF5 has a higher ability to distinguish mAb4 species with similar MW values. Since both SEC and HF5 analyses require almost then same amount of time (20 min) and taking into consideration all the observations made on the performance parameters, there is a clear advantage into employing the HF5 device instead of the SEC WTC column.

C. SEC AND HF5-UV-MALS IN LOWER IONIC STRENGTH MOBILE PHASE (180 MM)

Lastly, mAb4 was injected in HF5 and both SEC columns and separated employing carrier C reported in Table 1 (IS = 180 mM), which was also the recommended low IS elution buffer for the SEC Dionex column. The separation profiles at 280 nm of mAb4, as well as the MW value corresponding to each eluting peak, are reported in Figure 5, (a) the SEC separation employing the Dionex column, (b) SEC separation employing the WTC column and (b) the HF5 separation.

All separation profiles depicted in Figure 5 show only three peaks detected by UV absorbance at 280 nm, while MALS detection allows the detection of additional HMWS, whose presence would have otherwise been neglected. However, in the absence of UV signal in correspondence of the light scattering peak, the protein nature of these aggregates cannot be confirmed.

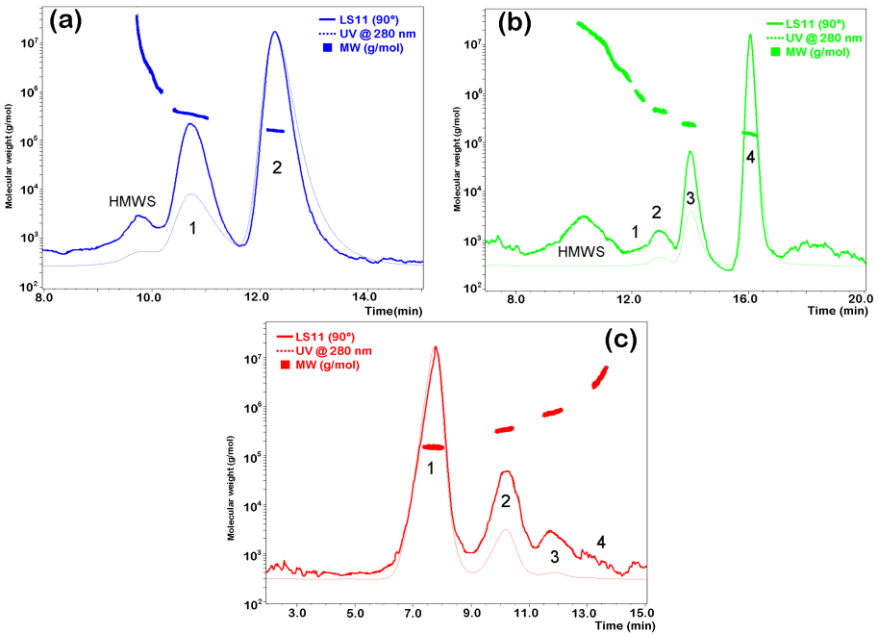

Figure 5 - UV-MALS separation profiles of mAb4 in carrier C employing (a) Dionex SEC column, (b) WTC SEC column and (c) HF5

The peaks assignments, based on the MW values calculated for each peak are reported in Table 8. The MW values derived from experimental data show that based on the MW_{HMWS}/MW_{1mer} ratios, SEC and HF5 do not separate exactly the same species.

Table 8 – Peak assignment for the separation profiles reported in Figure 5. Absolute MW values derived from MALS measurements.

Device	Peak #	MW (g/mol)	MW_{HMWS}/MW_{1mer}	Peak assignment
SEC Dionex	HMWS	$> 10^6$		Polydisperse population
(Figure 5a)	1	370.300	2.3	Dimer
	2	158.200	1.0	Monomer
SEC WTC	HMWS	$> 10^6$		Polydisperse population
(Figure 5b)	1	950.400	5.9	Hexamer
	2	459.400	2.8	Trimer
	3	262.600	1.7	Dimer
	4	159.400	1.0	Monomer
HF5	1	149.800	1.0	Monomer
(Figure 5c)	2	353.900	2.4	Dimer
	3	752.400	5.0	Pentamer
	4	4.024.589	26.9	Polydisperse population

Since this issue was already discussed in sections A and B, it can be interpreted like: (a) changes in the mAb4 composition caused by the dynamic and *spontaneous* dissociation of HMWS into species with smaller MW or (b) the SEC separation changing the oligomers distribution by *disrupting* the aggregates (interactions with the column matrix), documented in literature or (c) both.

Since it is not possible to determine the real cause of SEC and HF5 detecting different mAb4 species only based on UV-MALS data, it was considered appropriate to continue this study using the experimentally-derived value as such. Therefore, the MW-based selectivity of SEC and HF5 for the separation of mAb4 in carrier C was calculated from the experimental retention time and absolute MW values. The slope values corresponding to HF5 and SEC WTC were calculated on the first three eluting species, where the relationship between the two logarithms is linear and using only two points available for the SEC Dionex column. The selectivity plots are reported in Figure 6, (a) for the HF5 separation and (b) for the SEC separations.

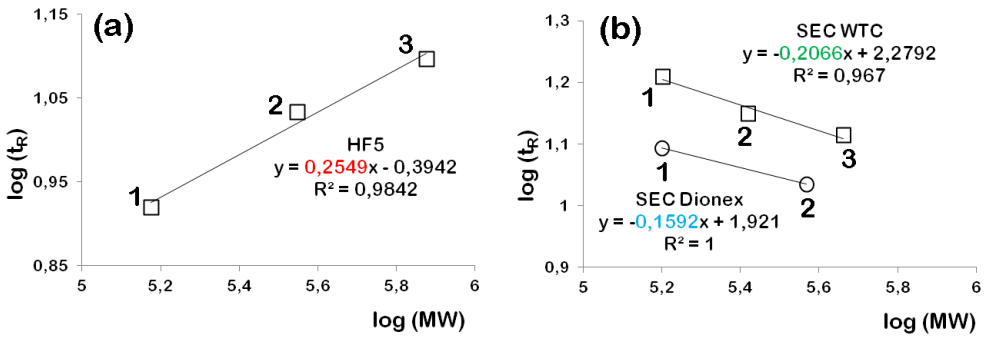

Figure 6 – Selectivity plots obtained in carrier C for (a) HF5 and (b) SEC. The numbers near the data points represent the peak numbers in their elution order.

As expected, once more, the HF5 selectivity for the separation of mAb4 is higher compared to both SEC Dionex and SEC WTC corresponding values, indicating that HF5 can separate mAb4 species with smaller differences in MW. Small MW differences correspond to significant differences in retention time. In order to compare the SEC and HF5 performance, the same specific separation parameters

discussed in section A and B were calculated and their values are reported in Table 7. The dead volumes of the SEC columns were calculated in sections A and B: a dead volume of 14.3 mL and a t_0 of 28.7 min for the SEC WTC column and a dead volume of 3.8 mL and a t_0 of 18.9 min for the SEC Dionex column. The t_0 was related afterwards to the retention time through the capacity factor, k for the analytes separated by SEC, instead of the retention level, R_L calculated for the analytes separated by HF5.

Table 9 – Separation performance parameters for SEC WTC and HF5 separations in carrier C

Device	Peak #	t_R (min)	Retention	MW (g/mol)	Efficiency (N)	Resolution R_S	Specific resolution (R_{sp})	Selectivity S_{MW}
			k					
SEC Dionex	1	10.8	0.43	370.300	4808			0.16
	2	12.4	0.34	158.200	1682	0.55	1.5	
			k					
SEC WTC	1	12.6	0.56	950.400	5327			0.21
	2	13.0	0.55	459.400	3261	0.56	1.8	
	3	14.1	0.51	262.600	4770	1.25	5.1	
	4	16.2	0.43	159.400	7822	2.69	12.4	
			R_L					
HF5	1	8.3	21.8	149.800	406			0.25
	2	10.8	28.4	353.900	840	1.56	4.2	
	3	12.5	32.9	752.400	958	1.10	3.4	
	4	13.6	35.8	4.024.589	616	0.60	0.8	

Even at low ionic strength, the SEC WTC column offers higher analytes retention compared to the Dionex column and the R_L obtained in HF5 employing carrier C are similar to the values obtained in other carriers (carrier A, Table 4 and carrier B, Table 7), always in the recommended range (< 50).

As expected, the efficiency in SEC is higher than in HF5 and the SEC WTC column offers, once more, an even higher efficiency compared to the Dionex column for the separation on mAb4.

As already observe din sections A and B, the R_{sp} in SEC and HF5 is similar and the resolution is obtained at baseline (Rs > 1.25) for the first two peaks in HF5 and the last three peaks in SEC, while the resolution in SEC Dionex is very low.

Once again, *selectivity* is higher in HF5 compared to SEC, which means that HF5 has a higher ability to distinguish mAb4 species with close MW values. Considering that both SEC WTE and HF5 analyses require almost then same amount of time (20 min) and taking into consideration all the observations made on the performance parameters, there is a net advantage into employing the HF5 device instead any of the SEC columns for the separation of mAb4. The selectivity of the SEC Dionex column does not change significantly when decreasing the ionic strength of the carrier (b = 0.16 at low IS vs. b = 0.15 at very high IS), thus demonstrating the *robustness* of the Dionex SEC column, while the SEC WTC column is the least selective among all separation devices (b = 0.21 at low IS vs. b = 0.13 at very high IS) in the low ionic strength buffer.

D. SAMPLE RECOVERY AND mAb4 SELF – DISSOCIATION DURING THE STUDY

The mAb4 recovery was calculated as the total area under peak for each experimental condition (carrier solutions A, B and C) and separating device (HF5, SEC WTC and SEC Dionex) and the results are reported in Figure 7. The highest area under the peak was associated to a complete (100%) sample recovery and all the other recovery values were calculated as relative to it.

The *self-dissociation* of mAb4 HMWS was monitored over 8 working days, which corresponded to the duration of the study presented in this sub-chapter, by calculating the under each eluting peak. In addition, the disaggregation phenomenon is displayed as % distribution of the mAb4 species over time (color coded in Figure 7).

As expected, the highest sample recovery is obtained employing the SEC Dionex column in carrier A, since it contains the highest amount of salt (NaCl). Nonetheless, even at low IS (carrier C), the SEC Dionex column offers the highest mAb4 recovery. Under all experimental conditions and employing different separation devices, the

mAb4 recovery is *always above 93%*.

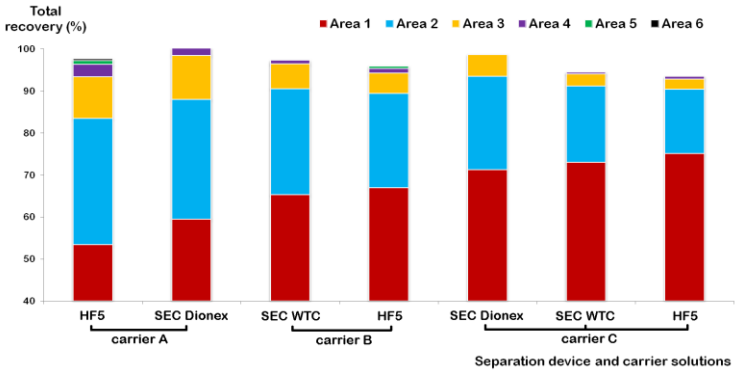

Figure 7 – Sample recovery and mAb4 species distribution (%) by SEC and HF5

The self-dissociation of mAb4 is a spontaneous phenomenon (dynamic), as seen for mAb1 in sub-chapter 4.1.3 (Chapter 4). It can be somewhat slowed down by storing the sample at 4°C, but not entirely stopped. Figure 7 shows that mAb4 oligomers co-exist with the monomer and, at room temperature, the trend of their dynamic equilibrium is shifted towards their dissociation into monomer.

The mAb4 conversion was monitored even after the SEC-HF5 comparison study was completed, by injecting the same mAb4 amount and separating by HF5 for the next few days and employing carrier solutions D and E. The mAb4 oligomers conversion into smaller MW species (usually monomer) is reported din Figure 8.

Figure 8 shows the tendency of the oligomers to dissociate into monomer as an increase in the monomer % (Area 1) and a simultaneous decrease in the % of the higher order oligomers (Areas 2-6). This conversion is faster in the beginning and slows down as the time passes. Figure 8 also shows the fact that HF5 at 97.5 hours allows the separation of more species than the previous SEC separation (SEC WTC at 96.0 hours), confirming the gentle separation mechanism of FFF. It is very likely that the SEC separation changed the aggregates % by disrupting high order oligomeric species through interactions with the column matrix.

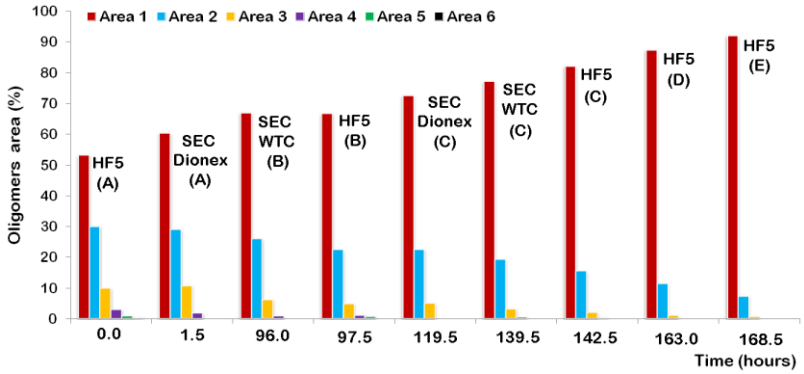

Figure 8 - mAb4 oligomers conversion into smaller MW species over 7 days. Carrier solutions indicated by letters A – E.

E. HF5-UV-MALS IN LOWER IONIC STRENGTH MOBILE PHASES: CARRIER D (55 MM) AND CARRIER E (171.5 MM)

Lastly, after the SEC-HF5 comparison was completed, HF5 was employed for the separation of mAb4 in low (E) and very low (D) ionic strength carrier solutions, to demonstrate the versatility of the technique residing in the wide choice of carrier solutions.

The exact composition of the mobile phases was reported in Table 1. The mAb4 sample was the same one used during the SEC-HF5 comparison study, therefore in an advanced stage of self-dissociation of the high order oligomers.

The HF5 separation profiles at 280 nm of mAb4, as well as the MW value corresponding to each eluting peak, are reported in Figure 9, (a) in carrier D and (b) in carrier E.

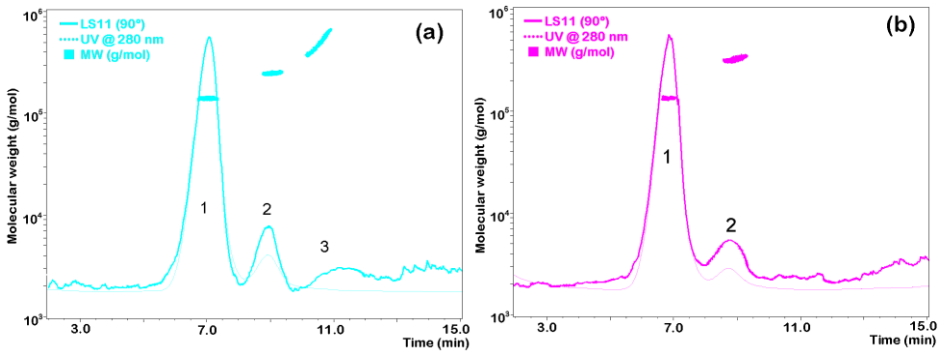

Figure 9 – HF5-UV-MALS separation profiles of mAb4 in (a) carrier D and (b) carrier E.

As expected, the separation profiles in Figure 9a and 9b show the separation of only 3 and, respectively 2 mAb4 species. The exact MW values, as well as the peaks assignment are reported in Table 10. The values reported in Table 10 confirm that peaks 1 and 2 in Figures 9 correspond to mAb4 monomer and respectively, mAb4 dimer.

A third peak, corresponding to a polydisperse population of mAb4, with an average MW between the trimer and the tetramer is observed only in Figure 9a. It is conceivable that, during the separation reported in Figure 9b, these HMWS have already dissociated into monomer, therefore they are no longer present at the time of the analysis. This explanation is supported by the oligomers % distribution in Figure 8, which shows the increased levels of monomer when carrier E is employed (time: 168.5 h) compared to the previous monomer % value obtained in carrier D (time: 163.0 h).

Table 10 – Peak assignment for the separation profiles reported in Figure 9. Absolute MW values derived from MALS measurements.

Carrier	Peak #	MW (g/mol)	MW_{HMWS}/MW_{1mer}	Peak assignment
D	1	153.400	1.0	Monomer
(Figure 9a)	2	315.300	2.1	Dimer
	3	534.000	3.5	Polydisperse population
E	1	149.500	1.0	Monomer
(Figure 9b)	2	355.600	2.4	Dimer / polydisperse

Next, the MW-based HF5 selectivity for the separation of mAb4 in carrier D and E was calculated from the experimental retention time and MW values. The slopes were calculated on the all the available experimental points and the selectivity plots are reported in Figure 10.

The selectivity values are very similar to the ones obtained in higher ionic strength, (reported in Tables 4, 7 and 9), therefore, a direct correlation between the ionic strength of the mobile phase and the HF5 selectivity could not be established based on this data. The HF5 selectivity remains high (around 0.3) and appears not to be

influenced by ionic strength.

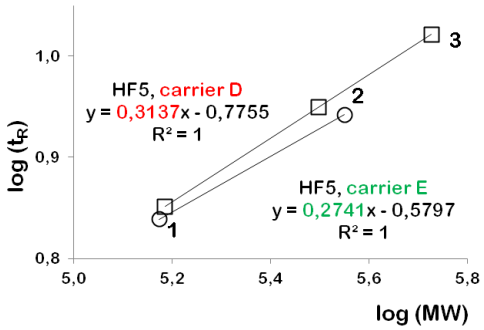

Figure 10 – HF5 selectivity plots obtained in carrier D and carrier E. The numbers near the data points represent the peak numbers in their elution order

The same specific separation parameters discussed in section A, B and C were calculated for the HF5 separations in carriers D and E and their values are reported in Table 11. The void time, t_0 was related to the retention time through the retention level, R_L.

Table 11 – Separation performance parameters for HF5 separations in carriers D and E

Carrier	Peak #	t_R (min)	Retention	MW (g/mol)	Efficiency (N)	Resolution R_S	Specific resolution (R_{sp})	Selectivity S_{MW}
			R_L					
D	1	7.1	17.8	153.400	471			0.31
	2	8.9	22.3	315.300	994	1.42	4.5	
	3	10.5	**26.3**	534.000	471	0.94	4.1	
			R_L					
E	1	6.9	17.3	149.500	930			0.27
	2	8.8	21.9	355.600	480	1.46	3.9	

The retention levels, R_L, as well as specific resolution values, R_{sp} obtained in HF5 in carriers D and E are similar to the values obtained in other carriers (carrier A, Table 4 and carrier B, Table 7 and carrier C, Table 9), with R_L always in the recommended range (< 50). Baseline or at least acceptable resolution among mAb4 species is always obtained in carriers D and E.

As mentioned previously in this section, the selectivity values are high (around 0.3) and apparently not influenced by the carrier solution ionic strength. Efficiency values

are even higher than the ones previously reported for carriers A – C.

4.1.6.4. CONCLUSIONS

HF5 has proven to be a highly selective (average S_{MW} = 0.3) separation tool for the characterization of mAb4, a representative protein formulation which contained high order oligomers in dynamic equilibrium with the monomer. As the time passed, this equilibrium shifted towards the monomer, therefore the oligomers dissociated into smaller MW species. Thanks to the gentle separation mechanism, HF5 online coupled with MALS detection was able to detect and quantify these changes in the mAb4 composition more accurately than SEC.

Even though the SEC separation is slightly faster, allowing the mAb4 separation in a short analysis time, it is very likely that some mAb4 species co-eluted with other species with similar MW value, therefore their presence was not detected. It is also very likely that, during the SEC separation, the loosely bound oligomers were disrupted, hence, the results obtained by SEC did not reflect the true mAb4 composition.

These two SEC issues (insufficient selectivity and changes in the sample composition caused by the separation mechanism / interactions with the column matrix) were overcome when HF5 was employed, thanks to the gentle separation mechanism (since the retention is achieved by applying an external field a not by the sample passing through a sieving matrix) and to the high HF5 selectivity, which allowed the separation and detection of HMWS present at trace levels.

Both SEC and HF5 provided a good sample recovery and the mAb4 oligomers dynamic dissociation was monitored over 7 days, providing valuable information regarding the spontaneous changes in the sample composition which were not necessarily related to the separation technique. Any separation technique intrinsically changes the sample composition, but the fact that we were able to

monitor these changes reflects the transient nature of these aggregates and the fact that these aggregates are, most likely, *metastable* higher order oligomeric species, as described by [Philo 2006, Philo and Arakawa 2009].

4.1.6.5. REFERENCES

[Arakawa et al. 2010] Arakawa T.; Ejima D.; Li T. and Philo J. S. (2010). "*The Critical Role of Mobile Phase Composition in Size Exclusion Chromatography of Protein Pharmaceuticals*." Journal of Pharmaceutical Sciences **99** (4): 1674-1692.

[Carpenter et al. 2010] Carpenter J. F.; Randolph T. W.; Jiskoot W.; Crommelin D. J. A.; Middaugh C. R. and Winter G. (2010). "*Potential Inaccurate Quantitation and Sizing of Protein Aggregates by Size Exclusion Chromatography: Essential Need to Use Orthogonal Methods to Assure the Quality of Therapeutic Protein Products*." Journal of Pharmaceutical Sciences **99** (5): 2200–2208.

[Gabrielson et al. 2007] Gabrielson J. P.; Brader M. L.; Pekar A. H.; Mathis K. B.; Winter G.; Carpenter J. F. and Randolph T. W. (2007). "*Quantitation of Aggregate Levels in a Recombinant Humanized Monoclonal Antibody Formulation by Size-Exclusion Chromatography, Asymmetrical Flow Field Flow Fractionation, and Sedimentation Velocity*." Journal of Pharmaceutical Sciences **96**: 268–279.

[Litzen et al. 1993] Litzen A.; Walter J. K.; Krischollek H. and Wahlund K. G. (1993). "*Separation and Quantitation of Monoclonal Antibody Aggregates by Asymmetrical Flow Field-Flow Fractionation and Comparison to Gel Permeation Chromatography*." Analytical Biochemistry **212** (2): 469-480.

[Lowe et al. 2011] Lowe D.; Dudgeon K.; Rouet R.; Schofield P.; Jermutus L. and Christ D. (2011). "*Aggregation, stability, and formulation of human antibody therapeutics*." Advances in Protein Chemistry and Structural Biology **84**: 41-61.

[Philo 2006] Philo J. S. (2006). "*Is Any Measurement Method Optimal for All Aggregate Sizes and Types?* ." The AAPS Journal **8** (3).

[Philo and Arakawa 2009] Philo J. S. and Arakawa T. (2009). "*Mechanisms of Protein Aggregation*." Current Pharmaceutical Biotechnology (10): 348-351.

[Wahlund 2013] Wahlund K.-G. (2013). "*Flow field-flow fractionation: Critical overview*." Journal of Chromatography A **1287** (2013): 97– 112.

4.1.7. *High reproducibility and low detection limit HF5 – MALS method for the characterization of aggregates in protein formulations. Case study: AvidinOX®*

In sub-chapter, the short-term accelerated stability study of a modified protein, stored in lyophilized form (AvidinOX®), was conducted by HF5 online coupled with UV and MALS detection.

The rapid development of protein-based pharmaceuticals highlights the need for robust analytical methods to ensure their quality (purity and stability). Monoclonal antibodies and large proteins that have an increasing role in biopharmaceutical applications for their highly specific action and are often modified to enhance or modulate their activity or stability when used as drugs. Their biological activity and the stability are closely related to the preservation of their complex structure, which is often subjected to stresses (external factors), which can cause their degradation and/or lead to aggregation.

Due to its ability to easily aggregate in solution, AvidinOX® is a model sample that gives the opportunity to demonstrate the various HF5 advantages (described in sub-chapters 4.1.1 – 4.1.6) for the of study the aggregation process, for the size and MW characterization and for the quantification of the various type of aggregates during several storage conditions in a relatively short time.

The detailed description of the HF5 method development is discussed in the first part of this study, where the design of experiments approach (a 2x2 factorial design) was employed and a simple algorithm was built to help choose the optimal combination of flow conditions for AvidinOX® formulation separation. Criteria like resolution, peak symmetry and valley height between species are employed for the construction of the algorithm.

The protein aggregates, present at trace levels, were successfully quantified and their MW values were calculated by MALS. This study also highlighted the miniaturization advantages regarding the decreased limit of detection of AvidinOX® (protein) aggregates and the HF5 versatility regarding the carrier solution composition (the possibility of working in denaturing vs. native mobile phase) that made possible the distinction and quantification of different types of protein aggregates (covalent vs. non-covalent).

The self-association process between units of an oxidized protein (AvidinOX®, each 64 kDa *unit* is actually a very stable tetramer, therefore made of 4x16 kDa sub-units), which have (most likely) suffered a conformational change due to chemical instability, and/or promoted by the presence of degradation products, was monitored by HF5-UV-MALS.

The definitions and formulas of all analytical parameters employed in this study were previously discussed in sub-chapter 2.4 (Chapter2).

4.1.7.1. EXPERIMENTAL SETUP

HF5 was performed using an Agilent 1200 HPLC system (Agilent Technologies, Santa Clara, CA, USA) consisting in a degasser, an isocratic pump, an auto sampler and a variable wavelength UV detector, combined with an Eclipse® DUALTEC™ FFF separation system (Wyatt Technology Europe, Dernbach, Germany). The ChemStation version B.04.03 [87] software for Agilent instrumentation (Agilent Technologies) was used to set and control the instrumentation and for the computation of various separation parameters. The software package Wyatt Eclipse @ ChemStation version 4.02 (Wyatt Technology Europe) was used to manage the FFF separation system.

The hollow fiber was a 17 cm long polyether-sulfone (PES) fiber, type FUS 0181 available from Microdyn-Nadir (Wiesbaden, Germany) with the following characteristics: 0.8 mm ID, 1.3 mm OD, and 10 kDa MWCO, corresponding to an average pore diameter of 5 nm.

An 18-angle multi angle light scattering (MALS) detector model DAWN® HELEOS™ (Wyatt Technology Corporation, Santa Barbara, CA, USA) operating at a wavelength of 658 nm was used to measure the absolute MW of proteins in solution. An UV detector operating at 280 nm was used as concentration detector. ASTRA® software version 5.3.2.14 (Wyatt Technology Corporation) was used to handle signals from the detectors (MALS, and UV), to compute the protein MW values and to quantify the aggregate levels.

4.1.7.2. SAMPLES AND REAGENTS

AvidinOX® (produced by Sigma Tau) is an oxidized form of avidin and indicated by its manufacturer as a ”pre-targeting receptor” for drug delivery in cancer, widely used *in vitro* for its capacity to bind biotin. However, due to its short residence in

blood and tissues, *in vivo* use of avidin is limited to therapeutic treatments where the radiolabelled biotin or its derivatives must be rapidly eliminated from the circulation. AvidinOX® is obtained by 4-hydroxyazobenzene-2′-carboxylic acid-assisted sodium periodate oxidation. Its synthesis method generates aldehyde groups from avidin carbohydrates, sparing biotin-binding sites from inactivation [Reschiglian et al. 2013].

AvidinOX® binds cellular and interstitial protein amino groups through Schiff bases, in both normal and neoplastic tissues, resulting in a tissue half-life of 2weeks, compared with 2 h of native avidin. AvidinOX® preserves the native structure of avidin, consisting in four identical subunits (homotetramer) of 16 kDa and high affinity and specificity for biotin. Nonetheless, as a consequence of the chemical modifications that lead to Schiff base formations, in solution at neutral pH, the protein easily tends to aggregate, thus it is stored in lyophilized conditions [Santis et al. 2010, Petronzelli et al. 2011].

Sodium chloride (NaCl), sodium acetate and urea were acquired from Sigma Aldrich Co. (St. Luis, MO, USA). Lyophilized AvidinOX® vials, supplied by Sigma-Tau, were reconstituted with ultrapure water to a final concentration of 3 mg/mL of protein in formulation buffer (mannitol 3 mg/mL, 0.067 M Sodium Acetate, pH 5.3). On one occasion, AvidinOX® was reconstituted in 4 M urea solution to the same final concentration, 3 mg/mL. Samples were injected immediately after preparation and after 3 h of storage at room temperature and 4°C or after 24 hours of storage at room temperature and 4°C.

4.1.7.3. RESULTS AND DISCUSSION

A. DESIGN OF EXPERIMENTS (DOE) APPLIED TO HF5 METHOD DEVELOPMENT. SIMPLE ALGORITHM PROPOSED TO DETERMINE THE OPTIMAL SEPARATION METHOD, UNDER DIFFERENT EXPERIMENTAL CONDITIONS. CASE STUDY: AVIDINOX® FORMULATION.

A 2x2 factorial design was employed during the HF5 method development. Two of the most important parameters that have great implications on the separation mechanism were considered as factors in the factorial design: the *channel flow rate*, v_c and the *cross-flow rate*, v_x. Each of them had two levels: a high value (+) and a low value (-), resulting in a total of 4 initial combinations. The flow rate values used for the 4 combinations are reported in Table 1.

Table 1 - Factorial design for the HF5 method development, part 1

Area	v_c (mL/min)	Variable 1	v_x (mL/min)	Variable 2	Combination
A	0.2	-	0.35	-	- -
B	0.2	-	0.85	+	- +
C	0.4	+	0.35	-	+ -
D	0.4	+	0.85	+	+ +

Taking into account the manufacturer's (Wyatt Technology Europe) recommendations regarding the flow rates that can be achieved during a typical HF5 run under optimal conditions with Eclipse® DUALTEC™ (0.1 – 1.0 mL/min for the *cross flow rate* and 0.1 – 0.5 mL/min for the *channel flow rate*), the instrumental operational range was divided into 4 initial areas and a combination between the two factors was placed inside of each one (see Figure 1).

Figure 1 depicts the approach used for the HF5 method development of AvidinOX®, considering also the MW of the protein (64 kDa): the instrument operational range was sliced into 4 sections and a flow rates combination was chosen inside each one.

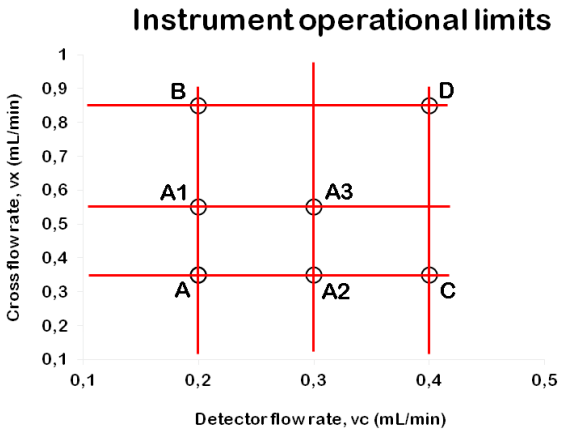

Figure 1 – HF5 operational limits and flow rate combinations for the experimental design

The experiments were performed following the order illustrated in Table 1. For each experiment, an amount of 9 µg of AvidinOX® was injected (3 µL of a 3 mg/mL solution) and separated in a carrier solution very similar to the protein's formulation buffer: 50 mM acetate buffer supplemented with 100 mM NaCl (total ionic strength 150 mM), at pH 5.3. A second mobile phase was employed to separate AvidinOX®, whose composition was identical to the first one, but supplemented with 4M urea, from this point forward called "*denaturing carrier solution*".

The *focus flow rate* (0.85 mL/min) and the *focus time* (3 min) were set constant for all experiments within the Eclipse method. The total elution time was set at 22 min (considered sufficient for all the species of interest to elute), followed by a 2 minutes field release to avoid possible sample carry over.

The HF5 elution profiles at 280 nm are reported in Figure 2, for both non-denaturing and denaturing separation conditions. Each flow rates combination (A-D) allows the separations of at least two AvidinOX® oligomers. As expected, the retention times of the same species increase when the separation is performed under denaturing conditions, because of the urea 4 M solution viscosity (η/η_0 = 1.2, therefore $t_{R,urea}/t_{R,water}$ = 1.2).

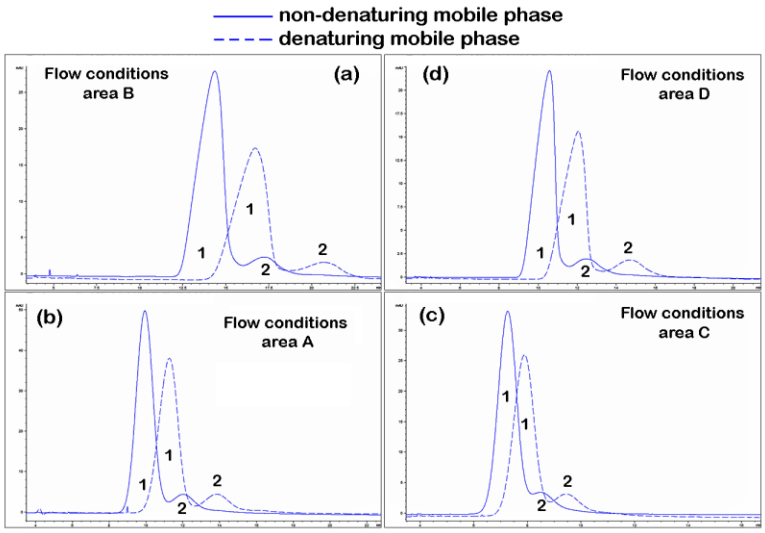

Figure 2 – HF5 separation profiles at 280 nm obtained under non-denaturing and denaturing conditions applying flow conditions A, B, C and D.

The separation was monitored by UV detection at 280 nm and the following separation parameters were calculated in order to choose the best out of the 4 combinations: *resolution*, *peak symmetry* and *valley height between peaks* (expressed as % of the smallest separated peak) and the values are reported in Table 2.

Table 2 – Separation performance parameters: resolution, peak symmetry and valley height between first and second peak (part 1)

Mobile phase	Area	Resolution	Monomer symmetry	Valley height as % of the smallest peak
Non denaturing	A (- -)	0.94	1.02	58.8
	B (- +)	0.82	1.77	58.8
	C (+ -)	0.85	1.03	94.4
	D (+ +)	0.79	2.19	56.2
Denaturing	A (- -)	1.07	1.18	35.2
	B (- +)	0.89	1.52	50.0
	C (+ -)	0.89	1.07	66.6
	D (+ +)	0.97	1.91	43.4

The best combination was found to be A, for both denaturing and non-denaturing separation conditions, not only based on the values corresponding to these separation parameters, but after careful observation of the UV elution profiles and after making sure that the values actually reflected the best separation conditions.

Flow rates combination A was further explored to narrow down to the most suitable

separation method for the AvidinOX® samples. The same 2x2 factorial design approach was used, but with different flow rate values (reported in Table 3*)* – at the border with the other areas (Figure 1). The same sample amount and volume were separated and the same carrier solutions were employed.

Table 3 - Factorial design for the HF5 method development, part 2

Area	vc (mL/min)	Variable 1	vx (mL/min)	Variable 2	Combination
A	0.2	-	0.35	-	- -
A1	0.2	-	0.55	+	- +
A2	0.35	+	0.35	-	+ -
A3	0.35	+	0.55	+	+ +

The separation parameters values obtained from experiments involving areas A, A1, A2 and A3 are summarized in Table 4.

Table 4 – HF5 performance parameters: resolution, peak symmetry and valley height between first and second peak (part 2)

Mobile phase	Area	Resolution	Monomer symmetry	Valley height as % of the smallest peak
Non denaturing	A (- -)	0.94	1.02	58.8
	A1 (- +)	1.15	1.36	31.5
	A2 (+ -)	1.11	1.5	33.3
	A3 (+ +)	0.89	1.22	55.5
Denaturing	A (- -)	1.07	1.18	35.2
	A1 (- +)	1.28	1.37	33.3
	A2 (+ -)	1.24	1.63	26.3
	A3 (+ +)	1.14	1.25	37.5

In order to facilitate data interpretation, the monomer symmetry value was plotted against the corresponding monomer-dimer resolution for each flow condition, under both non-denaturing (Figure 3a) and denaturing separation conditions (Figure 3b).
In Figure 3, the acceptable resolution value (1) and peak symmetry optimal value (1) are highlighted as red lines. These are the same values which will be used in the objective approach to choosing the optimal separation flow rates combination of

AvidinOX®.

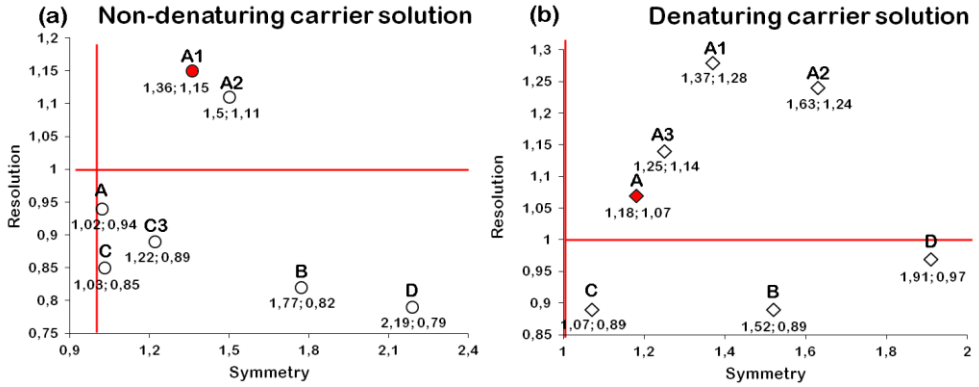

Figure 3 – HF5 performance under (a) non-denaturing and (b) denaturing conditions. Symmetry plotted against corresponding resolution for each flow rates combination. The (resolution; symmetry) values are displayed under each flow condition

Based on the computed separation parameters obtained with DOE approach, a simple algorithm is proposed in order help choose the optimal flow rates combination for the separation under both non-denaturing (Figure 4) and denaturing (Figure 5) separation conditions, represented as red dots in Figure 3.

The first decisional block of the algorithm represents the **resolution**. A score is calculated for each flow rates combinations, represented by the difference between the calculated resolution (R_s) and 1, which corresponds to an acceblable separation (when 2% of peak ares overlapse).

The *positive resolution scores* are tested according to the second decisional block, represented by the peak **symmetry** value, 1 representing a gausssian (symmetric peak). Negative values correspond to tailed peaks, while postive values correspond to fronted peaks.

The *negative resolution scores* are tested again, and the ones that match the criteria ($0.9<R_s<1$) arrive to the *symmetry* decisional block, and tested following the above described procedure.

A *total score*, represented by the sum between resolution score and symmetry score, is calculated for each value which passed the symmetry decisional block. The two

values closest to zero arrive to the third decisional block, which is represented by the **valley height between the separated species** and the other values are discarded. The flow rates combination with the smallest % is chosen as the optimal method.

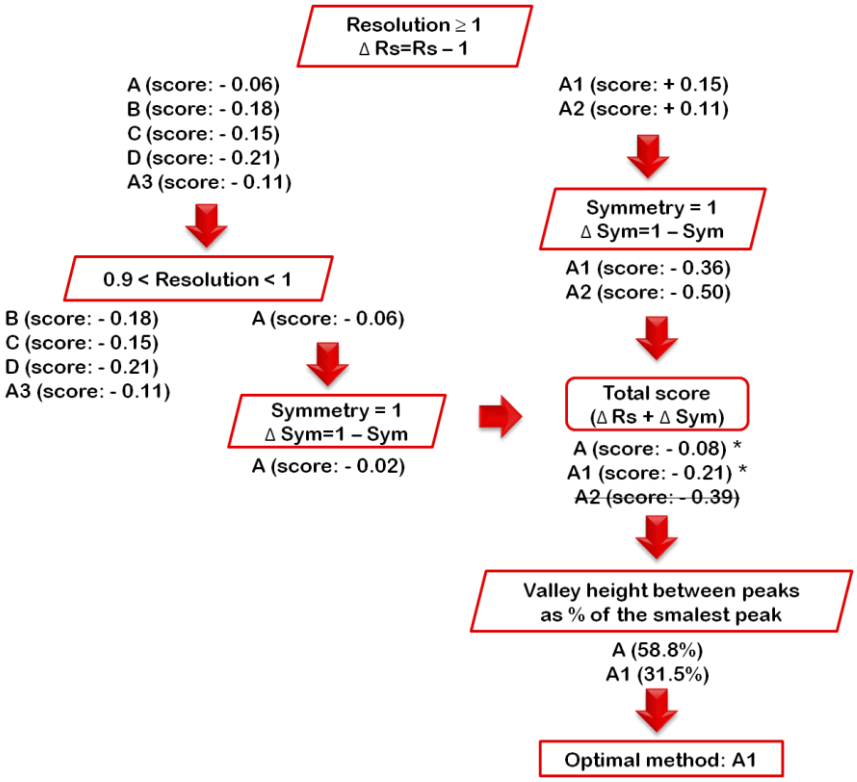

Figure 4 – Simple algorithm used to determine the optimal flow rates combination for the separation of AvidinOX® formulation under non-denaturing conditions

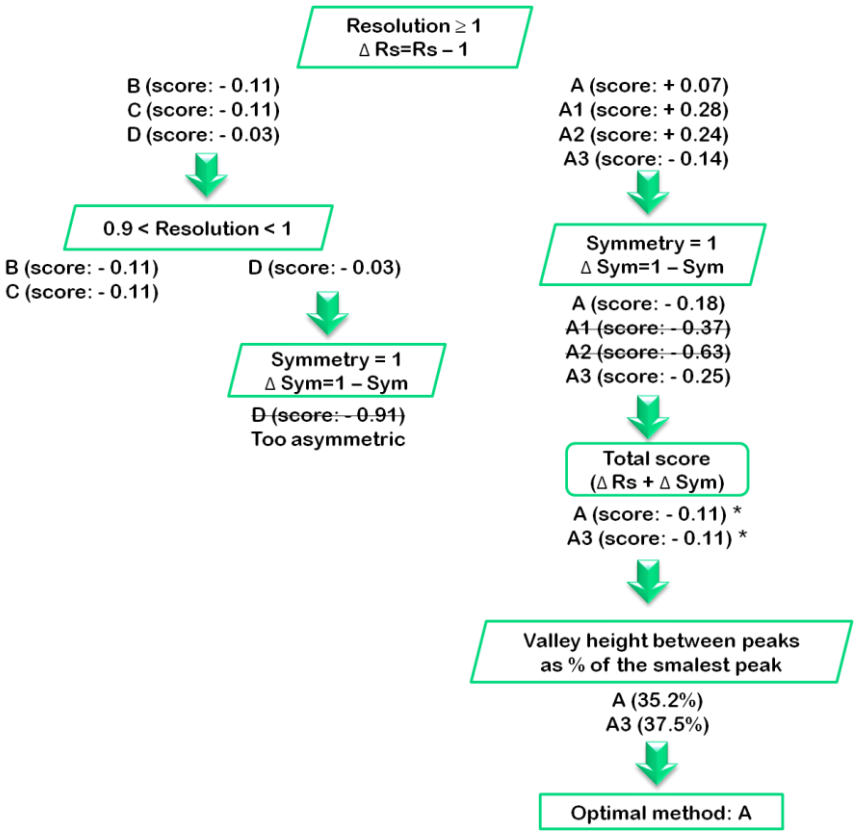

Figure 5 – Simple algorithm used to determine the optimal flow rates combination for the separation of AvidinOX® formulation under denaturing conditions

The factorial experiment approach (2x2 in this case, but it could be extended to other factors/variables or levels) provides a simple and quick, yet effective way to "scan" the whole instrumental range in search for most suitable separation method for the sample of interest. The number of experiments depends on the considered factors and on the number of levels for each one.

There are a few software meant for the design of experiments already commercially available that are able not only to generate the combinations (which becomes more difficult as the factors and/or the levels are more than 2) and to plan the order of experiments through randomization (to eliminate the succession of experiments as another variable to take into consideration), but are also able to calculate and represent visually the correlations between factors.

Since one of the major drawbacks of FFF in general is having to take into consideration too many parameters when developing a method, without knowing

exactly how and if one parameter could influence another (or more), the factorial design approach could prove itself very useful to study the correlations between separation variables and their impact on the separation parameters.

This approach could simplify immensely the method development step aimed for the separation of protein from their oligomeric species (i.e: antibodies), rendering FFF as separation method more "*user-friendly*", not to mention time-saving, all the while remaining versatile.

However, careful interpretation of the results is required, because the parameters values alone can be deceiving and could lead to an erroneous interpretation, if they are not supported by the confirmation from elution profiles.

B. HF5 – MALS METHOD FOR THE STUDY OF AVIDINOX® FORMULATION STABILITY AND AS MEANS OF INVESTIGATING THE NATURE OF AVIDINOX® HIGH MOLECULAR WEIGHT SPECIES (HMWS)

The HF5 methods that proved to be optimal for the separation of the AvidinOX® formulations were chosen applying the algorithms described in the previous section (marked with red dots in Figure 3) and are reported in Table 5.

Table 5 – HF5 methods for the AvidinOX® stability study

Mobile phase	v_c (mL/min)	v_{focus} (mL/min)	Focus time (min)	v_x (mL/min)
Non-denaturing	0.2	0.85	3	0.55
Denaturing	0.2			0.35

AvidinOX® formulation's stability was monitored over a series of injections at specific time intervals. More specifically, the variation of the protein oligomers levels was monitored by UV-MALS detection, immediately after the reconstitution (t_0), after 3h, at room temperature (t_1) and after 24h, at 4°C (t_2).

AvidinOX® stability was investigated under both native and denaturing conditions, in order to determine the true nature of the protein aggregates. For each experiment,

an amount of 9 µg of AvidinOX® was injected (3 µL of a 3 mg/mL solution) and separated in a carrier solution very similar to the protein's formulation buffer: 50 mM acetate buffer supplemented with 100 mM NaCl (total ionic strength 150 mM), at pH 5.3.

A denaturing mobile phase was also employed to separate AvidinOX®, which had a composition identical to the first one, but supplemented with 4M urea. Urea, as denaturant, has the ability to disrupt protein aggregates bound by weak interactions, such as hydrogen bonds or hydrophobic interactions.

The HF5 elution profiles, as well as the oligomers levels are reported in Figure 6. The blue traces correspond to separation performed under native (non-denaturing) conditions, while the red traces were obtained under denaturing conditions.

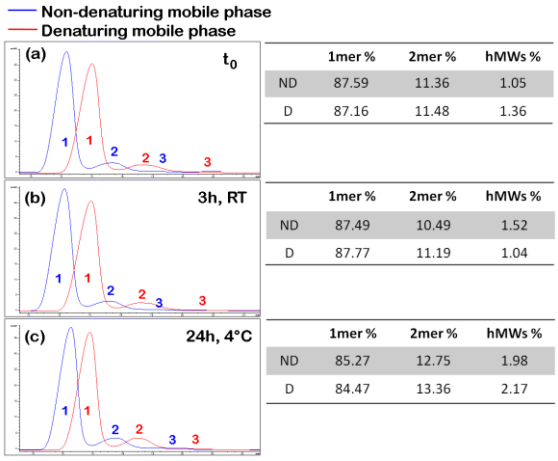

	1mer %	2mer %	hMWs %
ND	87.59	11.36	1.05
D	87.16	11.48	1.36

	1mer %	2mer %	hMWs %
ND	87.49	10.49	1.52
D	87.77	11.19	1.04

	1mer %	2mer %	hMWs %
ND	85.27	12.75	1.98
D	84.47	13.36	2.17

Figure 6 – HF5 separation profiles of AvidinOX® at 280 nm during the stability study (a) injected immediately after reconstitution; (b) injected after 3h of reconstitution and storage at room temperature and (c) injected after 24h of reconstitution and storage at 4°C

Each HF5 separation method allows the elution of three bands of AvidinOX®. The retention time difference between the red and the blue traces at each time point can be explained by the different viscosity of the mobile phase. When 4 M urea was added to the mobile phase, a retention time delay was to be expected: since η_{urea}/η_{water} = 1.2, the corresponding retention time delay will be directly related to the viscosity ratio according to HF5 retention theory (*Equations 11* and *12* discussed in

sub-chapter 2.2.2, Chapter 2).

From the retention time values, the peaks were assigned as follows: (1) AvidinOX® monomer, (2) AvidinOX® dimer and (3) AvidinOX® trimer. The oligomers levels have different trends under denaturing and non-denaturing separation conditions. Under native conditions, the trimer levels slightly increase over time, regardless of the storage temperature. Under denaturing conditions, the trimer levels decrease after 3h at room temperature, but increase when kept for 24h at 4°C. The dimer levels, under both non-denaturing and denaturing conditions, slightly decrease after 3h of storage at room temperature, but increase after 24h at 4°C.

The absolute MW values of the three elution bands were determined by online coupling Eclipse® DUALTEC™ (HF5) with a DAWN® HELEOS™ (MALS detector) and using a UV concentration detector set at 280 nm.

For each experiment, an amount of 9 µg of AvidinOX® was injected (3 µL of a 3 mg/mL solution) and the aggregate levels, as well as their absolute MW was monitored as follows: at t_0 (immediately after reconstitution) after 2h (kept at RT), 3h (kept at RT and at 4°C) and after 24h (kept at 4°C).

The elution profiles and the MW values corresponding to the three elution bands of AvidinOX® formulation kept at 4°C are reported in Figure 7 (a) separated in non-denaturing mobile phase and (b) separated in denaturing mobile phase.

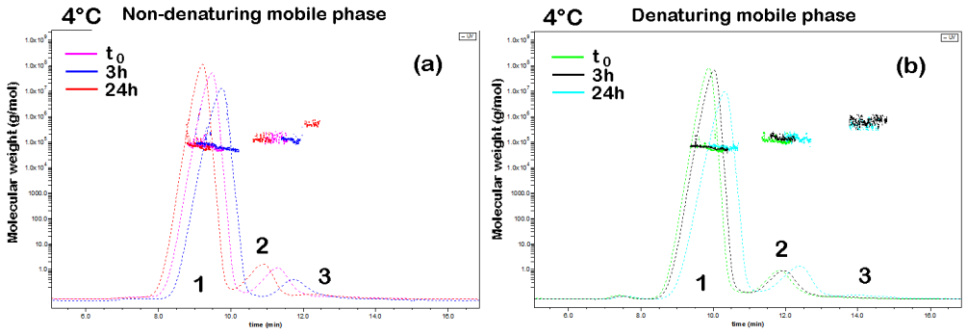

Figure 7 - HF5-MALS elution profiles and MW corresponding to the three elution bands of AvidinOX® kept at 4°C after reconstitution

With the passing of time, the elution bands tend to lose symmetry and the retention

times increase. The balance between the oligomers levels shifts slightly, as described before. The MW values were averaged over a series of 5 injections for each condition (5 x non-denaturing and 5 x denaturing) and the ratios $MW_{oligomer}/MW_{monomer}$ were found as follows: $MW_{peak\ 2}/MW_{peak\ 1} = 2.04 \pm 0.06$ and $MW_{peak\ 3}/MW_{peak\ 1} = 4.37 \pm 0.08$. These absolute MW values prove that the third peak was erroneously assigned (from the retention time value) to the AvidinOX® trimer, when, in fact, its MW value corresponds to the tetramer.

The elution profiles and the MW values corresponding to the three elution bands of AvidinOX® formulation stored at room temperature are reported in Figure 8 (a) separated in non-denaturing mobile phase and (b) separated in denaturing mobile phase.

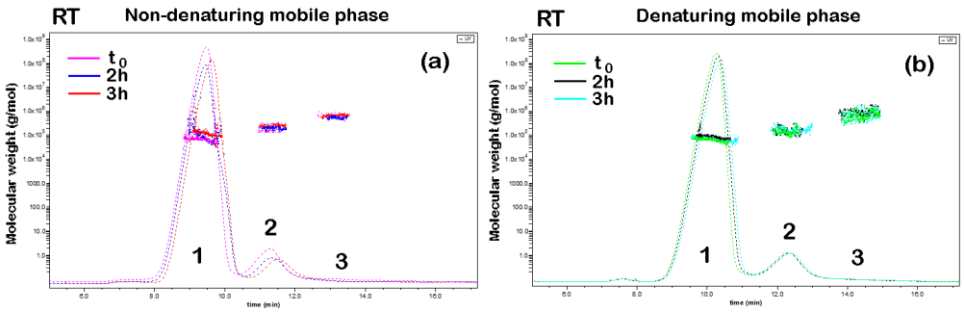

Figure 8 – HF5-UV-MALS elution profiles and MW corresponding to the three elution bands of AvidinOX® stored at room temperature after reconstitution

When stored at room temperature after reconstitution, AvidinOX® elution bands have highly reproducible retention times up to 3h since sample reconstitution. The $MW_{oligomer}/MW_{monomer}$ ratios are very similar to the ones already reported in the previous paragraph.

The aggregates levels for all experimental conditions are reported in Table 6. The tetramer levels decrease when the separations are performed in denaturing mobile phase. This finding suggests the presence of two types of AvidinOX® aggregates: *non-covalent*, which dissociate into smaller units when urea 4 M is present and *covalent*, which are not disrupted by urea. The two types of aggregate levels are reported in Table 7.

Table 6 – Aggregates levels during the stability study of AvidinOX® formulation

Time	t (°C)	Mobile phase	Monomer (%)	Dimer (%)	Tetramer (%)
reconstitution	any	Non denaturing	88.9	7.9	3.0
		Denaturing	85.0	11.0	2.6
2h	RT	Non denaturing	86.1	8.9	4.4
		Denaturing	86.5	10.1	3.8
3h	RT	Non denaturing	87.8	8.6	3.4
		Denaturing	86.5	10.9	2.1
3h	4°C	Non denaturing	86.4	9.1	3.9
		Denaturing	85.3	10.9	2.8
24h	4°C	Non denaturing	84.5	10.7	4.2
		Denaturing	82.2	13.1	3.6

The amount of covalent aggregates was calculated as the difference between the aggregate levels detected in non-denaturing and denaturing carrier solution and they are reported as % relative to the aggregates levels under non-denaturing conditions (100%). The dimer is the only oligomer whose levels increase under denaturing conditions.

Table 7 – True nature of AvidinOX® hMWs

Time	t°C	Tetramer *covalent* aggregates (%)	Tetramer *non-covalent* aggregates (%)	Dimer % increase under denaturing conditions
reconstitution	any	86.7	13.3	28.2
2h	RT	86.4	13.6	11.9
3h	RT	61.8	38.2	21.1
3h	4°C	71.8	28.2	16.5
24h	4°C	85.7	14.3	18.3

Table 7 reports that most of the aggregates in tetramer form are preserved under denaturing conditions, therefore stable to urea denaturation (most likely *covalent*), and the highest decrease occurs when the sample is stored at RT for 3h. The highest conversion rate occurs immediately after sample reconstitution, when 13.3% of tetramer dissociates into dimer units. The same phenomenon is observed in reverse, as a monomer dynamic association into dimer, occurring simultaneously with the

tetramer dissociation (4.4% of monomer converts into dimer).

The same trend, though less obvious, of *dynamic association* (monomer into dimer) / *dissociation* (tetramer into dimer) can be noticed along all the time points. This suggests that all oligomers tend towards the dimer form, which appears to be the most stable of all oligomers, but this process can be slowed down over time, by keeping the sample at 4°C.

In order to test the effectiveness of urea as denaturant and to understand whether the time that the denaturant spends in contact with the protein influences the aggregates levels, an AvidinOX® sample was reconstituted in 4M urea solution, separated under non-denaturing conditions after 3h and its elution profile was compared to the sample reconstituted in water. The comparison is reported in Figure 9.

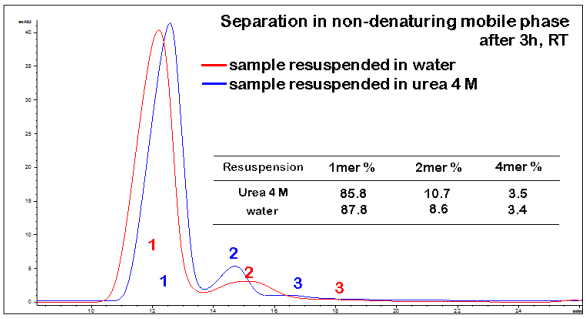

Figure 9 – AvidinOX® aggregates levels after 3h since sample reconstitution, storage at room temperature

Figure 9 shows that the AvidinOX® oligomers levels do not change significantly when the sample reconstitution is performed in 4 M urea and the 2% decrease in monomer levels appears to be directly related to the increase in the dimer levels. This finding suggests that the presence of urea causes the denaturation of the monomeric units leading to the aggregation of conformationally-altered monomers into dimers (probably according to aggregation mechanism 2, sub-chapter 4.1).

C. LIMIT OF QUANTIFICATION (LOQ) AND LIMIT OF DETECTION (LOD) ESTIMATION FOR HIGH MW AGGREGATES IN AVIDINOX® FORMULATION BY HF5 – UV.

The reproducibility of the HF5-UV method was tested under both native (non-denaturing) and denaturing conditions, at different time intervals from sample reconstitution and at different sample storage temperatures. In particular, the reconstituted sample was separated at t_0, after 3h (t_1) stored at RT and after 24h (t_2) stored at 4°C. Each separation was performed three times and the method repeatability was tested on the retention times of the three main bands. The retention time mean (average) value and the relative standard deviation (RSD%) calculated over three repeated runs are reported in Table 8.

No significant differences can be observed between the retention time values of the same species, repeated under the same experimental conditions. The HF5 method is therefore highly repeatable (first level of precision is met).

Table 8 – Average retention time values and standard deviation (n=3) for the three main elution bands in native (non-denaturing) and denaturing conditions.

	Non denaturing			Denaturing		
	# Peak	**Average t_R (min)**	**RSD%**	**# Peak**	**Average t_R (min)**	**RSD%**
t_0	1	8.7	4.6	1	10.6	7.5
	2	11.8	5.1	2	14.0	19.3
	3	14.2	5.6	3	16.3	7.4
3h (t1), RT	1	8.8	8.0	1	10.6	0.9
	2	11.7	7.7	2	14.0	11.4
	3	13.9	4.3	3	17.0	4.7
24h (t2), 4°C	1	9.0	2.2	1	10.2	2.9
	2	12.0	5.8	2	13.5	3.7
	3	14.3	11.9	3	15.9	3.1

Next, the reliability on the detection method was evaluated. For this purpose, the signal from a fluorescence detector was included in the study, along with the UV signal which was always recorded. The fluorescence detector was set on an excitation wavelength of 280 nm and an emission wavelength of 340 nm, specific for proteins.

The UV signal was set, as usual, to record an absorbance wavelength of 280 nm. Since both detectors were coupled online with the Eclipse® DUALTEC™ FFF separation system, their signals were recorded simultaneously.

Aliquots of the same AvidinOX® sample were placed in three different vials and the same sample amount (9 µg) was injected in sequence. Figure 10 reports the elution profiles of AvidinOX® injected immediately after reconstitution (a and c) and after 3h, samples stored at room temperature (b and d).

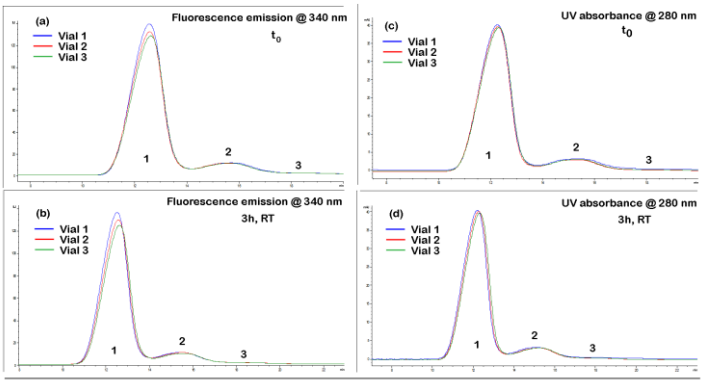

Fluorescence emission at 340 nm

Total area	Monomer area	RSD Total (%)	RSD Monomer (%)
13499.6	11824.3	2.850%	2.882%
12761.8	11198.4		
12576.8	10979.8		

UV absorbance at 280 nm

Total area	Monomer area	RSD Total (%)	RSD Monomer (%)
3780.7	3318.8	0.208%	0.218%
3771.9	3299.2		
3758.6	3305.9		

Figure 10 – HF5 elution profiles of different aliquots of AvidinOX®, fluorescence emission at 340 nm (a and b) and UV absorbance at 280 nm(c and d).

Figures 10a and 10b show the variation of the monomer peak height and the table below shows the same significant variations in the area under the peak (either total or monomer) when the fluorescence signal is used to monitor AvidinOX® separation. Figures 10c and 10d show that the elution profiles are identical under either separation conditions and the table below confirms the repeatability of the measurements, since the RSD is only 2%. This findings confirm that the UV absorbance signal in much more reliable for the quantification of the aggregates levels in AvidinOX® formulation than the fluorescence emission signal (as discussed in sub-chapters 3.2.1.2 and 4.1.5., the fluorescence signal might also reflect changes in the molecular conformation of AvidinOX®, which disturb the linear relationship between protein concentration and fluorescence emission).

Next, the Limit of Blank (LOB = $mean_{blank}$ + 1.645×$STDEV_{blank}$) was determined over 10 blank injections and was found to be 0.019 mAU.

The limit of detection (LoD) and of quantification (LoQ) for dimer and tetramer were determined from the corresponding calibration curves obtained by injecting different amounts of AvidinOX® and separating by HF5-UV under non-denaturing conditions. LoD and LoQ were determined on samples injected immediately after the reconstitution, when the aggregates level was the lowest.

The calibration curves were determined as dimer and tetramer height (expressed in mAU) plotted against the corresponding dimer and tetramer injected amount (expressed in μg). Since the sample recovery was considered complete and the injected amount was known at all times, the dimer amounts used in the calibration curves were estimated as % of the (total) injected amount. The calibration curves and their equations are reported in Figure 11.

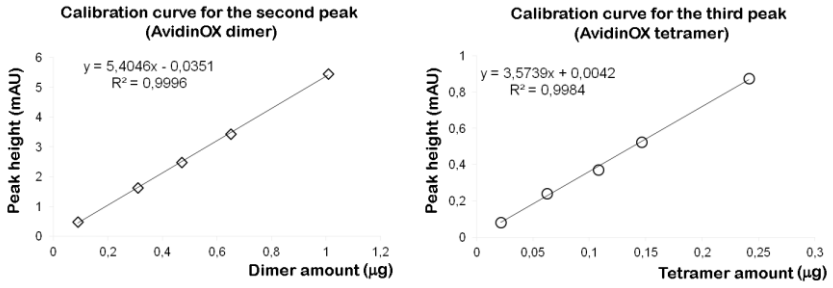

Figure 11 – Calibration curves for the calculation of LoD and LoQ of AvidinOX® aggregates

The limit of detection (LOD = 3 × LoB) and quantification (LoQ = 10 × LoB) are reported in Table 9, for both dimer and tetramer.

The following oligomers distribution was determined at t_0 under non-denaturing conditions: monomer (88.9%), dimer (7.9%) and tetramer (3.0%), previously reported in Table 6. Correlating this distribution with LoD and LoQ values from Table 9, the lowest AvidinOX® amount which needs to be injected in order for the **dimer** to be *detected* is 215 ng and 524.9 ng in order for the dimer to be *quantified* and, respectively, the lowest AvidinOX® amount which needs to be injected in order for

the **tetramer** to be *detected* is 489.7 ng and 1723.6 ng in order for the tetramer to be *quantified*.

Table 9 – LoD and LoQ determination of AvidinOX® aggregates

Aggregate type	Equation	x1 (ng)	x2 (ng)
Dimer	LoD = y1 = 5,4046 x1 - 0,0351	16.99	
	LoQ = y2 = 5,4046 x2 - 0,0351		41.46
Tetramer	LoD = y1 = 3,5739 x1 + 0,0042	14.69	
	LoQ = y2 = 3,5739 x2 + 0,0042		51.71
Where: LoD = 3 × LoB = 0.0567 mAU (y1) LoQ = 10 × LoB = 0.189 mAU (y2)			

4.1.7.4. CONCLUSIONS

Since one of the major drawbacks of FFF, in general, is having to take into consideration too many parameters when developing a method, design of experiments (DOE) approach could simplify immensely the method development process aimed at the separation of (therapeutic) protein self-associated species (monomers and their oligomeric species, rendering FFF more "*user-friendly*", not to mention time-saving and sample- customizable. A simple algorithm was successfully applied, which provided the optimal flow rates combination for the separation of AvidinOX® under both denaturing and non-denaturing conditions.

The versatility of HF5 allowed the use of a denaturing mobile phase containing a high urea concentration and the online coupling of HF5 with MALS provided the accurate MW of AvidinOX® elution bands. The stability of the AvidinOX® formulation was monitored over time and under different sample storage conditions. Employing denaturing and non-denaturing carrier solutions, the true nature of the aggregates was established and most of the high MW aggregates were found to be urea-insoluble, therefore considered covalent.

Lastly, the repeatability of the HF5 results was confirmed, meeting the first level of

precision and – after ascertaining the UV signal's reliability as detection method – the LoD, as well as LoQ values, were determined for both dimer and tetramer. The developed HF5-UV-(MALS) methods are highly sensitive, able to detect and quantify trace levels of AvidinOX® aggregates and it is proven that they provide repeatable results.

This study proves how, thanks to (a) the wide size range of separation and (b) the virtually infinite chromatographic space for the elution of aggregates, (c) the ability to analyze protein formulation under a variety of storage conditions and formulations and (d) the great versatility toward the choice of separation conditions (mobile phase composition, pH, additives) without loss of efficiency, HF5-UV-MALS could become the method of choice for the analysis of proteins formulations, where it can be invaluable in quantifying trace levels of high MW protein aggregates

Note: parts B and C of this sub-chapter were published as [Reschiglian et al. 2013]

4.1.7.5. REFERENCES

[Petronzelli et al. 2011] Petronzelli F.; Annam.Anastasi; Pelliccia A.; Santapaola D.; Albertoni C.; Rosi A.; Leoni B.; Ferrari L. E.; Paganelli G.; Gramiccioli G.; Pesce D.; Annam.Alfano; Stasi M. A. and Santis R. D. (2011). "*Preclinical Pharmacology and Safety of a Novel Avidin Derivative for Tissue-Targeted Delivery of Radiolabelled Biotin*." Basic & Clinical Pharmacology & Toxicology **109** (3): 145-155.

[Reschiglian et al. 2013] Reschiglian P.; Roda B.; Zattoni A.; Tanase M.; Marassi V. and Serani S. (2013). "*Hollow-fiber flow field-flow fractionation with multi-angle laser scattering detection for aggregation studies of therapeutic proteins*." Analytical and Bioanalytical Chemistry (Field-Flow Fractionation).

[Santis et al. 2010] Santis R. D.; Leoni B.; Rosi A.; Albertoni C.; Forni G.; Cojoca R.; Iezzi M.; Musiani P.; Paganelli G.; Chinol M. and Carminati P. (2010). "*AvidinOX™ for Highly Efficient Tissue-Pretargeted Radionuclide Therapy*." Cancer Biotherapy & Radiopharmaceuticals **25** (2): 143-148.

CHAPTER 4:

PART 2: STUDY OF OXIDATIVE STRESS-RELATED PROTEIN AGGREGATION PHENOMENA DURING BIOLOGICAL AGING

INTRODUCTION

SYNOPSIS: SENESCENCE

Senescence (from the Latin word: "*senescere*", meaning "*to grow old*") or biological aging represents an intrinsic process occurring in all living organisms that consists in the age-related progressive deterioration of all physiological functions, loss of viability, increased vulnerability towards pathogens, reflecting changes at molecular and cellular level and ultimately leading to death. At both organism and cellular level, the ability to respond to stressors declines and the homeostatic imbalance, as well as the risk of aging-associated diseases increase – all hallmarks or aging.

The factors that cause the development of cancer, neurodegenerative and cardiovascular diseases are all rooted in the natural biological aging process. Consequently, understanding the molecular mechanisms underlying aging is fundamental to understand many disease processes. For instance, the oxidation and nitration of intracellular proteins leading to the formation and accumulation of protein aggregates are suspected to be the culprits behind the loss of cellular function and the reduced ability of senescent animals to fight against physiological stresses [Squier 2001, Cannizzo et al. 2011] (and references therein).

Since oxidatively modified proteins are thermodynamically unstable and assume partially unfolded tertiary structures prone to form aggregates, it is very likely that oxidized proteins are intermediates in the formation if amyloid fibrils. Therefore, identifying oxidatively sensitive protein targets, which may play a protective role (by to down-regulating the energy metabolism and, consequently, reducing the generation of reactive oxygen species, ROS) is of particular interest.

Accordingly, regulating the rate of ROS generation, may enhance cellular maintenance and repair functions, which, in turn, have proven to enhance life-span and diminish a host of age-related diseases [Squier 2001] (and reference therein).

SYNOPSIS: OXIDATIVE STRESS

Inside any living organism, damaged cells are constantly being replaced and the proteins degraded to constituting AA and re-synthesized. The *reactive oxygen species* (ROS), such as hydrogen (H*), hydroxyl radical (OH*), transition metals (copper and iron), oxygen (O*and RO*), diatomic oxygen (O2*,HO_2*, RO_2*), and its superoxide (O_2^{*-}) [Cannizzo et al. 2011], highly reactive chemical species, are formed as a natural by-product of the normal metabolism of oxygen [Mirzaei and Regnier 2008] (and references therein). ROS are employed by the organism to fight against pathogens or to dispose of damaged cell components, thus, have important roles in cell signaling, homeostasis (maintaining the equilibrium inside the living organisms) and programmed cell death. Under normal circumstances, cells defend themselves from the damage caused by ROS through *antioxidants* like glutathione, vitamins A, C, and E, and flavonoids and *enzymatic scavengers* of ROS such as superoxide dismutase (SOD), catalase, and glutathione peroxide [Aiken et al. 2011] (and references therein), whose role is to prevent the unnecessary formation of ROS or to dispose of them before they can damage vital components of cells. ROS are present at very low levels and their damage is constantly repaired. Therefore, under normal circumstances, there is equilibrium between antioxidants and ROS levels, which makes it possible for the cells to be continuously renewed and disposed of [Bandyopadhyay et al. 1999] (and references therein).

Nonetheless, following natural aging/senescence, the body gradually loses its ability to repair itself, due to the loss of equilibrium between the oxidizing species (ROS) and antioxidants, which is believed to be the main cause of biological aging [Imlay 2003] (and references therein). This imbalance between the over-production (and action) of ROS and the reduced ability of the organism to readily dispose of the reactive intermediates or to repair the resulting damage is a condition called *oxidative stress*. The consequences of oxidative stress in the living organisms include toxicity induced by the production of peroxides and free radicals which damage cellular

components (proteins, lipids, and DNA). In addition, oxidative stress may disturb normal mechanisms of cellular signaling, since some ROS act as cellular messengers in redox signaling [Dare et al. 2014] (and references therein).

Oxidative stress is believed to be the root cause of a plethora of pathologies, including cancer, Parkinson's disease, Alzheimer's disease, Huntington's disease, atherosclerosis, heart failure, myocardial infarction, fragile X syndrome, Sickle Cell Disease, autism, and chronic fatigue syndrome [Rubinsztein et al. 2005, Patel and Chu 2011] (and references therein).

Associated with an increased production of ROS and/or significantly less efficacious antioxidant defenses, the effects of oxidative stress depend upon the entity of these changes. For instance, cells are able to overcome small perturbations and regain their function, nonetheless, even moderate oxidation can trigger apoptosis (programmed cell death), while more intense stresses may cause necrosis and severe oxidative stress can cause cell death [Imlay 2003] (and references therein).

A. REACTIVE OXYGEN SPECIES (ROS), OXIDATIVE STRESS AND SENESCENCE

The ROS are employed by the immune system as lethal weapons against pathogens, therefore, the production of ROS (and reactive nitrogen species) is a central part of this mechanism of pathogens disposal. The non-specific action of these highly reactive oxidants is advantageous because it targets and damages the entire cell, therefore impeding the pathogen to escape [Imlay 2003] (and references therein).

However, the production of ROS is a particularly destructive aspect of oxidative stress because, for instance, when reactive oxygen and nitrogen species overwhelm cellular antioxidants, it leads to oxidative damage to cellular proteins (and aggregation thereof) and impaired homeostasis. Furthermore, protein aggregation contributes to the formation of amyloid deposits that accumulate during biological aging [Squier 2001] (and references therein).

Due to their non-specific action, ROS (inescapable side-products of oxidative metabolism) can damage *lipids, nucleic acids* and ***proteins***. More specifically, ROS-mediated protein oxidation causes tertiary structural alterations (therefore loss or impairment of biological function) that promote protein aggregation and amyloid formation. The production of ROS roughly correlates with the life-span of living organisms, and is believed to represent a major determinant for the rate of aging and the development of numerous age-related diseases [Squier 2001] (and references therein).

Although, even under normal conditions, the efficiency of antioxidant and repair mechanisms cannot avoid completely the oxidation reaction mediated by ROS, during aging, the cellular homeostatic machinery becomes progressively impaired, which, in turn, increases the vulnerability towards oxidative damage. Oxidative processes cause reversible or irreversible changes/damage to macromolecules and their accumulation is associated to senescence [Valle 2011] (and references therein).

B. OXIDATIVE STRESS, SENESCENCE AND PROTEIN DAMAGE

PROTEIN POST-TRANSLATIONAL MODIFICATIONS

Protein oxidative modifications that occur during aging consist in post-translational modifications, which lead to altered stability and decreased function, observed in a variety of proteins isolated from senescent animals. Following oxidation, these proteins become conformationally unstable and prone to aggregation. Furthermore, it is highly probable that these oxidized proteins act as nucleation sites/intermediates in amyloid formation. The balance between protein oxidation and misfolding (leading to aggregation) and their degradation and repair (re-synthesis) will decide the aggregation extent. Thus, a decreased repair rate of damaged proteins and a consequent extended half-life of oxidized proteins in the cell, will promote

aggregation and amyloid fibril formation [Squier 2001] (and references therein).

Oxidative stress-mediated protein modifications that occur during senescence include *direct* amino acid (AA) modifications by hydroxylation and formation of carbonyl derivatives (aldehyde and ketonic groups on AA side chains), protein nitrosylation, or *indirect* AA modifications by addition of peroxidated lipids or products from glycation and glycoxidation. Among these modifications, ***protein carbonylation*** is the most frequent and a *true biomarker of aging* (or oxidative stress presence, in general). More specifically, AA like *lysine, arginine, threonine* and *proline* residues undergo aging-related carbonylation more frequent than others [Kopito 2000, Lindner and Demarez 2009, Scharf et al. 2013] (and references therein).

Other post-translation modifications include (a) *nitration*, which occurs at tyrosine residues (several nitro-tyrosines have been detected in aging proteins, as well as in proteins implicated in neurodegenerative diseases) or by cystein-s-thiolation, which has also been implicated as a post-translational protein modification occurring in aging (induces loss or gain of function in different proteins) and (b) *sulfoxidation* of several AA and, among them, methionine is particularly susceptible to this modification resulting in loss of biological function and conformational alterations.

Protein fragmentation, sub-unit dissociation, unfolding, and exposure of hydrophobic residues and aggregation, with an overall loss of function represent other consequences of protein degradation by oxidation during aging [David et al. 2010] (and references therein).

Therefore, protein aggregates are seen as an inherent part of aging and evidence points towards the primary AA sequence and the overall protein structure to play an important role in the tendency of the protein to form aggregates [Bandyopadhyay et al. 1999, Cannizzo et al. 2012] (and references therein).

CLEARANCE OF OXIDIZED PROTEINS AND FORMATION MECHANISM OF PROTEIN AGGREGATES: WHY DAMAGED PROTEINS AND AGGREGATES ACCUMULATE

Senescence-related AA substitutions or post-translational modifications of specific AA and/or decreases in the function of chaperones or proteases can result in an increase in the fraction of misfolded and damaged proteins, a process associated with the formation of protein aggregates. Consequently, protein aggregates interfere with the biological activity of native proteins by disrupting cellular functions and act as nuclei for the aggregation of other unrelated proteins, overloading chaperones and proteases in a way that progressively increases the fraction of misfolded proteins in the cell [Squier 2001] (and references therein).

The *extent of production* of oxidized species, and the *level of oxidation* are the two determinant factors for the clearance of oxidized proteins. When the oxidative damage is too extensive and irreversible, proteins are targeted for degradation [Kiffin et al. 2004] (and references therein). The main requirement for proteins to enter the narrow proteasome catalytic chamber is the proteasome protein unfolding capability. For instance, since a low oxidation extent still allows protein unfolding, mildly oxidized proteins are almost completely degraded by the proteasome system, while extensively oxidized proteins (often entangled in misfolded aggregates) cannot be unfolded for proteasome degradation [Kiffin et al. 2004] (and references therein). In this case, extensively damaged proteins will form an "inclusion-like" body named "*aggresome*", which actively seizes insoluble proteins, will be transported to the late endosomes and lysosomes by macroautophagy [Kopito 2000].

Moreover, extracellular aggregates and aggregates from cells which were programmed to die (apoptotic) are engulfed by tissue resident macrophages (phagocytes) and dendritic cells. Normally, damaged biomolecules are degraded to their constitutive AA inside the endosomal tract by a series of acidic hydrolases. Nonetheless, when the proteins suffer extensive damage, oxidized protein, together with carbohydrates and lipids often form entangled aggregates, which polymerize as

lipofuscin-like aggregates, which are resistant to endosomal degradation. These endosomal-resistant aggregates can increase progressively over time by the addition of newly damaged molecules, and induce cytotoxic cell death [Kiffin et al. 2004, Patel and Chu 2011, Cannizzo et al. 2012] (and references therein).

Amyloid fibrils formation occurs when protein aggregates form ordered filaments, and the underlying cause of a range of age-related disease (such as Alzheimer). Furthermore, amyloid fibrils are protease-resistant structures, therefore their formation is irreversible once initiated, behaving like nuclei for further aggregation [Squier 2001, Rubinsztein et al. 2005, Nixon 2013] (and references therein).

Recent advances in the understanding of proteasome structure and mechanism of action during oxidative stress were discussed by [Aiken et al. 2011], along with a visual description of how cells cope with oxidative stress through proteasome-mediated degradation pathways. The oxidative stress-triggered cellular response is summarized as a flowchart, reported in Figure 1([Aiken et al. 2011]):

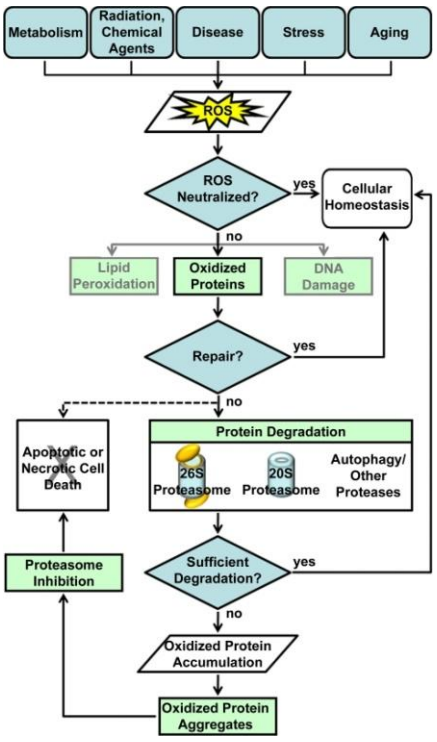

Figure 1 – Oxidative stress-triggered cellular response. The flow chart details the production of ROS and the consequent cellular response: either the restoration of normal cellular homeostasis or apoptotic/necrotic cell death [Aiken et al. 2011]

One common feature of oxidative stress-induced protein aggregates is that they are supposed to have a higher MW and size than the individual protein components of which they are composed. Furthermore, protein fragmentation is another effect of ROS damage and it was shown that protein fragments also have aggregation propensity [Mirzaei and Regnier 2008] (and references therein).

C. IMMUNOSENESCENCE, OXIDATIVE STRESS, PROTEIN DAMAGE AND ACCUMULATION OF PROTEIN AGGREGATES

Immunosenescence represents the progressive deterioration of the immune system as a consequence of natural aging. It manifests through a reduced capacity to respond to pathogens, as well as reduced vaccination efficacy (declining long-term immune memory) and is believed to be a function of age of the living organism relative to their life expectancy [Scharf et al. 2013] (and references therein).

There are two main biochemical mechanisms which relate immunosenescence to oxidative stress: (1) a decline in cellular functions consequent to protein, lipid and carbohydrate oxidative damage, and (2) cellular death subsequent to the progressive accumulation of oxidatively-damaged protein aggregates. As for any other aging cells inside the living organism, an increased amount of free radicals (ROS) was observed in the cells of the immune system. Consequently, *innate immune responses* (phagocytosis – dendritic cells, ROS production, and Toll Like Receptor functions) are generally compromised, as well as *adaptive immune responses* which are hampered by a decrease in the variety of the B and T immune cell repertoires,as well as their ability to clonally expand (proliferate from a common ancestor) following antigen stimulation. Furthermore, it was believed that endosomal accumulation of oxidatively-damaged proteins hinders the efficient processing of antigens and the macroautophagy-delivered degradation of proteins [Cannizzo et al. 2011] (and references therein).

An aspect of immunosenescence which was unknown until not so long ago was

whether the aging-related oxidative stress compromised the biological function of dendritic cells (major players in the innate immune system). In this regard, [Cannizzo et al. 2012] showed in a recent study the causality between the accumulation of oxidized products (damaged proteins and their aggregates) and the lack of efficacy of the immune response from dendritic cells, as well as an improvement in the adaptive immune system in recognizing antigens upon oxidative stress decrease, aspects which were not yet confirmed.

Moreover, the study showed *the accumulation of oxidatively damaged proteins in the dendritic cells from aging lymphatic organs*. The accumulation of oxidatively-damaged proteins in the endosomes of aging dendritic cells was investigated, showing that accumulation of such protein aggregates was not possible due to the short life span of dendritic cells. Large protein aggregates accumulate only in non-dividing cells endosomal compartments (neurons, cardiomyocytes and endothelial cells) [Cannizzo et al. 2012] (and references therein).

OXIDATIVE STRESS DAMAGE: PROTEIN CARBONYLATION

As previously stated, protein carbonylation of AA residues is as hallmark and a true biomarker for the age-related protein post-translational modifications. Protein carbonyls result from the oxidation of AA residues, the most frequent targeted being arginine, lysine and proline. Protein carbonyls can also arise from reactions of the AA like lysine, cysteine, or histidine with unsaturated aldehydes, which develop during the peroxidation of polyunsaturated fatty acids or from the oxidation of advanced glycation end (AGE) products [Cannizzo et al. 2011] (and references therein).

Typical post-translational protein modification associated with oxidative stress consists in the *addition of carbonyl groups* (aldehydes or ketones) to AA side chains. *Semialdehyde* carbonyls are mainly present on lysine, arginine and proline and represent the most abundant carbonyls observed in aging cells, while *ketone* carbonyls are mainly seen on histidine, proline, threonine and tryptophan residues

[Bandyopadhyay et al. 1999, Butterfield et al. 2012] (and references therein).

Another post-translational oxidative modification, introduced by either α-amidation or following oxidation of the glutamyl side chain, is the oxidative AA *side-chain cleavage*. In addition, some of the degradation products of *lipid oxidation* can directly bind AA side chains (mainly cysteine, lysine and histidine) through a Michael addition or Schiff base formation. Glycation, the non enzymatic addition of sugar to AA side chains, is also increased during oxidative stress conditions, while glycation additions to amine groups are collectively referred to as Maillard reactions. Advanced End Glycation products (AGE) are generated through aldose groups of a mono or polysaccharide binding to the amine groups on proteins, mainly on a lysine side chain. Most AGE products are rather unstable and promote further rearrangements, referred to as Amadori reactions [Imlay 2003, Cannizzo et al. 2011, Grune et al. 2013] (and references therein).

Another common modification following ROS-induced protein oxidation is *cross-linking*. The two most common cross-linking reactions are: (1) the formation of disulfide bonds between two oxidized cysteins and (2) Schiff base formation between carbonyl groups on different AA [Ishii et al. 2007, Butterfield et al. 2012].

Protein carbonylation is an *irreversible ROS-induced oxidative modification*, which often leads loss of protein activity and irreversible modification/damage promoted protein aggregation, followed by increased susceptibility to proteolysis. Consequently, protein carbonylation is considered a true *read-out of oxidative stress*. Moreover, carbonylated proteins are present in many aging-related inflammatory and neurodegenerative diseases [Aiken et al. 2011, Cannizzo et al. 2011, Cannizzo et al. 2012].

In the case of neurological diseases like Alzheimer's and Parkinson's disease, protein aggregates are generally composed of a single protein. Another consequence of carbonyl formation is the protein conformation alteration (these neurodegenerative disorders are also known as *protein misfolding diseases*), which, in turn, can increase protein hydrophobicity and enhance nonspecific protein–protein interactions, and

subsequent compromised cell viability and impaired protein turnover [Mirzaei and Regnier 2008] (and references therein).

IN VITRO AND *IN VIVO* EXPERIMENTAL MODELS FOR THE SIMULATION OF AGING EFFECTS: PARAQUAT – INDUCED OXIDATIVE STRESS

Paraquat is the commercial name for ***N,N'*-dimethyl-4,4'-bipyridinium dichloride**, a quaternary ammonium bipyridyl compound and one of the most widely used herbicides in the world. Paraquat has long been known to participate in cyclic reduction-oxidation reactions in biological systems, where it readily undergoes a single electron reduction in tissues, forming a free radical. Paraquat is often used in science as catalyst for the formation of ROS and more specifically, for the formation of the superoxide free radical [Takizawa et al. 2007]. In vivo, Paraquat is reduced by an electron donor such as NADPH, before being oxidized by an electron receptor such as dioxygen to produce the superoxide, a major ROS [Bus and Gibson 1984] (Figure 2).

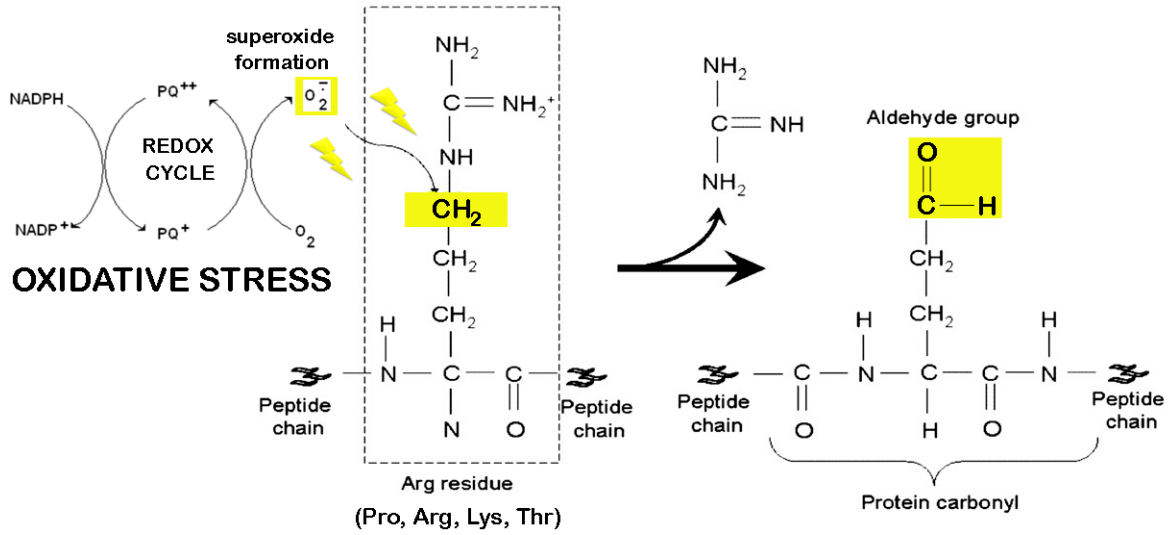

Figure 2 – Example of oxidative stress-induces (irreversible) protein carbonylation reaction, adapted from [Aslan et al. 2008] and [Bus and Gibson 1984]

Paraquat is used in murine models for the study of neurodegeneration [Manning-Bog et al. 2002, McCormack et al. 2002, McCarthy et al. 2004, Yang and Tiffany-

Castiglioni 2007] and leads to a reduced motor activity and, finally, cell death. Furthermore, the efficacy of Paraquat for oxidative stress generation purposes was reported in other types of cells. For example, used at low concentrations, Paraquat is able to induce protein aggregation in very short time, simulating the effects of aging both *in vitro* and *in vivo* [Scharf et al. 2013]. For *in vitro* studies of aging, solutions of known concentration of PQ are directly added to the cells in culture.

In this dissertation, Paraquat was employed to simulate the effects of aging in vitro as well as in vivo. Dendritic cells (Jaws II cell line culture) were treated with increasing molarities of Paraquat (in vitro) and mice were injected intra-peritoneally with Paraquat (in vivo). The efficacy of the Paraquat treatment, as well as the oxidatively-damaged proteins aggregates formation, isolation, characterization and quantification by HF5-(UV)-MALS are discussed in sub-chapters 4.2.1.4.B and C. The Paraquat controlled protein aggregation model was setup and served for the HF5 method development.

D. CURRENT PROTEOMIC TECHNOLOGIES AND THEIR LIMITATIONS

Proteomics technologies show certain limitations that are mostly related to the detection sensitivity of the analytical techniques employed for the study of difficult protein classes, such as low abundant, hydrophobic and basic proteins.

First of all, the selection of the proteomic methodology highly depends on the sample to be analyzed and the aim of the study. In general, the "*standard*" approach is the use of 2D gel/MALDI-TOF-MS and, since certain protein classes cannot be detected by these technologies, subsequent 2D LC–MS or tandem MS are necessary. However, it appears that the second approach is, generally, more effective. Moreover, as a rule of thumb, the complexity of the sample analysis protocol is directly related to the *chemical integrity* of the sample and *analysis reproducibility*, as well as the *sample recovery* [Garbis et al. 2005] (and references therein).

Basically, the limitations in a proteomic analysis can be classified as: (1) limitations

related to the complexity (the composition) of the proteome to be analyzed, the major issue being protein expression levels (which appear in all proteomics analyses), and (2) limitations of the analytical methods [Reschiglian and Moon 2008]. Consequently, the field of proteomics concentrates on both increasing the quantity of the low abundant proteins, to enable an efficient detection, and to applying the proper analytical methods to visualize all proteins in the mixture.

For instance, due to the vast protein diversity in terms of molecular sizes, charge state, hydrophobicity, protein conformational states, post-translational modifications or complex formation with other bio-macromolecules, it would be unfeasible to use a single sample preparation protocol, all the while capturing effectively the entire proteome. Since proteins are not expressed in equal amounts, there are large differences in the protein levels in all proteomes [Garbis et al. 2005] (and references therein).

A wide variety of analytical methods are applied to achieve the isolation and characterization of low-abundant proteins, which usually require enrichment of the low-abundant fraction and/or the depletion of highly abundant proteins that may interfere with the detection. For instance, in order to increase the probability to detect low abundant proteins, the original protein mixture (proteome) is separated into less complex fractions, where each of them contains a lower number of total proteins in comparison with the starting material [Garbis et al. 2005] (and references therein).

In a recent review, [Reschiglian and Moon 2008] discussed the pre-fractionation methods currently employed in proteomics, indicating the emerging role and gentle separation mechanism of Field Flow Fractionation (FFF) that allows proteins to maintain intact their biophysical properties (conformation included). In particular, the advantages brought by its miniaturized version, HF5, in terms of detection sensitivity, efficiency, solvent biocompatibility, as well as the possibility of on-line coupling with mass spectrometry (MS) are appealing features for proteomics.

Many publications support their findings in the field of proteomics:[Reschiglian et al. 2004, Reschiglian et al. 2005, Kang and Moon 2006, Reschiglian et al. 2006, Roda et al.

2006, Rambaldi et al. 2007, Kim et al. 2008, Lee et al. 2010, Reschiglian et al. 2011].

In this dissertation, HF5 was employed as a pre-fractionation method in a proteomic study. Since the aim of the study was to purify, characterize and quantify oxidatively-damaged protein aggregates present at trace levels, the complexity of the proteome (originating from different types of cells and different stages of aging) was reduced. Fractions were pooled from subsequent HF5 fractionations of the same sample, dialyzed and lyophilized to enrich the high MW aggregates fraction, discussed in sub-chapter 4.2.1.4.B and C.

E. IDENTIFICATION, ISOLATION AND PROTEOMIC ANALYSIS OF OXIDIZED PROTEINS AND PROTEIN AGGREGATES

OXIDATIVE STRESS DETECTION

The presence of oxidative stress can be achieved by fluorescent means, for instance, employing fluorogenic probes that can be used for measuring cellular oxidative stress in both live and fixed cell imaging. A highly efficient novel fluorogenic probe is CellROX® Deep Red Reagent (Life Technologies™), with absorption/emission maxima at ~644/665 nm. This dye is cell-permeant and is non-fluorescent in a reduced state, meanwhile, upon oxidation by reactive oxygen species (ROS), it exhibits bright fluorescence.

In this dissertation, the effectiveness of the in vivo Paraquat treatment, whose aim was to induce oxidative stress (and simulate in a brief time the effects of aging), was evaluated by fluorescent means, employing CellROX® Deep Red Reagent (Life Technologies™).The test, discussed in sub-chapter 4.2.1.4.C, showed highly increased fluorescence intensity in the Paraquat-treated mouse.

Recent developments in the field of functional proteomics have highlighted the selectivity of particular antibodies towards recognizing post-translational oxidative

modifications that occur following oxidative stress, therefore have provided the means for the detection, as well as affinity purification of aging-related oxidatively damaged entities. Coupled with proteomics and mass spectrometry, this selective purification has led the way towards mapping the oxidized proteins, and towards the identification of different types of oxidative modifications. [Cannizzo et al. 2011] (and references therein).

IDENTIFICATION AND ANALYSIS OF CARBONYLATED PROTEINS

The presence of carbonyl groups on oxidized proteins can be identified and quantified by derivatization with 2,4-dinitrophenylhydrazine (DNPH), which leads to the formation of hydrazones (Figure 3). When DNPH reacts with protein carbonyls, the amount of protein-hydrazone complex produced can also be measured spectrophotometrically at 375 nm and quantified against a calibration curve with a standard protein (such as BSA).

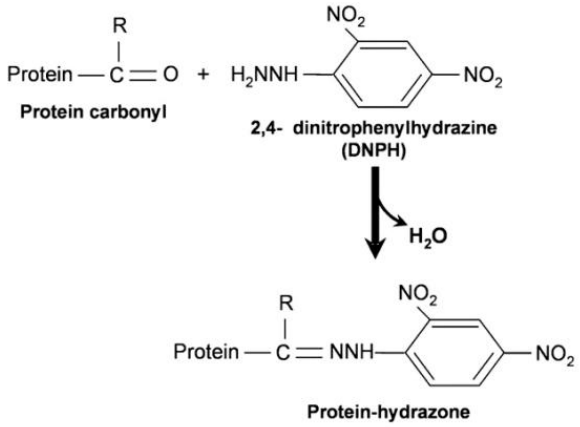

Figure 3 – Principle of carbonyl groups derivatization with DNPH [Aslan et al. 2008]

In this dissertation, the quantification of oxidative-stress induced carbonyl modifications was performed on two sets of samples, both treated with the pesticide Paraquat to induce oxidative stress: (a) in vitro Paraquat-treated Jaws II dendritic cell lysate samples and (b) in vivo

Paraquat-treated spleen cell lysate samples originating from mice. The protein carbonyl spectrophotometric assay discussed in sub-chapters 4.2.1.4.B (in vitro) and 4.2.1.4.C (in vivo) showed increased amounts of carbonyl in the Paraquat-treated samples as compared to control (non treated samples).

The DNPH-induced protein hydrazones can also be immunologically detected, using an anti-DNPH antibody that gives a precise indication on the amount of total protein carbonyls in a given sample. Furthermore, the advantage of having a DNPH specific antibody is that carbonylated proteins can be either immunoprecipitated or detected by SDS-PAGE or 2-D Fluorescence Difference Gel Electrophoresis (2-D DIGE), as preparative methods before mass spectrometry.

Following this procedure, reported schematically in Figure 4, [Cannizzo et al. 2012] showed that spleen and lymph node cells from aging mice accumulate oxidatively damaged proteins that presented hallmarks like carbonylated AA side-chains, AGE products and lipid peroxidation.

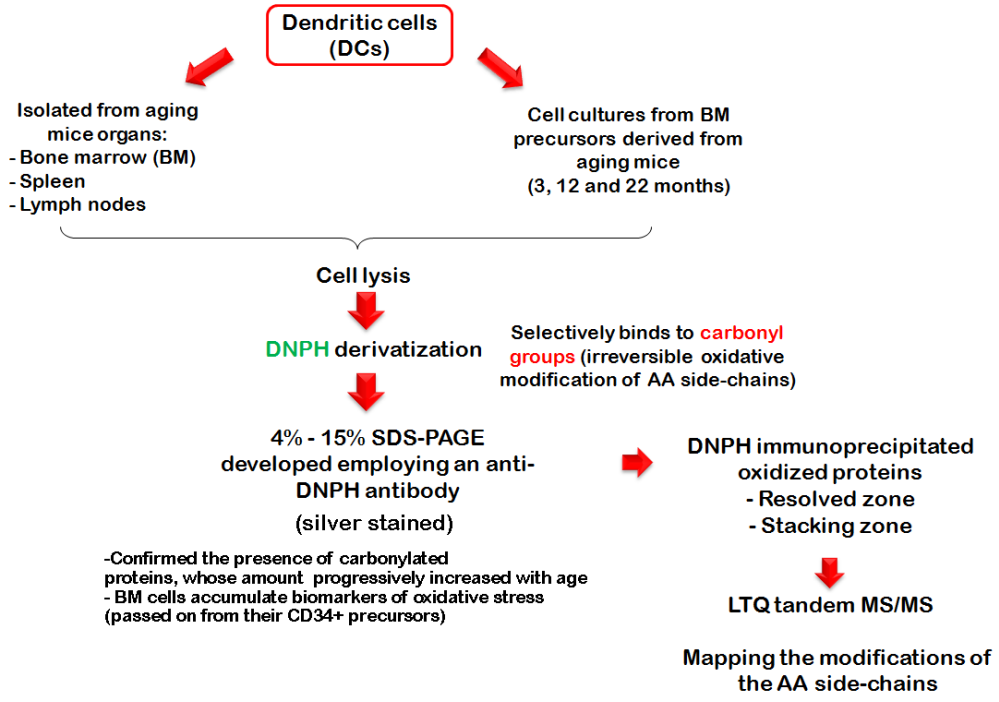

Figure 4 – Experimental procedure designed to identify the presence of oxidative stress-related protein modifications in dendritic cells, followed by the identification (mapping) of the modifications at biochemical level [Cannizzo et al. 2012]

SDS-PAGE performed on immunolabeled damaged proteins and protein aggregates showed an age-related progressively increased amount of high MW species (left in the stacking gel). Subsequent MS analyses performed on proteins excised from the stacking gel, as well as the resolved gel, allowed mapping the post-translational modifications suffered by proteins during aging. Moreover, the fact that damaged proteins and aggregates were found in dendritic cells derived from bone marrow (BM) CD34+ precursors indicates that these precursors are already compromised and is expected that they have a reduced biological function.

In this dissertation, HF5-(UV)-MALS analytical platform was employed for the size-separation, characterization (size and MW) and quantification of age-related protein aggregates in BM CD34+ precursor cells, discussed in sub-chapter 4.2.1.4.D. The results confirmed the previous finding by [Cannizzo et al. 2012].Furthermore, the offline MS analyses allowed the identification of age-related post-translational modifications and their extent.

Previous attempts by [Cannizzo et al. 2012] to isolate and characterize protein aggregates in CD34+ precursor cells are schematically reported in Figure 5. Their approach consisted in employing as first dimension of separation Fast Protein Liquid Chromatography (FPLC), a preparative separation technique routinely used in proteomics

Although FPLC was successfully employed by [Scharf et al. 2013] for the estimation of the oxidative post-translational modifications extent in structural proteins of intervertebral discs (IVDs) isolated from aging mice, where increased protein carbonylation was associated with protein fragmentation and aggregation, the study conducted by [Cannizzo et al. 2012] showed only the presence of age-related *micro-aggregates of carbonylated proteins* (1-3×10^6 Da, Figure 5), separated employing FPLC. However, FPLC fractions did not show the presence of large aggregates, concluding that DCs endosomal compartments do not accumulate such aggregates due to their short turn-over.

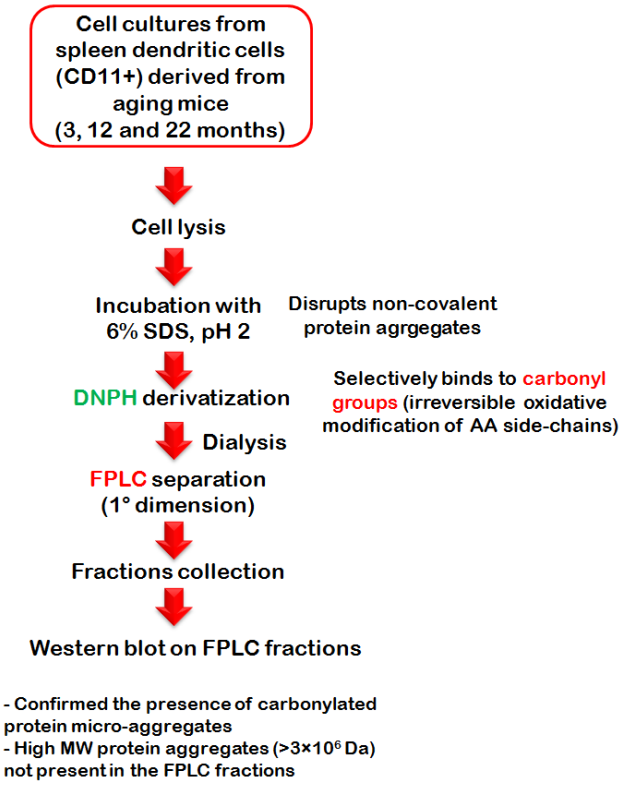

Figure 5 – Experimental procedure designed to for the isolation of oxidative stress-related protein aggregates in dendritic cells, followed by the Western blot performed on FPLC fractions [Cannizzo et al. 2012]

In this dissertation, FPLC was employed as first dimension of separation for the purifications of protein aggregates in oxidatively modified Jaws II dendritic cells (treated with Paraquat to induce oxidative stress and simulate the effects of aging in a short period of time). Nonetheless, FPLC proved not to be effective enough to resolve high MW protein aggregates, discussed in sub-chapter 4.2.1.4.B.

On the other hand, since HF5 is based on a different separation principle, allowing proteins (and protein aggregates) elution in increasing MW and size order (opposed to FPLC order of elution), provided enough separation space even for very high MW protein aggregates (>3×10⁶ Da). Moreover, thanks to HF5 versatility in terms of carrier solution composition, separations performed in denaturing carrier solution (containing different concentrations of urea), allowed the discrimination and quantification of urea-resistant covalent/irreversible protein aggregates, discussed in sub-chapters 4.2.1.4.B through 4.2.1.4.D.

Size exclusion chromatography (SEC) is another separation technique employed during proteomic procedures, recently used for the purification of oxidative stress-modified proteins and complexes in a study by [Mirzaei and Regnier 2008]. The effects of oxidative stress-induced protein aggregation were studied employing standard proteins and yeast cells. Oxidized standard proteins, at increasing ROS concentrations, were fractionated by SEC and displayed different elution profiles, indicating that protein aggregation occurs in stages and that protein fragments (result of ROS damage) also give rise to aggregates. Moreover, several carbonylated proteins and proteins known to form complexes with higher MW protein complexes were identified by MS on SEC fractions of oxidatively stressed yeast cells. In addition, these proteins were found to be part of the proteome known as the *aggresome* [Mirzaei and Regnier 2008] (and references therein).

REFERENCES

[Aiken et al. 2011] Aiken C. T.; Kaake R. M.; Wang X. and Huang L. (2011). "*Oxidative Stress-Mediated Regulation of Proteasome Complexes*." Molecular & Cellular Proteomics **10** (5).

[Aslan et al. 2008] Aslan M.; Cort A. and Yucel I. (2008). "*Oxidative and nitrative stress markers in glaucoma*." Free Radical Biology & Medicine **45**: 367–376.

[Bandyopadhyay et al. 1999] Bandyopadhyay U.; Das D. and Banerjee R. K. (1999). "*Reactive oxygen species: Oxidative damage and pathogenesis*." CURRENT SCIENCE **77** (5): 658-666.

[Bus and Gibson 1984] Bus J. S. and Gibson J. E. (1984). "*Paraquat: Model for Oxidant-Initiated Toxicity*." Environmental Health Perspectives **55**: 37-46.

[Butterfield et al. 2012] Butterfield D. A.; Perluigi M.; Reed T.; Muharib T.; Hughes C. P.; Robinson R. A. S. and Sultana R. (2012). "*Redox Proteomics in Selected Neurodegenerative Disorders: From Its Infancy to Future Applications*." ANTIOXIDANTS & REDOX SIGNALING **17** (11): 1610–1655.

[Cannizzo et al. 2012] Cannizzo E.; Clement C. C.; Morozova K.; Valdor R.; Kaushik S.; Almeida L. N.; Follo C.; Sahu R.; Cuervo A. M.; Macian F. and Santambrogio L. (2012). "*Age-related oxidative stress compromises endosomal proteostasis*." Cell Press **2** (1): 136-149.

[Cannizzo et al. 2011] Cannizzo E.; Clement C. C.; Sahu R.; Follo C. and Santambrogio L. (2011). "*Oxidative stress, inflamm-aging and immunosenescence*." Journal of Proteomics **74** (11): 2313–2323.

[Dare et al. 2014] Dare B. J.; Oyeniyi F. and Olaniyan O. T. (2014). "*Role of Antioxidant in Testicular Integrity*." SCIENCE DOMAIN International - Annual Research & Review in Biology **4** (7): 998-1023.

[David et al. 2010] David D. C.; Ollikainen N.; Trinidad J. C.; Cary M. P.; Burlingame A. L. and Kenyon C. (2010). "*Widespread Protein Aggregation as an Inherent Part of Aging in C. elegans*." PLoS Biology **8** (8): e1000450.

[Garbis et al. 2005] Garbis S.; Lubec G. and Fountoulakis M. (2005). "*Limitations of current proteomics technologies*." Journal of Chromatography A **1077** (1): 1-18.

[Grune et al. 2013] Grune T.; Catalgol B. and Jung T. (2013). *Chapter 1: Oxidative Stress and Protein Oxidation*. Protein Oxidation and Aging, First edition. Uversky V., John Wiley & Sons.

[Imlay 2003] Imlay J. A. (2003). "*PATHWAYS OF OXIDATIVE DAMAGE*." Annual Review of Microbiology **57**: 395-418.

[Ishii et al. 2007] Ishii T.; Yamada T.; Mori T.; Kumazawa S.; Uchida K. and Nakayama T. (2007). "*Characterization of acrolein-induced protein cross-links*." informa healthcare **41** (11): 1253-1260.

[Kang and Moon 2006] Kang D. and Moon M. H. (2006). "*Development of non-gel-based two-dimensional separation of intact proteins by an on-line hyphenation of capillary isoelectric focusing and hollow fiber flow field-flow fractionation.*" Analytical Chemistry **78** (16): 5789–5798.

[Kiffin et al. 2004] Kiffin R.; Christian C.; Knecht E. and Cuervo A. M. (2004). "*Activation of Chaperone-mediated Autophagy during Oxidative Stress*." Molecular Biology of the Cell **15** (11): 4829–4840.

[Kim et al. 2008] Kim K. H.; Kang D.; Koo H. M. and Moon M. H. (2008). "*Molecular mass sorting of proteome using hollow fiber flow field-flow fractionation for proteomics*." Journal of Proteomics **71** (1): 123–131.

[Kopito 2000] Kopito R. R. (2000). "*Aggresomes, inclusion bodies and protein aggregation*." Trends in Cell Biology **10** (12): 524-530.

[Lee et al. 2010] Lee J. Y.; Min H. K.; Choi D. and Moon M. H. (2010). "*Profiling of phospholipids in lipoproteins by multiplexed hollow fiber flow field-flow fractionation and nanoflow liquid chromatography–tandem mass spectrometry*." Journal of Chromatography A **1217** (10): 1660–1666.

[Lindner and Demarez 2009] Lindner A. B. and Demarez A. (2009). "*Protein aggregation as a paradigm of aging*." Biochimica et Biophysica Acta (BBA) - General Subjects **1790** (10): 980-996.

[Manning-Bog et al. 2002] Manning-Bog A. B.; Mccormack A. L.; Li J.; Uversky V. N.; Fink A. L. and Monte D. A. D. (2002). "*The Herbicide Paraquat Causes Up-regulation and Aggregation of α-Synuclein in Mice PARAQUAT AND α-SYNUCLEIN*." The Journal of Biological Chemistry **277**: 1641-1644.

[McCarthy et al. 2004] Mccarthy S.; Somayajulu M.; Sikorska M.; Borowy-Borowski H. and Pandey S. (2004). "*Paraquat induces oxidative stress and neuronal cell death; neuroprotection by water-soluble Coenzyme Q10.*" Toxicology and Applied Pharmacology **201** (1): 21–31.

[McCormack et al. 2002] Mccormack A. L.; Thiruchelvam M.; Manning-Bog A. B.; Thiffault C.; Langston J. W.; Cory-Slechta D. A. and Monte D. A. D. (2002). "*Environmental Risk Factors and Parkinson's Disease: Selective Degeneration of Nigral Dopaminergic Neurons Caused by the Herbicide Paraquat*." Neurobiology of Disease **10** (2): 119-127.

[Mirzaei and Regnier 2008] Mirzaei H. and Regnier F. (2008). "*Protein:protein aggregation induced by protein oxidation*." Journal of Chromatography B **873** (1): 8-14.

[Nixon 2013] Nixon R. A. (2013). "*The role of autophagy in neurodegenerative disease*." Nature Medicine **19**: 983–997.

[Patel and Chu 2011] Patel V. P. and Chu C. T. (2011). "*Nuclear transport, oxidative stress, and neurodegeneration*." International Journal of Clinical & Experimental Pathology **4** (3): 215–229.

[Rambaldi et al. 2007] Rambaldi D. C.; Zattoni A.; Casolari S.; Reschiglian P.; Roessner D. and Johann C. (2007). "*An Analytical Method for Size and Shape Characterization of Blood Lipoproteins*." Clinical Chemistry **53** (11): 2026-2029.

[Reschiglian and Moon 2008] Reschiglian P. and Moon M. H. (2008). "*Flow field-flow fractionation: A pre-analytical method for proteomics*." Journal of Proteomics **71** (3): 265–276.

[Reschiglian et al. 2004] Reschiglian P.; Zattoni A.; Cinque L. and Roda B. (2004). "*Hollow-Fiber Flow Field-Flow Fractionation for Whole Bacteria Analysis by Matrix-Assisted Laser Desorption/Ionization Time-of-Flight Mass Spectrometry*." Analytical Chemistry **76** (7): 2103–2111.

[Reschiglian et al. 2011] Reschiglian P.; Zattoni A.; Rambaldi D. C.; Roda A. and Moon M. H. (2011). *Hollow-Fiber Flow Field-Flow Fractionation for Mass Spectrometry: From Proteins to Whole Bacteria*. Detection of Biological Agents for the Prevention of Bioterrorism. Banoub J., Springer Netherlands**:** 13-36.

[Reschiglian et al. 2005] Reschiglian P.; Zattoni A.; Roda B. and Cinque L. (2005). "*On-Line Hollow-Fiber Flow Field-Flow Fractionation-Electrospray Ionization/Time-of-Flight Mass Spectrometry of Intact Proteins*." Analytical Chemistry **77** (1): 47-56.

[Reschiglian et al. 2006] Reschiglian P.; Zattoni A.; Roda B.; Roda A.; Parisi D.; Moon M.-H. and Min B.-R. (2006). "*Hollow-Fiber Flow Field-Flow Fractionation: A Gentle Separation Method for Mass Spectrometry of Native Proteins*." Annali di Chimica **96** (5-6): 253–257.

[Roda et al. 2006] Roda A.; Parisi D.; Guardigli M.; Zattoni A. and Reschiglian P. (2006). "*Combined Approach to the Analysis of Recombinant Protein Drugs Using Hollow-Fiber Flow Field-Flow Fractionation, Mass Spectrometry, and Chemiluminescence Detection*." Analytical Chemistry **78** (4): 1085–1092.

[Rubinsztein et al. 2005] Rubinsztein D. C.; Difiglia M.; Heintz N.; Nixon R. A.; Qin Z. H.; Ravikumar B.; Stefanis L. and Tolkovsky A. (2005). "*Autophagy and its possible roles in nervous system diseases, damage and repair*." Autophagy **1** (1): 11-22.

[Scharf et al. 2013] Scharf B.; Clement C. C.; Yodmuang S.; Urbanska A. M.; Suadicani S. O.; Aphkhazava D.; Thi M. M.; Perino G.; Hardin J. A.; Cobelli N.; Vunjak-Novakovic G. and Santambrogio L. (2013). "*Age-Related Carbonylation of Fibrocartilage Structural Proteins Drives Tissue Degenerative Modification*." Cell Press: Chemistry & Biology **20** (7): 922-934.

[Squier 2001] Squier T. C. (2001). "*Oxidative stress and protein aggregation during biological aging*." Experimental Gerontology **36** (9): 1539–1550.

[Takizawa et al. 2007] Takizawa M.; Komori K.; Tampo Y. and Yonaha M. (2007). "*Paraquat-induced oxidative stress and dysfunction of cellular redox systems including antioxidative defense enzymes glutathione peroxidase and thioredoxin reductase*." Toxicology in Vitro **21** (3): 355–363.

[Valle 2011] Valle L. G. d. (2011). "*Oxidative stress in aging: Theoretical outcomes and clinical evidences in humans*." Biomedicine & Aging Pathology **1** (1): 1-7.

[Yang and Tiffany-Castiglioni 2007] Yang W. and Tiffany-Castiglioni E. (2007). "*The Bipyridyl Herbicide Paraquat Induces Proteasome Dysfunction in Human Neuroblastoma SH-SY5Y Cells*." Journal of Toxicology and Environmental Health, Part A: Current Issues **70** (21): 1849-1857.

4.2.1. NOVEL METHODOLOGY BASED ON HF5 – MALS FOR THE SIZE-SEPARATION, CHARACTERIZATION AND QUANTIFICATION OF OXIDATIVE STRESS-RELATED PROTEIN AGGREGATES LEVELS IN WHOLE CELL LYSATES

STUDY IN COLLABORATION WITH THE PATHOLOGY, IMMUNOLOGY AND MICROBIOLOGY LABORATORY OF A. EINSTEIN COLLEGE OF MEDICINE (YESHIVA UNIVERSITY, NY, USA)

Protein aggregation is a common biological phenomenon, often occurring during pathological conditions, which can induce impaired proteostasis (proteostasis, "*protein*"+"*homeostasis*" is a concept which regards the plethora of competing and integrated biological pathways within cells that control the biogenesis, folding, trafficking and degradation of proteins present within and outside the cell).

An analytical platform, such as HF5-UV-MALS, capable of separating protein aggregates based on their biophysical properties, integrated as a *functional proteomics* methodology, would allow further understanding of the correlation between the protein sequence/structure and their tendency to aggregate, how different post-translational modifications affect unfolding and aggregation and the proteomic machinery associated with aggregates formation and degradation.

In this sub-chapter, a methodology which employs HF5 online coupled with UV and MALS detection was developed for the hydrodynamic *size-based separation*, *characterization* (MW, *rms radius* and molecular conformation) and *quantification* of protein aggregates from complex protein samples. Developed on an experimental model based on a set of *dendritic cells line* (Jaws II) samples, treated with progressively increasing concentrations of the pesticide Paraquat to induce oxidative

stress (and simulate the effects of aging in a short period of time), the HF5-(UV)-MALS method and was then applied on an *in vivo* Paraquat-treated murine model. The presence of high MW aggregates was observed in *spleen* and *brain cells*, as compared to control (non-treated) samples. The aggregates were isolated, characterized and quantified by HF5-(UV)-MALS and fractions were collected for complementary analyses.

Finally, the same HF5-(UV)-MALS method was and applied successfully to oxidative stress-related (damaged) protein aggregates present in aging samples, more in particular, *bone marrow CD34+ precursor cells*. The wide size and MW range of HF5 allowed the separation of highly complex samples (cell lysates) in a single-step analysis and in a relatively short time, therefore employed as the first dimension of separation in a functional proteomics study.

The HF5 method was, therefore, applied successfully to cell lysates containing in *vitro* and *in vivo* oxidative stress-induced aggregates, as well as to cell lysates containing aging-related protein aggregates.

Data processing allowed the analysis of the aggregates amount, absolute MW and size (r_h and *rms radius*). HF5 versatility allowed the samples separation under native conditions, as well as under different degrees of denaturing conditions (2 and/or 4 M Urea).

Offline native PAGE analyses conducted on protein fractions separated by HF5 corroborated the results obtained by HF5-(UV)-MALS: the separation occurred by molecular weight (MW), as well as by hydrodynamic size and the presence of aggregates above 5.0×10^6 Da only was observed only in conditions of oxidative stress.

Offline mass spectrometric (MS) analysis, performed on high MW protein (aggregates) fractions separated by HF5, confirmed the presence of several proteins previously reported to be insoluble or aggregation-prone and allowed the identification of post-translational modifications associated with increased unfolding, aggregation and targeting by proteasome and autophagic/endosomal degradation.

4.2.1.1. INSTRUMENTAL SETUP

All HF5 separations were performed employing an Agilent 1100 HPLC system (Agilent Technologies, Santa Clara, CA, USA) consisting in a degasser, a quaternary pump, an auto sampler and a diode array UV-Vis detector coupled with an Eclipse® DUALTEC™ flow FFF separation system (kindly provided by Superon GmbH, Dernbach, Germany).

The HF5 separation device was a 34 cm long cartridge assembled from two commercial (17 cm long) cartridges connected with a union piece, therefore called "*double length*" HF5 cartridge. Since a longer cartridge was employed successfully for the separation of a standard protein mixture in sub-chapter 4.1.2 (Chapter 2) without any downsides, on the contrary, allowing for a scale-up of the injected amount and complete sample recovery, the "double length" HF5 cartridge was considered the best solution for this study, able to provide enough protein per fraction for subsequent offline electrophoresis, MS analysis and other complementary assays.

The HF5 channel was equipped with a 34 cm long polyether-sulfone (PES) fiber, type FUS 0181 (Microdyn-Nadir, Wiesbaden, Germany) with the following characteristics: 0.8 mm inner diameter, 1.3 mm outer diameter and 10 kDa MWCO, corresponding to an average pore diameter of 5 nm. Its assembly and the modes of operation of the Eclipse® DUALTEC system have already been described in recent literature [Johann et al. 2010].

The ChemStation version B.04.03 (Agilent Technologies) software for Agilent was used to set and control the HPLC components and the software package Wyatt Eclipse @ ChemStation version 4.02 (Wyatt Technology Europe) was used to manage the Eclipse® DUALTEC separation system.

An 18-angle MALS detector model DAWN® EOS™ light scattering detector (provided by Wyatt Technology Corporation, Santa Barbara, CA, USA), employing a

laser operating at a wavelength of 658 nm, was used in all experiments.

An Agilent 1100 UV-Vis diode array detector operating at a wavelength of 280 nm was used as a concentration detector at all times. A second UV signal at 260 nm was registered to assess the DNA presence in the samples.

ASTRA® software version 6.0.6 (Wyatt Technology Corporation) was used to handle signals from the detectors (MALS and UV), for the determination of the molecular weight (MW) of proteins in solution and their size (*rms radius*).

4.2.1.2. SAMPLES

A mixture of native protein markers, NativeMark™ Unstained Protein Standard, (Novex®, Life Technologies™), employed as a sample model, was separated employing a native carrier solution in order to evaluate the performance of the HF5 method under optimal separation conditions.

MICE

C57BL/6J mice (3, 12 and 22 month old) were purchased from Harlam as part of the age-controlled NIH mouse colony program. All animal procedures were carried out according to a protocol approved by the Institutional Animal Care of Albert Einstein College of Medicine.

SAMPLE PREPARATIONS – *performed by the Laboratory of Pathology, Immunology and Microbiology of A. Einstein College of Medicine (Yeshiva University, NY, USA)*

- **BONE MARROW** cells were flushed from the femur and tibia of 3, 12 and 22 months old mice. Cells were centrifuged at 1500 rpm for 10 minutes, and CD34+ bone marrow precursors were purified by magnetic beads immunoselection (Miltenyi Biotec), following the manufacturer's instructions.

After positive immunoselection cells were washed with cold PBS three times and immediately lysed in 1% NP40, 50 mM Tris/HCl, 150 mM NaCl, 5mM EDTA and 10 mM DTT, supplemented with 1X protease inhibitor cocktail for 30 minutes on ice. Lysates were spun at 8,000 rpm and the supernatant collected for total protein determination using Bradford assay (Biorad).

- **SPLEEN** cells were harvested from C57Bl6 mice, and digested for 30 minutes at 37°C with 4000 U/ml of collagenase type II (Invitrogen) in sterile Hanks' balanced saline solution (HBSS) with $Ca2^{+}$ and $Mg2^{+}$ (Life Technologies). Cells were collected through a 70 ◎m sieve, centrifuged at 1500 rpm for 10 minutes and the cell pellet resuspended in red blood cell lysis buffer (8.3 g/L ammonium chloride in 0.01 M Tris-HCl buffer from Sigma, Aldrich). Following 5 minutes incubation at room temperature, complete media was added to stop the lysis reaction and the cells were pelleted at 1500 rpm for 10 min and further processed for HF5 separation or FACS analysis.
- **BRAIN** cells from control and Paraquat-treated mice were harvested and dissected on ice to separate their cortex regions. Upon pooling the cortex regions of three mice they were minced and immediately homogenated in 0.25M sucrose using a motorized homogenator with Teflon pestle (8 strokes at maximal speed). Protein concentration was estimated using Bradford assay (Biorad) and samples were stored frozen until use.

INDUCTION OF OXIDATIVE STRESS AND CELL LYSIS – *performed by the Laboratory of Pathology, Immunology and Microbiology of A. Einstein College of Medicine (Yeshiva University, NY, USA)*

- **IN VITRO**: Jaws II cells (CLR-11904; American Type Culture Collection), a DCs cell line established from C57Bl6 bone marrow were grown in complete media HyClone DMEM/High glucose (Thermo Scientific) supplemented with 10% FBS and 1% Hepes Buffer (Fisher Scientific), MEM Non-essential amino acids,

1mM sodium pyruvate, 10 U/ml penicillin and 100 μg/ml streptomycin all from Sigma. N,N′-dimethyl-4,4′-bipyridinium dichloride (Paraquat, PQ) was used to induce oxidative stress.

Three final concentrations of the drug, 0.25 mM, 5 mM and 10 mM were used. Control cells remained untreated. Twenty million cells for each condition were incubated at 37°C and 5% CO_2 for 6 hours, then collected, centrifuged at 1500 rmp for 5 minutes and washed twice with sterile PBS. Pellets were lysed in 150 mM Nacl, 50 mM Tris-HCl, 1% nonidet p-40 , 10 mM DTT, 5 mM EDTA supplemented with 1X of protease inhibitor cocktail (Sigma, St. Louis) and Bradford assay was performed to determine protein concentrations against a standard curve. The total carbonyl content from total cell lysates and from each HF5 collected fraction was determined spectrophotometrically with the OxiSelect Protein Carbonyl Spectrophotometric Assay kit (Cell Biolabs, CA). The absorbance of the DNPH-derivatized carbonyl groups was read at 375 nm. Results were normalized to the amount of total protein in each sample fraction.

- **IN VIVO**: Oxidative stress was induced in C57BL/6 mice by i.p injection with PQ-saline solution (2.5mg/25g body weight) on two consecutive days. Twenty four hours prior to the experiment, animals were fasted to minimize the potential background. Before imaging all animals were intravenously injected with Cell-ROX Deep Red (2.5mM, excitation 640 nm/emission 664 nm, Molecular Probes, CA) for *in vivo* fluorescent imaging using the IVIS (In-Vivo F PRO imaging system (Bruker BioSpin Molecular Imaging, CT) system. Whole animals were imaged 30 minutes post injection and images were captured at an excitation 610 nm/emission 700 nm using a built-in cooled closed-caption device camera. Images were threshold with respect to background intensity and different levels of fluorescence intensity were displayed using pseudo rainbow color scheme analyzed using built-in Carestream Molecular Imaging Software.

4.2.1.3. MATERIALS AND METHODS

REAGENTS

Trifluoroacetic acid, acetonitrile, acetic acid, formic acid, iodacetamide and methanol were purchased from Fisher Scientific (Pittsburgh, PA). Urea, thiourea, octylglucoside, dithiothreitol (DTT), iodoacetamide, ammonium bicarbonate, Coomassie Brilliant Blue R-250, KCl, KH_2PO4, H_3PO4 and Na_2CO_3 were purchased from SIGMA (St. Louis, MO, USA). Complete Proteinase inhibitor cocktail was also purchased from Sigma. Porcine trypsin (20 μg, specific activity > 5,000 units/mg seq. grade modified) and Lys-C (sequencing grade, 10μg) were purchased from Promega (Madison, WI).

Tris-HCl 1M and pH 8.0 was supplied by Teknova, while NaCl and urea were supplied by Sigma. All carrier solutions employed during this study were prepared using MilliQ water purified by an Elix 3 UV Water Purification System (Millipore, Billerica, USA) and filtered through 0.2 μm pore membrane sterile filter units (Steritop™, Millipore).

HF5 METHOD

Lysates were run in either *native* carrier solution buffer (50 mM Tris-HCl supplemented with 150 mM NaCl and proteases inhibitors, pH 7.4) or *denaturing* carrier solution, with a composition similar to the cells lysis buffer (50 mM Tris-HCl, supplemented with 150 mM NaCl, 2 or 4 M urea and proteases inhibitors, pH 8.0).

Cell lysates were injected during the focusing step, performed at 0.5 mL/min of focus flow rate for 5 minutes, after which each sample was eluted at 0.5 mL/min of longitudinal flow rate under a field gradient decreasing from 0.4 mL/min to 0.1 mL/min over 70 minutes.

Protein fractions were collected after HF5 separation. Samples separated under the

same conditions (either native or denaturing) and using the same flow rates were pooled (3-5 runs) for further analysis. To remove the high salt concentration (NaCl and urea), the fractions were dialyzed overnight against 10 mM Tris-Cl solution at pH 8.0 using Side – a – lyzer® cassettes (MWCO: 3500 Da, 3 – 15 mL, Pierce) or Snake Skin pleated dialysis tubing (MWCO: 3500 Da, capacity of 3.7 mL/cm, Pierce) for larger volumes. All fractions were lyophilized immediately after the dialysis was completed.

ASTRA® COMPUTATIONS

The Astra® software (version 6.0.6, Wyatt Technology Corporation) was used to calculate the MW ranges for all lysate samples. The light scattering intensity registered by detectors 2 through 18 and the concentration signal from the UV detector (280 nm) were correlated through a 1st degree Zimm model, thus providing the MW values. An average value of 1.0 (mL/mg×cm) for the extinction coefficient at 280 nm ($\varepsilon_{280nm}^{0.1\%}$) was used in all MW calculations. The ExPASy ProtParam free bioinformatics tool (http://www.expasy.org/) was used to compute the specific $\varepsilon_{280nm}^{0.1\%}$ for all protein standards in the mixture (Novex®, Life Technologies™), used as a model sample.

The angular dependency of the scattered light was correlated through a 1st degree Zimm model, thus providing the *rms radius* values. The sample recovery, as well as the protein aggregates amounts, calculated as % of the total protein amount in the lysates, were also quantified by Astra.

Astra software was also employed to determine the molecular conformation of the protein aggregates. The correlation plots (conformation plots) were generated from experimental data, by plotting the *rms radius* values against the corresponding MW values (both in logarithmic scale). The plots were fitted linearly and the slope values were assigned to known conformation types. A slope value of 1.0 corresponds to a *rod* conformation, a slope value of 0.5 – 0.6 corresponds to a *random coil* conformation and a slope value of 0.33 corresponds to a *sphere* conformation. The trend (slope

and/or change of the slope) of the molecular conformations was determined for *rms radius* values above 10 nm (due to DAWN EOS® instrumental range limitation), with corresponding MW values usually above 1×10^6 g/mol.

HYDRODYNAMIC RADIUS (r_H) CALCULATIONS

The Eclipse ISIS simulation software (Superon GmbH, Germany) was employed to predict the retention time (t_R), hydrodynamic radius (r_H) and diffusion coefficient (D) of each native marker in the mixture (Novex®, Life Technologies™), by inputting the HF5 method flow rates and the known MW values (declared by the manufacturer).
The same software was employed for the calculation of the r_H range for each cell lysate (reported in each graph as a secondary x axis), but based on the experimental t_R values instead of the ones predicted from the MW values.
The viscosity values for the carrier solutions were extrapolated from data found in literature [Kawahara and Tanford 1966] ($\eta_{water,25°C} = 10^{-3}$ N·s/m^2 for Tris-HCl buffer; 1.0909× $\eta_{water,25°C}$ for Tris-HCl + 2M urea and 1.2215× $\eta_{water,25°C}$ for Tris-HCl + 4M urea).

PROTEIN CARBONYL SPECTROPHOTOMETRIC ASSAY – *performed by the Laboratory of Pathology, Immunology and Microbiology of A. Einstein College of Medicine (Yeshiva University, NY, USA)*

The quantification of the protein carbonyl modifications was performed using the OxiSelect™ Protein Carbonyl Spectrophotometric Assay Kit supplied by Cell Biolabs, Inc. First, the protein carbonyls in BSA standards (1-10 mg/mL) were derivatized with DNPH. When DNPH reacts with protein carbonyls, the amount of protein-hydrozone produced can also be measured spectrophotometrically at 375 nm. Proteins were then precipitated following the TCA (trichloroacetic acid) precipitation protocol and free DNPH was removed by washing the protein pellet. After dissolving the protein pellet in GuHCl, the absorbance of protein-hydrozone was measured at 375 nm, and the protein carbonyl was calculated.

ELECTROPHORESIS – *performed by the Laboratory of Pathology, Immunology and Microbiology of A. Einstein College of Medicine (Yeshiva University, NY, USA)*

- **SDS-PAGE** was performed on whole cells lysates (before fractionation) in order to determine qualitatively the presence of HMW protein aggregates. Each cell lysate sample, containing approximately 20 μg of protein (previously quantified by BCA assay) were diluted in the recommended sample buffer 62.5 mM Tris-Cl, pH 6.8, 2% SDS, 25% glycerol, 0.01 % bromphenol blue), supplemented with 2-mercaptoethanol and incubated for 5 min at 110°C. After the protein denaturation was completed, a sample volume of 15μL was loaded in each well of a Mini-PROTEAN® TGX™ Gel (4 -15%), supplied by BioRad and recommended for the MW range of 20–250 kD.

  The electrophoretic run was performed in the recommended Tris/Glycine/SDS running buffer (25 mM Tris, 192 mM glycine, 0.1% SDS, pH 8.3) and was considered complete after approximately 1.5 hours. The gel was re-equilibrated in water for 5 min and stained employing the Pierce Color Silver Stain Kit (supplied by Pierce), following the manufacturer's instructions.

- **NATIVE PAGE.** The HF5 fractions were desalted by dialysis and concentrated by lyophilization. After lyophilization the powdered proteins were resuspended in a total volume of 100 μL of Milli-Q water. Aliquots of 25 μL of samples, either diluted in water or not, were further resuspended in a precast Native PAGE Sample Buffer (4X) and Cathode Buffer Additive (Invitrogen) and loaded in a NativePAGE™ Novex® Bis-Tris Gel System (3%-12%) supplied by Invitrogen and recommended in the MW range from 30 to 10.000 kDa. The same protein amount was loaded in each gel, based on previous protein quantification by BCA assay.

  The run was performed at 150 Volts for 110 minutes following the supplier's instructions. After the run was completed, the gel was re-equilibrated in water

for 5 min and stained employing the Pierce Color Silver Stain Kit (supplied by Pierce), following the manufacturer's instructions.

FPLC SIZE-EXCLUSION CHROMATOGRAPHY – *performed by the Laboratory of Pathology, Immunology and Microbiology of A. Einstein College of Medicine (Yeshiva University, NY, USA)*

An amount of 800 μg of total cell lysate, from untreated and Paraquat-treated samples, was loaded on a Superdex 200 column (HiLoad 16/60, prep grade, GE Healthcare Life Sciences) operated by a Biorad Biologic Duo Flow medium-pressure chromatographic system. PBS or 50 mM Tris-Cl were used as mobile phase, eluted at an isocratic flow rate of 1/mL minute. Protein elution was monitored at 280 nm.

FACS ANALYSIS – *performed by the Laboratory of Pathology, Immunology and Microbiology of A. Einstein College of Medicine (Yeshiva University, NY, USA)*

C57Bl6 spleen cells were harvested from control and PQ-treated mice, previously injected with Cell-ROX Deep Red. Spleens were digested for 30 minutes at 37°C with collagenase (4000 U/ml collagenase type II from Invitrogen) in sterile Hanks' balanced saline solution (HBSS) with Ca2+ and Mg2+ (Life Technologies). Cells were then collected using a 70 mm sieve, centrifuged at 1500 rpm for 10 minutes and the cell pellet resuspended in red blood cells lysis buffer for 5 min at RT (Sigma). Cells were then washed at 1500 rpm for 10 minutes and the pellet resuspended in FACS buffer (PBS supplemented with 4% FBS and 0.2% sodium azide). The following FITC labeled antibody were used for staining: CD3, CD19, CD11b, CD11c and GR-1 (Pharmingen). Finally, cells were analyzed by flow cytometry (Becton Dickinson, N.J, USA)

.

PROTEOMIC ANALYSIS OF HF5 PURIFIED AGGREGATES - *performed by the Laboratory of Pathology, Immunology and Microbiology of A. Einstein College of Medicine (Yeshiva University, NY, USA)*

Protein aggregates purified by HF5 (with the highest MW) were incubated in 0.1 M ammonium bicarbonate buffer with 4M urea and sonicated for 15 minutes at RT. The samples were further reduced with 10 mM TCEP-HCl in 0.1 M ammonium bicarbonate buffer, pH 8.9, for 30 minutes, at RT. The reduction was followed immediately by alkylation with 55 mM iodacetamide solution in 0.1 M ammonium bicarbonate, at RT, in the dark for 45 minutes.

Proteins were digested with trypsin and Lys-C (sequencing grade, Promega) at 37°C for 12 hours. Following digestion, the samples were subjected to desalting using ZipTip (C18) reversed-phase system (Millipore, Billerica, MA) and submitted for MS/MS peptide sequencing.

LTQ-MS/MS sequencing was performed using a Nanospray LC-MS/MS on a LTQ linear ion trap mass spectrometer (LTQ Thermo Scientific, San Jose, CA, USA) interfaced with a TriVersa NanoMate nanoelectrospray ion source (Advion BioSciences, Ithaca, NY, USA). The 15 most abundant ions were selected for MS/MS. Raw data files were converted to .mgf files using Proteome Discoverer 1.3 (Thermo Fisher Scientific).

All .mgf files were searched against the house mouse (*Mus musculus*; 16,230 sequences) in SwissProt 57.15 (515,203 total sequences; 181,334,896 total residues) using Mascot, in-house, (Matrix Science, London, UK; version 2.3.02). The following parameters were used for all searches: trypsin; 1 missed cleavage; fixed modification of carbamidomethylation (for Cys) and variable modifications: deamidation (Asn and Gln), oxidation (Met, Pro, Lys, Arg); monoisotopic masses: peptide precursor mass tolerance of 1.5 Da; and product ion mass tolerance of 0.5 Da.

A false discovery rate (FDR) for peptide identification was assessed by decoy database searching and was finally adjusted to less than 1.0% for proteins and peptides. Proteins were considered identified having at least one bold red (BR) significant peptide with an ion score cut-off of 40 or greater (corresponding to $p \leq 0.05$ and a FDR proteins ≤1.0%).

PATHWAYS ANALYSIS – *performed by the Laboratory of Pathology, Immunology and Microbiology of A. Einstein College of Medicine (Yeshiva University, NY, USA)*

The putative interactions among the identified proteins in the high MW aggregates, fractionated from 3 and 22 months old spleen and bone marrow, were analyzed using the functional networks interactive pathways analysis (IPA). The ArrayTrack™ **(**http://www.fda.gov**)** bioinformatics tool from the FDA web site was used to generate the heat map corresponding to the major up- and down-regulated pathways by importing the -log (p) values associated with each pathway as provided by IPA analysis.

4.2.1.4. RESULTS AND DISCUSSION

A. NATIVE PROTEINS MIXTURE

The developed HF5 method was simulated first, employing the ISIS simulation software (Superon GmbH), on a native proteins mixture (NativeMark™ Unstained Protein Standard, Novex®, Life Technologies™) used as a sample model, to check the correlations between retention time (t_R), hydrodynamic size (r_h), diffusion coefficient (D) and MW under ideal separation conditions (Figure 1).

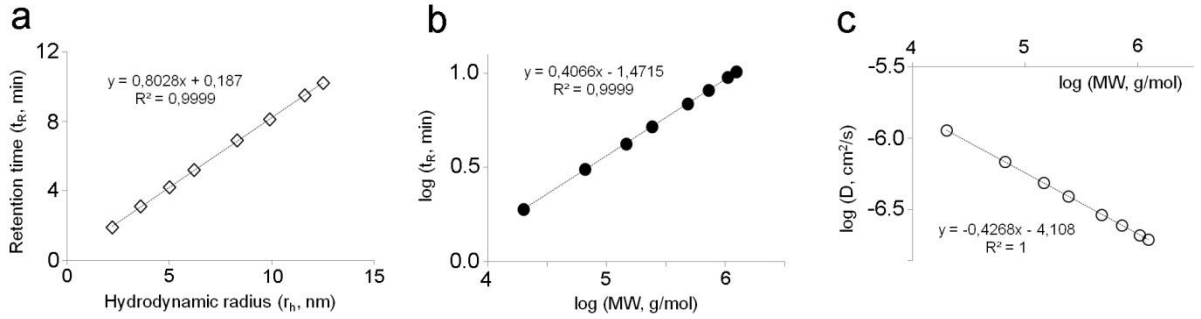

Figure 1 – Native markers: (a) relationship between hydrodynamic radius and retention time; (b) relationship between MW and retention time and (c) relationship between MW and D.

The Eclipse ISIS simulation software was employed to predict the (theoretical) t_R, r_H and D of each native marker, by inputting the HF5 method flow rates and the known MW values (declared by Life Technologies™ in the product sheet). Figure 1a shows how the protein size influences the t_R, therefore how the separation occurs according to size. Figure 1b shows how the protein MW influences the t_R, therefore how the separation occurs according to MW.

The slope of this plot (0.4) represents the value of parameter b, reported in *Equation 14* (sub-chapter 2.2.2 of Chapter 2). A slope value of 0.4 indicates molecular conformations between *hard sphere* (0.33) and *random coil* (0.5-0.6). Figure 1c shows how the diffusion coefficient, D (which determines the size, shape and surface

properties of proteins) is correlated to the proteins MW. The mathematical expression which represents *D* as a function of MW is reported in *Equation 14.*

In FPLC-UV or SEC-UV, the MW value of an unknown protein/protein aggregate in a complex sample like a cell lysate, is determined by interpolation using the *calibration curve,* which is built by plotting known MWs of standard proteins against their experimental retention time (t_R). This procedure assumes constant molecular conformations, usually globular (rigid sphere). The same approximation was made by the ISIS simulation software. Since the MW value assignment is based on a specific t_R, a slight change in the latter may lead to erroneous MW assignments, making this procedure faulty.

Indeed, when the HF5 method was applied experimentally to the same native markers mixture, discrepancies between the theoretical (Figure 1a) and experimental t_R (Figure 2) were observed, most likely caused by proteins shape deviation from rigid sphere (globular conformation), especially at high MW values.

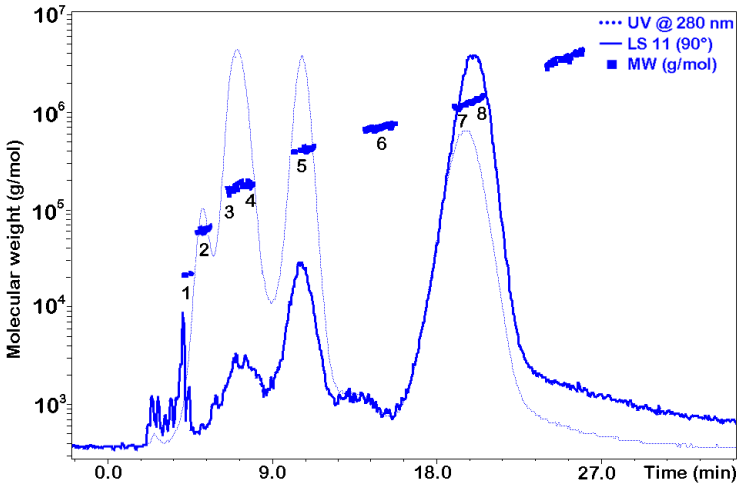

Figure 2 – HF5-UV-MALS separation profile of the standard protein mixture. The peak assignment was based on the absolute MW values computed by Astra®

Shifts in the t_R are very likely due to molecular conformational changes (like the ones caused by carbonylation of proteins side-chains, under the effect of oxidative stress or by protein denaturation, under the effect of urea), but also by specific/non-specific

interactions between the lysate components and the column matrix in FPLC and SEC. On the other hand, the MW determined by multi-angle light scattering (MALS) measurements is *absolute* (does not require calibration with molecular standard, nor makes approximations on the shape of the protein).

Based on differences in hydrodynamic size, proteins with the same MW may have different t_R, indicating molecular conformation differences. Indeed, the native proteins MW values derived from MALS measurements matched the ones declared by the manufacturer (Life Technologies™), even though there was a discrepancy between the experimental (Figure 2) and the predicted t_R values (Figure 1a).

The peaks were identified based on the absolute MW values, as follows: (1) soybean trypsin inhibitor, 20 kDa; (2) bovine serum albumin, 66 kDa; (3) lactate dehydrogenase, 146 kDa; (4) β-phycoerythrin, 242 kDa; (5) apoferritin band 1, 480 kDa; (6) apoferritin band 2, 720 kDa; (7) IgM pentamer, 1048 kDa and (8) IgM hexamer, 1236 kDa.

Given these satisfactory results, the next step consisted in applying the HF5-(UV)-MALS method to the cell lysate samples.

B. HF5-UV-MALS OF PROTEIN AGGREGATES GENERATED *IN VITRO*

To evaluate the capabilities of HF5 to separate over a wide MW range of proteins and complex protein aggregates, as present in a total cell lysate, an experimental culture of control cells and cells treated with different concentrations of Paraquat was setup. Paraquat is known to induce oxidative stress, a condition known to induce protein (irreversible) damage and promote protein aggregation. The Paraquat – induced oxidative stress is known to lead to the oxidation of the proteins side chains and the most frequent consequences are the carbonyl modifications, therefore considered markers of oxidative stress.

The Carbonyl spectrophotometric assay was performed on total cell lysates in order to determine the extent of the carbonyl modifications suffered upon Paraquat treatment, therefore to validate the efficacy of the Paraquat treatment and the results are reported in Figure 3a. The same samples were run on SDS-PAGE and the gel is reported in Figure 3b.

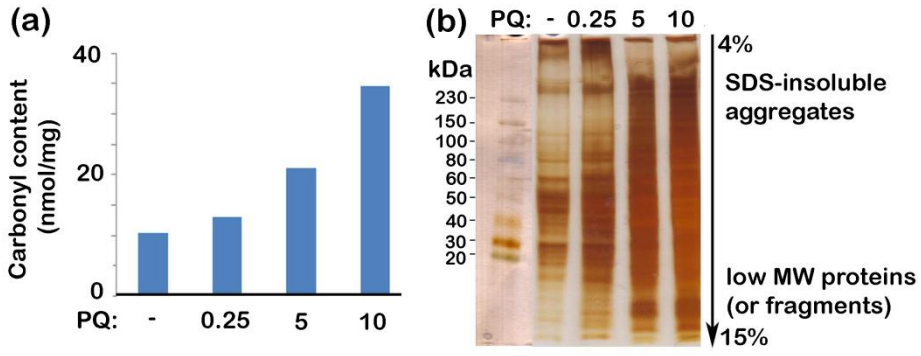

Figure 3 – Tests performed on whole cell lysates, following in vitro treatment with Paraquat: (a) protein carbonyl assay and (b) Silver staining of an SDS-PAGE. *Performed and kindly provided by the Laboratory of Pathology, Immunology and Microbiology of A. Einstein College of Medicine (Yeshiva University, NY, USA)*

Figure 3a demonstrates the efficacy of the Paraquat treatment, since an increased amount of total protein carbonylation was observed, directly proportional to the

molarities of Paraquat treatment. Figure 3b shows an increased amount of SDS-insoluble aggregates, as compared to untreated cells, also proportional to the amount of Paraquat added to the cell cultures. Moreover, Figure 3b shows an increased amount of low MW proteins/fragments in the Paraquat-treated cells, associated with oxidative cleavage.

Analysis of the samples by gel filtration (FPLC) employing a Superdex S 200 column confirmed high MW aggregates in the PQ treated samples, as well as presence of low MW cleavage products (Figure 4). However, the very high MW aggregates (MW > $1x10^6$ Da) did elute in the void volume with the dextran blue (MW = $2x10^6$ g/mol). Running the samples on a Sephadex column with increased porosity (S300) did not separate with enough resolution aggregates above $2x10^6$ g/mol (data not shown).

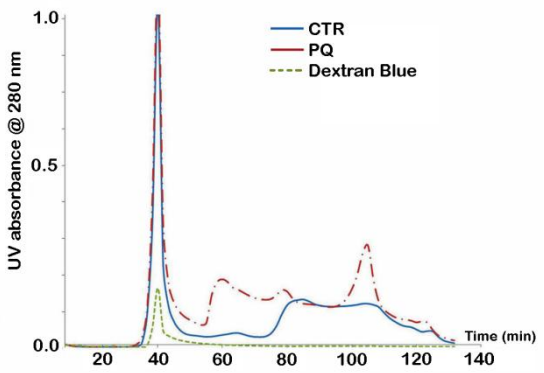

Figure 4 – FPLC separation profile at 280 nm of protein lysates from control cells and cells treated with 5 mM Paraquat. Dextran blue 2×106 MW elutes with the void volume. *Performed and kindly provided by the Laboratory of Pathology, Immunology and Microbiology of A. Einstein College of Medicine (Yeshiva University, NY, USA)*

Next, control and Paraquat-treated cell lysates were separated by HF5 under native conditions and the elution profiles, as well as the corresponding MW ranges are reported in Figure 5a. Figure 5a also reports the elution of the native protein markers (the same as reported in Figure 1) and the elution of Blue Dextran (MW: 2000 kDa). The *rms radius* ranges, derived from the MALS measurements and computed by Astra® are reported in Figure 5b.

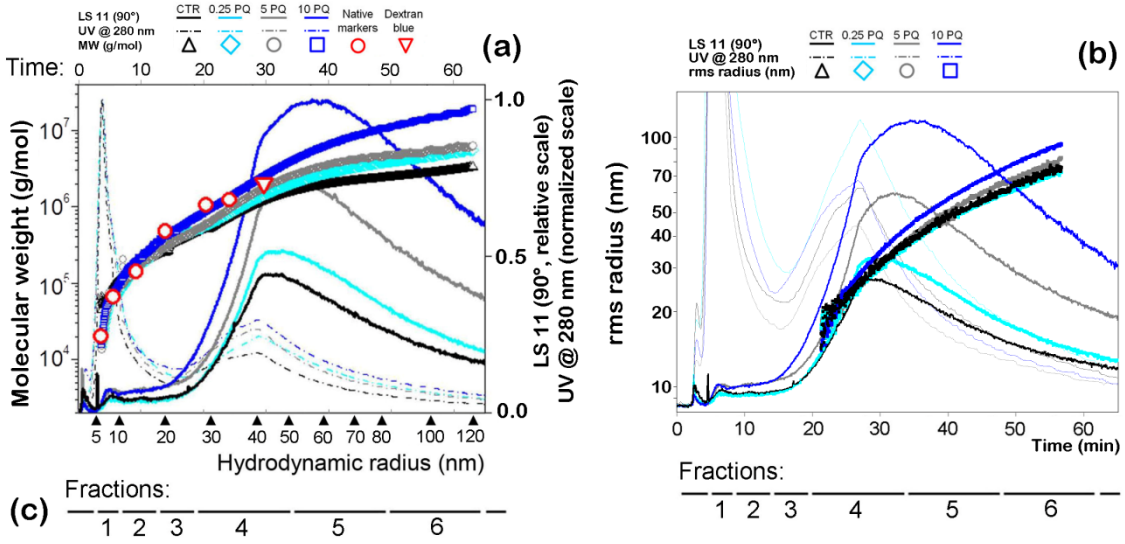

Figure 5 – HF5-UV-MALS elution profiles of the control and Paraquat-treated cell lysates, separated under native conditions, reporting: (a) MW range calculated by Astra; (b) *rms radius* range calculated by Astra and (c) lysate fractions collected for further characterization

Increased protein aggregation and the presence of HMW aggregates could be observed in Paraquat-treated samples, as compared to the untreated cells. All samples contain a common MW range of proteins and protein aggregates with MWs up to 3.3×10^6 g/mol. All Paraquat treated samples also show the presence of HMWs which are not present in the control sample, reported in Figure 5a and 6a. An increase in the protein aggregates upper MW limit with increasing Paraquat molarity is also observed in Figure 6a and the exact values are reported in Table 1.

Aggregates of the same MW value showed reduced r_H and *rms radius* values in the Paraquat treated samples when compared to the control, suggesting changes in the aggregate molecular conformation following carbonylation.

Conformational differences among the aggregates in the control and the treated samples were observed in the correlation plot reported in Figure 6b, obtained by plotting the log (*rms radius*) against the corresponding log (MW) values. The molecular conformation state (sphere, random coil or rod) was assigned based on the slope value of the correlation plot, as described in the Astra® Computations sub-section of Materials and Methods.

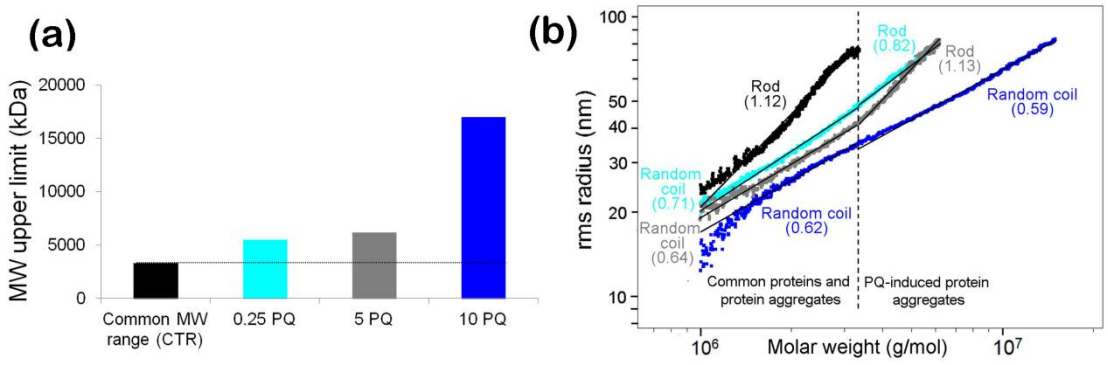

Figure 6 – Control and Paraquat treated samples (a) MW ranges of the Paraquat-treated samples compared to the control and (b) conformation plots, the number below the assigned molecular conformation represents the slope derived from experimental data

Figure 6b shows the conformation trend of the protein aggregates present in the Jaws II cell lysate samples separated under native conditions and how the increase in the Paraquat concentration progressively modifies the overall conformation trend of the protein aggregates.

The Paraquat treatment had two distinct effects on the proteins/protein aggregates and their HF5 elution behavior in native carrier solution:

(A) Conformation /shape effect: this led to observing different slope values in the correlation plot for the samples under examination. The protein aggregates are more compact in the treated samples and their compactness increases with the Paraquat concentration. Consequently, proteins aggregates with the same MW value have progressively anticipated retention times in the Paraquat-treated samples;

(B) Density effect: at equal MW value, protein aggregates in the treated samples have smaller *rms radii* compared to the control sample and the *rms radius* decreases with the Paraquat concentration. A smaller *rms radius* indicates that the scattering points are found closer to the mass center, leading to the same MW being concentrated in a smaller space. This implies that aggregates with the same MW have higher densities in the treated samples.

Moreover, the Paraquat has an overall effect on the elution behavior of all aggregates present in the treated samples, therefore even on aggregates whose formation was not mediated by the Paraquat treatment with MWs between 1.0×10^6 and 3.3×10^6 Da. It

is very likely that the Paraquat led to the carbonylation of the side chains causing a conformational change, but did not lead to further aggregation. The amount of the Paraquat – induced protein aggregates shows an increase with the Paraquat concentration and the values are reported in Table 1, along with the corresponding MW ranges and the elution times.

The next step consisted in determining whether HF5 runs employing a denaturing carrier solution could help establish the biophysical properties of the protein aggregates. Lysates from control sample and sample treated with the highest amount of Paraquat (10 mM) were separated under mild denaturing conditions (2 M urea) and the elution profiles, as well as the corresponding MW ranges are reported in Figure 7a. The *rms radius* ranges, derived from the MALS measurements and computed by Astra® are reported in Figure 7b.

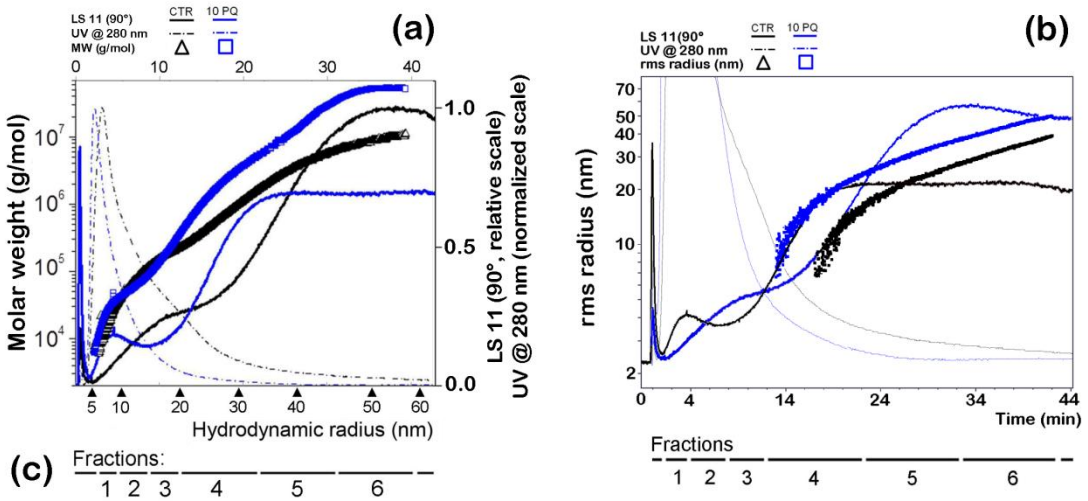

Figure 7 – HF5-UV-MALS elution profiles of the control and Paraquat-treated cell lysates, separated under denaturing conditions (2 M urea), reporting: (a) molecular weight range calculated by Astra; (b) *rms radius* range calculated by Astra and (c) lysate fractions collected for further characterization

Analysis of the r_H and *rms radius* showed that protein aggregates with the same MW eluted at different t_R, suggesting a reduced hydrodynamic size (for the aggregates with anticipated t_R). Moreover, aggregates with the same MW had similar *rms radius* values, even though eluted at different t_R. The results are reported in Table 2.

A drastic decrease in the percentage of the Paraquat-induced protein aggregates was observed (approximately 92%), indicating that many of the aggregates observed under native conditions are non-covalent. Nonetheless, Paraquat-induced aggregates representing 1.9% of the whole lysate, are present in the sample under denaturing condition (Table 1), therefore urea-resistant.

Indeed, at low concentration (2M) urea acts by disrupting the hydrogen bonds in the protein secondary structure thus disrupting non-covalent aggregates. As expected under denaturing conditions, the presence of new protein aggregates with MW above 1.7×10^7 g/mol, was also observed (Figure 7a, Tables 1 and 2).

Table 1 – Separation of Jaws II cell lysates under native and denaturing conditions

Jaws II cell lysates				
Native conditions – Figure 5a				
Sample	**CTR**	**0.25 mM PQ**	**5 mM PQ**	**10 mM PQ**
Common MW range (g/mol)	1.5×10^4 – 3.3×10^6			
Hydrodynamic radius range (nm)	2 – 115	2 – 74	2 – 61	2 – 45
MW range of Paraquat – induced aggregates (g/mol)	-	3.3×10^6 5.5×10^6	3.3×10^6 6.2×10^6	3.3×10^6 1.7×10^7
Hydrodynamic radius range (nm) of Paraquat – induced aggregates	-	74 – 115	61 – 115	45 – 115
Amount of Paraquat – induced aggregates	-	**12.5%**	**17.9%**	**25.1%**
Denaturing conditions – Figure 7a				
Sample	**CTR**		**10 PQ**	
Common MW range (g/mol)	1.5×10^4 – 3.3×10^6			
Hydrodynamic radius range (nm)	2 – 30		2 – 22	
MW range of Paraquat – induced aggregates (g/mol)	-		3.3×10^6 – 1.7×10^7	
Hydrodynamic radius range (nm) of Paraquat – induced aggregates	-		22 – 37	
Amount of Paraquat – induced aggregates	-		**1.9%**	
MW range of new aggregates (denaturing conditions)	3.3×10^6 – 1.7×10^7		1.7×10^7 – 4.3×10^7	
Hydrodynamic radius range (nm) of new aggregates	30 – 58		37 – 58	
Amount of new aggregates (denaturing conditions)	**8%**		**0.9%**	

The detailed fraction-by-fraction characterization by HF5-UV-MALS, containing the MW ranges, *rms radius* and hydrodynamic radius (r_H) ranges for each lysate fraction reported in Figures 5c (native) and 7c (denaturing), is reported in Table 2.

Table 2 - Fractions of Jaws II cell lysates separated under native and denaturing conditions. MW, rms radius and hydrodynamic radius (r_h) ranges.

Jaws II cell lysates fractions						
MW range (g/mol) – Figure 5a, fractions: Figure 5c						
Fractions	1	2	3	4	5	6
Control	4.4×10^4 1.5×10^5	1.5×10^5 2.8×10^5	2.8×10^5 6.5×10^5	6.5×10^5 2.2×10^6	2.2×10^6 3.0×10^6	3.0×10^6 3.3×10^6
r_h range (nm)	5 – 10	10 – 18	18 – 26	26 – 48	48 – 76	76 – 115
Treated (10PQ)	1.6×10^4 1.6×10^5	1.6×10^5 4.8×10^5	4.8×10^5 1.2×10^6	1.2×10^6 7.2×10^6	7.2×10^6 1.7×10^7	1.7×10^7 1.7×10^7
r_h range (nm)	5 – 10	10 – 18	18 – 26	26 – 48	48 – 76	76 – 115
Rms radius range (nm) – Figure 5b, fractions below figure						
Fractions	1	2	3	4	5	6
Control	N/A	N/A	N/A	20.9 – 46.6	46.6 – 71.0	71.0 – 108.6
Treated (10PQ)	N/A	N/A	N/A	18.0 – 52.6	52.6 – 88.5	88.5 – 126.4
MW range (g/mol) – Figure 7a, fractions: Figure 7c						
Fractions	1	2	3	4	5	6
Control	7.1×10^3 3.4×10^4	3.4×10^4 1.4×10^5	1.4×10^5 3.1×10^5	3.1×10^5 3.1×10^6	3.1×10^6 3.3×10^6	
New aggregates (denaturing conditions)					3.3×10^6 9.1×10^6	9.1×10^6 1.7×10^7
r_h range (nm)	5 – 8	8 – 14	14 – 19	19 – 32	32 – 43	43 – 58
Treated (10PQ)	6.2×10^3 3.9×10^4	3.9×10^4 1.2×10^5	1.2×10^5 6.8×10^5	6.8×10^5 1.0×10^7	1.0×10^7 1.7×10^7	
New aggregates (denaturing conditions)					1.7×10^7 3.9×10^7	3.9×10^7 4.3×10^7
r_h range (nm)	5 – 8	8 – 14	14 – 19	19 – 32	32 – 43	43 – 58
Rms radius range (nm) – Figure 7b, fractions below figure						
Fractions	1	2	3	**4**	**5**	**6**
Control	N/A	N/A	N/A	N/A	16.0 – 27.6	
New aggregates (denaturing conditions)					16.2 – 27.6	27.6 – 38.9
Treated (10PQ)	N/A	N/A	N/A	7.5 – 23.6	23.6 – 26.1	
New aggregates (denaturing conditions)					26.1 – 36.8	36.8 – 49.9

Under native conditions, the size of the aggregates progressively decreased as the Paraquat molarity increased. Moreover, under both denaturing and non denaturing conditions, aggregates of the same MW showed reduced r_H and *rms radius* values in the Paraquat treated samples when compared to the control, suggesting molecular conformation changes induced by the Paraquat treatment.

Figure 8 reports the correlation plots for the Jaws II cell lysates samples during the separation in denaturing buffer; the change in the slope value indicating the different molecular conformation trends, suggests overall modified conformations caused by the Paraquat treatment.

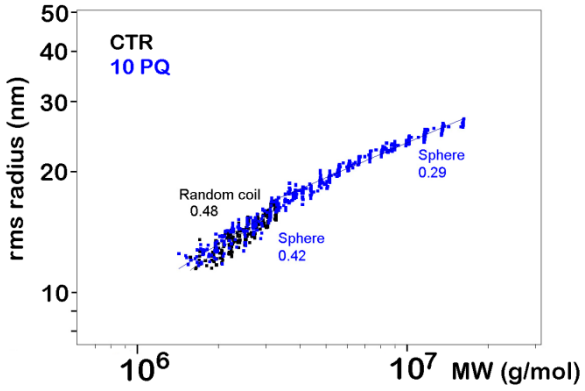

Figure 8 – Conformation plots of control and Paraquat treated sample separated under denaturing conditions (2 M urea); the number below the assigned molecular conformation represents the slope derived from experimental data

When separated under mild denaturing conditions, the aggregates in both control and treated samples tend to become more compact when compared to native conditions: their *rms radius* values decrease drastically (Table 2). Both samples contain protein aggregates with *random-coil* conformations in the common MW range (1.0×10^6 – 3.3×10^6 Da). In correspondence of the Paraquat-induced covalent aggregates (MWs above 3.3×10^6 Da), we observe a slope change towards even more compact, *sphere*-like, molecular conformations.

To confirm the suitability of the HF5 method to separate protein aggregates of different MWs, protein fractions were collected from control and Paraquat-treated

samples separated under native conditions (Figure 5c) and run on a native gel. The results are reported in Figure 9.

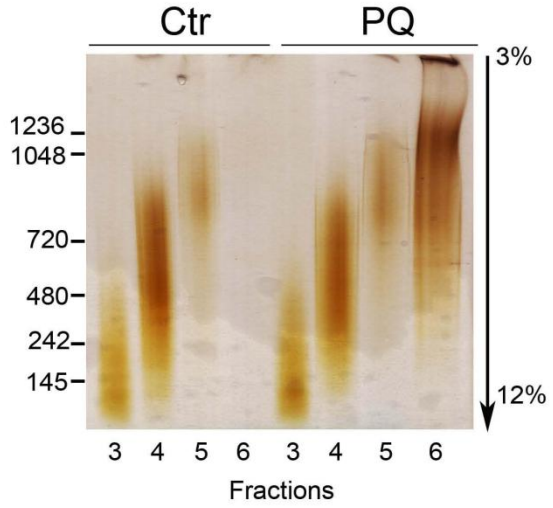

Figure 9 – Native-PAGE performed on the HF5 fractions form control and Paraquat-treated lysate samples. The fractions were dialyzed and lyophilized prior to electrophoresis. *Performed and kindly provided by the Laboratory of Pathology, Immunology and Microbiology of A. Einstein College of Medicine (Yeshiva University, NY, USA)*

The gel confirmed protein separation by HF5, detected as the increment in MW in progressive fractions from $1x10^5$ to over $2.5x10^6$. Additionally, fraction 6 collected after the elution of dextran blue ($2x10^6$ Da) indicated the presence of protein aggregates in the Paraquat-treated cells, but not control ones (Table 2).

Altogether, the results confirm the capability of HF5 to separate proteins and protein aggregates according to their MW, as well as hydrodynamic size, from a complex mixture of proteins as present in total cell lysate.

C. HF5-UV-MALS OF PROTEIN AGGREGATES GENERATED *IN VIVO*

Next, the HF5 capabilities were evaluated during the separation of protein aggregates formed *in vivo* and in primary cells, during conditions of increased oxidative stress. To this goal, mice were injected intraperitoneally with Paraquat (2.5mg/25g body weight) for two consecutive days. On day three mice were injected intravenously with the CellRox probe that fluoresces upon binding to reactive oxygen species and the results are displayed in Figure 10.

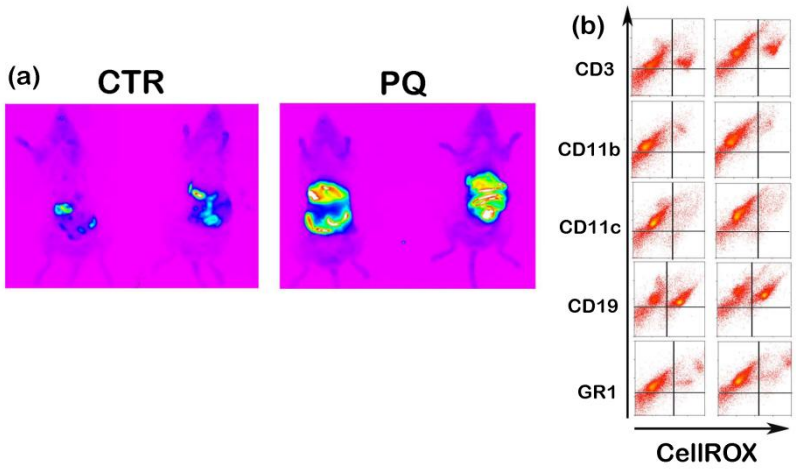

Figure 10 – (a) In vivo Detection of Oxidative Stress in control (CTR) and Paraquat (PQ) treated mice. The i*n vivo* detection of fluorescence was performed using the *In-Vivo* Imaging System FX PRO (Carestream); (b) FACS analysis of spleen cell subpopulations isolated *ex vivo*, following CellROX injection. *Performed and kindly provided by the Laboratory of Pathology, Immunology and Microbiology of A. Einstein College of Medicine (Yeshiva University, NY, USA)*

Increased fluorescence was observed in parenchyma organs in Paraquat-treated mice (Figure 10a). Similarly, increased ROS-generated fluorescence was also observed on *ex vivo* purified spleen cell subpopulations, as analyzed by FACS and reported in Figure 10b.

Next, total spleen lysates from control and Paraquat treated mice were run by HF5 and the elution profiles, as well as the corresponding MW ranges are reported in Figure 11.

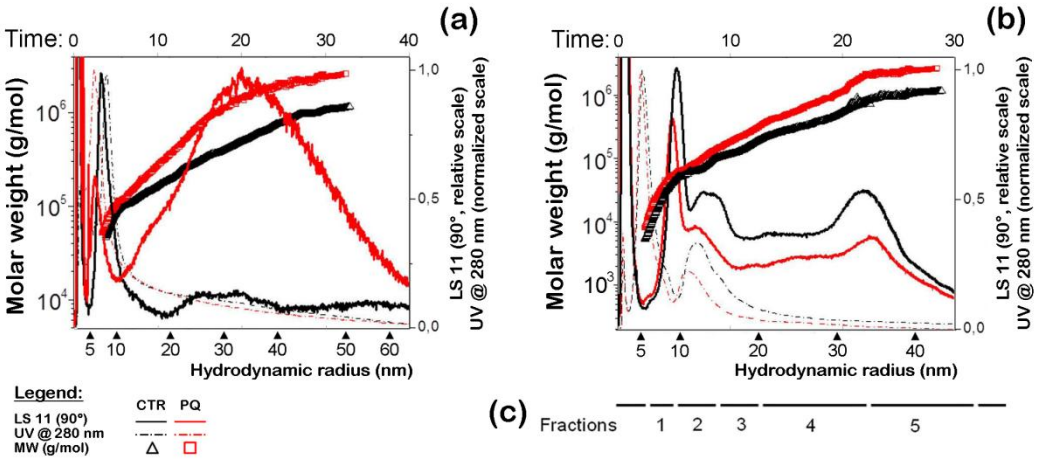

Figure 11 – HF5-UV-MALS elution profiles of the control and Paraquat-treated spleen cell lysates, separated under (a) native conditions and (b) denaturing conditions (2 M urea), both reporting the molecular weight range calculated by Astra, and (c) lysate fractions collected for further characterization

When separated under native conditions, both control and Paraquat-treated spleen cell lysate samples show a common MW range of proteins and protein aggregates, with MWs up to 1.2×10^6 g/mol. However, the treated sample also shows the presence of protein aggregates that are not present in the control sample (Figure 11a). The Paraquat–induced aggregates amounted to 21.4% of the total protein lysates of the treated sample, as reported in Table 3.

The biophysical nature of the Paraquat-induced aggregates was investigated further, by separating the same samples under mild denaturing conditions (2 M urea). The HMWs observed only in the treated sample were still present (Figure 11b), but their amount decreased significantly.

As reported previously for the *in vitro* Paraquat-induced aggregates (Table 1), the results indicate that most Paraquat-induced aggregates (approximately 74%) are non-covalent. The aggregates amounts along with the corresponding MW ranges and the elution times are reported in Table 3.

Once again, upon Paraquat treatment, aggregates having the same MW value showed reduced r_H values when compared to the control sample suggesting more compact aggregates following protein carbonylation. This observation is valid for separations under native and mild denaturing conditions.

Table 3 – Separation of spleen cell lysates (control and treated sample) under native and denaturing conditions

Native conditions – Figure 11a		
Sample	**CTR**	**PQ**
Common MW range (g/mol)	$5.0\times10^5 – 1.2\times10^6$	
Hydrodynamic radius range (nm)	2 – 55	2 – 23
MW range of Paraquat – induced aggregates (g/mol)	-	$1.2\times10^6 – 2.6\times10^6$
Hydrodynamic radius range (nm) of Paraquat – induced aggregates	-	23 – 55
Amount of Paraquat – induced aggregates	-	**21.4%**
Denaturing conditions – Figure 11b		
Sample	**CTR**	**PQ**
Common MW range (g/mol)	$5.0\times10^5 – 1.2\times10^6$	
Hydrodynamic radius range (nm)	2 – 40	2 – 26
MW range of Paraquat – induced aggregates (g/mol)	-	$1.2\times10^6 – 2.6\times10^6$
Hydrodynamic radius range (nm) of Paraquat – induced aggregates	-	26 – 40
Amount of Paraquat – induced aggregates	-	**5.5%**

Importantly, the quantification of protein carbonylation, as a measure of oxidative stress, showed an increase in the amount of carbonyl groups in each fraction of the Paraquat-treated cell lysate separated by HF5 (Figure 11c), but most predominantly in the high MW fractions of the spleen cell lysate. The results are reported in Figure 12.

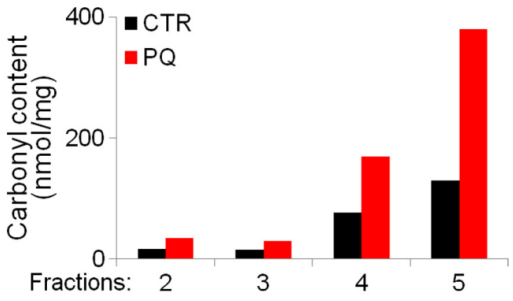

Figure 12 – Protein carbonyl assay performed of different fractions, collected from control and Paraquat spleen samples (Figure 11c). *Performed and kindly provided by the Laboratory of Pathology, Immunology and Microbiology of A. Einstein College of Medicine (Yeshiva University, NY, USA)*

Next, brain lysates from control and Paraquat-treated mice were analyzed by HF5-(UV)-MALS. Their elution profiles, as well as corresponding MW ranges are reported in Figure 13a (native) and 13b (denaturing, 2M urea). The *rms radius* ranges, derived from the MALS measurements and computed by Astra® are reported in Figure 13b.

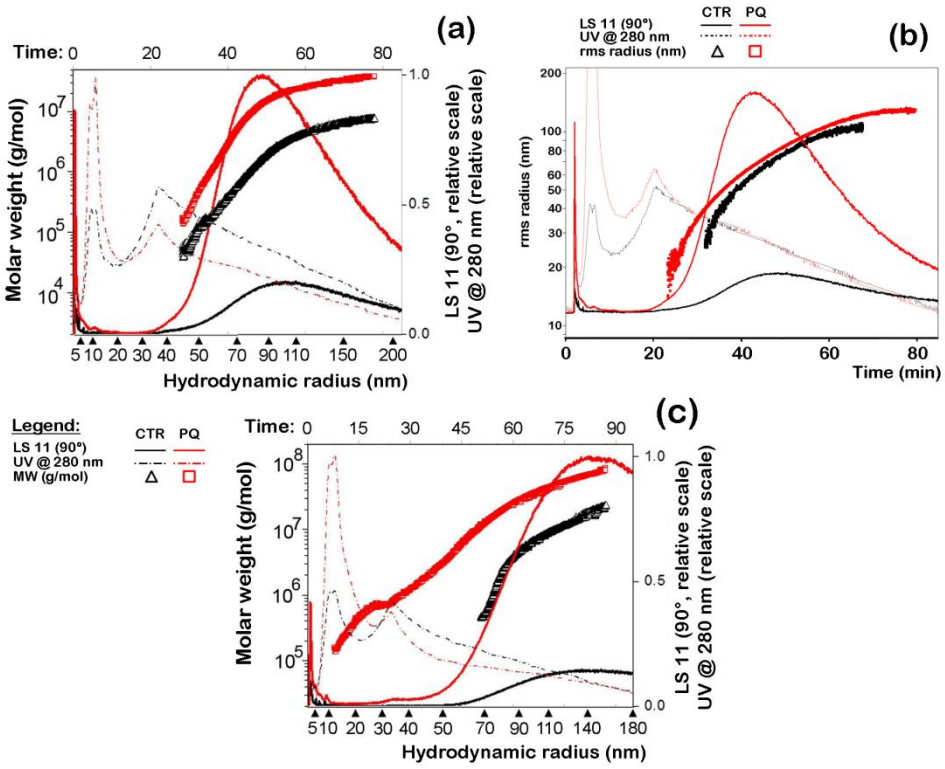

Figure 13 – HF5-UV-MALS elution profiles of the control and Paraquat-treated brain cell lysates, (a) separated under native conditions, reporting the MW ranges calculated by Astra and (b) *rms radius* ranges calculated by Astra and (c) separated under denaturing conditions (2 M urea), reporting MW ranges calculated by Astra

A common MW range of proteins and protein aggregates, with MWs up to 7.5×10^6 g/mol is observed for both control and treated sample, reported in Table 4. Once again, the brain sample from Paraquat-treated mice showed the presence of high MW aggregates, with MW above 7.5×10^6 g/mol, which were not detected in the control sample (Figure 13a). These aggregates amounted to up to the 26.1% of total proteins in the treated sample, reported in Table 4.

Table 4 – Separation of brain cell lysates (control and treated sample) under native and denaturing conditions

Native conditions – Figure 13a		
Sample	**CTR**	**PQ**
Common MW range (g/mol)	$1.0\times10^5 – 7.5\times10^6$	
Hydrodynamic radius range (nm)	4 – 203	4 – 100
MW range of Paraquat – induced aggregates (g/mol)	-	$7.5\times10^6 – 3.9\times10^7$
Hydrodynamic radius range (nm) of Paraquat – induced aggregates	-	100 – 200
Amount of Paraquat – induced aggregates	-	**26.1%**
Denaturing conditions – Figure 13c		
Sample	**CTR**	**PQ**
Common MW range (g/mol)	$1.0\times10^5 – 7.5\times10^6$	
Hydrodynamic radius range (nm)	0 – 116	0 – 68
MW range of Paraquat – induced aggregates (g/mol)	-	$7.5\times10^6 – 3.9\times10^7$
Hydrodynamic radius range (nm) of Paraquat – induced aggregates	-	68 – 115
Amount of Paraquat – induced aggregates	-	**14.8%**
MW range of new aggregates (denaturing conditions)	$7.5\times10^6 – 2.0\times10^7$	$3.9\times10^7 – 8.0\times10^7$
Hydrodynamic radius range (nm) of new aggregates	116 – 177	115 – 177
Amount of new aggregates (denaturing conditions)	12%	10%

Once again, upon Paraquat treatment, aggregates having the same MW value showed reduced r_H values (anticipated t_R) when compared to the control sample, suggesting more compact aggregates following protein carbonylation. Figure 13b shows a broad size range of proteins and protein aggregates for both lysates (control and treated sample) and, once again, at equal MW, the aggregates in the treated sample show reduced *rms radius*.

However, the Paraquat-induced aggregates, eluting from 31.5 to 55 min, are larger than previously observed in the control sample, arriving up to 120 nm of rms radius. These findings support the protein molecular conformational changes caused by carbonylation, already reported for the Jaws II cell lysates (Figures 6b and 8).

Once the samples were separated under denaturing conditions (4 M urea, Figure 13c), a decrease in their amount was observed, but less significantly of what observed in the spleen samples (Table 3), indicating that most Paraquat-induced aggregates in the brain samples are covalent (urea-resistant). As expected, under denaturing conditions, the presence of new protein aggregates was also observed and reported in Table 4

Altogether the data indicate MW and size-based HF5 separation of protein aggregates formed *in vivo* in primary cells. Additionally, it indicates that the majority of proteins modified by carbonylation, a post-translational modification typically observed in condition of oxidative stress, are predominantly observed in the HMW fractions.

D. HF5-UV-MALS OF AGING – RELATED PROTEIN AGGREGATES

The increasing protein tendency to aggregate with aging is a generally acknowledged fact. Indeed, increased amounts of protein post-translational modifications including glycation, carbonylation and lipoxidation in aging bone marrow lysates were previously reported by [Cannizzo et al. 2011, Cannizzo et al. 2012]. These modifications are normally associated with increased protein aggregation.

Thus, as next step we set to determine whether the proposed methodology could be successfully applied to protein aggregates as occurring in aging bone marrow precursors cell. $CD34^+$ cells were purified from the total bone marrow of 3, 12 and 22 months old mice and the lysates were run on an SDS-PAGE to confirm presence of protein aggregation. The results are reported in Figure 14 (Figure 4a). Indeed, a progressively increased amount of high MW aggregates was observed with aging.

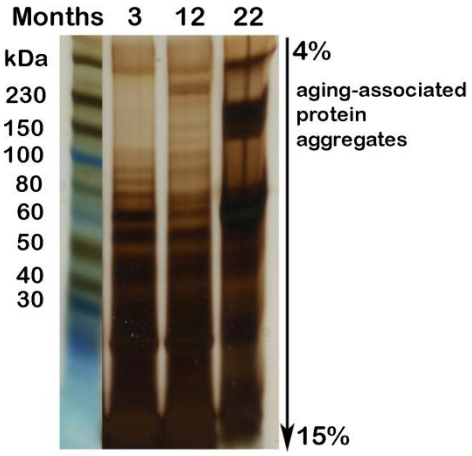

Figure 14 - Silver staining of an SDS-PAGE gel of total bone marrow cell lysate from 3, 12 and 22 months old mice. *Performed and kindly provided by the Laboratory of Pathology, Immunology and Microbiology of A. Einstein College of Medicine (Yeshiva University, NY, USA)*

Next, the same lysates were separated and characterized by HF5-(UV)-MALS using either native or denaturing carrier solutions. The elution profiles, as well as corresponding MW ranges are reported in Figure 15.

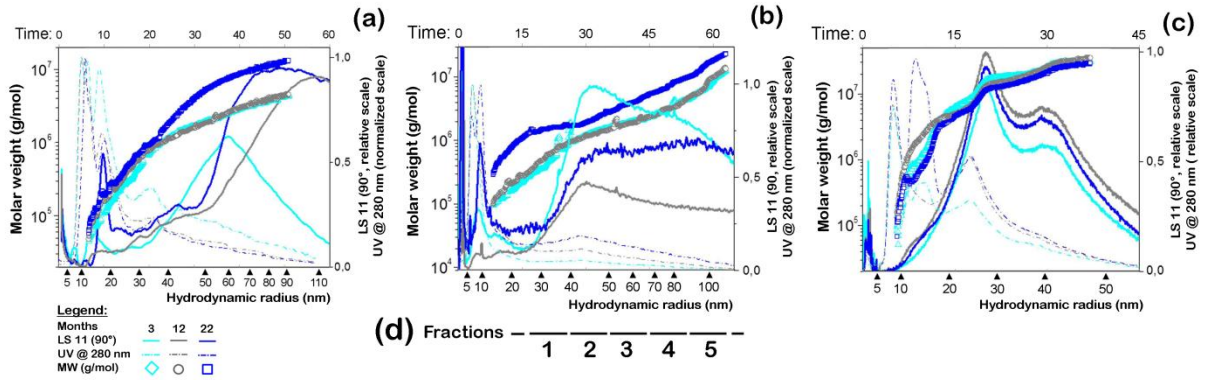

Figure 15 – HF5-UV-MALS elution profiles of bone marrow cell lysates from aging samples (mice of 3, 12 and 22 months), reporting the MW ranges calculated by Astra separated under: (a) native conditions, (b) mild denaturing conditions, 2 M urea and (c) denaturing conditions, 4 M urea; (d) protein fractions collected for further characterization.

Figure 15a shows that all three aging samples contained a common MW range of proteins and protein aggregates with MWs up to 4.4×10^6 g/mol, reported in Table 5. Additionally, the 22 months old bone marrow cell lysate also contained higher MWs that were not present in the samples from 3 and 12 months old mice, representing approximately 15.9% of the 22 months sample (Table 5).

Next, the samples were fractionated under denaturing conditions (2M and 4 M urea). Figures 15b and 15c show that the majority of aging-related protein aggregates, observed under native conditions, were still present in the 22 months sample. Indeed, their amount decreased only slightly as the urea concentration increased, indicating that many of the age-related aggregates presented covalent bonds (Table 5).

Importantly, aggregates, with the same MW, but collected from different ages, eluted at different retention times due to differences in the hydrodynamic sizes (r_h), also reported in Table 5. These r_h differences, between protein aggregates with the same MW value (but of different age), are due to changes in the aggregate molecular conformation, as previously reported for the Paraquat-treated cell lysates (Figure 6b and Figure 8). As expected under denaturing conditions, the formation of new aggregates was observed and reported in Table 5.

The *rms radius* ranges, derived from the MALS measurements and computed by Astra® are reported in Figure 16a; whereas Figure 16b reports the conformation trends of the covalent aggregates present in bone marrow cell lysates from aging samples (mice of 3, 12 and 22 months)

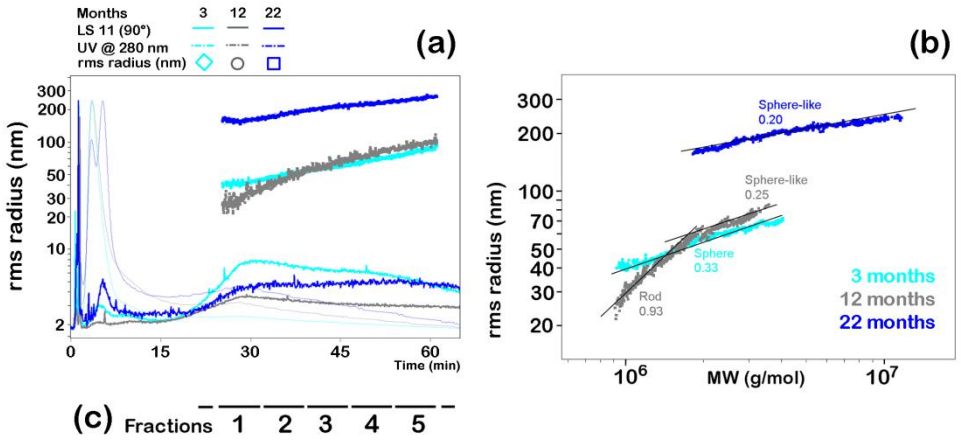

Figure 16 – HF5-UV-MALS elution profiles of the bone marrow aging (mice of 3, 12 and 22 months) cell lysates separated under mild denaturing conditions (2 M urea), reporting the (b) *rms radius* ranges calculated by Astra and (b) conformation plots; the number below the assigned molecular conformation represents the slope derived from experimental data

Table 5 – Separation of bone marrow cell lysates (3, 12 and 22 months under native and denaturing conditions

Bone marrow cell lysates			
Native conditions – Figure 15a			
Sample	**3 months**	**12 months**	**22 months**
Common MW range (g/mol)	$5.0\times10^4 – 4.4\times10^6$		
Hydrodynamic radius range (nm)	3 – 111	3 – 111	3 – 53
MW range of aging – induced aggregates (g/mol)	-	-	$4.4\times10^6 – 1.3\times10^7$
Hydrodynamic radius range (nm) of aging – induced aggregates	-	-	53 – 111
Amount of aging – induced aggregates	-	-	**15.9%**
Mild denaturing conditions (2 M urea) – Figure 15b			
Sample	**3 months**	**12 months**	**22 months**
Common MW range (g/mol)	$1.0\times10^5 – 4.4\times10^6$		
Hydrodynamic radius range (nm)	4 – 90	4 – 89	4 – 66
MW range of aging – induced aggregates (g/mol)	-	-	$4.4\times10^6 – 1.3\times10^7$
Hydrodynamic radius range (nm) of aging – induced aggregates	-	-	66 – 97
Amount of aging – induced aggregates	-	-	**11.5%**
MW range of new aggregates (denaturing conditions)	$4.4\times10^6 – 1.2\times10^7$	$4.4\times10^6 – 1.2\times10^7$	$1.3\times10^7 – 2.1\times10^7$
Hydrodynamic radius range (nm) of new aggregates	90 – 113	89 – 113	97 – 113
Amount of new aggregates (denaturing conditions)	**2%**	**3%**	**12%**
Denaturing conditions (4 M urea) – Figure 15c			
Sample	**3 months**	**12 months**	**22 months**
Common MW range (g/mol)	$1.0\times10^5 – 4.4\times10^6$		
Hydrodynamic radius range (nm)	3 – 7	3 – 7	3 – 9
MW range of aging – induced aggregates (g/mol)	-	-	$4.4\times10^6 – 1.3\times10^7$
Hydrodynamic radius range (nm) of aging – induced aggregates	-	-	9 – 18
Amount of aging – induced aggregates	-	-	**11%**
MW range of new aggregates (denaturing conditions)	$4.4\times10^6 – 3.0\times10^7$	$4.4\times10^6 – 3.0\times10^7$	$4.4\times10^6 – 1.5\times10^7$
Hydrodynamic radius range (nm) of new aggregates	7 – 51	7 – 51	18 – 51
Amount of new aggregates (denaturing conditions)	49%	56%	7%

Figure 16a shows the presence of very large protein aggregates in the 22 months sample that are not present in the younger ones. Figure 16b shows the differences in the conformation trends, indicated by the slope values and how the overall molecular conformations change due to modifications (mostly carbonylation, but also lipoxidation and glycation) caused by oxidative stress during the aging process. Indeed, the aging-related protein aggregates in the 22 months sample presented sphere-like, highly compact conformations, whereas aggregates found in younger bone marrow present a relaxed rod-like conformation (Figure 4e).

Additionally, the correlation plot reported in Figure 16b indicates different compactness degrees: the younger samples (3 and 12 months) show a very small *rms radius* increase over time, suggesting protein aggregates of very high density when compared to the oldest sample (22 months).
Moreover, correlating Figures 16a and 16b, is shown that the age-related aggregates that are present only in the oldest sample not only have higher MW values (as reported in Table 5), but have a much larger size and a more compact conformation when compared to the non age-related aggregates.

Analysis of the r_H and *rms radius* showed how protein aggregates with the same MW eluted at different t_R, suggesting a reduced hydrodynamic size for the aggregates with anticipated t_R, as already reported for other cell lysate samples. The detailed fraction-by-fraction characterization by HF5-UV-MALS, containing the MW ranges, *rms radius* and hydrodynamic radius (r_H) ranges for each lysate fraction depicted in Figures 15d and 16c is reported in Table 6.

Table 6 – Fractions of aging bone marrow cell lysates (3, 12 and 22 months old mice) separated under native and denaturing conditions. MW, rms radius and hydrodynamic radius (r_h) ranges.

Bone marrow cell lysates separated under mild denaturing conditions (2 M urea)						
Fractions		**1**	**2**	**3**	**4**	**5**
Hydrodynamic radius range (nm)		27 – 41	41 – 52	52 – 69	69 – 91	91 – 116
Mass fraction	**3 months**	8.3%	8.9%	6.1%	3.8%	1.7%
	12 months	11.4%	12.0%	8.2%	5.2%	2.5%
	22 months	12.1%	15.0%	11.5%	7.8%	4.5%
MW range (g/mol)	**3 months**	2.322×10^5 7.902×10^5	7.902×10^5 1.434×10^6	1.434×10^6 2.139×10^6	2.139×10^6 4.033×10^6	4.033×10^6 1.194×10^7
	12 months	2.722×10^5 8.655×10^5	8.655×10^5 1.321×10^6	1.321×10^6 2.323×10^6	2.323×10^6 4.129×10^6	4.129×10^6 1.244×10^7
	22 months	1.254×10^6 1.568×10^6	1.568×10^6 2.454×10^6	2.454×10^6 4.640×10^6	4.640×10^6 9.033×10^6	9.033×10^6 2.103×10^7
***Rms radius* range (nm)**	**3 months**	N/A	41.6 – 47.4	47.4 – 58.5	58.5 – 71.9	71.9 – 94.4
	12 months	N/A	26.2 – 41.6	41.6 – 67.8	67.8 – 84.5	84.5 – 99.2
	22 months	N/A	155.9 – 171.4	171.4 – 208.7	208.7 – 232.1	232.1 – 264.8

Altogether the data demonstrate that H5F-MALS can separate age-related aggregates from total cell lysates and characterize their MW, hydrodynamic radius and conformation.

E. Mass Spectrometric analysis of aging-related protein aggregates.

performed by the Laboratory of Pathology, Immunology and Microbiology of A. Einstein College of Medicine (Yeshiva University, NY, USA)

It has been recently reported that, during physiological aging, several hundred proteins tend to become more insoluble and aggregate (metastable proteins). Proteomic analysis of these proteins identified communality in biochemical and biological properties, including amino acids primary sequence, increased beta-sheets and grouping in specific biological pathways [Cannizzo et al. 2012].

To determine whether HF5-purified protein aggregates shared similarities with what was previously published, samples collected from the highest molecular weight fractions were digested using a combination of Lys-C and trypsin in 0.1 M bicarbonate buffer and 4M urea and peptide fragments analyzed by mass

spectrometry (Table 7).

In total bone marrow and spleen samples, 65% and 55% respectively of the proteins found in the high MW aggregate (MW>10^7) corresponded to proteins known to increase their tendency to aggregate in aging. Among those, several enzymes, histones and signaling molecules were found and reported in Figure 17 and Table 7.

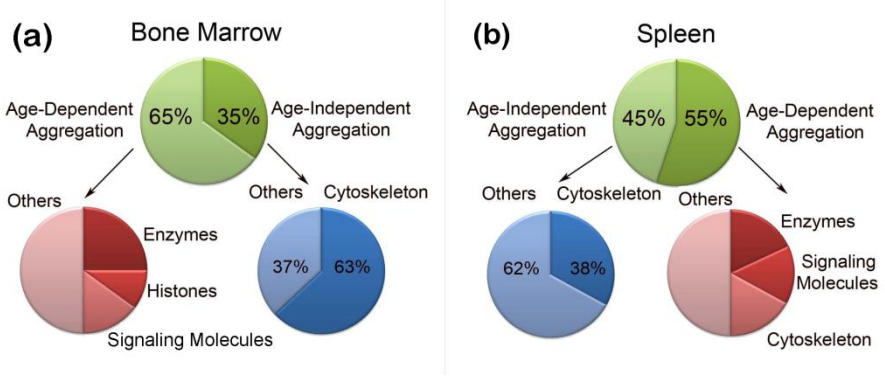

Figure 17 – (a) Pie charts of the aggregate proteome from 3 and 22 months old total bone marrow; b) Pie charts of the aggregate proteome from 3 and 22 months old spleen lysate. Proteins were identified by mass spectrometry and analyzed by scaffold analysis. *Kindly provided by the Laboratory of Pathology, Immunology and Microbiology of A. Einstein College of Medicine (Yeshiva University, NY, USA)*

The other 35% and 45% (bone marrow and spleen respectively) were proteins known to have a tendency to aggregate and being insoluble regardless the aging process. This category comprised several matrix proteins and cytoskeleton proteins.

Ingenuity pathway analysis of the urea collected high MW aggregates (MW>10^7) indicated grouping into few major pathways including cell growth, cellular respiration, metabolism, cytoskeleton and mobility and oxidative stress (Figure 18b).

Figure 18a shows the proteins distribution in the CD34+ bone marrow cell lysates aggregates from 3, 12, 22 months old mice. 171 proteins common proteins were identified for all three ages, several common proteins for each pair (3 – 12; 3 – 22 and 12 – 22 months), as well as age-specific proteins (13 proteins for the 3 months old, 14 for the 12 months old and 2 proteins for the 22 months old mice).

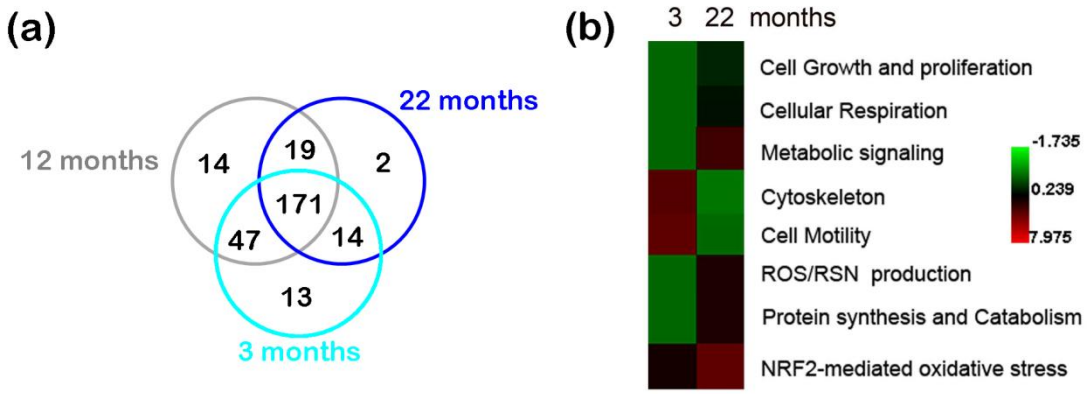

Figure 18 – (a) Scaffold analysis for proteins distribution in the CD34+ bone marrow cell lysates aggregates and (b) heat map of the major functional pathways represented in the aggregate proteome fractionated from bone marrow cells collected from 3, and 22 months old mice. *Kindly provided by the Laboratory of Pathology, Immunology and Microbiology of A. Einstein College of Medicine (Yeshiva University, NY, USA*

Table 7 – Mass spectrometry analysis of protein aggregates in bone marrow and spleen cell lysates.

Bone marrow			
Identified Proteins	**Accession Number**	**3months**	**22 months**
Protein Kinase A anchor protein	gi|6753026	26%	38%
Aldehyde dehydrogenase II	gi|191804	0	41%
B-cell scaffold protein 1	gi|110835719	29%	0
Beta actin	gi|4501885	100%	100%
Protein kinase 2, beta	gi|148687716	28%	40%
Cathepsin C	gi|45219895	0	91%
Cathepsin G	gi|6681083	0	100%
Collagen IV alpha-2	gi|556299	86%	90%
Peroxidase	gi|145966840	100%	100%
Ribonuclease A family, member 6	gi|21426871	0	91%
Ferritin light chain 1	gi|114326466	0	98%
Fibrillin 1	gi|118197277	100%	91%
Fibronectin 1	gi|148667849	99%	100%
High mobility group 1 protein	gi|600761	0	100
High mobility group protein B2	gi|11527222	0	47%
Histone 1, H1e	gi|13430890	86%	100%
Inhibitor of CDK interacting with cyclin A1	gi|47523979	0	38%
Myeloperoxidase	gi|226823250	0	91%

Rotamase	gi|118091	0	45%
Plectin-1	gi|122065897	55%	53%
Potassium voltage-gated channel A4	gi|3023498	0	35%
Cystatin-related protein 1	gi|82886009	0	41%
Collagen IV alpha 1	gi|148690109	86%	91%
Collagen XIX alpha 1	gi|111600306	0	53%
Prosaposin	gi|1381582	0	0
Protease, serine, 1	gi|16716569	78%	89%
Protein kinase C, beta 1	gi|148685332	0	44%
Proteoglycan 2	gi|6679457	98%	98%
Calgranulin B	gi|6677837	86%	100%
THAP domain containing 11	gi|10946934	0	37%
WD repeat domain 42A	gi|148707088	0	41%
Spleen			
Identified Proteins	**Accession Number**	**3 months**	**22 months**
Actin, gamma, cytoplasmic 1	gi|123298587	100%	100%
AHNAK nucleoprotein isoform 1	gi|61743961	100%	100%
Annexin A1	gi|124517663	86%	78%
Beta tubulin	gi|12846758	0	78%
Proteoglycan 2	gi|6679457	100%	100%
Collagen XIX, alpha 1	gi|111600306	65%	66%
Cytochrome P450	gi|148666702	31%	25%
DEAD box polypeptide 50	gi|60551791	0	0
Dpep1 protein	gi|13097534	0	34%
Peroxidase	gi|145966840	100%	100%
Ribonuclease A family, member 6	gi|21426871	0	78%
Fca/m receptor	gi|11071950	0	20%
Fibronectin 1	gi|148667849	97%	100%
Hist1h3e protein	gi|119850953	33%	24%
Igh-1 a protein similar	gi|1334091	0	100%
Major vault protein	gi|13879460	100%	100%
Myosin light chain kinase	gi|126157499	33%	0
Myosin-9 isoform	gi|114326446	100%	100%
Proline rich 12	gi|153791304	0	20%
Protein kinase C, beta 1	gi|148685332	0	18%

Myeloperoxidase	gi|129826	0	100%
P(4,5)P2 3-kinase alpha	gi|1171954	0	30%
Plectin-1	gi|122065897	39%	40%
Ribosomal L15 60S	gi|12846287	98%	97%
Ribosomal protein L27 60S	gi|6708474	79%	78%
Spastin isoform 1	gi|244790106	0	20%
Protein marked in red are equally expressed in aggregates from 3 and 22 months old mice			

4.2.1.5. CONCLUSIONS

The work presented in this chapter showed the importance of developing a methodology that allows separation of protein aggregates based on their size and biophysical properties, providing insight on the different type of aggregates. Further analyses on the isolated protein aggregates may provide insight upon their formation and disposal under different stress conditions, altogether furthering our knowledge on the mechanisms controlling cellular proteostasis.

Field-flow fractionation (FFF) and its miniaturized variant (HF5) was previously employed successfully for the separation of serum proteins including IgGs, albumin, hemoglobin and phospholipids in high-density and low-density lipoproteins from human plasma [Reschiglian et al. 2003, Kang and Moon 2006, Zattoni et al. 2007].
Herein, by online coupling HF5 and MALS we were able to separate for the first time protein aggregates, based on their size, molecular weight and biophysical properties, from a total cell lysate [Reschiglian et al. 2004, Reschiglian et al. 2006, Reschiglian et al. 2013]. Data processing allowed analysis of the aggregates amount, molecular weight and size (r_H and *rms radius*). Samples were run under non denaturing conditions using PBS or Tris-Buffer and under different degrees of denaturing conditions (2 and/or 4 M Urea). Further analysis of the collected fractions on native

gels confirmed separation by molecular weight and the presence of aggregates above 5.0×10^6 Da only in conditions of oxidative stress.

Additionally, proteomic analysis performed on the highest molecular weight aggregates (MW>10^7) confirmed the presence of several proteins previously reported to be insoluble or with increased tendency to aggregate during aging. The proteomic analysis on the purified aggregates presented here confirmed the presence of an aggregate proteome which share several proteins previously reported to be associated with age-related aggregation [David et al. 2010].

Altogether, several information could be gathered by HF5 purification that would have not be possible to obtain with traditional methods employed to separate protein aggregates, including filter assay, ultracentrifugation, agarose gels and size-exclusion chromatography (FPLC).

Firstly, and more importantly, we determined that HF5 does indeed separate proteins and protein aggregates over a wide range of sizes and molecular weights from complex protein mixtures such as the total cell lysates proteome, in a single step analysis.

Secondly, we observed how protein aggregates of the same MW eluted at different t_R because of different hydrodynamic sizes, which directly relate to their molecular conformation. Indeed, HF5-MALS online coupling allowed the determination of the molecular conformation of all protein aggregates, and showed that the oxidative stress-induced ones had a more compact conformation, following the protein modifications (carbonylation) caused by either Paraquat treatment or by the aging process. Thirdly, the ability to separate lysates under both physiological and denaturing conditions allowed establishing the biophysical nature of the aggregates. Schiff-base covalent bound protein aggregates that could not be disrupted by high molar urea were discriminated from the aggregates that were purely based on hydrophobic or electrostatic interactions and hydrogen bonds. In this respect, it is important to notice that samples obtained from mice, where oxidative stress was

induced for a short period of time, protein aggregates were indeed formed, but were readily solubilized in urea. However, we were able to report the percentages of the two types of oxidative stress-related aggregates. On the other hand, lysates from aging bone marrow presented high MW aggregates, as compared to the same specimens from younger mice, which could be fractionated in non-denaturing conditions and were poorly solubilized in high molar urea. This data indicates the suitability of HF5 (method and technique, in general) to separate aggregates with different biophysical properties.

Last, but not least, the subsequent offline MS analysis on the HF5 high MW fractions of bone marrow cell lysates from aging mice confirmed the presence of several proteins previously reported to be insoluble or with increased tendency to aggregate during aging.

Understanding the biophysical properties of the different species of protein aggregates can be highly relevant to predict their biological consequences. For instance, the compactness of the aggregates was shown recently to determine their ability to be cleared up by autophagy. The autophagic machinery required for the sequestration of the aggregates and delivery to lysosomes can only assembly in the surface of compact aggregates, whereas those showing active disassembly by chaperones cannot be targeted to this pathway [Wong et al. 2012]. Additionally, soluble or insoluble protein aggregates have different consequences on cellular toxicity [Kopito 2000]. Thus, being able to correlate the aggregates biophysical properties with their clearance and their overall effect on cellular proteostasis is highly significant.

In conclusion, this work shows for the first time that HF5 can be used to separate oxidative-stress and age-related protein aggregates from total cell lysates. By online coupling HF5 and MALS, important biophysical information on the separated aggregates can be gathered. The results provided by HF5-MALS were corroborated

by both native gel and proteomic analysis of the high molecular weight aggregates. In the future, the method could be applied for the separation of aggregates formed under different pathological conditions to better characterize their biochemical and biophysical properties and gain further insight into protein aggregation under different stressors.

4.2.1.6. REFERENCES

[Cannizzo et al. 2012] Cannizzo E.; Clement C. C.; Morozova K.; Valdor R.; Kaushik S.; Almeida L. N.; Follo C.; Sahu R.; Cuervo A. M.; Macian F. and Santambrogio L. (2012). "*Age-related oxidative stress compromises endosomal proteostasis*." Cell Press **2** (1): 136-149.

[Cannizzo et al. 2011] Cannizzo E.; Clement C. C.; Sahu R.; Follo C. and Santambrogio L. (2011). "*Oxidative stress, inflamm-aging and immunosenescence*." Journal of Proteomics **74** (11): 2313–2323.

[David et al. 2010] David D. C.; Ollikainen N.; Trinidad J. C.; Cary M. P.; Burlingame A. L. and Kenyon C. (2010). "*Widespread Protein Aggregation as an Inherent Part of Aging in C. elegans*." PLoS Biology **8** (8): e1000450.

[Johann et al. 2010] Johann C.; Elsenberg S.; Roesch U.; Rambaldi D. C.; Zattoni A. and Reschiglian P. (2010). "*A novel approach to improve operation and performance in flow field-flow fractionation*." Journal of Chromatography A **1218** (27): 4126–4131.

[Kang and Moon 2006] Kang D. and Moon M. H. (2006). "*Development of non-gel-based two-dimensional separation of intact proteins by an on-line hyphenation of capillary isoelectric focusing and hollow fiber flow field-flow fractionation.*" Analytical Chemistry **78** (16): 5789–5798.

[Kawahara and Tanford 1966] Kawahara K. and Tanford C. (1966). "*Viscosity and Density of Aqueous Solutions of Urea and Guanidine Hydrochloride*." The Journal of Biological Chemistry **241** (13): 3228-3232.

[Kopito 2000] Kopito R. R. (2000). "*Aggresomes, inclusion bodies and protein aggregation*." Trends in Cell Biology **10** (12): 524-530.

[Reschiglian et al. 2013] Reschiglian P.; Roda B.; Zattoni A.; Tanase M.; Marassi V. and Serani S. (2013). "*Hollow-fiber flow field-flow fractionation with multi-angle laser scattering detection for aggregation studies of therapeutic proteins*." Analytical and Bioanalytical Chemistry (Field-Flow Fractionation).

[Reschiglian et al. 2004] Reschiglian P.; Zattoni A.; Cinque L. and Roda B. (2004). "*Hollow-Fiber Flow Field-Flow Fractionation for Whole Bacteria Analysis by Matrix-Assisted Laser Desorption/Ionization Time-of-Flight Mass Spectrometry*." Analytical Chemistry **76** (7): 2103–2111.

[Reschiglian et al. 2003] Reschiglian P.; Zattoni A.; Roda B.; Cinque L.; Melucci D.; Min B. R. and Moon M. H. (2003). "*Hyperlayer hollow-fiber flow field-flow fractionation of cells*." Journal of Chromatography A **985** (1-2): 519–529.

[Reschiglian et al. 2006] Reschiglian P.; Zattoni A.; Roda B.; Roda A.; Parisi D.; Moon M.-H. and Min B.-R. (2006). "*Hollow-Fiber Flow Field-Flow Fractionation: A Gentle Separation Method for Mass Spectrometry of Native Proteins*." Annali di Chimica **96** (5-6): 253–257.

[Wong et al. 2012] Wong E.; Bejarano E.; Rakshit M.; Lee K.; Hanson H. H.; Zaarur N.; Phillips G. R.; Sherman M. Y. and Cuervo A. M. (2012). "*Molecular determinants of selective clearance of protein inclusions by autophagy*." Nature Communications **3** (1240).

[Zattoni et al. 2007] Zattoni A.; Casolari S.; Rambaldi D. C. and Reschiglian P. (2007). "*Hollow-fiber flow field-flow fractionation*." Current Analytical Chemistry **3** (4): 310-323.